



THE INTERPLAY BETWEEN EPIGENETIC REGULATION AND OTHER CELLULAR PROCESSES

EDITED BY: Kai Tang and Huiming Zhang

PUBLISHED IN: Frontiers in Genetics and
Frontiers in Cell and Developmental Biology



frontiers

Frontiers eBook Copyright Statement

The copyright in the text of individual articles in this eBook is the property of their respective authors or their respective institutions or funders. The copyright in graphics and images within each article may be subject to copyright of other parties. In both cases this is subject to a license granted to Frontiers.

The compilation of articles constituting this eBook is the property of Frontiers.

Each article within this eBook, and the eBook itself, are published under the most recent version of the Creative Commons CC-BY licence.

The version current at the date of publication of this eBook is CC-BY 4.0. If the CC-BY licence is updated, the licence granted by Frontiers is automatically updated to the new version.

When exercising any right under the CC-BY licence, Frontiers must be attributed as the original publisher of the article or eBook, as applicable.

Authors have the responsibility of ensuring that any graphics or other materials which are the property of others may be included in the CC-BY licence, but this should be checked before relying on the CC-BY licence to reproduce those materials. Any copyright notices relating to those materials must be complied with.

Copyright and source acknowledgement notices may not be removed and must be displayed in any copy, derivative work or partial copy which includes the elements in question.

All copyright, and all rights therein, are protected by national and international copyright laws. The above represents a summary only. For further information please read Frontiers' Conditions for Website Use and Copyright Statement, and the applicable CC-BY licence.

ISSN 1664-8714

ISBN 978-2-88966-976-9

DOI 10.3389/978-2-88966-976-9

About Frontiers

Frontiers is more than just an open-access publisher of scholarly articles: it is a pioneering approach to the world of academia, radically improving the way scholarly research is managed. The grand vision of Frontiers is a world where all people have an equal opportunity to seek, share and generate knowledge. Frontiers provides immediate and permanent online open access to all its publications, but this alone is not enough to realize our grand goals.

Frontiers Journal Series

The Frontiers Journal Series is a multi-tier and interdisciplinary set of open-access, online journals, promising a paradigm shift from the current review, selection and dissemination processes in academic publishing. All Frontiers journals are driven by researchers for researchers; therefore, they constitute a service to the scholarly community. At the same time, the Frontiers Journal Series operates on a revolutionary invention, the tiered publishing system, initially addressing specific communities of scholars, and gradually climbing up to broader public understanding, thus serving the interests of the lay society, too.

Dedication to Quality

Each Frontiers article is a landmark of the highest quality, thanks to genuinely collaborative interactions between authors and review editors, who include some of the world's best academicians. Research must be certified by peers before entering a stream of knowledge that may eventually reach the public - and shape society; therefore, Frontiers only applies the most rigorous and unbiased reviews.

Frontiers revolutionizes research publishing by freely delivering the most outstanding research, evaluated with no bias from both the academic and social point of view. By applying the most advanced information technologies, Frontiers is catapulting scholarly publishing into a new generation.

What are Frontiers Research Topics?

Frontiers Research Topics are very popular trademarks of the Frontiers Journals Series: they are collections of at least ten articles, all centered on a particular subject. With their unique mix of varied contributions from Original Research to Review Articles, Frontiers Research Topics unify the most influential researchers, the latest key findings and historical advances in a hot research area! Find out more on how to host your own Frontiers Research Topic or contribute to one as an author by contacting the Frontiers Editorial Office: frontiersin.org/about/contact

THE INTERPLAY BETWEEN EPIGENETIC REGULATION AND OTHER CELLULAR PROCESSES

Topic Editors:

Kai Tang, Purdue University, United States

Huiming Zhang, Shanghai Institute for Biological Sciences, China

Citation: Tang, K., Zhang, H., eds. (2021). The Interplay Between Epigenetic Regulation and Other Cellular Processes. Lausanne: Frontiers Media SA. doi: 10.3389/978-2-88966-976-9

Table of Contents

- 04 Editorial: The Interplay Between Epigenetic Regulation and Other Cellular Processes**
Kai Tang and Huiming Zhang
- 06 Target of Rapamycin Regulates Genome Methylation Reprogramming to Control Plant Growth in Arabidopsis**
Tingting Zhu, Linxuan Li, Li Feng, Huijuan Mo and Maozhi Ren
- 21 The Landscape of DNA Methylation Associated With the Transcriptomic Network of Intramuscular Adipocytes Generates Insight Into Intramuscular Fat Deposition in Chicken**
Meng Zhang, Donghua Li, Yanhui Zhai, Zhengzhu Wang, Xiangfei Ma, Daoyu Zhang, Guoxi Li, Ruili Han, Ruirui Jiang, Zhuanjian Li, Xiangtao Kang and Guirong Sun
- 36 Dopamine Receptor D1 Contributes to Cocaine Epigenetic Reprogramming of Histone Modifications in Male Germ Cells**
Betina González, Samanta N. Gancedo, Sahira A. Janeir Garazatua, Eduardo Roldán, Alfredo D. Vitullo and Candela R. González
- 45 ZNF143 in Chromatin Looping and Gene Regulation**
Bingyu Ye, Ganggang Yang, Yuanmeng Li, Chunyan Zhang, Qiwen Wang and Guoying Yu
- 55 Functional Implications of Active N⁶-Methyladenosine in Plants**
Hongxiang Zheng, Simin Li, Xiansheng Zhang and Na Sui
- 64 The Crosstalk Between Epigenetic Mechanisms and Alternative RNA Processing Regulation**
Jian Zhang, Yi-Zhe Zhang, Jing Jiang and Cheng-Guo Duan
- 74 The Role of HDACs and HDACi in Cartilage and Osteoarthritis**
He Zhang, Lu Ji, Yue Yang, Xiaoning Zhang, Yi Gang and Lunhao Bai
- 86 The Histone Methyltransferase SETDB1 Modulates Survival of Spermatogonial Stem/Progenitor Cells Through NADPH Oxidase**
Xueliang Li, Xiaoxu Chen, Yingdong Liu, Pengfei Zhang, Yi Zheng and Wenxian Zeng
- 98 Inhibition of DNA Methylation in *Picochlorum soloecismus* Alters Algae Productivity**
Christina R. Steadman, Shounak Banerjee, Yuliya A. Kunde, Claire K. Sanders, Babetta L. Marrone and Scott N. Twary
- 120 IFAIM Is Regulated by MiR-206, MiR-1-3p and MiR-133b**
Elena Coccia, Marc Masanas, Joaquín López-Soriano, Miguel F. Segura, Joan X. Comella and M. José Pérez-García



Editorial: The Interplay Between Epigenetic Regulation and Other Cellular Processes

Kai Tang^{1*} and Huiming Zhang^{2*}

¹ Department of Horticulture and Landscape Architecture, Purdue University, West Lafayette, IN, United States, ² Shanghai Center for Plant Stress Biology, CAS Center for Excellence in Molecular Plant Sciences, Chinese Academy of Sciences, Shanghai, China

Keywords: epigenetic regulation, cellular processes, DNA methylation, histone modification, RNA metabolism, lipid, folate, germ cells

Editorial on the Research Topic

The Interplay Between Epigenetic Regulation and Other Cellular Processes

Epigenetic changes can influence chromatin structure and, in turn, the accessibility of genetic information as well as the stability of the whole genome. As a result, epigenetic modifications are important to many biological processes, and disruption of epigenetic configuration can lead to developmental abnormalities in plants and mammals, such as failure in tomato fruit ripening (Zhong et al., 2013; Lang et al., 2017) and embryo lethality in mice (Cortázar et al., 2011; Blewitt and Whitelaw, 2013). In addition to coordinating with developmental processes, epigenetic regulation can also play an important role in organisms' responses and adaptation to environmental changes (Etchegaray and Mostoslavsky, 2016; Zhang et al., 2018). Thus, epigenetic processes are tightly regulated in coordination with other cellular processes.

On one hand, cellular processes with important functions can be mediated by epigenetic modifications at the transcriptional level. For instance, Steadman et al. reported that algae cultures treated with 5-aza-2'-deoxycytidine, an inhibitor of DNA methylation, resulted in a remarkable increase in the level of lipid accumulation and increased cell size. Similarly, Zhang M. et al. discovered that DNA methylation regulates fatty acid metabolism and intramuscular fat deposition in chicken. As reviewed in Zhang H. et al., histone deacetylation leads to the initiation and progression of osteoarthritis; while Li et al. showed that knockdown of SETDB1, a histone H3 lysine 9 (H3K9) methyltransferase, resulted in increased levels of reactive oxygen species and impaired proliferation of mouse spermatogonial stem cells.

On the other hand, epigenetic features can be affected by other important biological processes. Certain cellular processes are inherently required for epigenetic modifications, especially DNA methylation and histone post-transcriptional modifications, which are enzymatic processes that involve not only the chromatin but also donor molecules for the modifications. For instance, disruptions in the folate biosynthesis pathway impair the supply of methyl groups for DNA methylation and for histone methylation, resulting in transcriptional desilencing at certain genomic loci in *Arabidopsis thaliana* due to lowered levels of DNA methylation and histone H3K9 dimethylation (Zhang et al., 2012). In this Research Topic, González et al. revealed that, in mouse male germ cells, cocaine caused epigenetic reprogramming of histone modifications involved in gene silencing and the histone-to-protamine replacement, while the effects of cocaine on the histone modifications can be largely blocked by inhibition of the dopamine receptor 1 (DRD1), suggesting a novel connection between the DRD1-dependent dopaminergic system and epigenetic regulation. In *Arabidopsis thaliana*, Zhu et al. observed genome hypomethylation caused by chemical inhibition of the target of rapamycin (TOR), thereby pointing to a connection between

OPEN ACCESS

Edited by:

Rui Henrique,
Portuguese Oncology
Institute, Portugal

Reviewed by:

Alexander E. Berezin,
Zaporizhzhia State Medical
University, Ukraine

*Correspondence:

Kai Tang
tang58@purdue.edu
Huiming Zhang
hmzhang@psc.ac.cn

Specialty section:

This article was submitted to
Epigenomics and Epigenetics,
a section of the journal
Frontiers in Genetics

Received: 05 April 2021

Accepted: 13 April 2021

Published: 07 May 2021

Citation:

Tang K and Zhang H (2021) Editorial:
The Interplay Between Epigenetic
Regulation and Other Cellular
Processes. *Front. Genet.* 12:691202.
doi: 10.3389/fgene.2021.691202

epigenetic regulation and this evolutionarily conserved master regulator, which integrates multiple cellular processes to promote growth in all eukaryotes (Dobrenel et al., 2016). As reviewed by Ye et al., the transcription factor ZNF143, which shows higher expression in cancer cells than normal cells, connects promoters to distal regulatory elements and thereby mediates chromatin looping.

Many important biological processes involve RNA metabolism, such as N⁶-methyladenosine that carries many functions in plants as reviewed by Zheng et al., as well as the newly identified miRNAs that silence an important regulator of apoptosis in the report by Coccia et al. Epigenetic regulation of the chromatin are often closely related to RNA metabolism. As reviewed by Zhang J. et al., a crosstalk exists between epigenetic regulation and alternative RNA processing including alternative splicing and alternative polyadenylation. Apparently, the interplay between epigenetic regulation and certain cellular processes can be bidirectional.

The interplay between epigenetic regulation and diverse cellular processes has become increasingly valued over the past few years. While this theme is highlighted by the articles in this

Research Topic, the need for a thorough understanding of the epigenetics-connected cellular network continues to urge more discoveries and new insights in this important research area.

AUTHOR CONTRIBUTIONS

All authors listed have made a substantial, direct and intellectual contribution to the work, and approved it for publication.

FUNDING

Research in HZ lab has been supported by the Chinese Academy of Sciences.

ACKNOWLEDGMENTS

We thank all authors who submitted their work for this Research Topic as well as the invaluable help of reviewers in manuscript evaluation and the support of professional Editorial staff at Frontiers.

REFERENCES

- Blewitt, M., and Whitelaw, E. (2013). "The use of mouse models to study epigenetics." *Cold Spring Harbor Perspect. Biol.* 5:a017939. doi: 10.1101/cshperspect.a017939
- Cortázar, D., Kunz, C., Selfridge, J., Lettieri, T., Saito, Y., MacDougall, E., et al. (2011). "Embryonic lethal phenotype reveals a function of TDG in maintaining epigenetic stability." *Nature*. 470, 419–423. doi: 10.1038/nature09672
- Dobrenel, T., Camila, C., Johannes, H., Christophe, R., Michel, V., Bruce, V., et al. (2016). "TOR signaling and nutrient sensing." *Annu. Rev. Plant. Biol.* 67, 261–285. doi: 10.1146/annurev-arplant-043014-114648
- Etchegaray, J. P., and Mostoslavsky, R. (2016). "Interplay between metabolism and epigenetics: a nuclear adaptation to environmental changes." *Mol. Cell*. 62, 695–711. doi: 10.1016/j.molcel.2016.05.029
- Lang, Z., Wang, Y., Tang, K., Tang, D., Datsenko, T., Cheng, J., et al. (2017). "Critical roles of DNA demethylation in the activation of ripening-induced genes and inhibition of ripening-repressed genes in tomato fruit." *Proc. Natl. Acad. Sci. U. S. A.* 2017:5233. doi: 10.1073/pnas.1705233114
- Zhang, H., Xiangyang, D., Daisuke, M., Sean, C., Jee-Eu, O., and Jian-Kang, Z. (2012). Sulfamethazine suppresses epigenetic silencing in Arabidopsis by impairing folate synthesis. *Plant Cell*. 24, 1230–1241. doi: 10.1105/tpc.112.096149
- Zhang, H., Zhaobo, L., and Jian-Kang, Z. (2018). Dynamics and function of DNA methylation in Plants. *Nat. Rev. Mol. Cell Biol.* 19, 489–506. doi: 10.1038/s41580-018-0016-z
- Zhong, S., Fei, Z., Chen, Y. R., Zheng, Y., Huang, M., Vrebalov, J., et al. (2013). "Single-base resolution methylomes of tomato fruit development reveal epigenome modifications associated with ripening." *Nat. Biotechnol.* 31, 154–159. doi: 10.1038/nbt.2462

Conflict of Interest: The authors declare that the research was conducted in the absence of any commercial or financial relationships that could be construed as a potential conflict of interest.

Copyright © 2021 Tang and Zhang. This is an open-access article distributed under the terms of the Creative Commons Attribution License (CC BY). The use, distribution or reproduction in other forums is permitted, provided the original author(s) and the copyright owner(s) are credited and that the original publication in this journal is cited, in accordance with accepted academic practice. No use, distribution or reproduction is permitted which does not comply with these terms.



Target of Rapamycin Regulates Genome Methylation Reprogramming to Control Plant Growth in *Arabidopsis*

Tingting Zhu^{1,2†}, Linxuan Li^{1†}, Li Feng^{1,3}, Huijuan Mo³ and Maozhi Ren^{1,3*}

¹ Institute of Urban Agriculture, Chinese Academy of Agricultural Sciences, Chengdu, China, ² School of Life Sciences, Chongqing University, Chongqing, China, ³ Zhengzhou Research Base, State Key Laboratory of Cotton Biology, Zhengzhou University, Zhengzhou, China

OPEN ACCESS

Edited by:

Kai Tang,
Purdue University, United States

Reviewed by:

Yu-Hung Hung,
Donald Danforth Plant Science
Center, United States
Zoltan Magyar,
Biological Research Centre,
Hungarian Academy of Sciences
(MTA), Hungary

*Correspondence:

Maozhi Ren
renmaozhi01@caas.cn

[†]These authors have contributed
equally to this work

Specialty section:

This article was submitted to
Epigenomics and Epigenetics,
a section of the journal
Frontiers in Genetics

Received: 04 November 2019

Accepted: 17 February 2020

Published: 03 March 2020

Citation:

Zhu T, Li L, Feng L, Mo H and
Ren M (2020) Target of Rapamycin
Regulates Genome Methylation
Reprogramming to Control Plant
Growth in *Arabidopsis*.
Front. Genet. 11:186.
doi: 10.3389/fgene.2020.00186

DNA methylation is an indispensable epigenetic modification that dynamically regulates gene expression and genome stability during cell growth and development processes. The target of rapamycin (TOR) has emerged as a central regulator to regulate many fundamental cellular metabolic processes from protein synthesis to autophagy in all eukaryotic species. However, little is known about the functions of TOR in DNA methylation. In this study, the synergistic growth inhibition of *Arabidopsis* seedlings can be observed when DNA methylation inhibitor azacitidine was combined with TOR inhibitors. Global DNA methylation level was evaluated using whole-genome bisulfite sequencing (WGBS) under TOR inhibition. Hypomethylation level of whole genome DNA was observed in AZD-8055 (AZD), rapamycin (RAP) and AZD + RAP treated *Arabidopsis* seedlings. Based on functional annotation and KEGG pathway analysis of differentially methylated genes (DMGs), most of DMGs were enriched in carbon metabolism, biosynthesis of amino acids and other metabolic processes. Importantly, the suppression of TOR caused the change in DNA methylation of the genes associated with plant hormone signal transduction, indicating that TOR played an important role in modulating phytohormone signals in *Arabidopsis*. These observations are expected to shed light on the novel functions of TOR in DNA methylation and provide some new insights into how TOR regulates genome DNA methylation to control plant growth.

Keywords: target of rapamycin, DNA methylation, AZD-8055, rapamycin, plant growth, *Arabidopsis*

INTRODUCTION

DNA methylation is an important part of epigenetics, which is widely distributed in microbes, animals and plants. DNA methylation plays an important role in controlling transcriptional silencing of transposon, regulating gene expression and maintaining plant development (Moore et al., 2013; Bouyer et al., 2017; Zhang et al., 2018), which is one of the most studied epigenetic modifications in epigenetics. The methyl of DNA methylation provided by S-adenosylmethionine

is transferred to the cytosine of genome DNA under the catalysis of DNA methyltransferase (Razin and Riggs, 1980). Mammals mainly methylate cytosine at symmetrical CG site, while plant DNA methylation occurs in all cytosine sequence contexts: CG, CHG, and CHH (H represents A, T, or C) (Lister et al., 2008). DNA methylation regions are mainly found in highly repetitive sequences (transposon and rDNA), promoter region (suppressing gene expression), coding sequence region and intergenic region. More than 5% of the expressed genes have DNA methylation in their promoter region, and more than 33% of genes contain DNA methylation within the coding sequence region in *Arabidopsis* (Zhang et al., 2006). Promoter-methylated genes are low expressed and show a greater degree of tissue specific expression, whereas genes methylated in transcribed regions are highly expressed (Zhang et al., 2006). However, recently study also showed that methylation in transcribed regions can negatively regulate the gene expression (Long et al., 2014; Lou et al., 2014).

DNA methylation is critically important for normal growth and development in both animals and plants; null mutations of DNA methyltransferase DNMT1 or DNMT3 result in embryonic lethality in mouse, and *drm1/drm2/cmt3* triple mutants exhibit developmental abnormalities in *Arabidopsis* (Grace and Bestor, 2005; Chan et al., 2006). 5-Azacytidine (Azacitidine) is a nucleoside analog of cytidine that specifically inhibits DNA methylation by capturing DNA methyltransferase in bacteria and mammalian (Christman, 2002). In plants, genome-wide demethylation caused by methylation inhibitor azacitidine leads to growth retardation, malformations, and changes in the flowering time or flower sexuality (Fieldes et al., 2005; Marfil et al., 2012). Interestingly, azacitidine can increase amounts of somatic embryos in somatic embryogenesis stage, indicating that DNA demethylation caused by azacitidine promotes the reprogramming of gene expression, acquisition of totipotency and initiation of embryogenesis in explant (Osorio-Montalvo et al., 2018).

The target of rapamycin (TOR) is an evolutionarily conserved protein kinase that integrates nutrient and energy signaling to regulate growth and homeostasis in fungi, animals and plants. TOR is activated by both nitrogen and carbon metabolites and promotes energy-consuming processes such as mRNA translation, protein biosynthesis and anabolism while represses autophagy and catabolism in times of energy abundance (Dobrenel et al., 2016; Juppner et al., 2018; Ahmad et al., 2019). However, deregulated mammalian target of rapamycin (mTOR) signaling is implicated in the progression of cancer and diabetes, and the aging process in mammalian (Saxton and Sabatini, 2017). Genetic, physiological and genomic studies revealed that TOR plays central roles in plant embryogenesis, seedling growth, root and shoot meristem activation, root hair elongation, leaf expansion, flowering and senescence (Ren et al., 2011, 2012; Xiong et al., 2013; Yuan et al., 2013; Xiong and Sheen, 2014; Deng et al., 2017; Shi et al., 2018). TOR gene was originally identified by genetic mutant screens for resistance to rapamycin in budding yeast (Heitman et al., 1991). Subsequent research showed that null mutation of *tor* resulted in embryonic lethality in yeast, animals and plants (Heitman et al., 1991;

Ren et al., 2011; Saxton and Sabatini, 2017), indicating that TOR was an essential kinase in eukaryotes. Since rapamycin acts as a specific inhibitor of the TOR kinase, the TOR signaling pathway is quickly considered as a central regulator by application of rapamycin in yeast and animals (Benjamin et al., 2011). However, TOR is insensitive to rapamycin in plants, which is mainly due to evolutionary mutation of the *FK506-binding protein 12 (FKBP12)* gene, resulting in loss of function to bind rapamycin (Xu et al., 1998). To dissect TOR signaling pathway in *Arabidopsis* by using rapamycin, Ren et al. (2012) generated a rapamycin-hypersensitive line (BP12-2) by introducing yeast *FKBP12* gene into *Arabidopsis*. Inhibition of AtTOR in BP12-2 line by rapamycin resulted in slower root, shoot and leaf growth and development, leading to poor carbon and nitrogen metabolism, nutrient uptake and light energy utilization (Ren et al., 2012). Additionally, the ATP competitive TOR kinase inhibitors including Torin2, WYE-132, Ku-0063794, and AZD-8055 (AZD) were also applied to study the TOR pathway in plants (Montane and Menand, 2013; Li et al., 2015; Song et al., 2017, 2018). As revealed by recent studies, AZD had high specificity and strong inhibitory effects on TOR activity in flowering plants (Montane and Menand, 2013; Li et al., 2015), implying that AZD can be preferentially applied to plants to dissect TOR signaling pathway compared with other TOR kinase inhibitors in angiosperms.

The TOR signaling pathway is a central regulator in regulating cell growth, homeostasis, proliferation and metabolism (Dobrenel et al., 2016; Saxton and Sabatini, 2017; Shi et al., 2018). DNA methylation is an epigenetic mechanism that plays key roles in genome integrity, suppression of transposon, gene expression and somatic embryogenesis in plants (Osorio-Montalvo et al., 2018; Zhang et al., 2018). However, it has not been reported whether TOR directly or indirectly regulates the methylation level of genome DNA to control plant growth and development. In this study, we performed base-resolution whole-genome bisulfite sequencing (WGBS) under TOR inhibition in *Arabidopsis*. Differentially methylated regions and genes support the evolutionarily conserved TOR functions in ribosome biogenesis, metabolism, and cell growth. Our detailed genome-wide analysis of DNA methylation under TOR inhibition provides new insights into how TOR regulates global DNA methylation to control plant growth.

MATERIALS AND METHODS

Plant Materials and Growth Conditions

WT *Arabidopsis* Columbia (Col-0) and the transgenic *Arabidopsis* BP12-2 line were used in this study (Ren et al., 2012). Sterile treatment of *Arabidopsis* seeds surface prior to plating. The seeds first repeatedly were shook in 75% ethanol for 2 min and the supernatant was discarded. Then, shaking the seeds repeatedly with 10% sodium hypochlorite containing 0.3% Tween-20 for 4 min, and discarding the supernatant; followed by four or five rinses with sterile water, and the supernatant was discarded. Finally, the seeds were suspended in 0.15% sterile agarose solution and kept at 4°C for 2 days. Sterilized seeds were plated

on plates, and then grown in a controlled environment at 22°C under 16 h 60–80 $\mu\text{E}\cdot\text{m}^{-2}\text{s}^{-1}$ continuous light and 8 h darkness.

DNA Library Construction and Whole-Genome Bisulfite Sequencing

BP12-2 seedlings of 7 days were treated with DMSO, AZD (1 μM), RAP (5 μM), and AZD (1 μM) + RAP (5 μM) for 24 h, and each sample contained three biological replicates. Total genomic DNA was extracted using a plant genomic DNA kit (TIANGEN, Beijing, China) according to the manufacturer's instructions. Genomic DNA degradation and contamination was monitored on agarose gels. DNA purity was checked using the NanoPhotometer® spectrophotometer (IMPLEN, Westlake Village, CA, United States). DNA concentration was measured using Qubit® DNA Assay Kit in Qubit® 2.0 Fluorometer (Life Technologies, CA, United States). A total amount of 5.2 microgram genomic DNA spiked with 26 ng lambda DNA were fragmented by sonication to 200–300 bp with Covaris S220, followed by end repair and adenylation. Cytosine-methylated barcodes were ligated to sonicated DNA as per manufacturer's instructions. Then these DNA fragments were treated twice with bisulfite using EZ DNA Methylation-Gold Kit™ (Zymo Research). In addition, the resulting single-strand DNA fragments were PCR amplified using KAPA HiFi HotStart Uracil + ReadyMix (2X). Library concentration was quantified by Qubit® 2.0 Fluorometer (Life Technologies, CA, United States) and quantitative PCR, and the insert size was checked on Agilent Bioanalyzer 2100 system. The clustering of the index-coded samples was performed on a cBot Cluster Generation System using TruSeq PE Cluster Kit v3-cBot-HS (Illumina) according to the manufacturer's instructions. After cluster generation, the prepared library were sequenced on an Illumina HiSeq 2000/2500 platform, and 100/50 bp single-end reads were generated. Image analysis and base calling were performed with the standard Illumina pipeline, and finally 100 bp paired-end reads were generated.

Estimating Methylation Level

To identify the methylation level, we employed a sliding-window approach, which was conceptually similar to approaches that have been used for bulk BS-Seq. With window size = 3,000 bp and step size = 600 bp (Smallwood et al., 2014), the sum of methylated cytosine (mC) and unmethylated cytosine (C) read counts in each window were calculated. Methylation level (ML) for each cytosine site showed the fraction of methylated C, and was defined as: $\text{ML (mC)} = \text{reads (mC)} / (\text{reads (mC)} + \text{reads (C)})$. Calculated ML was further corrected with the bisulfite non-conversion rate according to previous studies (Lister et al., 2013).

Analysis of Methylation Levels in Genomic Functional Regions

Analysis of the average methylation level of the CG, CHG, and CHH sites in genomic functional regions including promoter (2 kb region upstream of the transcription start site), 5'UTR, exon, intron and 3'UTR regions. Divided each functional element region in the genome annotation into 20 bins, and counted the

number of mC and C reads in each bin. For average plots, average values in 20 bins were calculated and plotted.

Differentially Methylated Regions (DMRs) Analysis

Differentially methylated regions (DMRs) were identified using the Bseq R package software, which used a sliding-window approach (reads coverage ≥ 5). The window was set to 1,000 bp and step length was 100 bp. The main steps of identification DMR were as follows: First set the sliding window and sliding step size, every 1000 bp as a window and 100 bp as the step size. Selected the DNA methylation level difference value > 0.1 and the DNA methylation difference fold-change > 2 between the treatment and the control sample, and the number of cytosine > 10 as potential DMRs. Next, probabilities were calculated using a Fisher's exact test. The regions with significant differences ($p < 0.05$) were considered as DMRs. Then, moved to the next window with the step size and repeated the above steps to obtain DMRs information of the whole genome. FDR (FDR < 0.05) was used to correct the p value of all DMRs.

GO and KEGG Enrichment Analysis of DMR-Related Genes (DMGs)

Gene Ontology (GO) enrichment analysis of genes related to DMRs was implemented by the Goseq R package (Young et al., 2010), in which gene length bias was corrected. GO terms with corrected P -value less than 0.05 were considered significantly enriched by DMGs. Kyoto Encyclopedia of Genes and Genomes (KEGG) (Minoru et al., 2008) is a database resource for understanding high-level functions and utilities of the biological system, such as the cell, the organism and the ecosystem, from molecular-level information, especially large-scale molecular datasets generated by genome sequencing and other high-throughput experimental technologies¹. We used KOBAS software (Mao et al., 2005) to test the statistical enrichment of DMGs in KEGG pathways.

Quantitative Real-Time PCR

Total RNA of transgenic *Arabidopsis* BP12-2 seedlings which treated for 24 h in mediums containing DMSO, AZD (1 μM), RAP (5 μM), and AZD (1 μM) + RAP (5 μM) was isolated using the RNeasy Pure Plant Kit (TIANGEN, Beijing, China). Total RNA was reverse transcribed into cDNA using the PrimeScript R RT reagent kit (Takara, Dalian, China). Relative transcript levels were assayed by the CFX96 real-time PCR system (BIO-RAD, United States). *AtACTIN2* was used as an internal control. Real-time PCR primers were shown in **Supplementary Table S1**. Reaction was performed in a final volume of 20 μL containing 10 μL of 2 \times Power Top Green qPCR SuperMix (TRANSGEN, Beijing, China). RNA relative quantification analyses were performed with the Bio-Rad CFX manager software. The data represented the mean \pm SD of three independent experiments.

¹<http://www.genome.jp/kegg/>

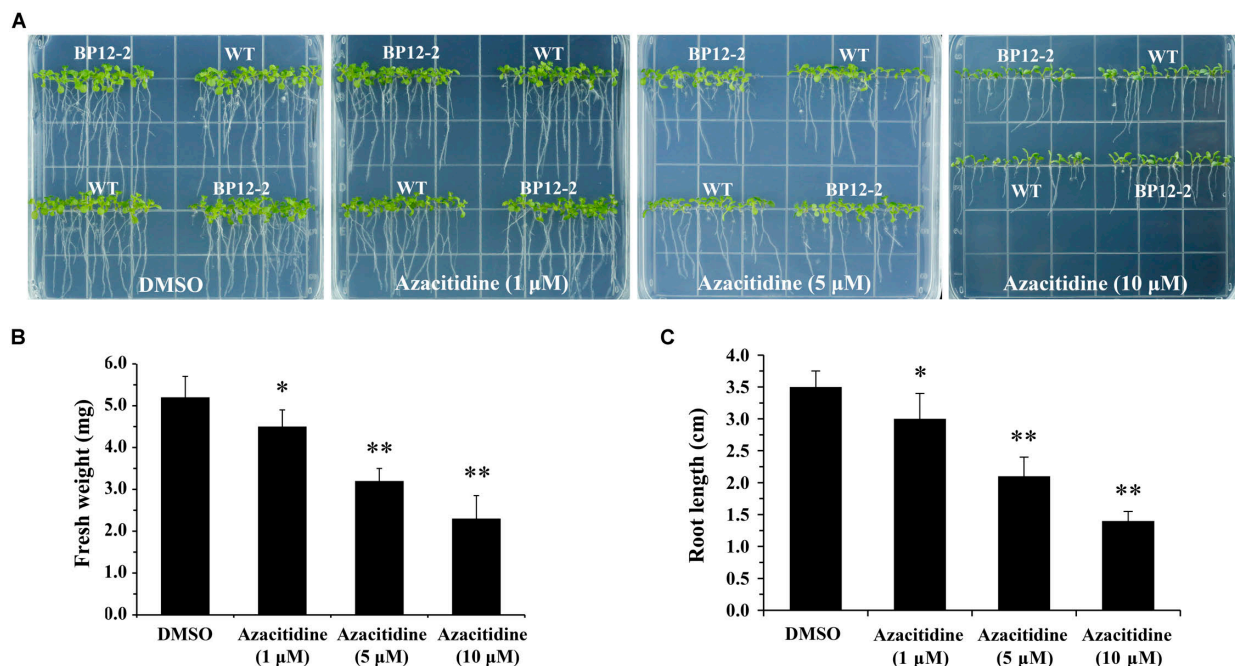


FIGURE 1 | Azacitidine inhibits seedlings growth in dose-dependent manner in *Arabidopsis*. **(A)** Phenotypes of WT and BP12-2 seeds cultured on 1/2 MS medium containing increasing concentrations of azacitidine for 10 days. **(B,C)** Fresh weight and root length of WT seedlings growing on different azacitidine concentrations for 10 days. Each graph represents the average of 30 seedlings. Error bars indicate means \pm SD of three biological replicates. Asterisks denote Student's *t*-test significant difference compared with DMSO (* $P < 0.05$, ** $P < 0.01$).

Combination Index (CI) Value Measurement

Combination index (CI) values were used to evaluate the interaction between azacitidine and AZD/RAP. The degree of reagents interaction was based on synergistic effect ($CI < 1$), additive effect ($CI = 1$), or antagonism ($CI > 1$) (Chou, 2006). WT and BP12-2 seeds were sown on plates containing DMSO, azacitidine, RAP, AZD, and pairwise combination for 10 days, and then fresh weight was measured for CI value assessment. Experiments were repeated at least three times. The values of affected fraction (Fa) were calculated according to the CompuSyn software program (Chou and Talalay, 1984; Chou, 2006).

RESULTS

Azacitidine and TOR Inhibitors Synergistically Inhibit Seedlings Growth in *Arabidopsis*

Azacitidine is a specific inhibitor of DNA methylation, which interacts with DNA methyltransferase to inhibit DNA methylation in mammalian (Christman, 2002). To test the effect of azacitidine on seeds germination and seedlings growth in *Arabidopsis*, we treated *Arabidopsis* seeds with different concentrations of azacitidine. With the increase of azacitidine concentrations, Col-0 (WT) and BP12-2 seeds germination was not affected by azacitidine, whereas the seedlings growth was

subjected to different degrees of inhibition, reflecting in the reduction of fresh weight and shorter root length (Figure 1). The 50% growth inhibitory dose (GI50) of azacitidine was 10 μ M in accordance with fresh weight (Figure 1B). The phenotype of azacitidine-treated *Arabidopsis* seedlings is similar to that of TOR kinase inhibitors, implying that TOR may play a role in regulating DNA methylation in *Arabidopsis*. Interestingly, the transcription level of *AtTOR* did not significantly change in azacitidine-treated WT and BP12-2 seedlings (Supplementary Figure S1A), indicating that azacitidine had no effect on TOR expression.

To examine the roles of TOR in the regulation of DNA methylation, we used combinations of TOR inhibitors and azacitidine to treat *Arabidopsis* seeds. Rapamycin (RAP) and AZD-8055 (AZD) that act as different types of TOR kinase inhibitors were selected to treat WT and BP12-2 *Arabidopsis* seeds. Consistent with the previous reports (Ren et al., 2012), RAP had no obvious inhibitory effect on WT seedlings, whereas significantly inhibited roots and shoots elongation and leaves expansion in BP12-2 seedlings (Figure 2A). The combination of RAP and azacitidine enhanced the inhibition of seedlings growth compared with RAP or azacitidine alone treatment, resulting in leaves yellowing and growth retardation in BP12-2 seedlings (Figures 2A,B). Meanwhile, the combination of AZD and azacitidine also enhanced the inhibition of seedlings growth, implying that TOR inhibitors and azacitidine may synergistically inhibit seedlings growth in *Arabidopsis*. To further explore whether TOR inhibitors and azacitidine synergistically inhibit seedlings growth, we used a combination index (CI) to calculate

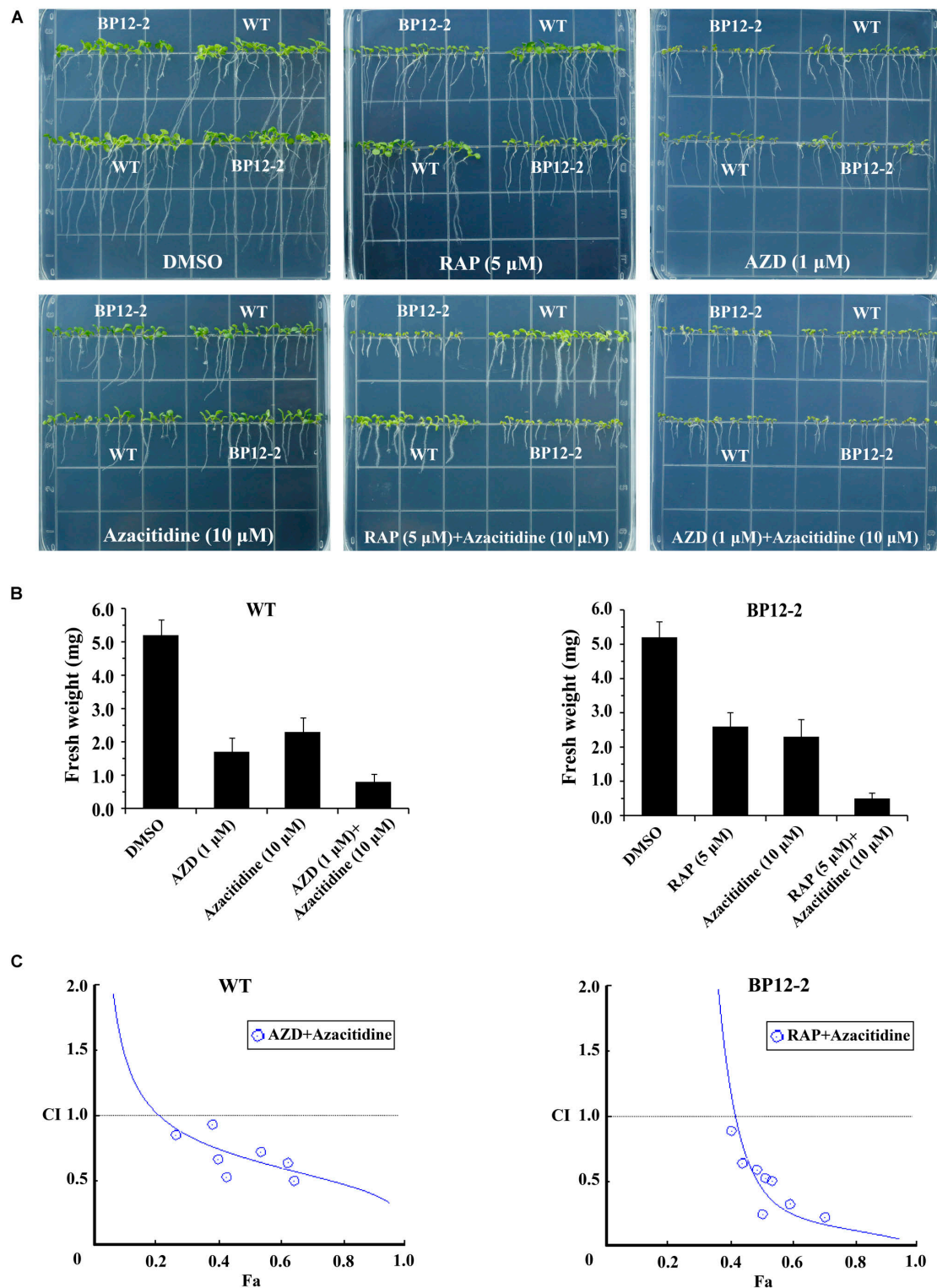


FIGURE 2 | Azacitidine and TOR inhibitors synergistically inhibit seedlings growth in *Arabidopsis*. **(A)** Phenotypes of 10-day-old WT and BP12-2 seeds sown on 1/2 MS medium containing DMSO, azacitidine (10 μ M), RAP (5 μ M), AZD (1 μ M), and the combination of RAP (5 μ M) + azacitidine (10 μ M) and AZD (1 μ M) + azacitidine (10 μ M). **(B)** Fresh weight of WT and BP12-2 seedlings sown on different plates for 10 days. Each graph represents the average of 30 seedlings. Error bars indicate means \pm SD of three biological replicates. **(C)** Azacitidine and TOR inhibitors synergistically inhibit plant growth *in vitro*. WT and BP12-2 seeds were sown on plates containing DMSO, azacitidine, RAP, AZD, and pairwise combination for 10 days, and then fresh weight was measured for CI value assessment. The Fa-CI curve shows synergistic effects ($CI < 1$) between AZD + azacitidine and RAP + azacitidine in WT and BP12-2 seedlings, respectively.

TABLE 1 | Data generated by whole-genome bisulfite sequencing (WGBS).

Samples	Raw reads	Clean reads	GC content	Total reads	Mapped reads	Mapping rate	Uniquely mapping rate	Bisulfite conversion rate
DMSO	56035294	53295965	20.12%	26438527	19114111	71.97%	58.56%	99.56%
AZD	59270545	55453129	20.43%	27726565	19734425	71.22%	59.59%	99.62%
RAP	57042080	51115347	20.35%	25557673	18379669	71.20%	59.48%	99.59%
AZD + RAP	64675954	58197908	20.45%	29098954	20895769	71.85%	58.49%	99.56%

the interaction between TOR inhibitors and azacitidine in *Arabidopsis*. The combination treatment of RAP and azacitidine generated a strong synergistic effect ($CI < 0.5$) in BP12-2 seedlings. Meanwhile, the combination treatment of AZD and azacitidine also generated the synergistic effects ($CI < 1$) in WT plants (**Figure 2C**). These results indicated that TOR inhibitors and azacitidine synergistically inhibit the growth of *Arabidopsis* seedlings, implying the functions of TOR in DNA methylation.

Inhibition of TOR Reduces Whole-Genome Methylation Level in *Arabidopsis*

To further analyze the functions of TOR in the regulation of DNA methylation, we performed base-resolution whole-genome bisulfite sequencing (WGBS) under TOR inhibition by AZD, RAP, and AZD + RAP treatment in *Arabidopsis*. Each sample contained more than 51 million clean reads after removing the low-quality reads, duplicate reads and adapters. The bisulfite conversion efficiency exceeded 99.5% in all samples, providing a reliable guarantee of the accuracy of WGBS (**Table 1**). We used Bowtie2 (Bismark) software to map the clean reads to the reference genome, and more than 58% of the reads were uniquely mapped to the *Arabidopsis* genome in each sample (**Table 1**). Further statistical analysis found that DNA methylation occurred mainly at three different sequence sites: CG, CHG, and CHH sites ($H = A, T, \text{ or } C$) in all samples, we calculated methylation ratio of the three sequence contexts in the genome. The methylation ratio of the CG sequence was the highest, followed by the CHG sequence and the CHH sequence in all samples (**Table 2**). Among them, the methylation ratio of CG context was decreased, while the methylation ratio of CHH context was increased under TOR inhibition. Importantly, the total mCX methylation ratio was reduced in TOR-inhibited samples compared to DMSO control group (**Table 2**). Furthermore, genome-wide methylation level was decreased in TOR-inhibited samples, of which the methylation level was most obviously decreased in AZD + RAP treated sample (**Figure 3A**). Additionally, we analyzed the proportion of methylated C site on each chromosome and found that the methylation ratio of CG site on each chromosome was higher than the CHG and CHH sites. Consistent with the above findings, inhibition of TOR also reduced the proportion of methylated CX sites on each chromosome (**Figure 3B**).

To explore the role of DNA methylation in regulating gene expression, we analyzed the changes of DNA methylation levels on genomic functional elements including promoters, exons, introns and UTR regions. Similar methylation levels were observed in the three methylated CX contexts in each

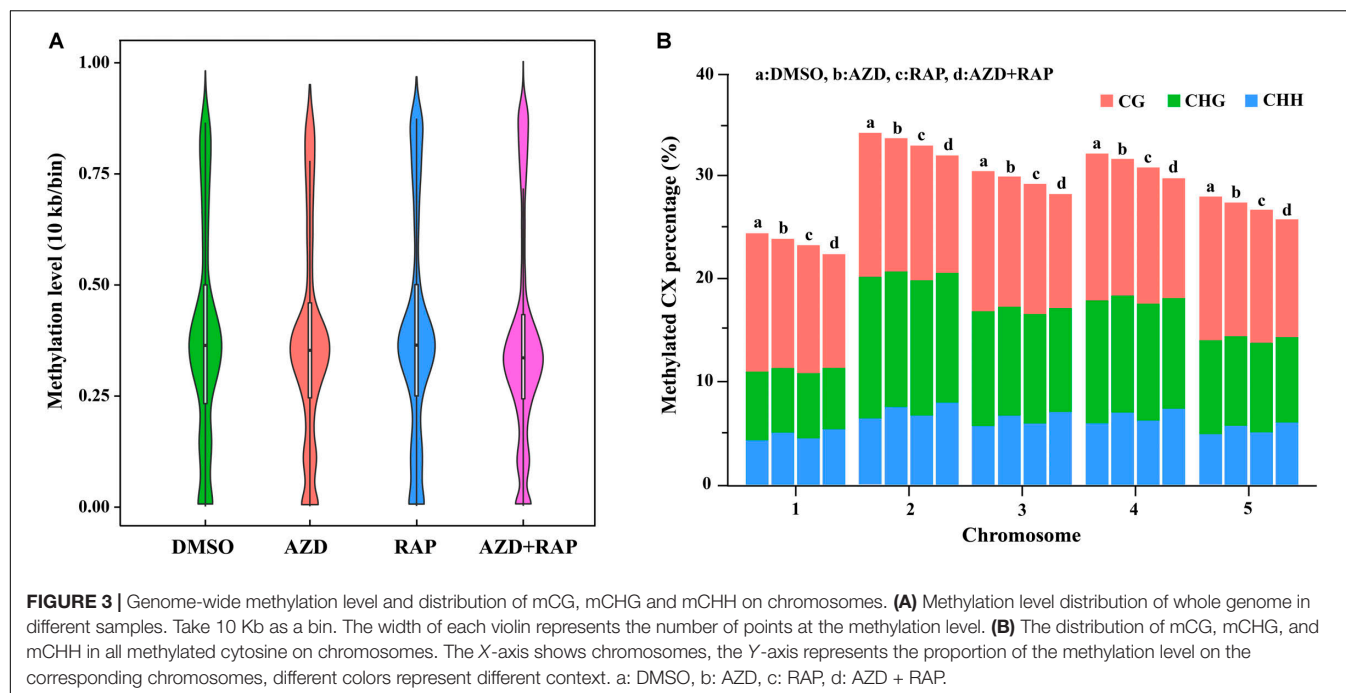
functional element of all samples. Among them, the promoter had the highest DNA methylation ratio, followed by the exon region, and the 5'UTR had the lowest DNA methylation ratio in all samples (**Figure 4**). Interestingly, we found that inhibition of TOR increased the average methylation level of mCHH in the promoter region whereas mCG and mCHG had no obvious change, implying that TOR plays an important role in regulation of methylation of CHH site in promoter region. To investigate whether the reduction in genome-wide methylation was caused by methyltransferases, we examined the transcription levels of methyltransferase and demethylase genes under TOR inhibition. The transcription level of *METHYLTRANSFERASE 1 (MET1)* that maintains CG methylation in plants was down-regulated in TOR-inhibited seedlings (**Supplementary Figure S2A**). However, *DOMAINS REARRANGED METHYLASE 1 (DRM1)* and *DRM2* genes, which maintain asymmetric CHH site methylation in plants (Chan et al., 2005), were up-regulated under TOR inhibition, which could account for high methylation level of CHH site in the promoter region under TOR inhibition. Besides, the transcription levels of demethylase genes including *ROS1*, *MBD7*, and *IBM1* were significantly up-regulated in TOR-inhibited seedlings (**Supplementary Figure S2B**). These results indicated that TOR regulated DNA methylation by altering the transcription levels of methyltransferase and demethylase genes in *Arabidopsis*.

Analysis of Differentially Methylated Region (DMR) Under TOR Inhibition

Whole genome differential methylation analysis was performed in AZD vs. DMSO, RAP vs. DMSO, and AZD + RAP vs. DMSO groups. Total 1417, 4664, and 5282 DMRs were identified in AZD vs. DMSO, RAP vs. DMSO, and AZD + RAP vs. DMSO groups, respectively. All DMRs were classified into five types according to genome elements, most of which were distributed in promoter and exon regions. Moreover, hypermethylated DMRs were more than hypomethylated DMRs under TOR inhibition, of which hypermethylated DMRs were also mainly distributed in promoter and exon regions (**Figure 5A**). We further mapped the obtained DMRs of promoter, 5'UTR, exon, intron, and 3'UTR to genes.

TABLE 2 | The proportion of methylated C site in the genome.

Samples	mCpG (%)	mCHG (%)	mCHH (%)	Total mCX (%)
DMSO	29.17	15.41	5.29	49.87
AZD	27.66	15.68	6.23	49.57
RAP	27.96	15.18	5.53	48.67
AZD C RAP	27.01	15.24	6.58	48.83



A total of 1296, 4015, and 4520 differentially methylated genes (DMGs) were found in AZD vs. DMSO, RAP vs. DMSO, and AZD + RAP vs. DMSO groups, respectively. The Venn diagram displayed that 314 DMGs were overlapping among three groups, while approximately 50% of the DMGs were not overlapping between these groups (**Figure 5B**). Furthermore, hierarchical cluster analysis of DMGs was performed using Cluster software, and methylated genes were clustered using a distance metric based on the Pearson correlation. The results showed that some DMGs had a hypomethylated status under TOR inhibition (**Figure 5C**). Especially, some significant hypomethylated genes were found in RAP-treated seedlings (**Supplementary Table S2**).

Gene Ontology (GO) and KEGG Pathway Enrichment Analysis of DMGs

We further functionally categorized the DMGs and analyzed their significant differences by using the Goseq R package (Young et al., 2010). These DMGs were assigned to one or more of three categories: biological process, cellular component, and molecular function base on the GO assignments, and they were significantly enriched in 25, 132, and 198 terms of three GO categories in AZD vs. DMSO, RAP vs. DMSO, and AZD + RAP vs. DMSO groups, respectively (corrected $P < 0.05$) (**Supplementary Table S3**). The top three significantly enriched GO terms were “cell periphery,” “plasma membrane,” and “catalytic activity” in AZD vs. DMSO group, “catalytic activity,” “nucleotide binding,” and “nucleoside phosphate binding” in RAP vs. DMSO group, and “nucleotide binding,” “nucleoside phosphate binding,” and “ribonucleoside binding” in AZD + RAP vs. DMSO group (**Figure 6A** and **Supplementary Figure S3A**), suggesting that these GO terms may play important roles in TOR-regulated genomic methylation. Furthermore, the largest number of functional GO

term was “cell” under TOR inhibition, which distributed in the cellular component category, implying that TOR may participate in the regulation of cellular component GO terms.

To provide further insight into the pathways, we performed KEGG pathway analysis of the DMGs under TOR inhibition. The major metabolic pathways and signal transduction pathways of DMGs were identified by KEGG significant enrichment. The top two enriched KEGG pathways were “Carbon metabolism” and “Biosynthesis of amino acids” under TOR inhibition (**Figure 6B** and **Supplementary Figure S3B**). In addition, DMGs in “RNA transport,” “Ribosome biogenesis in eukaryotes,” and “beta-Alanine metabolism” pathways were also found under TOR inhibition.

DMGs Involved in the Regulation of Cell Growth

Carbon metabolism and synthesis of proteins are important limiting factors for cell growth and proliferation (Webb and Satake, 2015; Saxton and Sabatini, 2017). Among these altered metabolic processes in KEGG pathways, the number of “Carbon metabolism” and “Biosynthesis of amino acids” pathways was the largest (**Figure 6B**), indicating that TOR controlled cell growth and proliferation by regulating the methylation level of the genes. We further analyzed the methylation levels of “Carbon metabolism” and “Biosynthesis of amino acids” pathways in RAP vs. DMSO group. A total of 21 and 17 DMGs had significant changed methylation levels in “Carbon metabolism” and “Biosynthesis of amino acids” pathways, respectively (methylation ratio > 1.5 -fold) (**Table 3**). The genes encoding rate-limiting enzymes of carbon metabolism and biosynthesis of amino acids such as 6-phosphofructokinase (*PFK6*) and isocitrate dehydrogenase

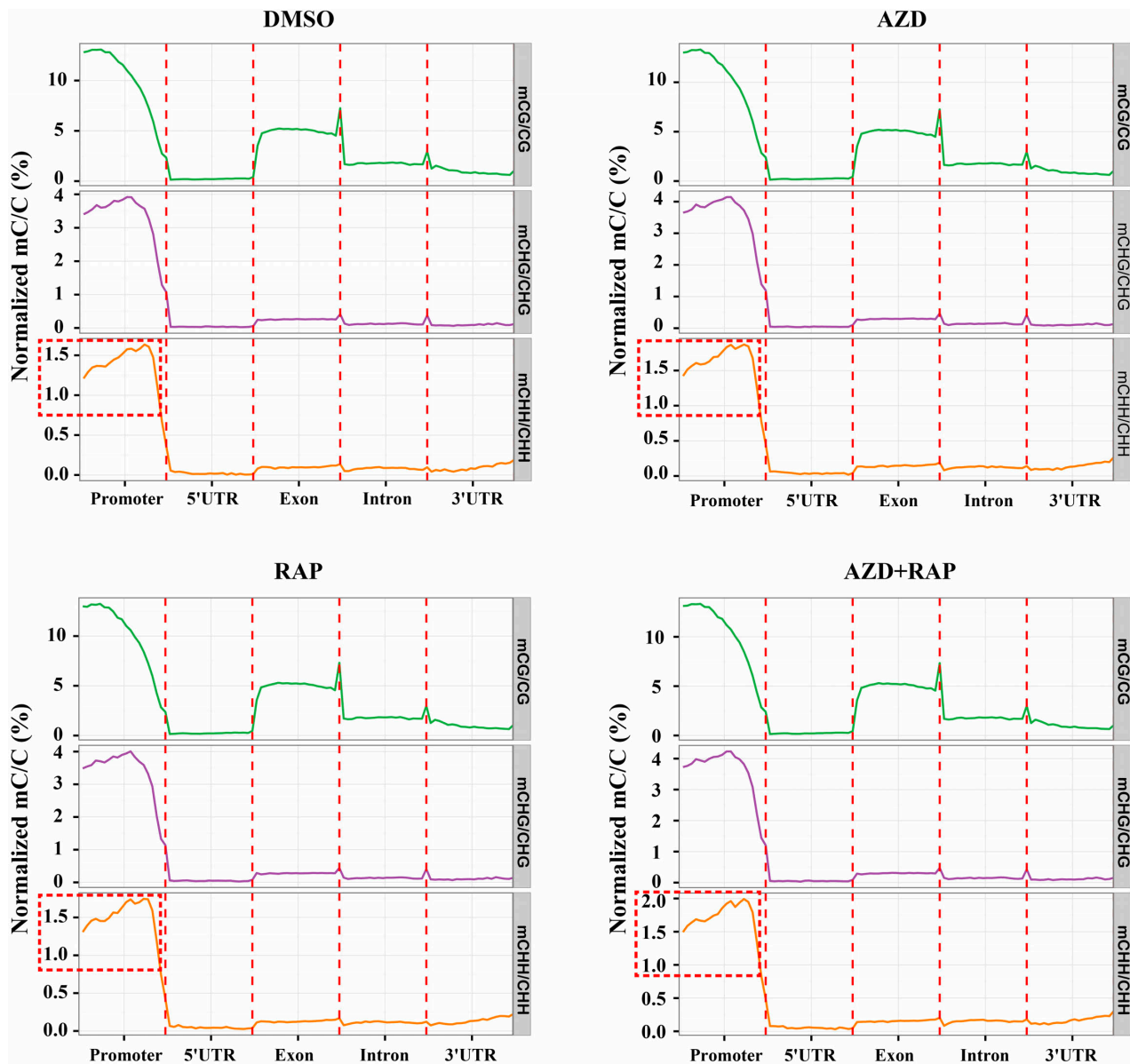


FIGURE 4 | Distribution of methylation levels of all samples on different genomic elements. Abscissa represented different genomic elements, ordinate represented the average level of methylation, and different colors represented different sequence contexts (CG, CHG, and CHH). The promoter region is a 2 kb region upstream of the TSS site.

(*IDH5*) were hypermethylated, suggesting that TOR inhibition by RAP reduced the carbon metabolism levels in *Arabidopsis*. In addition, the methylation levels of genes in “Carbon metabolism” and “Biosynthesis of amino acids” pathways were also changed in AZD-treated samples (**Supplementary Table S4**). These results indicated that TOR regulated multiple metabolic processes by altering the methylation levels of related genes.

The ribosome, composed of ribosomal RNAs and ribosomal proteins, is responsible for the synthesis of proteins in prokaryotes and eukaryotes (Adam et al., 2011; Opron and Burton, 2018). TORC1 positively regulates multiple steps

including ribosomal RNAs transcription, the synthesis of ribosomal proteins and other components in ribosome biogenesis (Iadevaia et al., 2014; Kos-Braun and Kos, 2017). We found that 38 DMGs associated with ribosome genes in RAP vs. DMSO group (**Table 3**). Besides, a large number of DMGs associated with ribosome were also found in AZD and AZD + RAP treated samples (**Supplementary Tables S4, S5**). Interestingly, “Ribosome biogenesis in eukaryotes” was the most enriched pathway in AZD + RAP vs. DMSO group, of which 31 DMGs were found in this pathway (**Supplementary Figure S3B and Table S5**). Additionally, we found that the methylation level of *TOR* was reduced whereas the transcription level of

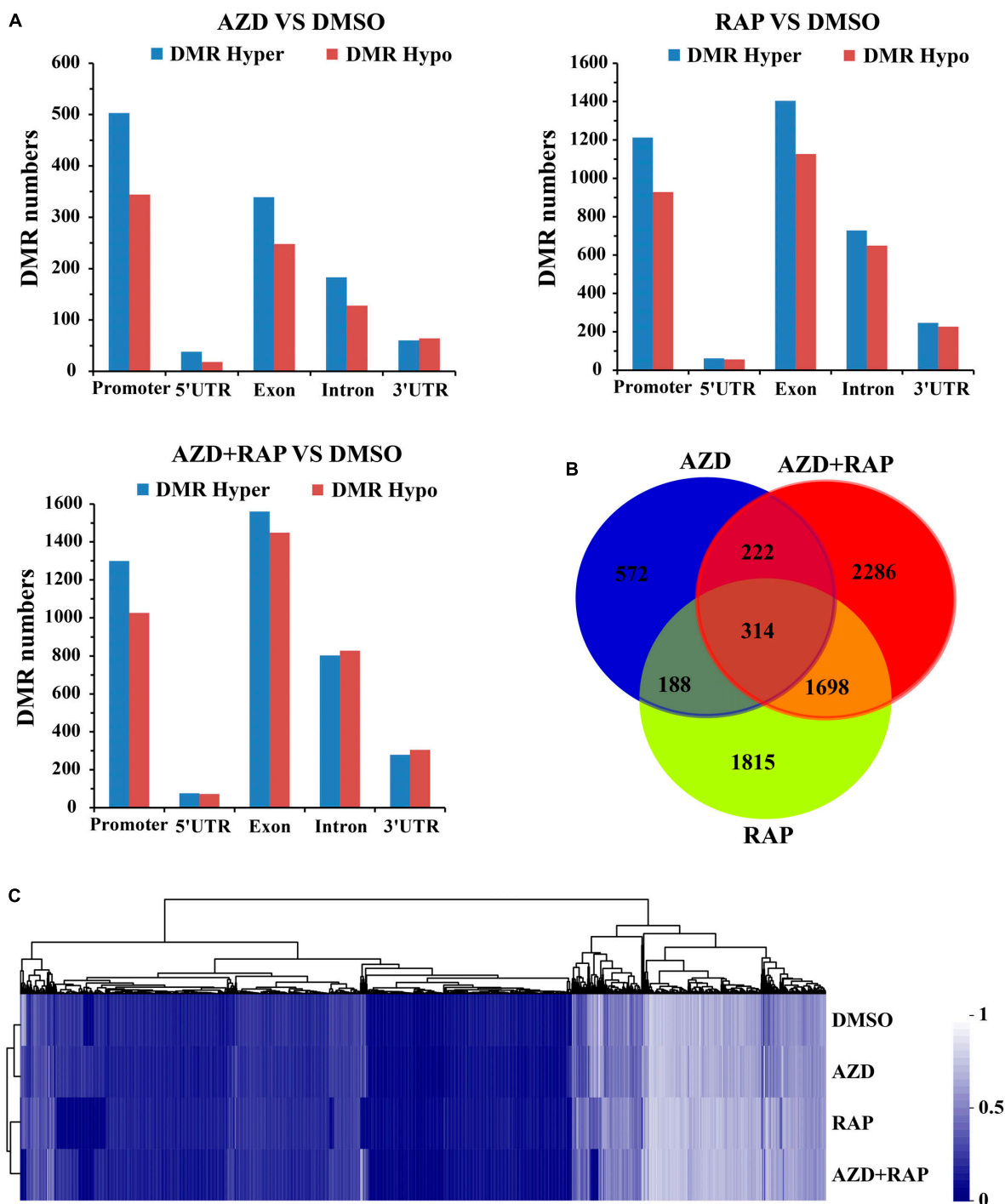
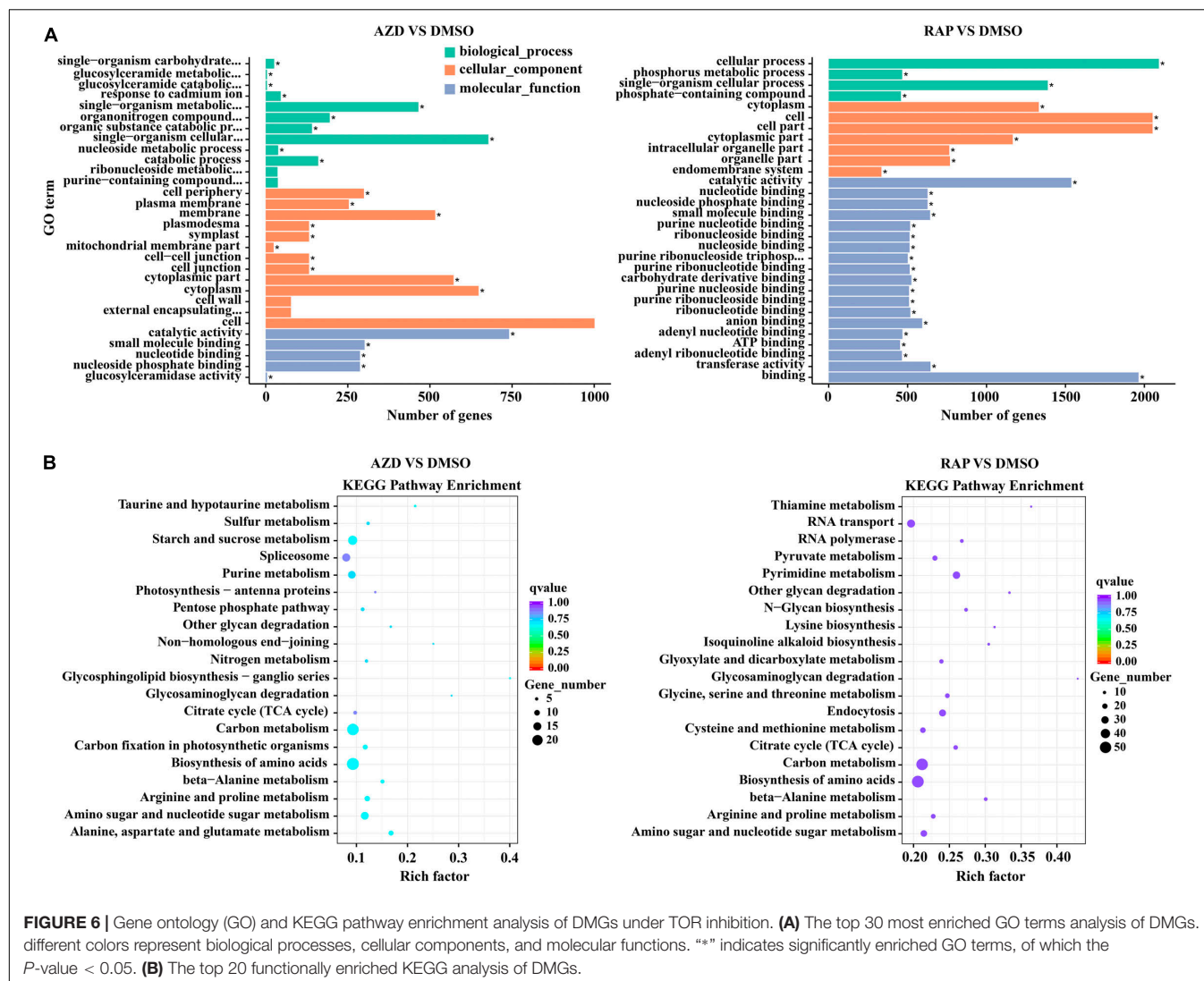


FIGURE 5 | Differentially methylated regions (DMRs) analysis of DMSO, AZD, RAP, and AZD + RAP samples. **(A)** The numbers of DMRs in genome elements. Histograms showing the overall DMRs numbers of genome elements: promoter, 5'UTR, exon, intron, and 3'UTR regions. Hyper: high methylation level, hypo: low methylation level. **(B)** The Venn diagram of differentially methylated genes (DMGs) among different combinations of AZD vs. DMSO, RAP vs. DMSO, and AZD + RAP vs. DMSO groups. **(C)** Cluster analysis of DMGs for DMSO, AZD, RAP, and AZD + RAP treated samples. The blue color represented lower methylation level and the white color represented higher methylation level. Each row represented a sample, each column represented a gene.

TOR was up-regulated under TOR inhibition (**Supplementary Figure S1B**), suggesting a feedback regulation of TOR inhibition in *Arabidopsis*. Collectively, these results and observations

suggested that TOR plays a crucial role in plant growth and development through regulating multiple metabolic processes and protein synthesis.



DMGs Involved in the Regulation of Plant Hormone Signal Transduction

Plant hormones play indispensable roles in mediating cellular metabolism, regulating plant growth and development, and resisting biotic and abiotic stresses (Rubio et al., 2009). Based on the WGBS data, DMGs associated with auxin, cytokinin (CK), brassinosteroid (BR), abscisic acid (ABA), ethylene (ET), and jasmonic acid (JA) were detected under TOR inhibition (Supplementary Table S6). Among these phytohormone signaling pathways, the top three largest number of DMGs were CK, BR, and ABA signaling pathways. Recent studies showed that TOR interacted with ABA signaling to balance plant growth and stress responses in plants (Wang et al., 2018). Based on our data, several ABA signaling pathway-related genes were significantly differentially methylated. In detail, the protein kinase *SnRK2* of the ABA signaling pathway was hypermethylated, whereas protein phosphatase *PP2CA* was hypomethylated. Besides, some important plant hormone-related genes were differentially methylated. For example, auxin

responsive SAUR proteins were hypermethylated in the promoter region, and BR signaling protein kinases *BSK1* and *BSK2* were hypomethylated under TOR inhibition (Supplementary Table S6). The transcription levels of *ABI5*, *BSK2*, and *PP2CA* genes were up-regulated whereas methylation levels of these genes were decreased in the promoter regions under TOR inhibition (Supplementary Figure S2C and Supplementary Table S6). These results showed that TOR may act as a regulator to mediate plant hormone signals transduction in *Arabidopsis*.

Association of DMGs With Gene mRNA Expression Level

To dissect the relationship between DMGs and gene mRNA expression level, we examined the expression levels of related genes using qRT-PCR. Eight DMGs were randomly selected for the real-time PCR, of which three DMGs involved in stresses response and five DMGs involved in metabolism and cell growth. Consistent with the previous study (Zhang et al., 2006), gene mRNA expression level was decreased in the

TABLE 3 | Differentially methylated genes (DMGs) of carbon metabolism, biosynthesis of amino acids and ribosome in RAP vs. DMSO group.

Gene id	Methylation ratio	Status	Regions	Annotation
Carbon metabolism				
AT1G17745	0.0065	Hypo	Promoter	PGDH2 Allosteric substrate binding domain
AT3G52200	0.3913	Hypo	Exon/intron	LTA3 2-oxoacid dehydrogenase acyltransferase
AT5G08300	0.5078	Hypo	Promoter	ATP-citrate lyase/succinyl-CoA ligase
AT1G04410	0.5323	Hypo	Promoter	MDH1 Lactate dehydrogenase/glycoside hydrolase
AT4G13890	0.5464	Hypo	Exon	SHM5 Pyridoxal phosphate-dependent transferase
AT5G23250	0.6175	Hypo	Exon/intron/utr3	ATP-citrate lyase/succinyl-CoA ligase
AT4G26970	0.6402	Hypo	Exon/intron	ACO3 Aconitase/3-isopropylmalate dehydratase
AT1G22020	0.6478	Hypo	Exon/intron	SHM6 Pyridoxal phosphate-dependent transferase
AT5G11670	0.6696	Hypo	Promoter	NADP-ME2 Malic enzyme, NAD-binding
AT1G79530	0.6699	Hypo	Promoter	GAPCP1 Glyceraldehyde 3-phosphate dehydrogenase
AT2G07732	1.5040	Hyper	Promoter	Ribulose biphosphate carboxylase, large subunit
AT4G32840	1.5343	Hyper	Promoter	PFK6 Phosphofructokinase
AT2G36460	1.5464	Hyper	Exon	Fructose-bisphosphate aldolase
AT1G54220	1.5971	Hyper	Promoter	2-oxoacid dehydrogenase acyltransferase
AT1G36370	1.6290	Hyper	Exon	SHM7 Pyridoxal phosphate-dependent transferase
AT1G74030	1.6688	Hyper	Exon/intron/utr3	ENO1 Enolase
AT3G49360	1.9074	Hyper	Promoter	PGL2 6-phosphogluconolactonase, DevB-type
AT5G03290	1.9497	Hyper	Exon	IDH5 Isocitrate dehydrogenase NAD-dependent
AT3G12780	1.9568	Hyper	Exon/intron	PGK1 Phosphoglycerate kinase
AT1G01090	2.0177	Hyper	Exon/intron	PDH-E1 Pyruvate dehydrogenase E1 component
AT1G17650	2.6505	Hyper	Exon/intron	GLYR2 6-phosphogluconate dehydrogenase
Biosynthesis of amino acids				
AT5G11880	0.1681	Hypo	Exon/intron	LYSA2 Diaminopimelate decarboxylase, LysA
AT1G58080	0.2884	Hypo	Exon/intron	HISN1A ATP phosphoribosyltransferase
AT3G22425	0.4460	Hypo	Promoter	HISN5A Imidazoleglycerol-phosphate dehydratase
AT4G13890	0.5464	Hypo	Exon	SHM5 Pyridoxal phosphate-dependent transferase
AT4G37670	0.5988	Hypo	Exon/intron	NAGS2 Acyl-CoA N-acyltransferase
AT4G26970	0.6402	Hypo	Exon/intron	ACO3 Aconitase dehydratase large subunit
AT1G22020	0.6478	Hypo	Exon/intron	SHM6 Pyridoxal phosphate-dependent transferase
AT1G79530	0.6699	Hypo	Promoter	GAPCP1 Glyceraldehyde 3-phosphate dehydrogenase
AT4G32840	1.5343	Hyper	Promoter	PFK6 Phosphofructokinase
AT2G36460	1.5464	Hyper	Exon	Fructose-bisphosphate aldolase, class-I
AT1G36370	1.6290	Hyper	Exon	SHM7 Pyridoxal phosphate-dependent transferase
AT1G74030	1.6688	Hyper	Exon/intron/utr3	ENO1 Enolase
AT2G45440	1.6816	Hyper	Intron	DHDPS2 Dihydrodipicolinate synthase, DapA
AT4G01850	1.7869	Hyper	Exon	SAM2 S-adenosylmethionine synthetase
AT4G23590	1.9377	Hyper	Exon	Pyridoxal phosphate-dependent transferase
AT5G03290	1.9497	Hyper	Exon	IDH5 Isocitrate dehydrogenase NAD-dependent
AT3G12780	1.9568	Hyper	Exon/intron	PGK1 Phosphoglycerate kinase
Ribosome				
AT4G27490	0.2287	Hypo	Promoter	Ribosomal protein S5 domain 2-type fold
AT1G23280	0.2364	Hypo	Promoter	Mak16 Ribosomal L28e
AT1G52930	0.2828	Hypo	Exon/intron	BRX1 Ribosome biogenesis protein
AT5G59180	0.3100	Hypo	Exon/utr3	NRPB7 Ribosomal protein S1, RNA-binding domain
AT1G04170	0.3194	Hypo	Promoter	EIF2γ Translation elongation factor EF1A gamma
AT1G32990	0.4472	Hypo	Promoter	RPL11 Ribosomal protein L11
AT1G07210	0.4729	Hypo	Exon/intron	Ribosomal protein S18
AT5G05470	0.4853	Hypo	Exon/intron	EIF2α Translation initiation factor 2, alpha subunit
AT4G10450	0.5106	Hypo	Promoter	RPL9D Ribosomal protein L6
AT1G07770	0.5567	Hypo	Exon/intron	RPS15AA Ribosomal protein S8
AT3G06580	0.5818	Hypo	Exon/intron	GAL1 Ribosomal protein S5 domain 2-type

(Continued)

TABLE 3 | Continued

Gene id	Methylation ratio	Status	Regions	Annotation
AT1G02830	0.6042	Hypo	Promoter	RPL22A Ribosomal protein L22e
AT3G63490	0.6304	Hypo	Exon/intron/utr3	RPL1 Ribosomal protein L1
AT2G44860	0.6369	Hypo	Exon/utr3	Ribosomal protein L24e, conserved site
AT2G25210	0.6443	Hypo	Exon/intron/utr5/promoter	Ribosomal protein L39e
AT5G64650	0.6492	Hypo	Exon/intron	Ribosomal protein L17
AT1G41880	1.5163	Hyper	Exon/utr3	RPL35AB Ribosomal protein L35Ae
AT1G24240	1.5289	Hyper	Promoter	Ribosomal protein L19
AT3G10950	1.5472	Hyper	Promoter	RPL37AB Ribosomal protein L37ae
AT1G31355	1.5676	Hyper	Promoter	Translation protein SH3-like family protein
AT4G16030	1.5756	Hyper	Promoter	Ribosomal protein L19/L19e
AT5G16130	1.5889	Hyper	Promoter	RPS7C Ribosomal protein S7e
AT3G49010	1.6060	Hyper	Promoter	RPL13B Ribosomal protein L13e
AT1G13950	1.6211	Hyper	Promoter	ELF5A-1 Ribosomal protein L2 domain 2
AT5G02870	1.7028	Hyper	Promoter	RPL4D 60S ribosomal protein L4, C-terminal domain
AT1G26630	1.7231	Hyper	Exon/intron	ELF5A-2 Ribosomal protein L2 domain 2
AT5G53920	1.8060	Hyper	Promoter	Ribosomal protein L11 methyltransferase
AT2G45030	1.9131	Hyper	Exon/utr3	MEFG2 Ribosomal protein S5 domain 2-type fold
AT3G20260	1.9516	Hyper	Promoter	Ribosomal protein L34Ae
AT2G40205	1.9979	Hyper	Promoter	RPL41E Ribosomal protein L41
AT4G34730	2.1114	Hyper	Intron	Ribosome-binding factor A
AT1G31355	2.1706	Hyper	Promoter	Translation protein SH3-like family protein
AT5G19720	2.2472	Hyper	Promoter	Ribosomal protein L25, beta-barrel domain
AT1G01220	2.4560	Hyper	Promoter	FKGP Ribosomal protein S5 domain 2-type fold
AT4G29060	2.9800	Hyper	Exon/utr3	emb2726 Ribosomal protein S1
AT2G20060	2.9911	Hyper	Promoter	Ribosomal protein L4
AT3G53890	3.4514	Hyper	Exon/utr3	RPS21B Ribosomal protein S21e
AT5G39785	6.5648	Hyper	Exon/intron	Ribosomal protein L34Ae

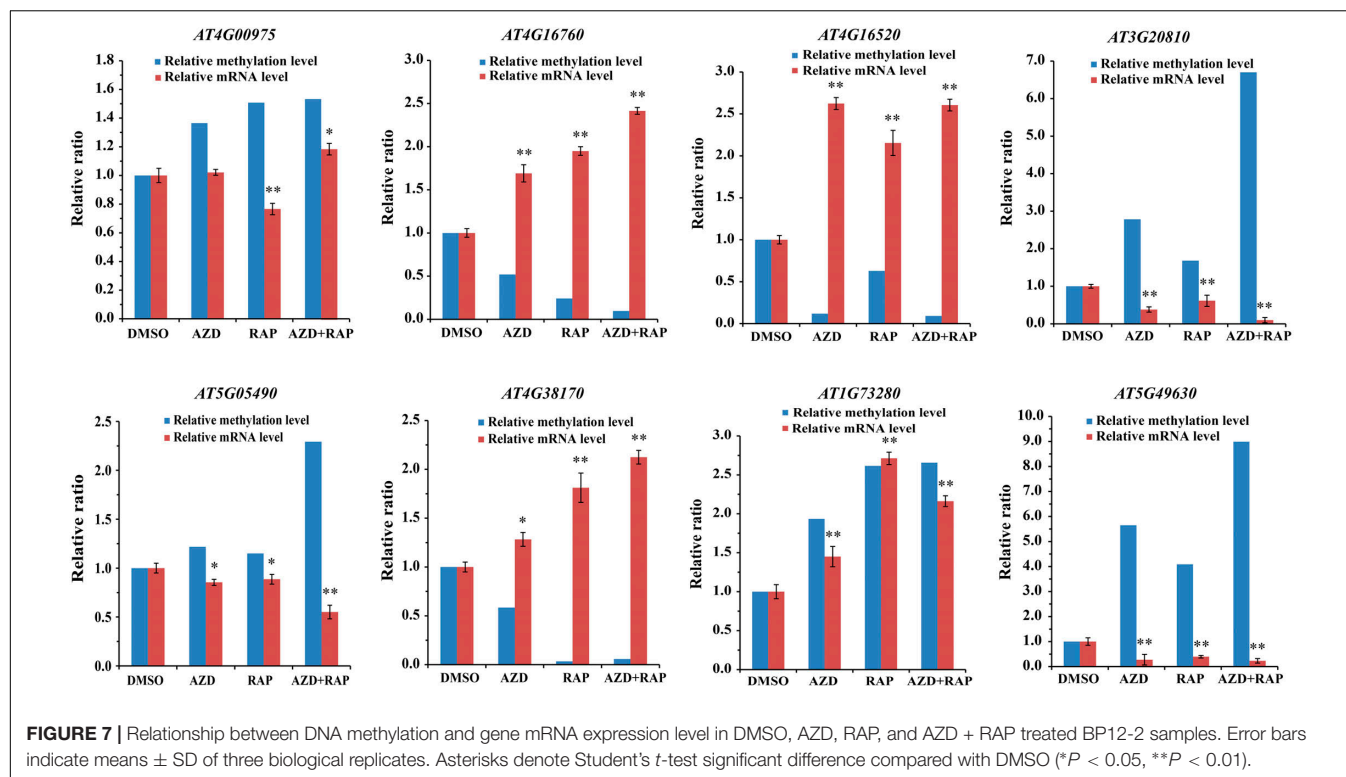
hypermethylated promoter region in this study (**Figure 7**). For example, *AT4G16520* (*ATG8F*) and *AT4G16760* (*ACX1*) induced by stresses were hypomethylated in the promoter region, while mRNA expression level was upregulated under TOR inhibition. *AT5G05490* (*SYN1*) and *AT5G49630* (*AAP6*) that involved in cell growth were hypermethylated whereas mRNA expression level was downregulated. Besides, some genes hypermethylated in transcribed regions were highly expressed whereas other genes were low expressed (**Figure 7** and **Supplementary Table S7**), demonstrating methylation in transcribed regions both positive and negative relationships to gene expression (Zhang et al., 2006; Lou et al., 2014).

DISCUSSION

In this study, we analyzed the functions of TOR in the regulation of DNA methylation using WGBS. We found that inhibition of TOR reduced whole-genome methylation levels whereas the methylation level of CHH site in the promoter region was increased. CHH methylation is maintained by DRM1 or DRM2 in plants. Through RNA-directed DNA methylation (RdDM) pathway, DRM2 maintains CHH methylation at RdDM target regions (Zhang et al., 2018). The transcription level of *MET1* gene was down-regulated whereas *DRM1* and *DRM2*

genes were up-regulated under TOR inhibition. Furthermore, the transcription level of DNA demethylation genes were significantly up-regulated in TOR-inhibited seedlings. These results explained that inhibition of TOR results in lower genome-wide methylation levels but increases methylation level of CHH site in the promoter region. Besides, CHROMOMETHYLASE 2 (*CMT2*) is also involved in maintaining CHH methylation in plants (Zemach et al., 2013; Stroud et al., 2014). Methylation level of *CMT2* was decreased in AZD + RAP treated sample, implying that TOR inhibition may activate DRM2 or *CMT2* to maintain CHH methylation level. Interestingly, our study showed that TOR regulated genome DNA methylation to control plant growth in *Arabidopsis*, while curcumin induced the promoter hypermethylation of *mTOR* gene in myeloma cells (Chen et al., 2019), suggesting that TOR had a feedback regulation mechanism in the process of regulating DNA methylation. The detailed regulatory mechanisms of TOR and DNA methyltransferases still need further study in the future.

In addition to reduced genome-wide methylation, we also identified 1296, 4015, and 4520 DMGs in AZD vs. DMSO, RAP vs. DMSO, and AZD + RAP vs. DMSO groups, respectively. The difference of DMGs between AZD and RAP may be caused by off-target effects in *ScFKBP12*-overexpressed *Arabidopsis*. Previous studies suggested that the expression of *FKBP12* in *Arabidopsis* might have unexpected molecular phenotypes unrelated to



TOR signaling pathway due to its peptidyl-prolyl isomerase activity (Gerard et al., 2011; Alavilli et al., 2018). Changes of non-TOR-kinase specific in intracellular metabolism caused by RAP off-targets in *ScFKBP12*-overexpressed *Arabidopsis* still need further study.

TOR signaling is indispensable for growth and development from embryogenesis to senescence by modulating translation, autophagy, metabolism, and cell cycle in plants (Ren et al., 2012; Xiong and Sheen, 2014; Shi et al., 2018). In our study, many genes of cellular metabolic processes and signal pathways were differentially methylated under TOR inhibition, especially carbon metabolism and biosynthesis of amino acids. Furthermore, DMGs associated with ribosome and ribosome biogenesis were detected. It is well known that TOR controls protein synthesis at multiple levels from transcription, ribosome biogenesis to protein translation in various eukaryotes (De Virgilio and Loewith, 2006; Xiong et al., 2013; Yang et al., 2013; Xiong and Sheen, 2014; Dong et al., 2015; Li et al., 2019). Our results indicated that TOR involved in the regulation of ribosome and ribosome biogenesis by changing the methylation levels of related genes, which is responsible for protein synthesis and plant growth.

Plant hormones play essential roles in plant growth, development and reproduction (Durbak et al., 2012). Previous studies demonstrate that TOR is indispensable for auxin signaling transduction, and auxin activates TOR to promote translation reinitiation in *Arabidopsis* (Deng et al., 2016; Schepetilnikov et al., 2017). Moreover, TOR signaling also promotes accumulation of BZR1 protein to promote plant growth in *Arabidopsis* (Zhang et al., 2016). Nevertheless, TOR signal and ABA or JA signal are antagonism to balance plant growth and stress

response (Song et al., 2017; Wang et al., 2018). Based on the WGBS data, we found some DMGs in plant hormone signal transduction including auxin, BR and ABA signals. The differential methylation of these genes may result in changes in gene expression level, providing a new insight of the involvement of TOR in phytohormone signaling.

In summary, DNA methylation inhibitor azacitidine and TOR inhibitors synergistically inhibited the growth of *Arabidopsis* seedlings, implying that TOR played a role in DNA methylation. We therefore further systematically investigated changes in genome DNA methylation levels under TOR inhibition by high-throughput bisulfite sequencing, and we obtained a large number of differentially methylated regions and genes. Based on the whole-genome DNA methylation data, hypomethylation level of whole-genome DNA was observed in AZD, RAP, and AZD + RAP treated *Arabidopsis*. KEGG pathway enrichment showed that DMGs were involved in many metabolic pathways, such as carbon metabolism and biosynthesis of amino acids. Additionally, we also found that some plant hormone signal transduction-related genes displayed significant differences in methylation level under TOR inhibition. In conclusion, the above studies revealed the genome methylation pattern under TOR inhibition, providing important clues for further analysis of the functions of TOR in DNA methylation.

DATA AVAILABILITY STATEMENT

The datasets generated for this study can be found in the NCBI Sequence Read Archive (SRA) accession: PRJNA606264.

AUTHOR CONTRIBUTIONS

MR, TZ, and LL designed the experiments. TZ and LL performed the experiments. LL, LF, and HM analyzed the data. MR, TZ, and LL wrote the manuscript.

FUNDING

This work was supported by grants from the National Natural Science Foundation of China (Nos. U1804231 and 31972469), the Genetically Modified Organisms

Breeding Major Project of China (No. 2019ZX08010004-004), Central Public-interest Scientific Institution Basal Research Fund (No. Y2020XK04), and Chengdu Agricultural Science and Technology Center local financial special fund project (NASC2019T113).

SUPPLEMENTARY MATERIAL

The Supplementary Material for this article can be found online at: <https://www.frontiersin.org/articles/10.3389/fgene.2020.00186/full#supplementary-material>

REFERENCES

- Adam, B. S., Nicolas, G. D. L., Sergey, M., Lasse, J., Gulnara, Y., and Marat, Y. (2011). The structure of the eukaryotic ribosome at 3.0 Å resolution. *Science* 334, 1524–1529. doi: 10.1126/science.1212642
- Ahmad, Z., Magyar, Z., Bogre, L., and Papdi, C. (2019). Cell cycle control by the target of rapamycin signalling pathway in plants. *J. Exp. Bot.* 70, 2275–2284. doi: 10.1093/jxb/erz140
- Alavilli, H., Lee, H., Park, M., Yun, D. J., and Lee, B. H. (2018). Enhanced multiple stress tolerance in *Arabidopsis* by overexpression of the polar moss peptidyl prolyl isomerase FKBP12 gene. *Plant Cell Rep.* 37, 453–465. doi: 10.1007/s00299-017-2242-9
- Benjamin, D., Colombi, M., Moroni, C., and Hall, M. N. (2011). Rapamycin passes the torch: a new generation of mTOR inhibitors. *Nat. Rev. Drug Discov.* 10, 868–880. doi: 10.1038/nrd3531
- Bouyer, D., Kramdi, A., Kassam, M., Heese, M., Schnittger, A., Roudier, F., et al. (2017). DNA methylation dynamics during early plant life. *Genome Biol.* 18:179. doi: 10.1186/s13059-017-1313-0
- Chan, S. W., Henderson, I. R., and Jacobsen, S. E. (2005). Gardening the genome: DNA methylation in *Arabidopsis thaliana*. *Nat. Rev. Genet.* 6, 351–360.
- Chan, S. W., Henderson, I. R., Zhang, X., Shah, G., Chien, J. S., and Jacobsen, S. E. (2006). RNAi, DRD1, and histone methylation actively target developmentally important non-CG DNA methylation in *Arabidopsis*. *PLoS Genet.* 2:e83. doi: 10.1371/journal.pgen.0020083
- Chen, J., Ying, Y., Zhu, H., Zhu, T., Qu, C., Jiang, J., et al. (2019). Curcumin-induced promoter hypermethylation of the mammalian target of rapamycin gene in multiple myeloma cells. *Oncol. Lett.* 17, 1108–1114. doi: 10.3892/ol.2018.9662
- Chou, T. C. (2006). Theoretical basis, experimental design, and computerized simulation of synergism and antagonism in drug combination studies. *Pharmacol. Rev.* 58, 621–681.
- Chou, T. C., and Talalay, P. (1984). Quantitative analysis of dose-effect relationships: the combined effects of multiple drugs or enzyme inhibitors. *Adv. Enzyme Regul.* 22, 27–55.
- Christman, J. K. (2002). 5-Azacytidine and 5-aza-2'-deoxycytidine as inhibitors of DNA methylation: mechanistic studies and their implications for cancer therapy. *Oncogene* 21, 5483–5495.
- De Virgilio, C., and Loewith, R. (2006). Cell growth control: little eukaryotes make big contributions. *Oncogene* 25, 6392–6415.
- Deng, K., Dong, P., Wang, W., Feng, L., Xiong, F., Wang, K., et al. (2017). The TOR pathway is involved in adventitious root formation in *Arabidopsis* and potato. *Front. Plant Sci.* 8:784. doi: 10.3389/fpls.2017.00784
- Deng, K., Yu, L., Zheng, X., Zhang, K., Wang, W., Dong, P., et al. (2016). Target of rapamycin is a key player for auxin signaling transduction in *Arabidopsis*. *Front. Plant Sci.* 7:291. doi: 10.3389/fpls.2016.00291
- Dobrenel, T., Caldana, C., Hanson, J., Robaglia, C., Vincentz, M., Veit, B., et al. (2016). TOR signaling and nutrient sensing. *Plant Biol.* 67, 261–285.
- Dong, P., Xiong, F., Que, Y., Wang, K., Yu, L., Li, Z., et al. (2015). Expression profiling and functional analysis reveals that TOR is a key player in regulating photosynthesis and phytohormone signaling pathways in *Arabidopsis*. *Front. Plant Sci.* 6:677. doi: 10.3389/fpls.2015.00677
- Durbak, A., Yao, H., and Mcsteen, P. (2012). Hormone signaling in plant development. *Curr. Opin. Plant Biol.* 15, 92–96. doi: 10.1016/j.pbi.2011.12.004
- Fieldes, M. A., Schaeffer, S. M., Krech, M. J., and Brown, J. C. (2005). DNA hypomethylation in 5-azacytidine-induced early-flowering lines of flax. *Theor. Appl. Genet.* 111, 136–149.
- Gerard, M., Deleersnijder, A., Demeulemeester, J., Debyser, Z., and Baekelandt, V. (2011). Unraveling the role of peptidyl-prolyl isomerases in neurodegeneration. *Mol. Neurobiol.* 44, 13–27. doi: 10.1007/s12035-011-8184-2
- Grace, G. M., and Bestor, T. H. (2005). Eukaryotic cytosine methyltransferases. *Annu. Rev. Biochem.* 74, 481–514.
- Heitman, J., Movva, N. R., and Hall, M. N. (1991). Targets for cell cycle arrest by the immunosuppressant rapamycin in yeast. *Science* 253, 905–909.
- Iadevaia, V., Liu, R., and Proud, C. G. (2014). mTORC1 signaling controls multiple steps in ribosome biogenesis. *Semin. Cell Dev. Biol.* 36, 113–120. doi: 10.1016/j.semcdb.2014.08.004
- Juppner, J., Mubeen, U., Lisse, A., Caldana, C., Wiszniewski, A., Steinhäuser, D., et al. (2018). The target of rapamycin kinase affects biomass accumulation and cell cycle progression by altering carbon/nitrogen balance in synchronized *Chlamydomonas reinhardtii* cells. *Plant J.* 93, 355–376. doi: 10.1111/tpj.13787
- Kos-Braun, I. C., and Kos, M. (2017). Post-transcriptional regulation of ribosome biogenesis in yeast. *Microb. Cell* 4, 179–181.
- Li, L., Song, Y., Wang, K., Dong, P., Zhang, X., Li, F., et al. (2015). TOR-inhibitor insensitive-1 (TRIN1) regulates cotyledons greening in *Arabidopsis*. *Front. Plant Sci.* 6:861. doi: 10.3389/fpls.2015.00861
- Li, L., Zhu, T., Song, Y., Luo, X., Feng, L., Zhuo, F., et al. (2019). Functional characterization of target of rapamycin signaling in *Verticillium dahliae*. *Front. Microbiol.* 10:501. doi: 10.3389/fmicb.2019.00501
- Lister, R., Mukamel, E. A., Nery, J. R., Urich, M., Puddifoot, C. A., Johnson, N. D., et al. (2013). Global epigenomic reconfiguration during mammalian brain development. *Science* 341:1237905. doi: 10.1126/science.1237905
- Lister, R., O'malley, R. C., Tonti-Filippini, J., Gregory, B. D., Berry, C. C., Millar, A. H., et al. (2008). Highly integrated single-base resolution maps of the epigenome in *Arabidopsis*. *Cell* 133, 523–536. doi: 10.1016/j.cell.2008.03.029
- Long, J., Zhi, J., Xia, Y., Lou, P. E., Lei, C., Wang, H., et al. (2014). Genome-wide DNA methylation changes in skeletal muscle between young and middle-aged pigs. *BMC Genomics* 15:653. doi: 10.1186/1471-2164-15-653
- Lou, S., Lee, H. M., Qin, H., Li, J. W., Gao, Z., Liu, X., et al. (2014). Whole-genome bisulfite sequencing of multiple individuals reveals complementary roles of promoter and gene body methylation in transcriptional regulation. *Genome Biol.* 15:408. doi: 10.1186/s13059-014-0408-0
- Mao, X., Tao, C. J. G. O., and Wei, L. (2005). Automated genome annotation and pathway identification using the KEGG orthology (KO) as a controlled vocabulary. *Bioinformatics* 21, 3787–3793.
- Marfil, C. F., Asurmendi, S., and Masuelli, R. W. (2012). Changes in micro RNA expression in a wild tuber-bearing *Solanum* species induced by 5-azacytidine treatment. *Plant Cell Rep.* 31, 1449–1461. doi: 10.1007/s00299-012-1260-x
- Minoru, K., Michihiro, A., Susumu, G., Masahiro, H., Mika, H., Masumi, I., et al. (2008). KEGG for linking genomes to life and the environment. *Nucleic Acids Res.* 36, 480–484.
- Montane, M. H., and Menand, B. (2013). ATP-competitive mTOR kinase inhibitors delay plant growth by triggering early differentiation of meristematic cells but

- no developmental patterning change. *J. Exp. Bot.* 64, 4361–4374. doi: 10.1093/jxb/ert242
- Moore, L. D., Le, T., and Fan, G. (2013). DNA methylation and its basic function. *Neuropsychopharmacology* 38, 23–38. doi: 10.1038/npp.2012.112
- Opron, K., and Burton, Z. F. (2018). Ribosome structure, function, and early evolution. *Int. J. Mol. Sci.* 20:E40.
- Osorio-Montalvo, P., Sáenz-Carbonell, L., and De-La-Peña, C. (2018). 5-azacytidine: a promoter of epigenetic changes in the quest to improve plant somatic embryogenesis. *Int. J. Mol. Sci.* 19:3182. doi: 10.3390/ijms19103182
- Razin, A., and Riggs, A. D. (1980). DNA methylation and gene function. *Science* 210, 604–610.
- Ren, M., Qiu, S., Venglat, P., Xiang, D., Feng, L., Selvaraj, G., et al. (2011). Target of rapamycin regulates development and ribosomal RNA expression through kinase domain in *Arabidopsis*. *Plant Physiol.* 155, 1367–1382. doi: 10.1104/pp.110.169045
- Ren, M., Venglat, P., Qiu, S., Feng, L., Cao, Y., Wang, E., et al. (2012). Target of rapamycin signaling regulates metabolism, growth, and life span in *Arabidopsis*. *Plant Cell* 24, 4850–4874. doi: 10.1105/tpc.112.107144
- Rubio, V., Bustos, R., Irigoyen, M. L., Cardona-López, X., Rojas-Triana, M., and Paz-Ares, J. (2009). Plant hormones and nutrient signaling. *Plant Mol. Biol.* 69, 361–373. doi: 10.1007/s11103-008-9380-y
- Saxton, R. A., and Sabatini, D. M. (2017). mTOR signaling in growth, metabolism, and disease. *Cell* 168, 960–976. doi: 10.1016/j.cell.2017.02.004
- Schepetilnikov, M., Makarian, J., Srouf, O., Geldreich, A., Yang, Z., Chicher, J., et al. (2017). GTPase ROP2 binds and promotes activation of target of rapamycin, TOR, in response to auxin. *EMBO J.* 36, 886–903. doi: 10.15252/emboj.201694816
- Shi, L., Wu, Y., and Sheen, J. (2018). TOR signaling in plants: conservation and innovation. *Development* 145:dev160887. doi: 10.1242/dev.160887
- Smallwood, S. A., Lee, H. J., Angermueller, C., Krueger, F., Saadeh, H., Peat, J., et al. (2014). Single-cell genome-wide bisulfite sequencing for assessing epigenetic heterogeneity. *Nat. Methods* 11, 817–820. doi: 10.1038/nmeth.3035
- Song, Y., Li, L., Yang, Z., Zhao, G., Zhang, X., Wang, L., et al. (2018). Target of rapamycin (TOR) regulates the expression of lncRNAs in response to abiotic stresses in cotton. *Front. Genet.* 9:690. doi: 10.3389/fgene.2018.00690
- Song, Y., Zhao, G., Zhang, X., Li, L., Xiong, F., Zhuo, F., et al. (2017). The crosstalk between target of rapamycin (TOR) and jasmonic acid (JA) signaling existing in *Arabidopsis* and cotton. *Sci. Rep.* 7:45830. doi: 10.1038/srep45830
- Stroud, H., Do, T., Du, J., Zhong, X., Feng, S., Johnson, L., et al. (2014). Non-CG methylation patterns shape the epigenetic landscape in *Arabidopsis*. *Nat. Struct. Mol. Biol.* 21, 64–72. doi: 10.1038/nsmb.2735
- Wang, P., Zhao, Y., Li, Z., Hsu, C. C., Liu, X., Fu, L., et al. (2018). Reciprocal regulation of the TOR kinase and ABA receptor balances plant growth and stress response. *Mol. Cell* 69, 100–112.e6. doi: 10.1016/j.molcel.2017.12.002
- Webb, A. A., and Satake, A. (2015). Understanding circadian regulation of carbohydrate metabolism in *Arabidopsis* using mathematical models. *Plant Cell Physiol.* 56, 586–593. doi: 10.1093/pcp/pcv033
- Xiong, Y., McCormack, M., Li, L., Hall, Q., Xiang, C., and Sheen, J. (2013). Glucose-TOR signalling reprograms the transcriptome and activates meristems. *Nature* 496, 181–186. doi: 10.1038/nature12030
- Xiong, Y., and Sheen, J. (2014). The role of target of rapamycin signaling networks in plant growth and metabolism. *Plant Physiol.* 164, 499–512. doi: 10.1104/pp.113.229948
- Xu, Q., Liang, S., Kudla, J., and Luan, S. (1998). Molecular characterization of a plant FKBP12 that does not mediate action of FK506 and rapamycin. *Plant J.* 15, 511–519.
- Yang, H., Rudge, D. G., Koos, J. D., Vaidialingam, B., Yang, H. J., and Pavletich, N. P. (2013). mTOR kinase structure, mechanism and regulation. *Nature* 497, 217–223.
- Young, M. D., Wakefield, M. J., Smyth, G. K., and Oshlack, A. (2010). Gene ontology analysis for RNA-seq: accounting for selection bias. *Genome Biol.* 11:R14. doi: 10.1186/gb-2010-11-2-r14
- Yuan, H. X., Xiong, Y., and Guan, K. L. (2013). Nutrient sensing, metabolism, and cell growth control. *Mol. Cell* 49, 379–387. doi: 10.1016/j.molcel.2013.01.019
- Zemach, A., Kim, M. Y., Hsieh, P. H., Coleman-Derr, D., Eshed-Williams, L., Thao, K., et al. (2013). The *Arabidopsis* nucleosome remodeler DDM1 allows DNA methyltransferases to access H1-containing heterochromatin. *Cell* 153, 193–205. doi: 10.1016/j.cell.2013.02.033
- Zhang, H., Lang, Z., and Zhu, J. K. (2018). Dynamics and function of DNA methylation in plants. *Nat. Rev. Mol. Cell Biol.* 19, 489–506. doi: 10.1038/s41580-018-0016-z
- Zhang, X., Yazaki, J., Sundaresan, A., Cokus, S., Chan, S. W., Chen, H., et al. (2006). Genome-wide high-resolution mapping and functional analysis of DNA methylation in *Arabidopsis*. *Cell* 126, 1189–1201.
- Zhang, Z., Zhu, J. Y., Roh, J., Marchive, C., Kim, S. K., Meyer, C., et al. (2016). TOR signaling promotes accumulation of BZR1 to balance growth with carbon availability in *Arabidopsis*. *Curr. Biol.* 26, 1854–1860. doi: 10.1016/j.cub.2016.05.005

Conflict of Interest: The authors declare that the research was conducted in the absence of any commercial or financial relationships that could be construed as a potential conflict of interest.

Copyright © 2020 Zhu, Li, Feng, Mo and Ren. This is an open-access article distributed under the terms of the Creative Commons Attribution License (CC BY). The use, distribution or reproduction in other forums is permitted, provided the original author(s) and the copyright owner(s) are credited and that the original publication in this journal is cited, in accordance with accepted academic practice. No use, distribution or reproduction is permitted which does not comply with these terms.



The Landscape of DNA Methylation Associated With the Transcriptomic Network of Intramuscular Adipocytes Generates Insight Into Intramuscular Fat Deposition in Chicken

Meng Zhang¹, Donghua Li¹, Yanhui Zhai², Zhengzhu Wang², Xiangfei Ma¹, Daoyu Zhang², Guoxi Li¹, Ruili Han¹, Ruirui Jiang¹, Zhuangjian Li¹, Xiangtao Kang¹ and Guirong Sun^{1*}

¹ College of Animal Science and Veterinary Medicine, Henan Agricultural University, Zhengzhou, China, ² The First Clinical Hospital, Jilin University, Changchun, China

OPEN ACCESS

Edited by:

Kai Tang,
Purdue University, United States

Reviewed by:

Guiping Zhao,
Chinese Academy of Agricultural
Sciences, China

Hui Li,
Northeast Agricultural University,
China

*Correspondence:

Guirong Sun
grsun2000@126.com

Specialty section:

This article was submitted to
Epigenomics and Epigenetics,
a section of the journal
Frontiers in Cell and Developmental
Biology

Received: 12 November 2019

Accepted: 10 March 2020

Published: 02 April 2020

Citation:

Zhang M, Li D, Zhai Y, Wang Z,
Ma X, Zhang D, Li G, Han R, Jiang R,
Li Z, Kang X and Sun G (2020) The
Landscape of DNA Methylation
Associated With the Transcriptomic
Network of Intramuscular Adipocytes
Generates Insight Into Intramuscular
Fat Deposition in Chicken.
Front. Cell Dev. Biol. 8:206.
doi: 10.3389/fcell.2020.00206

Intramuscular fat (IMF), which regulated by genetics, nutrition and environment is an important factor that influencing meat quality. Up to now, the epigenetic regulation mechanism underlying poultry IMF deposition remains poorly understood. Here, we focused on the DNA methylation, which usually regulate genes in transcription level. To look into the essential role of DNA methylation on the IMF deposition, chicken intramuscular preadipocytes were isolated and cultured *in vitro*, and a model of intramuscular adipocyte differentiation was constructed. Combined the whole genome bisulfite sequencing (WGBS) and RNA-Seq technologies, we identified several methylated genes, which mainly affecting fatty acid metabolism and muscle development. Furthermore, we reported that DNA methylation regulate intramuscular adipogenesis by regulating the genes, such as collagen, type VI, alpha 1 (*COL6A1*) thus affecting IMF deposition. Overexpression of *COL6A1* increases the lipid droplet and inhibits cell proliferation by regulating *CHAD* and *CAMK2* in intramuscular adipocytes, while knockdown of *COL6A1* shows the opposite effect. Taken together, our results reveal that DNA methylation plays an important role in poultry IMF deposition.

Keywords: DNA methylation, transcriptome, intramuscular adipocytes differentiation, *COL6A1*, IMF deposition

INTRODUCTION

Intramuscular fat (IMF) is one of the most important factors that affect meat quality (Fanatico et al., 2007; Ros-Freixedes et al., 2014; Li et al., 2019). Previous researches have indicated that IMF improved the quality of meat by improving the flavor, juiciness and tenderness (Gao and Zhao, 2009). IMF deposition is primarily dependent on the differentiation, maturation and proliferation of intramuscular preadipocytes (Cristancho and Lazar, 2011; Zhang et al., 2019). Previous studies have identified about several genes related to chicken IMF, including *PPARG*, *GPAT1*, *ACC*, *CD36*, *AGPAT1*, and *DGAT2*, *FABP*, *LPL*, *DGAT1*, and *SCL27A1* (Ye et al., 2010; Serão et al., 2011; Jeong et al., 2012; Li et al., 2013; Qiu et al., 2017). The mechanism that underlies chicken IMF deposition is very complicated obviously, involving many metabolic pathways and genes.

As one of the earliest discovered epigenetic modification, DNA methylation plays an extremely significant role in sustaining cell's normal function in animals, gene expression regulation (Razin and Cedar, 1984), genetic imprinting (Jaenisch, 1997), embryonic development (Li et al., 2018), and tumor formation (Shivapurkar et al., 1986; Bender et al., 1998). Growing number of studies suggested that DNA methylation played significantly role in adipogenesis (Broholm et al., 2016; Chen et al., 2016; Lim et al., 2016). Previous studies recommended that *DNMT3A* inhibited porcine intramuscular preadipocytes differentiation by changing the methylation levels of *p21* and *PPAR γ* (Abdalla et al., 2018; Qimuge et al., 2019). Zhang et al. (2014) found that *MBD4* inhibited porcine preadipocytes differentiation by changing the DNA methylation levels of adipogenic genes. Li et al. suggested that DNA methylation regulated chicken *PPARG* and *CEBPA* during the development of chicken adipose tissue (Sun et al., 2014; Gao et al., 2015). Our previous study identified large amount of differentially expressed genes (DEGs) during intramuscular adipogenic differentiation (Zhang et al., 2019). The epigenetic molecular mechanism, especially DNA methylation that underlies IMF deposition remains, however, poorly investigated.

In order to investigate the potential functions of DNA methylation that affected the poultry intramuscular adipogenesis. Whole genome single-base DNA methylation profiles of intramuscular preadipocytes and differentiated adipocytes were generated by whole genome bisulfite sequencing (WGBS). The present study integrated the RNA-Seq and WGBS data, aimed to describe the DNA methylation patterns in chicken intramuscular

adipocytes and reveal the novel methylated candidate genes related to intramuscular adipogenesis. Our results offered basic research data about intramuscular adipogenesis and the IMF deposition in poultry.

RESULTS

The Identification of Chicken Intramuscular Adipocyte Differentiation Model

To investigate the IMF deposition of poultry, chicken intramuscular adipogenic differentiation model *in vitro* was constructed in the present study. After 80–90% confluence, cells were exposed to MDIO differentiation medium. As shown in **Figure 1A**, cells were filled with lipid droplets after 10 days' induction. Furthermore, qRT-PCR results suggested that the adipogenic markers *PPARG*, *FABP4*, *CEBPA*, and *FASN* significantly increased with adipogenic differentiation ($p < 0.01$) (**Figure 1B**).

Difference in DNA Methylation Level Between Intramuscular Preadipocytes and Adipocytes in Chickens

To explore the role of DNA methylation in intramuscular adipogenic differentiation, 5 mC and 5 hmC levels were detected by immunofluorescence staining. Compared with intramuscular preadipocytes, the 5 mC levels of intramuscular adipocytes

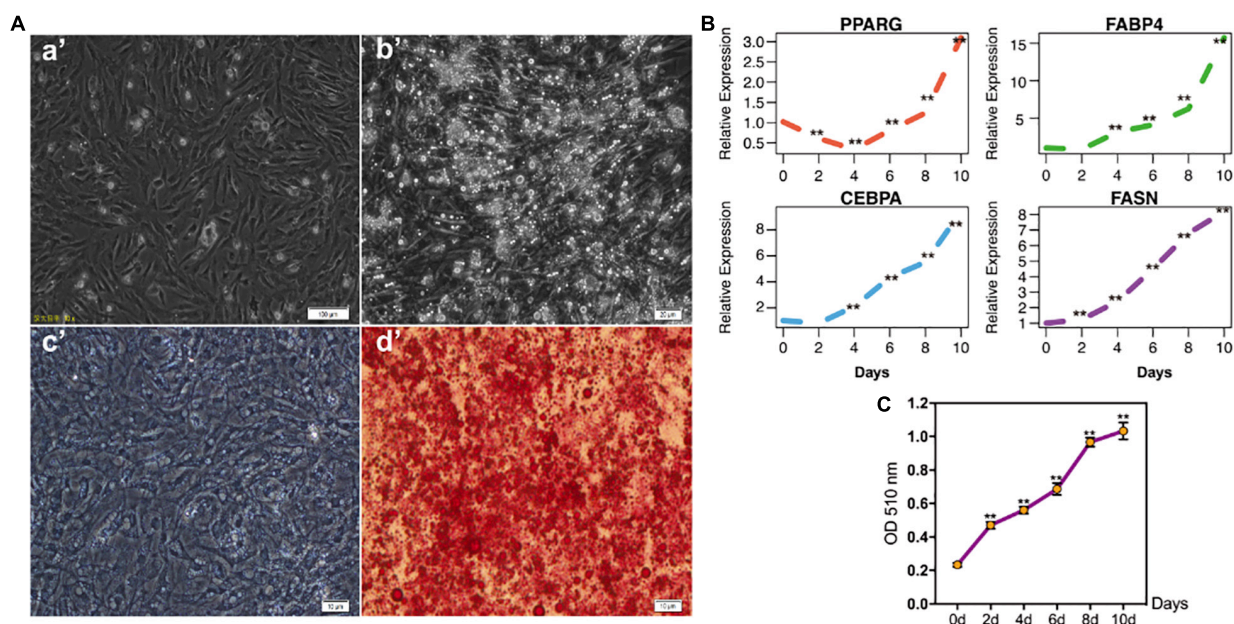


FIGURE 1 | The identification of chicken intramuscular preadipocytes differentiation model. **(A)** The shape of chicken intramuscular preadipocytes before (a') and after (b') adipogenic differentiation for 10 days. The oil red O staining of chicken intramuscular preadipocytes (c') and mature adipocytes (d'); **(B)** qRT-PCR analysis of adipogenic makers *PPARG*, *FABP4*, *CEBPA*, and *FASN* during chicken intramuscular preadipocyte differentiation. The mRNA levels of adipogenic makers were detected by qRT-PCR at 0, 2, 4, 6, 8, 10 days after induced differentiation. **(C)** The OD value at 510 nm of Oil Red O staining during intramuscular preadipocyte differentiation. ($n = 3$, $**p < 0.01$).

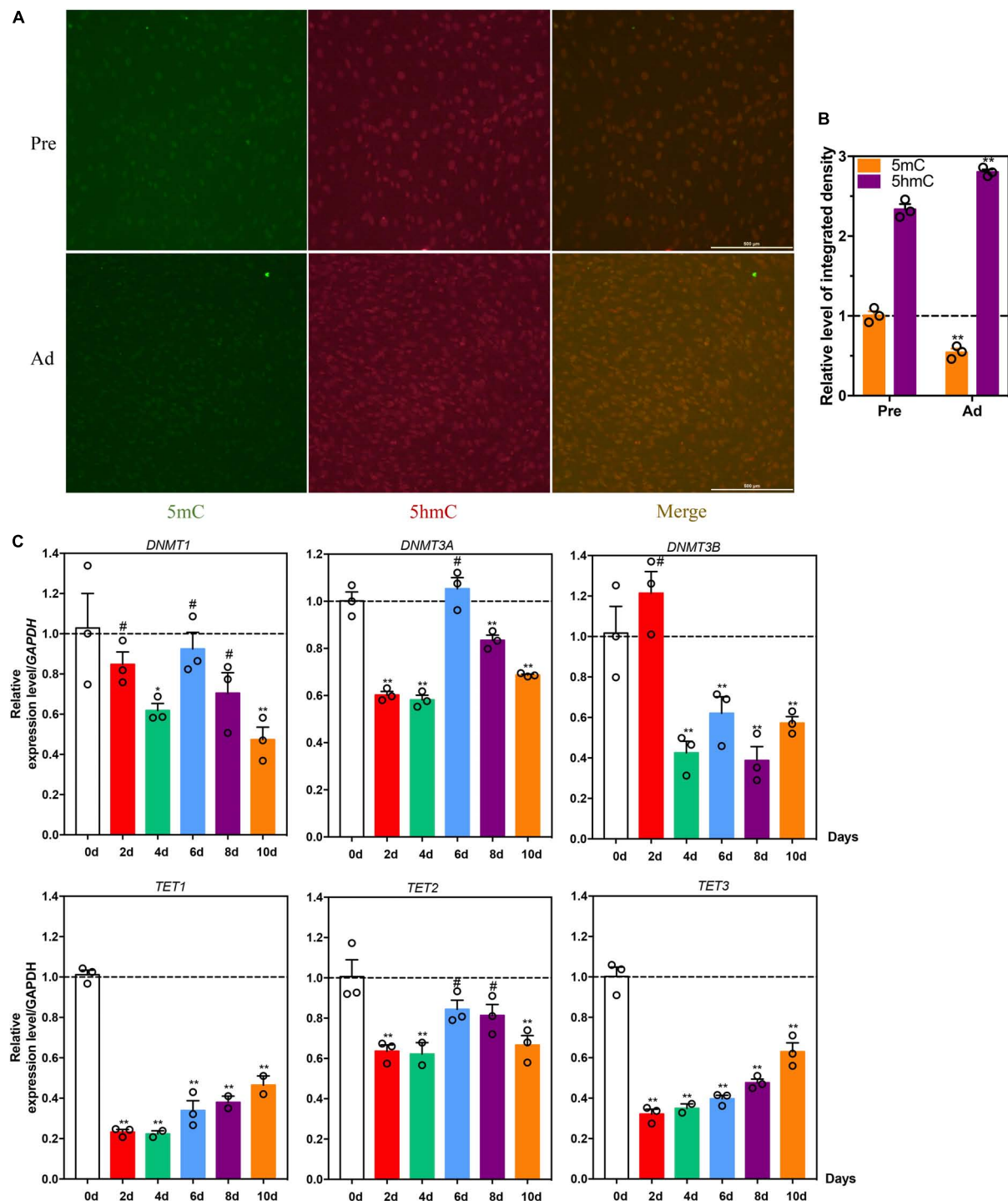


FIGURE 2 | Difference in DNA methylation levels between intramuscular preadipocytes and adipocytes in chickens. **(A)** Immunofluorescence staining and quantification **(B)** of 5mC (green) and 5hmC (red) abundance in intramuscular preadipocytes and mature adipocytes. **(C)** Relative mRNA abundance of TET1/2/3, DNMT1, DNMT3A, and DNMT3B during the intramuscular adipogenic differentiation. qRT-PCR analysis of the relative mRNA levels DNA methyltransferase DNMT1, DNMT3A/3B, and TET1/2/3 during chicken intramuscular preadipocyte differentiation. ($n = 3$, ** $p < 0.01$; # $p > 0.05$).

were significantly decreased (Figures 2A,B), whereas 5hmC levels were higher in the intramuscular adipocytes compared to intramuscular preadipocytes (Figures 2A,B). At the same

time, the mRNA expression levels of DNA methylation-related enzymes showed that mRNA expression levels of DNA methyltransferases *DNMT3A/3B* and *DNMT1* were significantly

decreased after induction of differentiation ($p < 0.01$, **Figure 2C**), while the demethylase *TET1/2/3* were significantly increased after induction of differentiation (from days 2 to 4) (**Figure 2C**).

The DNA Methylation Atlas of Intramuscular Preadipocytes and Adipocytes in Chickens

In the present study, 34.43 and 35.29 G raw data were generated in intramuscular preadipocytes and matured intramuscular adipocytes, respectively. After taking the low quality, N (unknown) and connector contamination reads off, we finally got 212,981,499 and 232,403,717 clean reads in IM_Pre and IM_Ad groups, respectively (**Table 1**). There were 68.6 and 72% of chicken genome were covered with the uniquely mapped reads in the preadipocytes and adipocytes groups, respectively (**Table 1**). The unique alignments rate of was more than 80%. The Q30 value was more than 0.9, these results indicated a reliable sequencing outcome. In addition, Circos plot displayed the DNA methylation levels in the various sequence contexts (mCG, mCHG, and mCHH) (where H is A, C, or T) in chicken chromosomes (1–32 and the Z, W, MT chromosome; **Figure 3**).

Global DNA Methylation Patterns Intramuscular Adipocytes in Chickens

Pearson correlation analysis of the CpG base suggested that our samples have good data repeatability ($r > 0.87$) (**Figure 4A**). To investigate the differences of global DNA methylation profile between the two groups, DNA methylation levels in three contexts: CG, CHG, and CHH (where H is A, C, or T) were analyzed in the present study. As shown in **Figure 4B**, most proportion (60%) of cytosines were methylated in CpG context, only small proportion (1.2%) of cytosines were methylated in non-CG context (CHG and CHH context). To explore the patterns of methylated cytosines in chicken intramuscular adipocytes, we analyzed the genome-wide mC sequence preferences in various sequence contexts. Our results showed that the methylated cytosines preference for being located in CG, CHG, and CHH ($H = A > T$) (**Figure 4C**). The DMRs of the CGI were mainly located in the openSea (60.4%) and CpG island (CGI) (25.1%) (**Figures 4D,E**). The DMRs were mainly located in the intergenic region (42.9%), followed by the introns (31.25%) and the TSS region (16.9%) (**Figures 4F,G**).

Functional Characterization of Differentially Methylated Genes (DMGs)

In the present study, a total of 7580 DMRs were discovered. The DNA methylation level of adipocytes in the chicken genome showing a “V” trend around the promoter region (**Figure 5A**), which is consistent with previous studies in chicken breast muscle tissues (Zhang et al., 2017). Furthermore, we found that hypomethylation level in the promoter region and higher genome-wide gene expression level in intramuscular adipocytes groups compared with the preadipocytes group (**Figures 5A,B**). In addition, a large proportion of DMRs were intron and exon regions (**Figure 5C**). We noticed that most DMRs were length 100–200 bp and short than 1000 bp (**Figure 5D**). To look into the

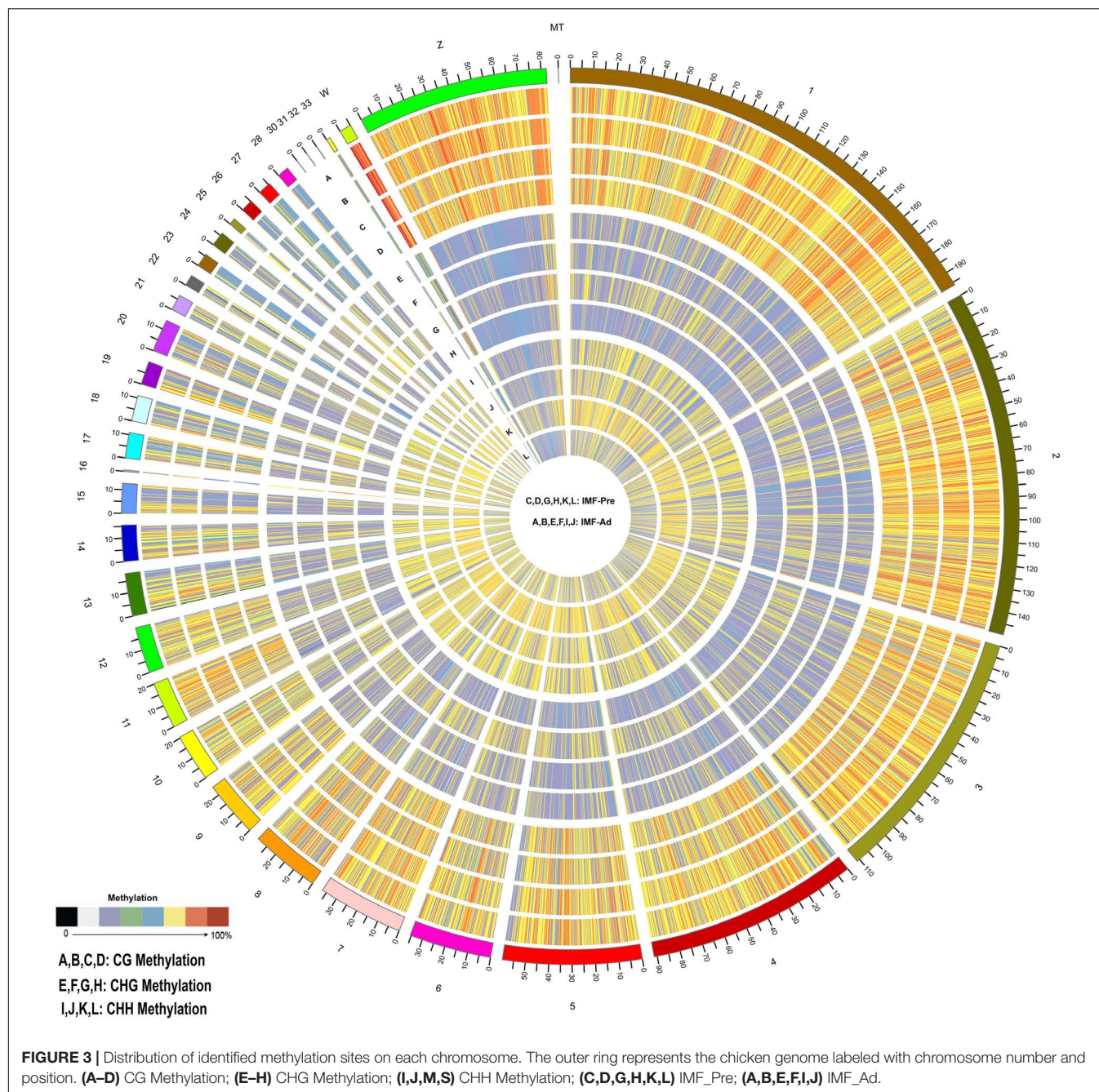
TABLE 1 | The summary of data generated by genome-wide bisulfite sequencing.

Sample ID	Raw reads	Clean reads	Clean rate (%)	Mapping rate (%)	Unique alignments	
					rate (%)	Q30
IM_Pre1	376,952,718	347,396,358	92.20	68.60	83.8	0.90
IM_Pre2	293,867,266	276,661,137	94.10	68.60	84.5	0.91
IM_Ad1	359,297,694	330,787,356	92.10	71.70	80.3	0.90
IM_Ad2	329,939,770	316,350,010	95.90	65.80	84.6	0.91

DMGs' potential biological roles, gene ontology (GO) analysis and KEGG pathway analysis were performed. Our results showed that the DMGs mainly enriched in the regionalization and skeletal system development terms (**Figure 5E**), focal adhesion, fatty acid metabolism, ECM-receptor interaction and PPAR signaling pathways (**Figure 5F**).

Candidate DMGs Associated With IMF Deposition

To explore whether the candidate DMGs are related to IMF deposition, we integrated the RNA-Seq and WGBS data to reveal methylated candidate genes associated with IMF deposition. Our results showed that there were 324 (hypermethylated and down-regulated) and 338 (hypomethylated and up-regulated) differentially expressed DMGs during adipocytes differentiation process (**Figure 6A**), several lipid metabolism-related and adipogenic differentiation genes, such as *FASN*, *HADHA*, *INSIG1*, *BMP4*, and *LCLAT1* were found in the present study (**Figure 6B**). Besides, we observed that several genes were involved in the ECM-receptor interaction, insulin signaling pathway and fatty acid metabolism pathway, such as *COL6A1*, *THBS1*, *LAMA2*, *HADHA*, *ACAA2*, *ELOVL7*, *ACADL*, *LCLAT1*, *INSIG1*, and *FOXO3* (**Figure 6C**). Moreover, the protein-protein interaction (PPI) network analysis illustrated that these DMGs were correlated with each other highly (**Figure 6C**). The DNA methylation and gene expression levels of three DMGs, *INSIG1*, *BMP4*, and *COL6A1* were showed in **Figure 6D**. Furthermore, the correlations between IMF content and gene mRNA levels at different age stages were analyzed. Our results suggested that the expression levels of *COL6A1* and *ABCA1* were positively correlated with the IMF content ($r = 0.980$ and 0.994 , $p < 0.05$) (**Figure 6E**). To study the expression trend of candidate genes in the differentiation of intramuscular adipocytes, the total RNA of intramuscular adipocytes differentiated at different periods was analyzed by qRT-PCR. Our results suggested that the mRNA level of *COL6A1* was significantly increased during adipogenic differentiation of intramuscular preadipocytes. The mRNA level of *ABCA1* significantly increased in the day 2, while declined slowly from days 4 to 10. And *GSTTIL* mRNA expression level was downregulated in day 2, while increased slowly after from days 4 to 10 (**Figure 6F**). Furthermore, our results suggested that the mRNA level of *COL6A1* was significantly positive correlative with the TG content of intramuscular adipocytes during differentiation process ($r = 0.84$, $p = 0.03$), while *ABCA1* and *GSTTIL* were was not significant correlative with the



TG content ($r = 0.14$, $p = 0.78$ and $r = 0.24$, $p = 0.65$) (Supplementary Figure S1).

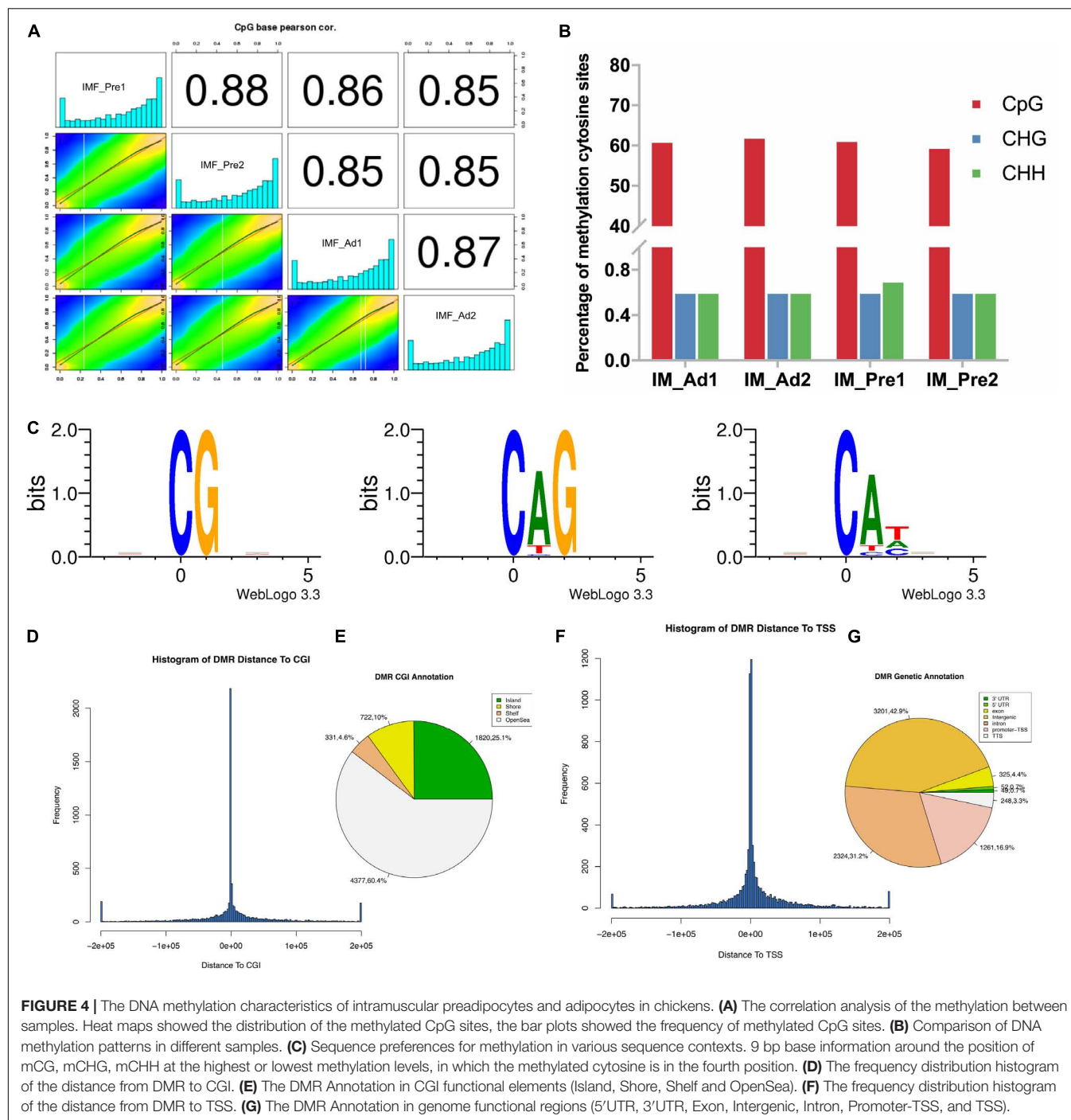
DNA Methylation of COL6A1 Promoter Region

According to the BSP results, there was a hypermethylated (72%) promoter region of *COL6A1* in the intramuscular preadipocytes compared with differentiated adipocytes, while a low methylation level (28%) in the matured intramuscular adipocytes (Figures 7A,B). Furthermore, we found that the methylation of *COL6A1* promoter were significantly negatively

correlated with the mRNA level ($r = -0.908$, $p < 0.05$) (Figure 7C). And the DNA methylation levels of *ABCA1* and *GSTTIL* promoter were significantly negatively correlated with their mRNA levels ($r = -0.94$, $p < 0.01$, and $r = -0.87$, $p < 0.05$) (Supplementary Figures S2, S3).

Effect of 5-Azacytidine (5-AZA) on Intramuscular Preadipocytes Differentiation

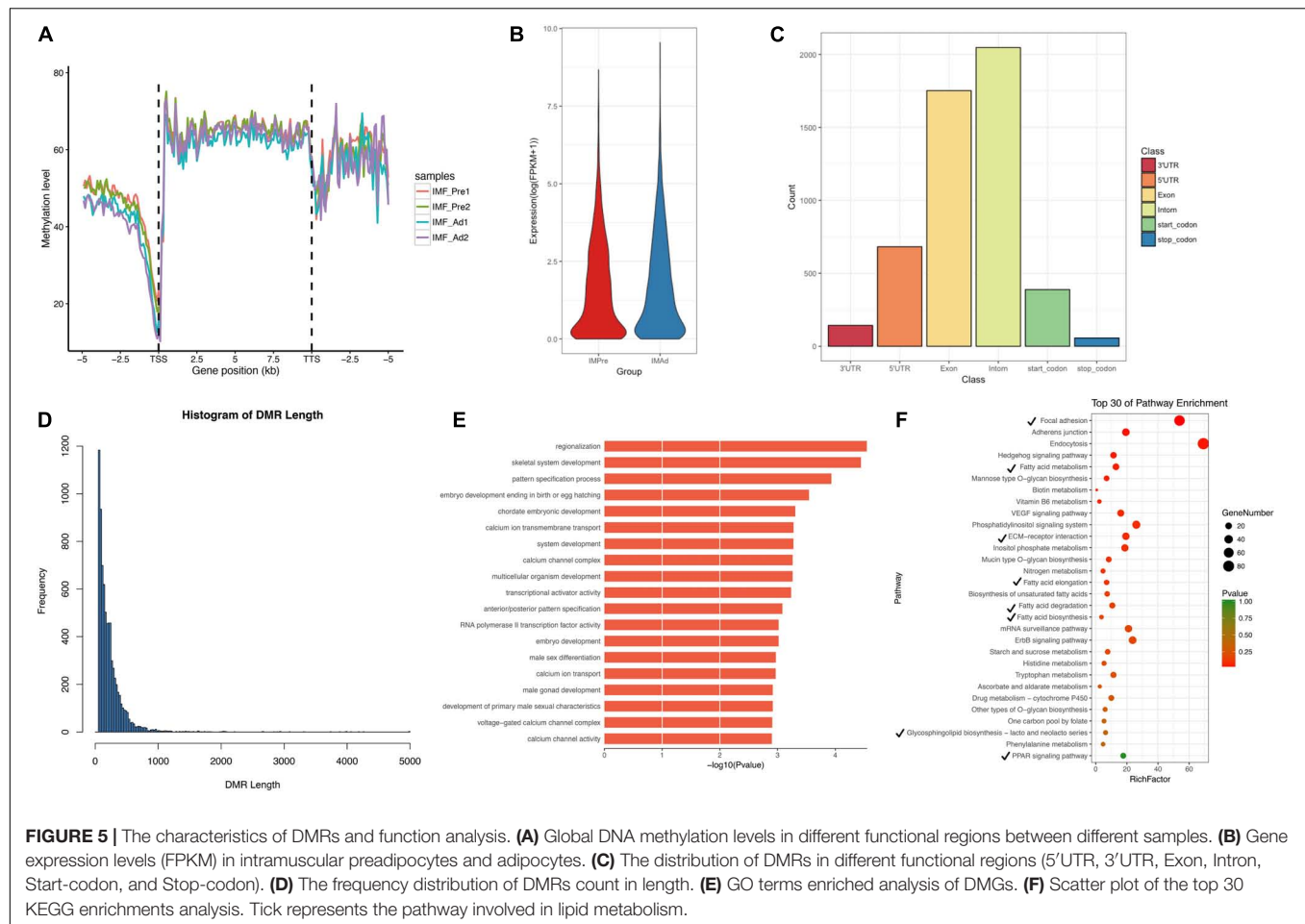
To further investigate whether the DNA methylation influence intramuscular adipogenesis, the methylation inhibitor, 5-AZA



was used to treat intramuscular preadipocytes. As shown in **Figure 8A**, the methylation level declined 60% in preadipocytes in the presence of 5-AZA relative to the control cells. Meanwhile, the mRNA levels of *COL6A1* and adipogenic makers, *PPARG* and *CEBPA* were significantly up-regulated after differentiation induction for 48 h in treating with 5-AZA cells (**Figure 8B**). In addition, Oil Red O staining showed that 5-AZA promoted the intramuscular adipogenesis (**Figures 8C,D**).

Chicken COL6A1 Promoted Intramuscular Preadipocytes Proliferation and Differentiation

To find out the potential role of *COL6A1* in chicken intramuscular preadipocyte proliferation and differentiation, *COL6A1* overexpression [pcDNA3.1(+)-*COL6A1* vs. pcDNA3.1(+)-EGFP] and knockdown (siRNA-NC vs. siRNA-*COL6A1*)



experiments were performed. The mRNA levels of *COL6A1* increased over 13-fold in pcDNA3.1(+)-*COL6A1*-transfected group compared with control pcDNA3.1(+)-EGFP-transfected group (Figure 9A). Overexpressed *COL6A1* significantly increased the mRNA expression levels of adipogenic makers *PPARG*, *CEBPA*, *FABP4*, and ECM-related genes *CHAD*, *MMP7*, *MMP9*, and *CAMK2* (Figure 9B). In contrast, knockdown the *COL6A1* down-regulated their mRNA expression levels (Figures 9C,D). EDU staining suggested that *COL6A1* promoted intramuscular preadipocytes proliferation (Figure 9E). BODIPY staining showed that overexpressed *COL6A1* significantly promoted the formation of lipid droplet in the intramuscular adipocytes, while decreased lipid droplet formation after RNA interference with *COL6A1* (Figure 9F). Wound healing test suggested that *COL6A1* promoted intramuscular adipocytes migration (Figure 9G).

MATERIALS AND METHODS

Ethics Statement

All animal experiments were conducted with the guidelines of Institutional Animal Care and Use Committee (IACUC)

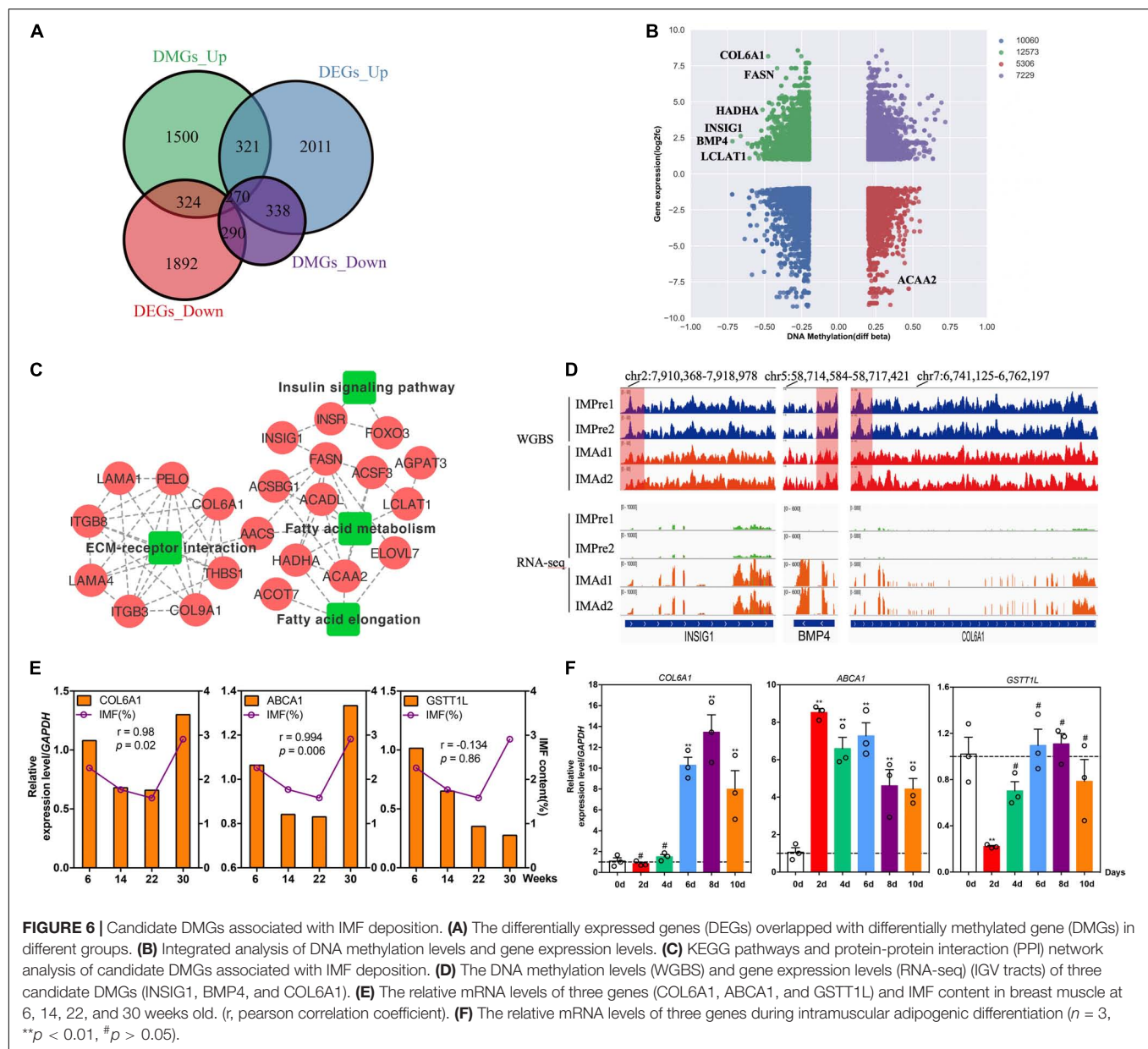
at the Henan Agricultural University (Zhengzhou, Henan, China) (#11-0085).

Animals and Cells

All of the Gushi chickens were purchased from the Animal Center of Henan Agricultural University (Zhengzhou, Henan, China). Chickens were fed with the same diet *ad libitum* in the same environment. Tissues used for tissues expression profiles were collected and stored at -80°C until use. The breast muscle tissues were used for the IMF preadipocytes isolation according to our previous methods (Zhang et al., 2019).

DNA Extraction, Library Construction, and Whole Genome Bisulfite Sequencing (WGBS)

Genomic DNA used for WGBS was extracted by an animal genomic DNA kit (Tiangen, China) according to the manufacturer's instructions. genomic DNA was interrupted into fragments and purified by PCR purification kit. Fragmented DNA was end-repaired, added "A" nucleotide to the 3' end and ligated with methylated adapters. Fragments with adapters were used for bisulfite conversion by a methylation-gold kit (ZYMO, Los Angeles, CA, United States). Furthermore,



converted DNA fragments were sequenced by Illumina HiSeq 2500. After removing unknown nucleotides and low-quality reads of raw reads, clean reads were got and used for the downstream analysis.

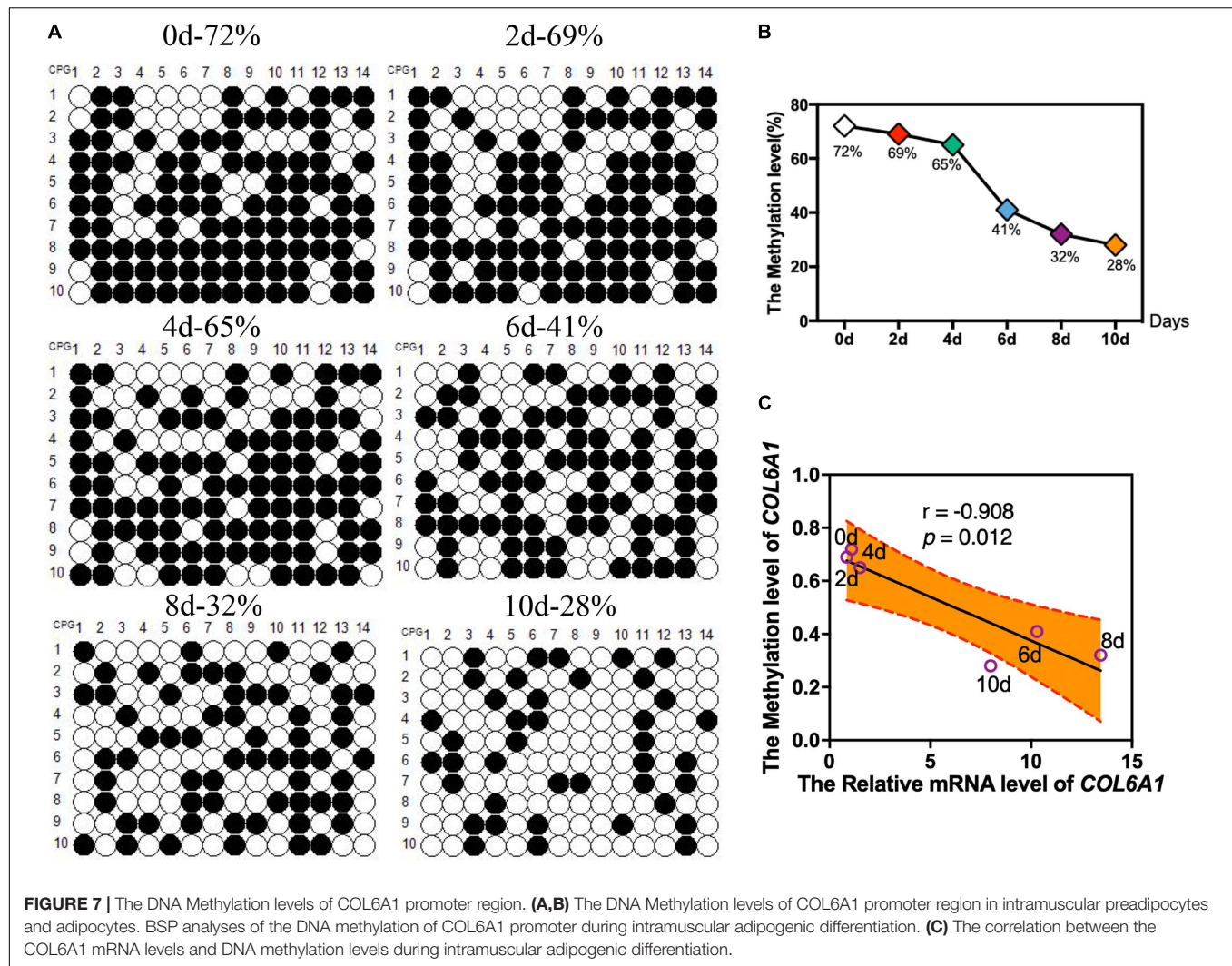
Data Analysis

Produced clean reads were mapped to chicken reference genome (GGA_5.0) using the Bismark software (version: 2.90) (Krueger and Andrews, 2011). Then, a methylkit R package (Akalin et al., 2012) was used to estimate methylation status and ratio of the CpG sites, promoter region, CpG island region and gene annotation. To get different methylation status in the chicken different genomic regions, methylation levels at 5'-flanking 2 kb regions and gene sequences in different samples were plotted. The

RNA-Seq data used in the present study come from our present study (Zhang et al., 2019). The IMF content data used in the present study came from our previous study (Fu et al., 2018).

Identification of DMRs and Functional Analysis of DMR-Related Genes

The methylation regions with $p \leq 0.05$ (chi-square test) and the degree of difference methylation $>20\%$ were considered as differentially methylated regions (DMRs). DMRs that overlapping with genes body or up or downstream 2 kb of body regions were considered as differentially methylated genes (DMGs). To investigate the functions of the DMGs, GO, and KEGG pathway analysis were conducted in the present study. Fisher's Exact Test is $p \leq 0.05$ as threshold.



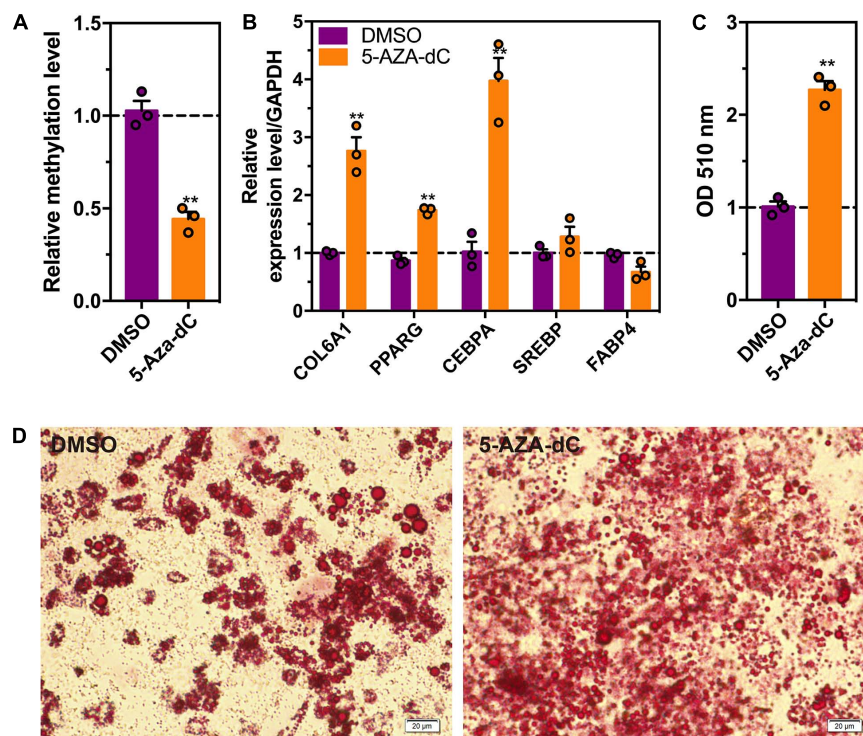


FIGURE 8 | The effects of 5-AZA-dC treatment on intramuscular adipocytes differentiation. **(A)** The DNA methylation level (5 mC) in intramuscular preadipocytes treated with or without 5-AZA-dC (5 μ M) for 96 h. **(B)** The relative mRNA levels in intramuscular adipocytes treated with or without 5-AZA-dC (5 μ M) for 96 h. **(C,D)**. Oil-red O staining of intramuscular adipocytes treated with or without 5-AZA-dC (5 μ M) for 96 h. ($n = 3$). ** $p < 0.01$.

Immunofluorescence Staining

For immunofluorescence, intramuscular adipocytes were fixed with 4% PFA (Beyotime) for 40 min, permeabilized 0.5% Triton X-100 for 10 min, and then blocked with 2% bovine serum albumin (BSA) for 2 h. Following incubated overnight at 4°C with anti-5 mC (Active Motif, 1:200) and anti-5 hmC (Active Motif, 1:200), stained at room temperature for 1 h with Alexa Fluor 488 goat anti-mouse or 594 goat anti-rabbit. The DNA were stained with DAPI (10 μ g/mL, Beyotime) for 5 min. The images were captured with fluorescence microscopy (Nikon, Tokyo, Japan). The fluorescence intensity was analyzed by ImageJ software.

5-aza-2'-Deoxycytidine (5-Aza-dC) Treatments

After reaching 70–80% confluent, intramuscular preadipocytes were treated with demethylation agent 5-aza-dC (Sigma) (dissolved in DMSO) at 5 μ M for 96 h. DMSO treatment was used as a control. Then cells were induced differentiation for 96 h, then for downstream experiment.

5-Methylcytosine (5-mC) Analysis of Genomic DNA

The genomic DNAs were extracted with TIANamp Genomic DNA Kit (TIANGEN) following the instruction of manufacturers. The methylation analysis was performed

by the 5 mC DNA ELISA Kit (Zymo Research, United States) following the manufacturer's instructions. The microplate reader (Thermo Fisher) was used to detect the absorbance at 405 nm.

5-Ethynyl-2'-Deoxyuridine (EdU) Assay

After transfection for 48 h, intramuscular adipocytes were incubated at 37°C with 50 μ M EdU (RiboBio, China) for 2 h, then cells were fixed with 4% PFA for 30 min and neutralized by 2 mg/mL glycine solution, permeabilized with 0.5% Triton X-100. Then cells were incubated with Apollo Reaction Cocktail (RiboBio, China) for 30 min at room temperature. The DNA was stained with DAPI (Beyotime) for 15 min. The EDU-positive cells were observation with a fluorescence microscope (Nikon, Tokyo, Japan).

Wound Healing Test

After reached 70–80% confluence, intramuscular preadipocytes were transfected with plasmid or RNA oligos. Subsequently, 10 μ L pipette tips were used to generated linear wound. The width of the scratches was measured by microscope (Nikon, Japan) at 0 and 72 h.

Oil Red O and BODIPY 493/503 Staining

Oil red O staining was performed following our previously method (Zhang et al., 2018). Cells were fixed with 10% PFA for 40 min, and then stained with oil red O for 20 min. The dye was extracted by isopropanol incubation

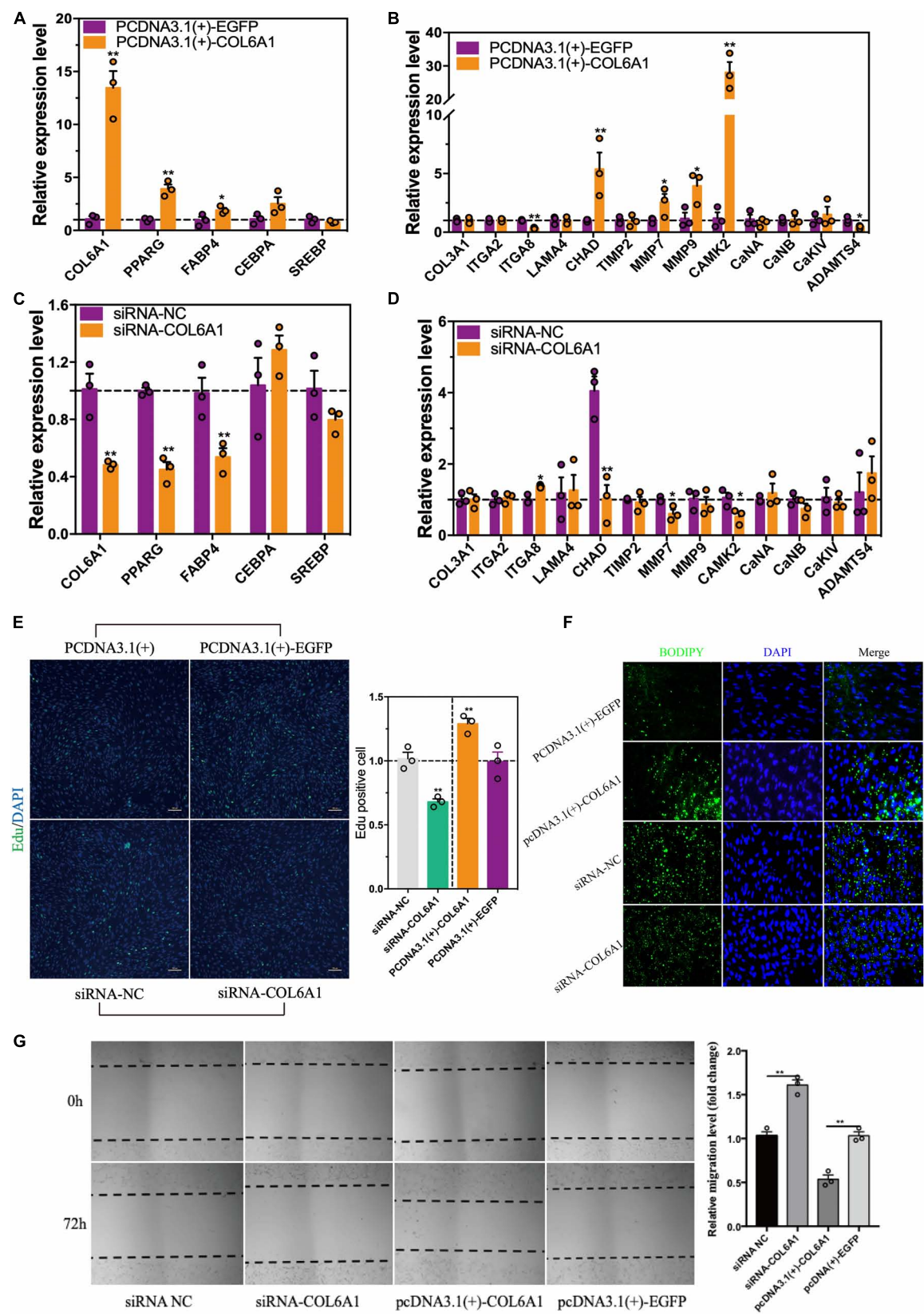


FIGURE 9 | Continued

FIGURE 9 | Continued

The effects of COL6A1 overexpression and knockdown on cell proliferation, differentiation and migration. **(A)** Overexpressed of COL6A1 promoted the expression of adipogenic differentiation and ECM-related genes **(B)** of intramuscular adipocytes. The relative mRNA levels of genes were detected by qRT-PCR after transfected with plasmid for 48 h. **(C)** Knockdown of COL6A1 suppressed the expression of adipogenic differentiation and ECM-related genes **(D)** of intramuscular adipocytes. The relative mRNA levels of genes were detected by qRT-PCR after transfected with RNA oligos for 24 h. **(E)** COL6A1 promoted intramuscular preadipocytes proliferation. The percentage of EDU positive cells was quantified after transfected with plasmid or RNA oligos. **(F)** COL6A1 accelerated intramuscular preadipocytes differentiation. BODIPY (green) and DAPI (blue) staining of intramuscular adipocytes after transfected with plasmid or RNA oligos. **(G)** COL6A1 promoted intramuscular adipocytes migration. The width of the scratches was measured by microscope after transfected with plasmid or RNA oligos for 72 h ($n = 3$), $*p < 0.05$, $**p < 0.01$.

for 15 min at room temperature. Quantitative assessment was obtained by microplate reader (Thermo Scientific) at 510 nm. Where indicated, lipids were co-stained by adding BODIPY 493/503 (1 mg/mL, Molecular Probes #D3922) to secondary antibody solution. Cells were washed three times with PBS prior to imaging.

Statistical Analysis

Statistical analyses were performed using SPSS19 software (SPSS Inc., Chicago, IL, United States). In the present study, the results were presented as mean \pm SEM, were subjected to statistical analysis by two-tailed *t*-test. The level of significance was presented as $*p < 0.05$ and $**p < 0.01$.

DISCUSSION

IMF content contributes to the meat juiciness and tenderness. Our previous study suggested that the breast muscle of later laying-period hens had higher IMF content than that of juvenile hens, while they exhibited higher global DNA methylation levels (Zhang et al., 2017). Growing numbers of studies demonstrated that DNA methylation played important roles in adipogenesis. Therefore, we speculated that DNA methylation might have great influences on adipogenic differentiation of chicken intramuscular adipocytes *in vitro*.

According to our WGBS data, 60% of mC were found to be existed in the CG context, 0.6% in the CHG context, and 0.7% in the CHH context in the present study. The methylation level at the genome-wide scale was significantly reduced in the mature intramuscular adipocytes. We noticed that the DNA methylation level declined aggressively prior to TSS and gradually rose in the coding region of the chicken genome, which is consistent with previous studies in chicken (Zhang et al., 2017). The exon and intron regions of the chicken genome consisted of a large proportion of the DMRs, a small part of DMRs were belong to the 5'UTR and 3'UTR (Figure 5). The methylation regulation of the intron regions underlying adipocytes differentiation was worth to study in the future.

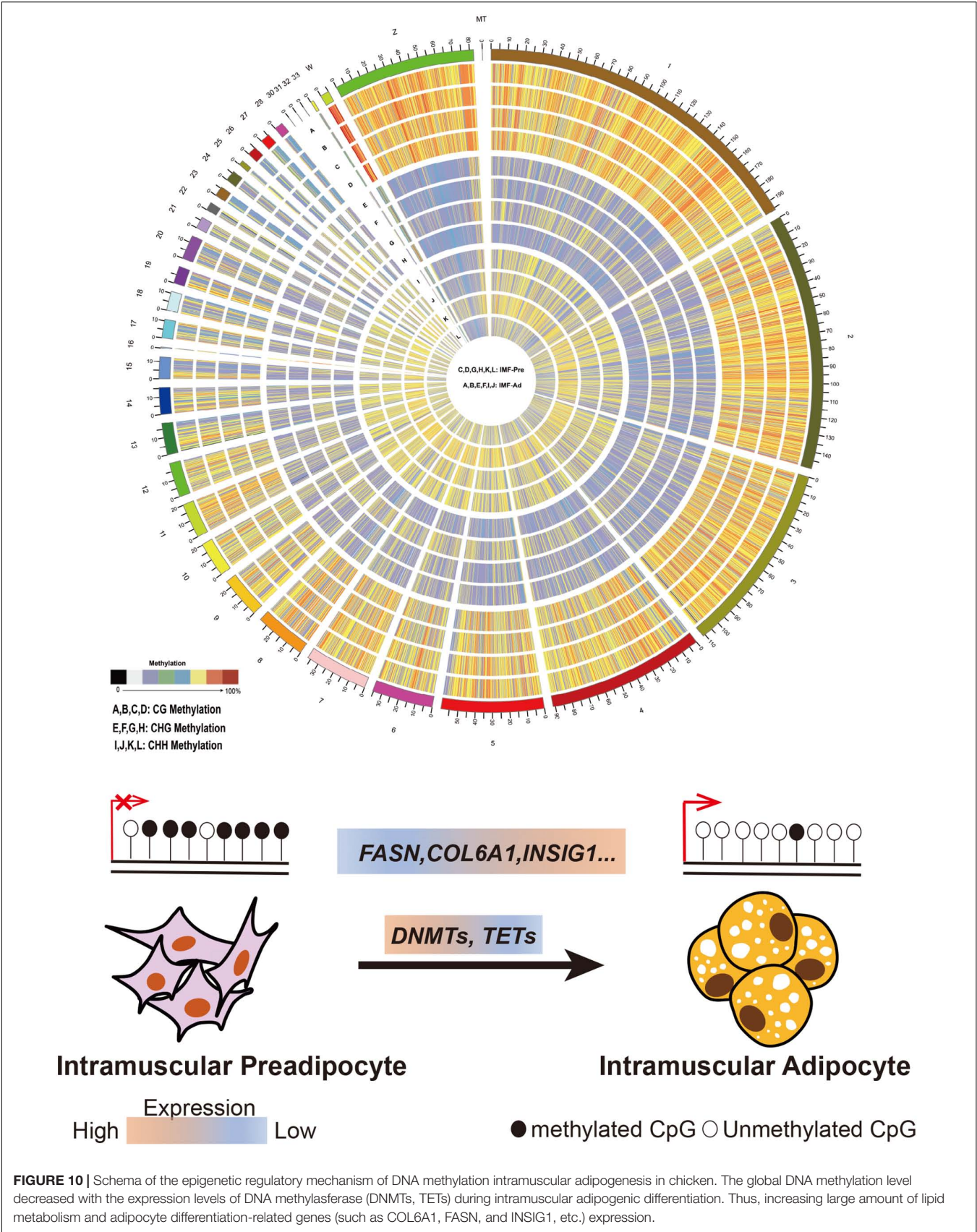
DNMT1 mainly involved in maintain methylation (Song et al., 2012), while *DNMT3A/3B* mainly involved in the *de novo* DNA methylation (Li et al., 2007; Hervouet et al., 2009). Tet methylcytosine dioxygenases (*TET1/2/3*) play important roles in elimination of methylation (Williams et al., 2011). qPCR results showed that the mRNA levels of DNA methyltransferases *DNMT1*, *DNMT3A/3B*, and *TET1/2/3* were significantly down-regulated during intramuscular adipocyte differentiation,

suggesting that whole-genome DNA demethylation may occur during adipocyte differentiation. The process of adipocyte differentiation requires the initiation of a large number of genes and transcription factors for synergistic expression, which may be related to the differentiation of adipocytes (Mersmann and Ding, 2001). Our previous study found that the hypermethylation in the promoters of *ABCA1*, *COL6A1*, and *GSTT1*, thus inhibiting their expression in the later laying-period hens (Zhang et al., 2017). Interestingly, we noticed that they were up-regulated after adipocyte differentiation, suggesting that they may play crucial roles in the differentiation of intramuscular preadipocytes.

ABCA1 maintains cholesterol homeostasis, regulates lipid metabolism in adipocytes (Schmitz et al., 1999; Schmitz and Langmann, 2005). The DNA methylation level of *ABCA1* affects high density lipoprotein cholesterol (HDL) levels in patients with familial hypercholesterolemia (Yasuaki et al., 2017). *ABCA1* expression influenced triglyceride metabolism in bovine mammary epithelial cells by regulating the expression of related genes in the lipid metabolism pathway (Chen et al., 2019). *ABCA1* silencing by siRNA also reduce peroxisome proliferator-activated receptor γ (*PPAR* γ) expression and triglyceride content during 3T3-L1 pre-adipocyte differentiation (Cuffe et al., 2018). *ABCA1* is significantly up-regulated after differentiation of 3T3-L1 adipocytes, which is consistent with our study on chicken intramuscular adipocytes (Le et al., 2003). Glutathione S-transferases (*GSTT1*) Glutathione S-transferases influencing the lipid peroxides metabolism during adipocytes differentiation process (Jowsey et al., 2003; Corton et al., 2008). Wang et al. (2009) found that *GSTT1* were upregulated in the adipose tissues of fat line birds compared with lean line birds.

Muscle tenderness is closely related with the content of collagen. The ECM not only affects the development of muscle fibers, but also has an effect on IMF content and tenderness (Cánovas et al., 2010). *COL6A1* gene is involved in cell adhesion and extracellular matrix (ECM). Previous studies suggested that the expression of collagen synthesis related-genes is related to the meat quality of beef (Zhang et al., 2011).

To further investigate the effects of DNA methylation on intramuscular preadipocytes differentiation, we focused on collagen type VI alpha 1 chain gene (*COL6A1*), which is located in the extracellular matrix (ECM) receptor interaction and focal adhesion pathway. With the differentiation of preadipocytes, the lipid droplets gradually fill the cytoplasm, and the cells are easily crushed and ruptured. At this time, the collagen components that act as protective cells in the extracellular matrix are synthesized in large amounts. It is generally believed that DNA methylation of the gene promoter region inhibits



gene expression (Lorincz et al., 2004). In our study, we found that the DNA methylation level of *COL6A1* promoter was decreased while the mRNA level was increasing after adipogenic differentiation. The methylation inhibitor, 5-AZA-dC promotes intramuscular adipocytes differentiation by increasing the core adipogenic factors, *PPARG* and *CEBPA*. Furthermore, function loss and gain of experiment of *COL6A1* suggested that DNA methylation can regulate the chicken intramuscular adipocytes differentiation by affecting the expression of ECM-related genes (such as *COL6A1* gene).

CONCLUSION

In conclusion, our study firstly supplies comprehensive DNA methylation atlas in chicken adipocytes. Integrated DNA methylation with transcriptome, the present study revealed several potential genes (such as *COL6A1*, *FASN*, and *INSIG*, etc.) and pathways related to lipid metabolism and adipocytes differentiation regulated by DNA methylation (Figure 10). Our study will accelerate the study of genome epigenetic mechanism in adipocytes differentiation and IMF deposition in poultry.

DATA AVAILABILITY STATEMENT

The datasets generated for this study can be found in the PRJNA429489 and PRJNA428933.

ETHICS STATEMENT

The animal study was reviewed and approved by Institutional Animal Care and Use Committee (IACUC).

AUTHOR CONTRIBUTIONS

MZ, GS, and XK conceived of and designed the experiments. MZ, DL, YZ, and ZW performed the experiments. MZ, DL,

and YZ analyzed the data. ZL, GL, XM, DZ, RH, and RJ contributed reagents, materials, and analysis tools. MZ wrote the manuscript. ZL reviewed the manuscript. All authors approved the final manuscript.

FUNDING

This research was supported by the China Agriculture Research System (CARS-40-K04), National Natural Science Foundation of China (31572356 and 31501948), Research on the Foundation and Frontier Technology of Henan Science and Technology Department (162300410162), Program for Innovation Research Team of Ministry of Education (IRT16R23) and Key Science and Technology Research Project of Henan Province (151100110800).

SUPPLEMENTARY MATERIAL

The Supplementary Material for this article can be found online at: <https://www.frontiersin.org/articles/10.3389/fcell.2020.00206/full#supplementary-material>

FIGURE S1 | The correlation between the mRNA levels of *COL6A1*, *ABCA1*, and *GSTT1L* and the TG content of intramuscular adipocytes during differentiation process.

FIGURE S2 | The DNA Methylation levels of *ABCA1* promoter region. (A,B) The DNA Methylation levels of *ABCA1* promoter region in intramuscular preadipocytes and adipocytes. BSP analyses of the DNA methylation of *ABCA1* promoter during intramuscular adipogenic differentiation. (C) The correlation between the *ABCA1* mRNA levels and DNA methylation levels during intramuscular adipogenic differentiation.

FIGURE S3 | The DNA Methylation levels of *GSTT1L* promoter region. (A,B) The DNA Methylation levels of *GSTT1L* promoter region in intramuscular preadipocytes and adipocytes. BSP analyses of the DNA methylation of *GSTT1L* promoter during intramuscular adipogenic differentiation. (C) The correlation between the *GSTT1L* mRNA levels and DNA methylation levels during intramuscular adipogenic differentiation.

TABLE S1 | Primer sequences for BSP and qRT-PCR.

REFERENCES

- Abdalla, B. A., Li, Z., Ouyang, H., Jebessa, E., Sun, T., Yu, J. A., et al. (2018). A novel *Dnmt3a1* transcript inhibits adipogenesis. *Front. Physiol.* 9:1270. doi: 10.3389/fphys.2018.01270
- Akalin, A., Kormaksson, M., Li, S., Garrett-Bakelman, F. E., Figueroa, M. E., Melnick, A., et al. (2012). methylKit: a comprehensive R package for the analysis of genome-wide DNA methylation profiles. *Genome Biol.* 13:R87. doi: 10.1186/gb-2012-13-10-r87
- Bender, C. M., Pao, M. M., and Jones, P. A. (1998). Inhibition of DNA methylation by 5-Aza-2'-deoxycytidine suppresses the growth of human tumor cell lines. *Cancer Res.* 58, 95–101.
- Broholm, C., Olsson, A. H., Perfilov, A., Gillberg, L., Hansen, N. S., Ali, A., et al. (2016). Human adipogenesis is associated with genome-wide DNA methylation and gene expression changes. *Epigenomics* 8, 1601–1617. doi: 10.2217/epi-2016-0077
- Cánovas, A., Quintanilla, R., Amills, M., and Pena, R. N. (2010). Muscle transcriptomic profiles in pigs with divergent phenotypes for fatness traits. *BMC Genomics* 11:372. doi: 10.1186/1471-2164-11-372
- Chen, Y. S., Wu, R., Yang, X., Kou, S., MacDougald, O. A., Yu, L., et al. (2016). Inhibiting DNA methylation switches adipogenesis to osteoblastogenesis by activating *Wnt10a*. *Sci. Rep.* 6:25283. doi: 10.1038/srep25283
- Chen, Z., Chu, S. F., Wang, X. L., Fan, Y., Zhan, T., Arbab, A. A. I., et al. (2019). microRNA-106b regulates milk fat metabolism via ATP binding cassette subfamily A member 1 (*ABCA1*) in bovine mammary epithelial cells. *J. Agric. Food Chem.* 67, 3981–3990. doi: 10.1021/acs.jafc.9b00622
- Corton, M., Botella-Carretero, M., Lopez, J. A., Camafeita, E., San Millan, J. L., Escobar-Morreale, H. F., et al. (2008). Proteomic analysis of human omental adipose tissue in the polycystic ovary syndrome using two-dimensional difference gel electrophoresis and mass spectrometry. *Hum. Reprod.* 23, 651–661. doi: 10.1093/humrep/dem380
- Cristancho, A. G., and Lazar, M. A. (2011). Forming functional fat: a growing understanding of adipocyte differentiation. *Nat. Rev. Mol. Cell Biol.* 12, 722–734. doi: 10.1038/nrm3198
- Cuffe, H., Liu, M. X., Key, C.-C. C., Boudyguina, E., Sawyer, J. K., Weckerle, A., et al. (2018). Targeted deletion of adipocyte *Abca1* (ATP-binding cassette transporter A1) impairs diet-induced obesity. *Arterioscler. Thromb. Vasc. Biol.* 38, 733–743. doi: 10.1161/ATVBAHA.117.309880

- Fanatico, A. C., Pillai, P. B., Emmert, J. L., and Owens, C. M. (2007). Meat quality of slow- and fast-growing chicken genotypes fed low-nutrient or standard diets and raised indoors or with outdoor access. *Poult. Sci.* 86, 2245–2255. doi: 10.1093/ps/86.10.2245
- Fu, S., Zhao, Y. L., Li, Y. F., Li, G., Xi, L., Chen, Y., et al. (2018). Characterization of miRNA transcriptome profiles related to breast muscle development and intramuscular fat deposition in chickens. *J. Cell Biochem.* 119, 7063–7079. doi: 10.1002/jcb.27024
- Gao, S. Z., and Zhao, S. M. (2009). Physiology, affecting factors and strategies for control of pig meat intramuscular fat. *Recent Pat. Food Nutr. Agric.* 1, 59–74. doi: 10.2174/2212798410901010059
- Gao, Y., Sun, Y., Duan, K., Shi, H., Wang, S., Li, H., et al. (2015). CpG site DNA methylation of the CCAAT/enhancer-binding protein, alpha promoter in chicken lines divergently selected for fatness. *Anim. Genet.* 46, 410–417. doi: 10.1111/age.12326
- Hervouet, E., Vallette, F. M., and Pierre-Fancois, C. (2009). Dnmt3/transcription factor interactions as crucial players in targeted DNA methylation. *Epigenetics* 4, 487–499. doi: 10.4161/epi.4.7.9883
- Jaenisch, R. (1997). DNA methylation and imprinting: why bother? *Trends Genet.* 13, 323–329. doi: 10.1016/s0168-9525(97)01180-3
- Jeong, J., Kwon, E. G., Im, S. K., Seo, K. S., and Baik, M. (2012). Expression of fat deposition and fat removal genes is associated with intramuscular fat content in longissimus dorsi muscle of Korean cattle steers1. *J. Anim. Sci.* 90, 2044–2053. doi: 10.2527/jas.2011-4753
- Jowsey, I. R., Smith, S. A., and Hayes, J. D. (2003). Expression of the murine glutathione S-transferase $\alpha 3$ (GSTA3) subunit is markedly induced during adipocyte differentiation: activation of the GSTA3 gene promoter by the pro-adipogenic eicosanoid 15-deoxy- $\Delta 12,14$ -prostaglandin J2. *Biochem. Biophys. Res. Commun.* 312, 1226–1235. doi: 10.1016/j.bbrc.2003.11.068
- Krueger, F., and Andrews, S. R. (2011). Bismark: a flexible aligner and methylation caller for bisulfite-Seq applications. *Bioinformatics* 27, 1571–1572. doi: 10.1093/bioinformatics/btr167
- Le, L., Robichon, C., Le, Liepvre X., Dagher, G., Ferre, P., and Dugail, I. (2003). Regulation of ABCA1 expression and cholesterol efflux during adipose differentiation of 3T3-L1 cells. *J. Lipid Res.* 44, 1499–1507. doi: 10.1194/jlr.M200466-JLR200
- Li, C., Fan, Y., Li, G., Xu, X., Duan, J., Li, R., et al. (2018). DNA methylation reprogramming of functional elements during mammalian embryonic development. *Cell Discov.* 4:41. doi: 10.1038/s41421-018-0039-9
- Li, F., Li, D. H., Zhang, M., Sun, J. W., Li, W. T., Jiang, R. R., et al. (2019). miRNA-223 targets the GPAM gene and regulates the differentiation of intramuscular adipocytes. *Gene* 15, 106–113. doi: 10.1016/j.gene.2018.10.054
- Li, T., Xu, D., Zuo, B., Lei, M., Xiong, Y., Chen, H., et al. (2013). Ectopic overexpression of porcine DGAT1 increases intramuscular fat content in mouse skeletal muscle. *Transgenic Res.* 22, 187–194. doi: 10.1007/s11248-012-9633-z
- Li, Y. Q., Zhou, P. Z., Zheng, X. D., Walsh, C. P., and Xu, G. L. (2007). Association of Dnmt3a and thymine DNA glycosylase links DNA methylation with base-excision repair. *Nucleic Acids Res.* 35, 390–400. doi: 10.1093/nar/gkl1052
- Lim, Y. C., Chia, S. Y., Jin, S., Han, W., Ding, C., and Sun, L. (2016). Dynamic DNA methylation landscape defines brown and white cell specificity during adipogenesis. *Mol. Metab.* 5, 1033–1041. doi: 10.1016/j.molmet.2016.08.006
- Lorincz, M. C., Dickerson, D. R., Schmitt, M., and Groudine, M. (2004). Intragenic DNA methylation alters chromatin structure and elongation efficiency in mammalian cells. *Nat. Struct. Mol. Biol.* 11, 1068–1075. doi: 10.1038/nsmb840
- Mersmann, H. J., and Ding, S. T. (2001). Fatty acids modulate porcine adipocyte differentiation and transcripts for transcription factors and adipocyte-characteristic proteins? *J. Nutr. Biochem.* 12, 101–108. doi: 10.1016/S0955-2863(00)00136-4
- Qimuge, N., He, Z., Qin, J., Sun, Y., Wang, X., Yu, T., et al. (2019). Overexpression of DNMT3A promotes proliferation and inhibits differentiation of porcine intramuscular preadipocytes by methylating p21 and PPARG promoters. *Gene* 696, 54–62. doi: 10.1016/j.gene.2019.02.029
- Qiu, F., Liang, X., Jing-e, M., Wen, L., Li, Z., Zhe, C., et al. (2017). Lower expression of SLC27A1 enhances intramuscular fat deposition in chicken via down-regulated fatty acid oxidation mediated by CPT1A. *Front. Physiol.* 8:449. doi: 10.3389/fphys.2017.00449
- Razin, A., and Cedar, H. (1984). DNA methylation and gene expression. *Microbiol. Rev.* 55, 451–458. doi: 10.1007/978-1-4613-8519-6-8
- Ros-Freixedes, R., Reixach, J., Bosch, L., Tor, M., and Estany, J. (2014). Genetic correlations of intramuscular fat content and fatty acid composition among muscles and with subcutaneous fat in Duroc pigs. *J. Anim. Sci.* 92, 5417–5425. doi: 10.2527/jas.2014-8202
- Schmitz, G., Kaminski, W. E., Porsch-Ozcürümez, M., Klucken, J., Orsó, E., Bodzioch, M., et al. (1999). ATP-binding cassette transporter A1 (ABCA1) in macrophages: a dual function in inflammation and lipid metabolism? *Pathobiology* 67, 236–240. doi: 10.1159/000028100
- Schmitz, G., and Langmann, T. (2005). Transcriptional regulatory networks in lipid metabolism control ABCA1 expression. *Biochim. Biophys. Acta.* 1735, 1–19. doi: 10.1016/j.bbali.2005.04.004
- Serão, N. V., Veroneze, R., Ribeiro, A. M., Verardo, L. L., Braccini Neto, J., Gasparino, E., et al. (2011). Candidate gene expression and intramuscular fat content in pigs. *J. Anim. Breed. Genet.* 128, 28–34. doi: 10.1111/j.1439-0388.2010.00887.x
- Shivapurkar, N., Wilson, M. J., Hoover, K. L., Mikol, Y. B., Creasia, D., and Poirier, L. A. (1986). Hepatic DNA methylation and liver tumor formation in male C3H mice fed methionine- and choline-deficient diets. *J. Natl. Cancer Inst.* 77, 213–217.
- Song, J. K., Teplova, M., Ishibe-Murakami, S., and Patel, D. J. (2012). Structure-based mechanistic insights into DNMT1-mediated maintenance DNA Methylation. *Science* 335, 709–712. doi: 10.1126/science.1214453
- Sun, Y. N., Gao, Y., Qiao, S. P., Wang, S. Z., Duan, K., Wang, Y. X., et al. (2014). Epigenetic DNA methylation in the promoters of peroxisome proliferator-activated receptor γ in chicken lines divergently selected for fatness. *J. Anim. Sci.* 92, 48–53. doi: 10.2527/jas.2013-6962
- Wang, D., Wang, N., Li, N., and Li, H. (2009). Identification of differentially expressed proteins in adipose tissue of divergently selected broilers. *Poult. Sci.* 88, 2285–2292. doi: 10.3382/ps.2009-00190
- Williams, K., Christensen, J., and Helin, K. (2011). DNA methylation: TET proteins-guardians of CpG islands? *EMBO Rep.* 13, 28–35. doi: 10.1038/embor.2011.233
- Yasuaki, T., Yuko, U., Akira, A., Daisuke, M., Keiji, Y., Takata, K., et al. (2017). Increased hepatic ABCA1 transporter is associated with hypercholesterolemia in a cholestatic rat model and primary biliary cholangitis patients. *Med. Mod. Morphol.* 50, 227–237. doi: 10.1007/s00795-017-0166-7
- Ye, M. H., Chen, J. L., Zhao, G. P., Zheng, M. Q., and Wen, J. (2010). Associations of A-FABP and H-FABP markers with the content of intramuscular fat in Beijing-You chicken. *Anim. Biotechnol.* 21, 14–24. doi: 10.1080/10495390903328116
- Zhang, L. J., Zhu, Y. N., Gao, Y., Liu, S. Y., Zhai, B., Li, C. H., et al. (2014). The MBD4 gene plays an important role in porcine adipocyte differentiation. *Cell Physiol. Biochem.* 34, 1216–1226. doi: 10.1159/000366333
- Zhang, M., Li, D. H., Li, F., Sun, J. W., Jiang, R. R., Li, Z. J., et al. (2018). Integrated analysis of MiRNA and genes associated with meat quality reveals that Gga-MiR-140-5p affects intramuscular fat deposition in chickens. *Cell Physiol. Biochem.* 46, 2421–2433. doi: 10.1159/000489649
- Zhang, M., Li, F., Ma, X. F., Li, W. T., Jiang, R. R., Han, R. L., et al. (2019). Identification of differentially expressed genes and pathways between intramuscular and abdominal fat-derived preadipocyte differentiation of chickens *in vitro*. *BMC Genomics* 20:743. doi: 10.1186/s12864-019-6116-0
- Zhang, M., Yan, F. B., Li, F., Jiang, K. R., Li, D. H., Han, R. L., et al. (2017). Genome-wide DNA methylation profiles reveal novel candidate genes associated with meat quality at different age stages in hens. *Sci. Rep.* 7:45564. doi: 10.1038/srep45564
- Zhang, Y. Y., Zan, L., and Wang, H. (2011). Screening candidate genes related to tenderness trait in qinchuan cattle by genome array. *Mol. Biol. Rep.* 38, 2007–2014. doi: 10.1007/s11033-010-0323-8

Conflict of Interest: The authors declare that the research was conducted in the absence of any commercial or financial relationships that could be construed as a potential conflict of interest.

Copyright © 2020 Zhang, Li, Zhai, Wang, Ma, Zhang, Li, Han, Jiang, Li, Kang and Sun. This is an open-access article distributed under the terms of the Creative Commons Attribution License (CC BY). The use, distribution or reproduction in other forums is permitted, provided the original author(s) and the copyright owner(s) are credited and that the original publication in this journal is cited, in accordance with accepted academic practice. No use, distribution or reproduction is permitted which does not comply with these terms.



Dopamine Receptor D1 Contributes to Cocaine Epigenetic Reprogramming of Histone Modifications in Male Germ Cells

Betina González¹, Samanta N. Gancedo¹, Sahira A. Janeir Garazatua², Eduardo Roldán³, Alfredo D. Vitullo² and Candela R. González^{2*}

¹ Instituto de Investigaciones Farmacológicas, Universidad de Buenos Aires–Consejo Nacional de Investigaciones Científicas y Técnicas, Buenos Aires, Argentina, ² Centro de Estudios Biomédicos Básicos, Aplicados y Desarrollo, Universidad Maimónides, Buenos Aires, Argentina, ³ Departamento de Biodiversidad y Biología Evolutiva, Museo Nacional de Ciencias Naturales, Madrid, Spain

OPEN ACCESS

Edited by:

Huiming Zhang,
Shanghai Center for Plant Stress
Biology (SIBS-CAS), China

Reviewed by:

Daniel Vaiman,
Institut National de la Santé et de la
Recherche Médicale (INSERM),
France
Rodolfo Negri,
Sapienza University of Rome, Italy

*Correspondence:

Candela R. González
gonzalez.candela@maimonides.edu;
cande.gonz80@gmail.com

Specialty section:

This article was submitted to
Epigenomics and Epigenetics,
a section of the journal
Frontiers in Cell and Developmental
Biology

Received: 03 February 2020

Accepted: 12 March 2020

Published: 03 April 2020

Citation:

González B, Gancedo SN, Janeir Garazatua SA, Roldán E, Vitullo AD and González CR (2020) Dopamine Receptor D1 Contributes to Cocaine Epigenetic Reprogramming of Histone Modifications in Male Germ Cells. *Front. Cell Dev. Biol.* 8:216. doi: 10.3389/fcell.2020.00216

Paternal environmental perturbations, including cocaine intake, can affect the development and behavior of the offspring through epigenetic inheritance. However, the mechanism by which cocaine alters the male germ cells epigenome is almost unexplored. Here, we report that cocaine-treated male mice showed alterations on specific histone post-translational modifications (PTMs) including increased silent chromatin marks H3K9me3 and H3K27me3 and decreased active enhancer and promoter marks H3K27ac and H3K4me3 in isolated germ cells. Also, cocaine increased H3K9ac and H4K16ac levels, involved in the replacement of histones by protamines that take place at round spermatid stage. Cocaine also altered histones H3/H4 epigenetic enzymes by increasing acetyltransferase KAT8/MOF, deacetylase SIRT1 and methyltransferase KMT1C/G9A, and decreasing deacetylases HDAC1/2 and demethylase KDM1A/LSD1 protein levels. Moreover, a pre-treatment with dopamine receptor 1 (DRD1) antagonist SCH23390 (SCH) blocked cocaine effects on H3K4me3, H3K27me3, and H4K16ac epigenetic marks. Interestingly, treatment with SCH-only was able to modify most of the histone marks tested here, pointing to a dopamine role in controlling histone PTMs in germ cells. Taken together, our data suggest a key role for DRD1 in mediating cocaine-triggered epigenetic modifications related to the silencing of gene transcription and the histone-to-protamine replacement that controls chromatin architecture of maturing sperm cells, and pinpoints a novel role of the dopaminergic system in the regulation of male germ cells reprogramming.

Keywords: cocaine, male germ cells, epigenetics, dopamine receptor 1, histone post-translational modifications

INTRODUCTION

In the last years, there has been special interest in the characterization of epigenetic mechanisms during spermatogenesis that control the reprogramming of the paternal genome, due to the possible trans-generational transmission of acquired traits (Lacal and Ventura, 2018; Galan et al., 2019). Epigenetic reprogramming involves histones post-translational modifications (PTMs),

DNA methylation, and changes in small non-coding RNAs that modulate gene expression in response to basal transcriptional programs and environmental signals (Jenkins and Carrell, 2012). Histones PTMs differentially signal chromatin states such as open/transcription-permissive or closed/repressed, as well as regulatory elements in DNA including active enhancers and promoters (Miller and Grant, 2013). The spermatogenesis in particular is characterized by an epigenetic program that enables the multiple chromatin reorganizations and unique transcriptional regulation that are required for proper meiotic divisions and sperm maturation. During spermiogenesis, the histone-to-protamine replacement occurs to facilitate chromatin compaction in the sperm, and histones H3/H4 hyperacetylation is essential for this process (Hazzouri et al., 2000; Steilmann et al., 2011; Shirakata et al., 2014; Bao and Bedford, 2016). Importantly, not all histones are removed from the sperm nucleus; a small percentage (5–15%, depending on the species) is retained at specific loci of key spermatogenesis and embryonic developmental genes (Rajender et al., 2011; Carrell, 2012). It is important to point out that, once paternal DNA compaction has occurred, epigenetic marks may not be altered, creating windows of vulnerability in male germs cells to environmental reprogramming during spermatogenesis (Bale, 2015).

In line with this, recent evidence suggests that cocaine administration in animal models can trigger non-genetic inheritance of addiction traits from father to offspring, including negative birth outcomes, increased rates of anxiety and depression as well as impaired cognition affecting development and behavior (Vassoler et al., 2013; White et al., 2016; Wimmer et al., 2017). This paternal transmission is partly due to the incomplete replacement of histones by protamines. For instance, it has been reported an increased H3K9K14ac2 mark associated with the *Bdnf* promoter in the sperm of cocaine-experienced rats as well as their male offspring (Vassoler et al., 2013). Also, we have recently reported that chronic cocaine treatment increased specific germ cell H3/H4 acetylation (González et al., 2018). Thus, histones PTMs represent epigenetic marks potentially inheritable to offspring (Rajender et al., 2011; Vassoler et al., 2013). However, the mechanism by which cocaine alters male germ cells epigenome has been poorly investigated.

Cocaine intake has been associated with impaired male reproductive function including increased oxidative stress, fibrosis of the seminiferous tubules and germ cell apoptosis that leads to a reduction in sperm production (Bracken et al., 1990; Rodriguez et al., 1992; George et al., 1996; Li et al., 1999; Brown et al., 2006; Fronczak et al., 2012; González et al., 2015). In other tissues, cocaine binds to transporters, receptors, voltage-gated ion channels, and plasma proteins and metabolic enzymes (Heard et al., 2008). Importantly, cocaine inhibits monoamine transporters increasing the synaptic concentration of dopamine, nor-epinephrine and serotonin, and which is responsible for cocaine reinforcing and sympathomimetic effects (Heard et al., 2008). It has been established that the major adverse effects of cocaine are due to increased dopamine binding to dopamine receptor 1 (DRD1) in the mesocorticolimbic system (Anderson and Pierce, 2005; Heard et al., 2008). Concerning the testis, we

have previously described that cocaine administration in mice increases tyrosine hydroxylase expression, the rate-limiting enzyme of catecholamine synthesis, and downregulates DRD1 and DRD2, similarly to the mechanism described in the brain (González et al., 2015). Interestingly, we found that the DRD1 receptor was the only one expressed in the spermatogonia nearest the basal lamina of the seminiferous tubules (González et al., 2015). In line with this, early reports have found dopamine located in the wall of seminiferous tubules and interstitial cells (Zieher et al., 1971). Taken together, these findings suggest that the dopamine system could be involved in the epigenetic reprogramming of germ cells.

To date, the mechanisms by which environmental traits can be codified into the male germ cells epigenome and transmitted to the progeny are the focus of intense research. Here, we evaluated the effects of chronic cocaine treatment in adult male mice, and participation of DRD1, on specific histone modifications and epigenetic enzymes, and involved in the structural and dynamic changes of chromatin in isolated male germ cells.

MATERIALS AND METHODS

Animals

Male C57BL/6 mice (10–12 weeks old) from the School of Exact and Natural Sciences of the University of Buenos Aires (UBA) were housed in a light- and temperature-controlled room. Principles of animal care were followed in accordance with “Guidelines for the Care and Use of Mammals in Neuroscience and Behavioral Research” (National Research Council (US) Committee on Guidelines for the Use of Animals in Neuroscience and Behavioral Research, 2003) and approved by IACUC Committee of the Faculty of Pharmacy and Biochemistry, Universidad de Buenos Aires (Protocol Number: EXP-FYB N° 52867/2019 RES(D) N° 2019-3534).

Pharmacological Treatment

Mice were treated with cocaine (Sigma-Aldrich, St. Louis, MO, United States) or vehicle (sterile 0.9% saline), in an intermittent *binge* protocol: 3 i.p. injections, 1 h apart, one day on/off for 13 days (González et al., 2015, 2018). To evaluate the involvement of DRD1 in the deleterious action of cocaine, DRD1 antagonist SCH23390 (TOCRIS bioscience, Ellisville, MO, United States) was injected 15 min before each cocaine or vehicle injection (González et al., 2016). Animals were assigned to four different groups: COC (3 × saline s.c + 3 × cocaine 10 mg/kg i.p.), SCH (3 × SCH23390 0.5 mg/kg s.c + 3 × saline i.p.), SCH-COC (3 × SCH23390 0.5 mg/kg s.c + 3 × cocaine 10 mg/kg i.p.), and VEH (3 × saline s.c + 3 × saline i.p.). Mice were euthanized 24 h after the last binge on day 14 and testes removed for isolation of germ cells.

Germ Cells Isolation

Germ cells were isolated from the testes of the four experimental groups as was previously described (González et al., 2018). The right and left testes of each animal were decapsulated

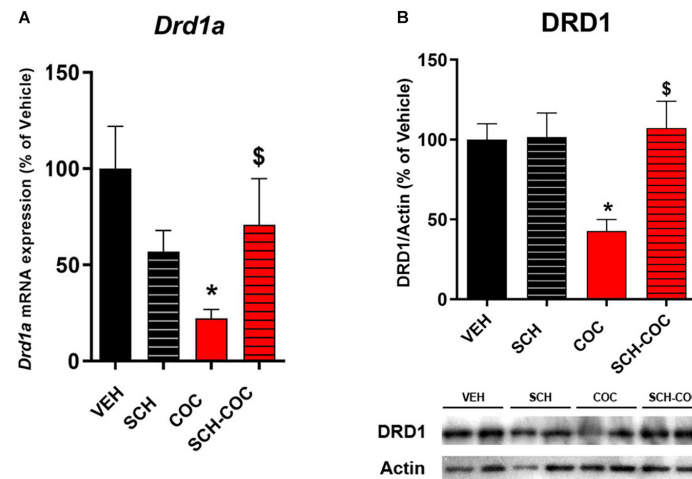


FIGURE 1 | Effect of cocaine (COC), SCH23390 (SCH), and SCH 15 min before COC (SCH-COC) treatments on DRD1 mRNA and protein expression in male germ cells. **(A)** DRD1 mRNA expression (RT-PCR), Kruskal–Wallis-paired comparisons $H = 12.86$, $p = 0.005$. **(B)** DRD1 protein levels (western blot), ANOVA–Bonferroni $F_{(3,23)} = 4.49$, $p = 0.014$. Values indicate mean \pm SEM ($n = 5-7$). * $p < 0.05$ different from VEH, \$ $p < 0.05$ different from COC.

and digested with type I collagenase (0.23 mg/ml, Sigma) in phosphate-buffered saline (PBS) with 0.1% bovine serum albumin for 10 min at 34°C in a shaking water bath. Collagenase activity was stopped by adding cold PBS and the seminiferous tubules were allowed to settle and washed three times with PBS. Then, the seminiferous tubules were mechanically dispersed and the supernatants were filtered (cell strainer, 41 μ m) and centrifuged at 150 g for 15 min. Finally, PBS was removed and the cells were kept at -80°C for molecular studies.

Western Blot

Western blot analyses were conducted as previously described (González et al., 2018). Briefly, homogenates were prepared in a solution containing 50 mM Tris–HCl pH 7.5, 150 mM NaCl, 0.1% Triton X100, 0.5% sodium deoxycholate, 0.1% SDS, 1 mM PMSF, 5 μ g/ml leupeptin, and 5 μ g/ml aprotinin. After removal of cell debris by centrifugation, the protein concentration of the cell lysate was determined. The homogenates were combined with loading buffer containing 4% SDS, 20% glycerol, 10% β -mercaptoethanol, 125 mM Tris, (pH 6.8), and boiled at 100°C for 5 min. Protein samples (15–50 μ g) were separated by 10–12% SDS-PAGE, and the proteins transferred to a PVDF membrane. Blots were incubated with the following primary antibodies: anti-DRD1 (1:50, sc33660), anti-HDAC2 (1:1000, sc-7899), anti-G9a (1:250, sc515726), anti-Tip60 (1:250, sc166323), anti-MOF (1:250, sc81163), anti-LSD1 (1:250, sc271720), and anti-SIRT1 (1:500, sc74465) from Santa Cruz Biotechnology Inc., United States; anti-H3K4me3 (1:1500, ab1012), anti-H3K27me3 (1:250, ab192985), anti-H4K16ac (1:250, ab109463), anti-H3K9me3 (1:1000, ab8898), and anti-H3K27ac (1:1000, ab4729) from Abcam, United Kingdom; anti-HDAC1 (1:1000, 05-100-I) from Millipore, PAIS; anti-H3K9ac (1:500, #9649) from Cell Signaling Technology, United States; and anti-Actin (1:5000, A5441) and anti- α -tubulin (1:10000, T9026) were from Sigma, United States. Immune complexes were

detected with anti-rabbit or anti-mouse secondary antibodies and chemiluminescence reagents (Amersham, United States), and bands were visualized with the image reader ImageQuant 350 (GE Healthcare). The resulting images were quantified with ImageJ (NIH) software. Original blots shown in this study are available in **Supplementary Material**.

Real Time PCR

RT-PCR was conducted as previously described (González et al., 2015, 2018). Briefly, total germ cells RNA was extracted with TRIzol (Invitrogen, Carlsbad, CA, United States) according to the manufacturer's instructions. Total RNA (1 μ g) was treated with DNaseI (Invitrogen, Carlsbad, CA, United States) and used for reverse transcription in a 20 μ l final volume containing M-MLV reverse transcriptase (200 U/ μ l) (Promega, Madison, WI, United States), and random hexamer primers (Biodynamics, Milwaukee, WI, United States). Reverse transcribed cDNA was employed for quantitative PCR using SYBR Green PCR Master Mix and specific primers in a Stratagene MPX500 cyciler (Stratagene, San Diego, United States). Primers sequences for DRD1 and GAPDH are published in González et al. (2015). Data from the reaction were collected and analyzed by the complementary computer software (MxPro3005P v4.10 Build 389, Schema 85). Relative quantitation of gene expression was calculated using standard curves and normalized to GAPDH in each sample.

Statistical Analysis

Statistics were performed using one-way ANOVA followed by Bonferroni *post hoc* test. Data were transformed when required. For data that did not comply with parametric test assumptions, Kruskal–Wallis ANOVA on ranks followed

by paired comparisons was applied. InfoStat 2010 software¹ was used for statistical analysis. Differences were considered significant if $p < 0.05$.

RESULTS

Cocaine Elicits DRD1 Downregulation in Germ Cells via a DRD1-Dependent Mechanism

We have previously reported that male mice spermatogonia express DRD1, and that cocaine administration affects the testicular dopaminergic system decreasing DRD1 mRNA (González et al., 2015). Therefore, we evaluated the effect of cocaine (COC), DRD1 antagonist SCH23390 (SCH) receptor, and SCH administered 15 min before COC (SCH-COC) on DRD1 expression levels in isolated mouse germ cells. Both DRD1 mRNA (Figure 1A) and protein (Figure 1B) expression were significantly reduced in germ cells from cocaine-treated mice compared to vehicle (VEH). Combined SCH-COC treatment was able to revert the effect of cocaine on DRD1 mRNA and protein levels (Figure 1). No differences in mRNA and protein expression of DRD1 were detected in SCH group compared to VEH under these experimental conditions.

Cocaine Elicits Epigenetic Reprogramming of Histone PTMs in Male Germ Cells: Role of DRD1

We evaluated the effect of COC, SCH, and SCH-COC treatments on protein expression levels of specific H3/H4 PTMs related to the epigenetic regulation of gene expression and chromatin remodeling during spermatogenesis: (i) H3K9me3 and H3K27me3 as silent chromatin marks, (ii) H3K27ac and H3K4me3 as active enhancer and promoter marks, and (iii) H3K9ac and H4K16ac as marks of open chromatin states and the replacement of histones by protamines. We found a significant increase in H3K9me3, H3K27me3, H3K9ac, and H4K16ac protein levels in isolated germ cells of COC group compared to VEH (Figure 2). Pre-treatment with SCH counteracted cocaine-increased protein levels of H4K16ac and H3K27me3 (Figure 2). On the other hand, we observed a decrease in H3K27ac and H3K4me3 in isolated germ cells of COC group compared to VEH (Figure 2). Pre-treatment with SCH was able to re-establish protein levels of H3K4me3 (Figure 2).

Cocaine Affects the Expression of Epigenetic Enzymes: Role of DRD1

We evaluated protein expression levels of histone modifying enzymes acetyltransferases/deacetylases (KATs/HDACs) and methyltransferases/demethylases (KMTs/KDMs) in isolated germ cells from all groups. We found decreased protein levels of class I deacetylases HDAC1 and HDAC2 and increased class III deacetylase SIRT1 in COC group compared to VEH, which reverted under pre-treatment with SCH (Figure 3).

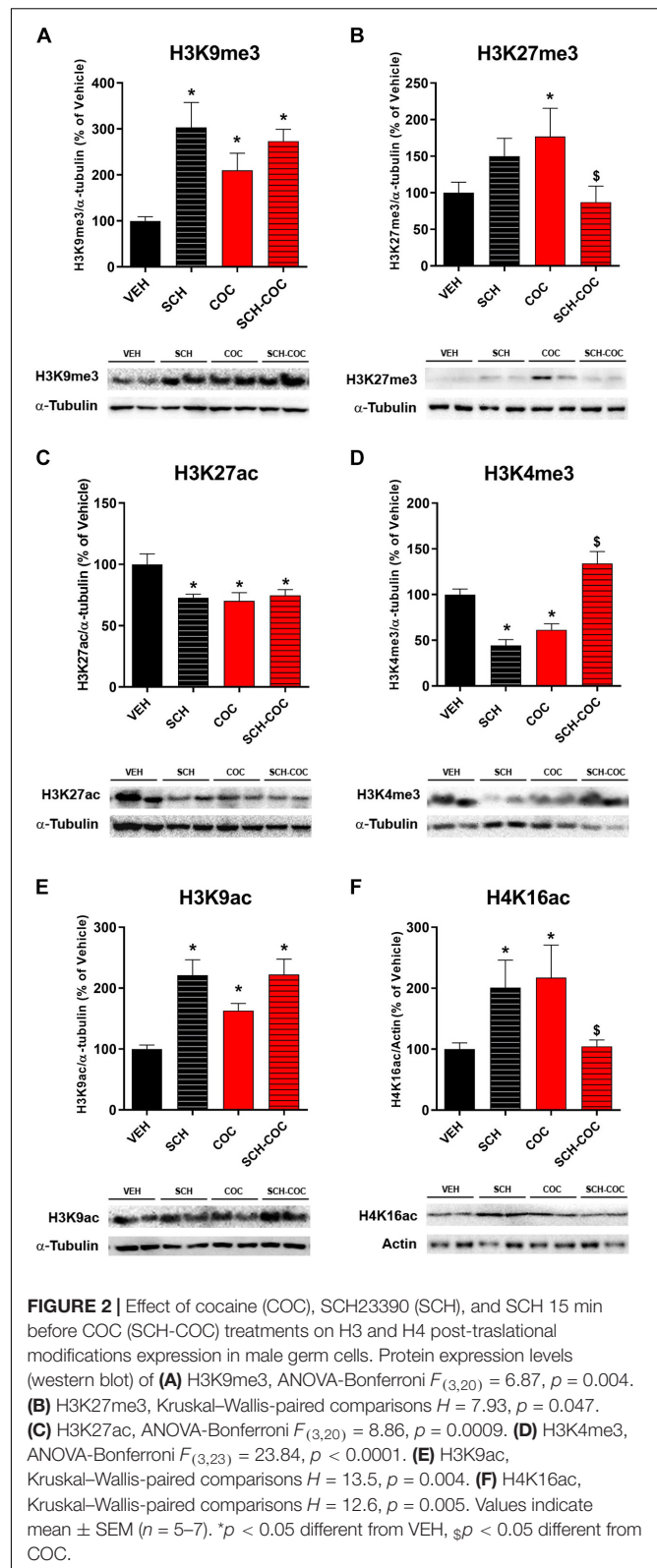


FIGURE 2 | Effect of cocaine (COC), SCH23390 (SCH), and SCH 15 min before COC (SCH-COC) treatments on H3 and H4 post-translational modifications expression in male germ cells. Protein expression levels (western blot) of (A) H3K9me3, ANOVA-Bonferroni $F_{(3,20)} = 6.87$, $p = 0.004$. (B) H3K27me3, Kruskal-Wallis-paired comparisons $H = 7.93$, $p = 0.047$. (C) H3K27ac, ANOVA-Bonferroni $F_{(3,20)} = 8.86$, $p = 0.0009$. (D) H3K4me3, ANOVA-Bonferroni $F_{(3,23)} = 23.84$, $p < 0.0001$. (E) H3K9ac, Kruskal-Wallis-paired comparisons $H = 13.5$, $p = 0.004$. (F) H4K16ac, Kruskal-Wallis-paired comparisons $H = 12.6$, $p = 0.005$. Values indicate mean \pm SEM ($n = 5-7$). * $p < 0.05$ different from VEH, \$ $p < 0.05$ different from COC.

SCH-only treatment was also able to increase SIRT1 (Figure 3). Protein levels of acetyltransferase KAT8/MOF, which catalyzes the specific acetylation of H4K16, increased in COC group

¹ www.infostat.com.ar

compared to VEH and reverted under pre-treatment with SCH (Figure 3). No differences in KAT5/TIP60 protein levels were detected between groups under these experimental conditions (Figure 3). We also found that KDM1A/LSD1, which can demethylate both H3K4me and H3K9me, decreased both in COC and SCH groups compared to VEH, whereas SCH-COC was neither different from VEH nor COC groups. Protein levels of KMT1C/G9A, which catalyzes H3K9 methylation, increased in SCH, COC, and SCH-COC groups compared to VEH (Figure 3).

DISCUSSION

The once controversial idea that parental lifestyle can shape the physiology and behavior of their offspring via epigenetic inheritance has become a vibrant area of research. Accumulating data has shown that male germ cells are epigenetically modified at various time points during spermatogenesis to condense and protect paternal DNA, and also to provide epigenetic information for future embryo development. Here, we report that cocaine, through both DRD1-dependent and independent mechanisms, altered specific histones PTMs and epigenetic modifying enzymes related to the control of gene transcription and to the histone-to-protamine replacement, suggesting a novel role for the dopaminergic system in the regulation of germ cells reprogramming.

It has been found that H3 retention sites in normal sperm are highly conserved, and specific PTMs alterations were linked to epigenetic transgenerational transmission of environmental toxicants exposure traits (Ben Maamar et al., 2018). Retained H3 PTMs in the sperm epigenome were located at key genes that control the spermatogenesis, showing a so-called “spermatogenic memory,” as well as at developmental genes that will take part in the future embryonic program (Carrell and Hammoud, 2010). The active transcription mark H3K4me3 was highly detected in the sperm nucleosome fraction and enriched at gene clusters of developmental genes, non-coding RNAs and spermatogenesis-related genes (Erkek et al., 2013). Also, sperm-retained H3K27ac was found enriched at super-enhancers that are active in adult tissues, suggesting that cis-regulatory elements critical for adult cell differentiation are already specified in sperm (Jung et al., 2017). On the other hand, H3K9me3 was found retained at satellite repeats in mouse sperm, whereas H3K27me3 was found enriched in promoters of developmental genes that are repressed in the early pre-implantation stages of embryogenesis (Hammoud et al., 2009; Brykczynska et al., 2010; Carrell, 2012; Erkek et al., 2013). Here, we found that cocaine treatment increased silent chromatin marks H3K9me3/H3K27me3 and decreased active enhancer and promoter marks H3K27ac/H3K4me3 in mouse germ cells. It has been shown that DNA methylation induces H3K27me3 deposition at specific gene promoters (Hammoud et al., 2009; King et al., 2016), and we have previously found that cocaine increased 5-mC levels in DNA from isolated germ cells and sperm (González et al., 2018). Interestingly, blockade of DRD1 was only able to revert cocaine-induced effects on the functionally opposite histone marks H3K4me3

and H3K27me3. Sperm retained nucleosomes often contain H3K4me3/H3K27me3 bivalent marking, characteristic of gene preactivation termed “poising” (Hammoud et al., 2014), and localize at the promoters of hundreds of developmental genes, including Hox-, Fox-, Sox-, and Gata-families (Hammoud et al., 2009; Brykczynska et al., 2010). Therefore, our data suggest that cocaine, through DRD1 activation, may cause H3K4me3/H3K27me3 imbalance potentially affecting the embryonic developmental program. In line with this, we found that cocaine treatment increased KMT1C/G9A and decreased KDM1A/LSD1 enzymes. KMT1C/G9A is a key mediator of the epigenetic effects of cocaine in the mesolimbic system (Maze et al., 2010; Anderson et al., 2019) and has been described as a crucial epigenetic marker of heterochromatin formation during meiosis (Tachibana et al., 2007). KDM1A/LSD1 participates in the demethylation of H3K4/K9 and is required for spermatogonial differentiation and germ cell survival in mice (Myrick et al., 2017). Also, it has been found that many bivalent genes have increased H3K4me3 and decreased H3K27me3 levels and are occupied by KDM1A/LSD1 to maintain low levels of H3K4me2 that often co-localized with H3K4me3 (Adamo et al., 2011; Whyte et al., 2012). Additionally, KDM1A/LSD1 inactivation results in increased global H3K27me3 leading to suppression of gene expression (Leis et al., 2012). Interestingly, KDM1A/LSD1 was found in the same transcriptional repressor complex with HDAC1/2 (Kelly et al., 2018), which were also downregulated in germ cells after cocaine treatment (González et al., 2018), and its expression tightly correlated with H3K4me3 levels in male germ cells (Godmann et al., 2007). Altogether, these data suggest that cocaine promotes alterations in KDM/KMT enzymes that would trigger altered methylation patterns of H3 lysine residues associated with the silencing of genetic transcription in mouse germ cells.

During spermatogenesis, specific histones PTMs work together to facilitate genome re-organization and packaging of the sperm nucleus. Hyperacetylation of H3K9 and H4K16 triggers the histone-to-protamine replacement, which takes place at stage 8–12 round spermatids (Hazzouri et al., 2000; Steilmann et al., 2011; Shirakata et al., 2014). Here, we found increased H3K9ac and H4K16ac in mouse germ cells after cocaine treatment. We also found altered levels of the H4K16-specific acetyltransferase KAT8/MOF and deacetylases HDAC1/2 and SIRT1, which were all found to participate in the histone-to-protamine transition at round spermatid stage (Fenic et al., 2004; Bell et al., 2014; Jiang et al., 2018). In addition, we found that SCH pre-treatment was able to revert cocaine-induced effects on H4K16ac as well as HDAC1/2, SIRT1, and KAT8/MOF. These data suggest that cocaine, via DRD1 regulation, has a key role in modulating the acetylation status of male epigenome most likely interfering with histone eviction and chromatin reassembly.

The data presented here showed that DRD1 blockade is able to re-establish the levels of some epigenetic marks altered by cocaine. Also, SCH-only treatment was able to modify most of the epigenetic histone PTMs as well as SIRT1, KDM1A/LSD1, and KMT1C/G9A, further supporting a novel role of dopamine controlling epigenetic marks during spermatogenesis. Noteworthy, H4K16ac, H3K4me3, H3K27me3,

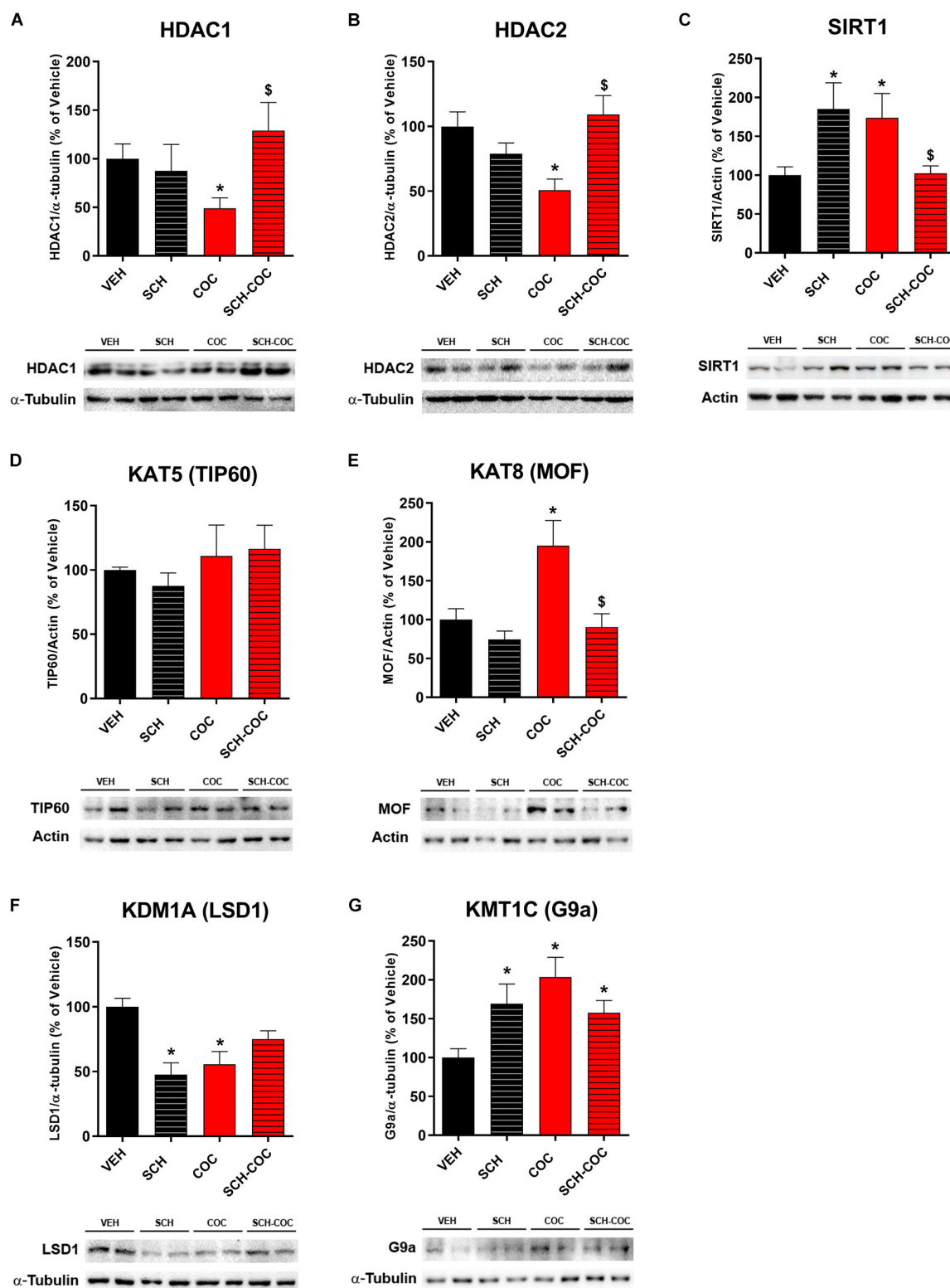


FIGURE 3 | Effect of cocaine (COC), SCH23390 (SCH), and SCH 15 min before COC (SCH-COC) treatments on histone modifying enzymes expression in male germ cells. Protein expression levels (western blot) of **(A)** HDAC1, Kruskal–Wallis-paired comparisons $H = 7.9$, $p = 0.048$. **(B)** HDAC2, ANOVA–Bonferroni $F_{(3,24)} = 6.32$, $p = 0.003$. **(C)** SIRT1, Kruskal–Wallis-paired comparisons $H = 10.2$, $p = 0.016$. **(D)** TIP60, ANOVA–Bonferroni $F_{(3,20)} = 1$, $p > 0.05$. **(E)** MOF, ANOVA–Bonferroni $F_{(3,24)} = 6.8$, $p = 0.002$. **(F)** LSD1, ANOVA–Bonferroni $F_{(3,20)} = 9.5$, $p = 0.0009$. **(G)** G9a, Kruskal–Wallis-paired comparisons $H = 11.3$, $p = 0.01$. * $p < 0.05$ different from VEH, \$ $p < 0.05$ different from COC.

and SIRT1 showed that SCH-only treatment behaved like cocaine, but returned to control values in the combined SCH-COC group. This type of response is typical of the so-called “inverted U-shaped” effect of DRD1, extensively studied in brain cortical cells, where both low (as in SCH) and high (as in COC) dopamine concentrations impact DRD1 signaling causing similar detrimental effects in cells function and cognition (Williams and Castner, 2006; González et al., 2016). Here, cocaine may have increased local dopamine production by TH-expressing neuron-like-cells and meiotic germ cells (Frungieri et al., 2000; González et al., 2015), as well as plasmatic dopamine through sympathetic nerves and/or adrenal medulla release (Rubí and Maechler, 2010). Also, the DRD1-mediated effects found in germ cells could have been triggered by autocrine-paracrine effects of DRD1-expressing spermatogonia (González et al., 2015), by interstitial-tubular effects of Leydig cells expressing DRD1 (González et al., 2015), and also by endocrine hypothalamic-pituitary factors under the control of the central tubero-infundibular dopamine circuit such as prolactin (Rubí and Maechler, 2010). Our data point to DRD1 involvement in germ cell epigenetic homeostasis, but also, that these cocaine-reprogramming effects in germ cells are potentially reversible. This type of evidence becomes of great importance due to the existence of several therapeutic drugs that affect the dopaminergic system and cause male infertility. For instance, it was found that dopamine antagonists and antidepressants such as reserpine (Yamauchi et al., 2000), dopamine agonist bromocriptine (Richardson et al., 1984), and antihypertensive drug methyl dopa (Chapin and Williams, 1989) cause testicular atrophy. Thus, epigenetic changes induced by dopamine imbalance in male germ cells could be reversible if the environmental conditions return to normal.

CONCLUSION

In conclusion, our findings strongly suggest that cocaine can induce an epigenetic reprogramming of male germ cells through changes in epigenetic enzymes and histones specific PTMs which could trigger silencing of genetic expression and, moreover, alter the histone-to-protamine replacement event necessary to chromatin reorganization and DNA compaction. Although this is a preliminary study performed in samples containing all the germ cells populations, we show novel evidence that pinpoint a key role for DRD1 in mediating specific epigenetic modifications induced by cocaine in mouse germ cells. Further studies in specific cell stages of spermatogenesis obtained by cell sorting will be performed in order to expand to the knowledge about the mechanisms by which environmental effects such as addictive stimulants consumption can be codified in the paternal epigenome and transmitted across generations.

REFERENCES

- Adamo, A., Sesé, B., Boue, S., Castaño, J., Paramonov, I., Barrero, M. J., et al. (2011). LSD1 regulates the balance between self-renewal and differentiation in human embryonic stem cells. *Nat. Cell Biol.* 13, 652–659. doi: 10.1038/ncb2246

DATA AVAILABILITY STATEMENT

The datasets generated for this study are available on request to the corresponding author.

ETHICS STATEMENT

The animal study was reviewed and approved by Principles of animal care were followed in accordance with “Guidelines for the Care and Use of Mammals in Neuroscience and Behavioral Research” (National Research Council (US) Committee on Guidelines for the Use of Animals in Neuroscience and Behavioral Research, 2003) and approved by IACUC Committee of the Faculty of Pharmacy and Biochemistry, Universidad de Buenos Aires (Protocol Number: EXP-FYB N° 52867/2019 RES(D) N° 2019-3534).

AUTHOR CONTRIBUTIONS

CG and BG contributed to conception and design of the study. CG, BG, SG, and SJ contributed to the methodology. BG performed the statistical analysis. CG and BG wrote the first draft of the manuscript. AV and ER contributed to the writing and editing of the manuscript. All authors read and approved the submitted version.

FUNDING

This work was supported by Agencia Nacional de Promoción Científica y Tecnológica (PICT 2017-0267, CG) and Fundación Científica Felipe Fiorellino (AV and CG).

ACKNOWLEDGMENTS

CG has been authorized to study drug abuse substances in animal models by ANMAT (National Board of Medicine Food and Medical Technology, Ministerio de Salud, Argentina).

SUPPLEMENTARY MATERIAL

The Supplementary Material for this article can be found online at: <https://www.frontiersin.org/articles/10.3389/fcell.2020.00216/full#supplementary-material>

- Anderson, E. M., Sun, H., Guzman, D., Taniguchi, M., Cowan, C. W., Maze, I., et al. (2019). Knockdown of the histone di-methyltransferase G9a in nucleus accumbens shell decreases cocaine self-administration, stress-induced reinstatement, and anxiety. *Neuropsychopharmacology* 44, 1370–1376. doi: 10.1038/s41386-018-0305-4

- Anderson, S. M., and Pierce, R. C. (2005). Cocaine-induced alterations in dopamine receptor signaling: implications for reinforcement and reinstatement. *Pharmacol. Ther.* 106, 389–403. doi: 10.1016/j.pharmthera.2004.12.004
- Bale, T. L. (2015). Epigenetic and transgenerational reprogramming of brain development. *Nat. Rev. Neurosci.* 16, 332–344. doi: 10.1038/nrn3818
- Bao, J., and Bedford, M. T. (2016). Epigenetic regulation of the histone-to-protamine transition during spermiogenesis. *Reproduction* 151, 55–70.
- Bell, E. L., Nagamori, I., Williams, E. O., Del Rosario, A. M., Bryson, B. D., Watson, N., et al. (2014). SirT1 is required in the male germ cell for differentiation and fecundity in mice. *Development* 141, 3495–3504. doi: 10.1242/dev.110627
- Ben Maamar, M., Sadler-Riggleman, I., Beck, D., and Skinner, M. K. (2018). Epigenetic transgenerational inheritance of altered sperm histone retention sites. *Sci. Rep.* 8:5308. doi: 10.1038/s41598-018-23612-y
- Bracken, M. B., Eskenazi, B., Sachse, K., McSharry, J. E., Hellenbrand, K., and Leo-Summers, L. (1990). Association of cocaine use with sperm concentration, motility, and morphology. *Fertil. Steril.* 53, 315–322. doi: 10.1016/s0015-0282(16)53288-9
- Brown, T. T., Wisniewski, A. B., and Dobs, A. S. (2006). Gonadal and adrenal abnormalities in drug users: cause or consequence of drug use behavior and poor health outcomes. *Am. J. Infect. Dis.* 2, 130–135. doi: 10.3844/ajidsp.2006.130.135
- Brykczynska, U., Hisano, M., Erkek, S., Ramos, L., Oakeley, E. J., Roloff, T. C., et al. (2010). Repressive and active histone methylation mark distinct promoters in human and mouse spermatozoa. *Nat. Struct. Mol. Biol.* 17, 679–687. doi: 10.1038/nsmb.1821
- Carrell, D. T. (2012). Epigenetics of the male gamete. *Fertil. Steril.* 97, 267–274. doi: 10.1016/j.fertnstert.2011.12.036
- Carrell, D. T., and Hammoud, S. S. (2010). The human sperm epigenome and its potential role in embryonic development. *Mol. Hum. Reprod.* 16, 37–47. doi: 10.1093/molehr/gap090
- Chapin, R. E., and Williams, J. (1989). Mechanistic approaches in the study of testicular toxicity: toxicants that affect the endocrine regulation of the testis. *Toxicol. Pathol.* 17, 446–451. doi: 10.1177/019262338901700220
- Erkek, S., Hisano, M., Liang, C. Y., Gill, M., Murr, R., Dieker, J., et al. (2013). Molecular determinants of nucleosome retention at CpG-rich sequences in mouse spermatozoa. *Nat. Struct. Mol. Biol.* 20, 868–875. doi: 10.1038/nsmb.2599
- Fenic, I., Sonnack, V., Failing, K., Bergmann, M., and Steger, K. (2004). In vivo effects of histone-deacetylase inhibitor trichostatin-A on murine spermatogenesis. *J. Androl.* 25, 811–818. doi: 10.1002/j.1939-4640.2004.tb02859.x
- Fronczak, C. M., Kim, E. D., and Barqawi, A. B. (2012). The insults of illicit drug use on male fertility. *J. Androl.* 33, 515–528. doi: 10.2164/jandrol.110.011874
- Frungeri, M. B., Urbanski, H. F., Höhne-Zell, B., and Mayerhofer, A. (2000). Neuronal elements in the testis of the rhesus monkey: ontogeny, characterization and relationship to testicular cells. *Neuroendocrinology* 71, 43–50. doi: 10.1159/000054519
- Galan, C., Krykbaeva, M., and Rando, O. J. (2019). Early life lessons: the lasting effects of germline epigenetic information on organismal development. *Mol. Metab.* doi: 10.1016/j.molmet.2019.12.004 [Epub ahead of print].
- George, V. K., Li, H., Teloken, C., Grignon, D. J., Lawrence, W. D., and Dhabuwala, C. B. (1996). Effects of long-term cocaine exposure on spermatogenesis and fertility in peripubertal male rats. *J. Urol.* 155, 327–331. doi: 10.1097/00005392-199601000-00133
- Godmann, M., Auger, V., Ferraroni-Aguai, V., Di Sauro, A., Sette, C., Behr, R., et al. (2007). Dynamic regulation of histone H3 methylation at lysine 4 in mammalian spermatogenesis. *Biol. Reprod.* 77, 754–764. doi: 10.1095/biolreprod.107.062265
- González, B., Pantoja, C. R. G., Sosa, M. H., Vitullo, A. D., Bisagno, V., and González, C. R. (2018). Cocaine alters the mouse testicular epigenome with direct impact on histone acetylation and DNA methylation marks. *Reprod. Biomed. Online* 37, 269–278. doi: 10.1016/j.rbmo.2018.05.014
- González, B., Rivero-Echeto, C., Muñoz, J. A., Cadet, J. L., García-Rill, E., Urbano, F. J., et al. (2016). Methamphetamine blunts Ca(2+) currents and excitatory synaptic transmission through D1/5 receptor-mediated mechanisms in the mouse medial prefrontal cortex. *Addict. Biol.* 21, 589–602. doi: 10.1111/adb.12249
- González, C. R., González, B., Matzkin, M. E., Muñoz, J. A., Cadet, J. L., García-Rill, E., et al. (2015). Psychostimulant-induced testicular toxicity in mice: evidence of cocaine and caffeine effects on the local dopaminergic system. *PLoS One* 10:e0142713. doi: 10.1371/journal.pone.0142713
- Hammoud, S. S., Low, D. H., Yi, C., Carrell, D. T., Guccione, E., and Cairns, B. R. (2014). Chromatin and transcription transitions of mammalian adult germline stem cells and spermatogenesis. *Cell Stem Cell* 7, 239–253. doi: 10.1016/j.stem.2014.04.006
- Hammoud, S. S., Nix, D. A., Zhang, H., Purwar, J., Carrell, D. T., and Cairns, B. R. (2009). Distinctive chromatin in human sperm packages genes for embryo development. *Nature* 460, 473–478. doi: 10.1038/nature08162
- Hazzouri, M., Pivot-Pajot, C., Faure, A. K., Usson, Y., Pelletier, R., Sèle, B., et al. (2000). Regulated hyperacetylation of core histones during mouse spermatogenesis: involvement of histone deacetylases. *Eur. J. Cell Biol.* 79, 950–960. doi: 10.1078/0171-9335-00123
- Heard, K., Palmer, R., and Zahniser, N. R. (2008). Mechanisms of acute cocaine toxicity. *Open Pharmacol. J.* 2, 70–78. doi: 10.2174/1874143600802010070
- Jenkins, T. G., and Carrell, D. T. (2012). The sperm epigenome and potential implications for the developing embryo. *Reproduction* 143, 727–734. doi: 10.1530/REP-11-0450
- Jiang, H., Gao, Q., Zheng, W., Yin, S., Wang, L., Zhong, L., et al. (2018). MOF influences meiotic expansion of H2AX phosphorylation and spermatogenesis in mice. *PLoS Genet.* 14:e1007300. doi: 10.1371/journal.pgen.1007300
- Jung, Y. H., Sauria, M. E. G., Lyu, X., Cheema, M. S., Ausio, J., Taylor, J., et al. (2017). Chromatin states in mouse sperm correlate with embryonic and adult regulatory landscapes. *Cell Rep.* 18, 1366–1382. doi: 10.1016/j.celrep.2017.01.034
- Kelly, R. D., Chandru, A., Watson, P. J., Song, Y., Blades, M., Robertson, N. S., et al. (2018). Histone deacetylase (HDAC) 1 and 2 complexes regulate both histone acetylation and crotonylation in vivo. *Sci. Rep.* 8:14690. doi: 10.1038/s41598-018-32927-9
- King, A. D., Huang, K., Rubbi, L., Liu, S., Wang, C. Y., and Wang, Y. (2016). Reversible regulation of promoter and enhancer histone landscape by DNA methylation in mouse embryonic stem cells. *Cell Rep.* 17, 289–302. doi: 10.1016/j.celrep.2016.08.083
- Lacal, I., and Ventura, R. (2018). Epigenetic inheritance: concepts, mechanisms and perspectives. *Front. Mol. Neurosci.* 11:292. doi: 10.3389/fnmol.2018.00292
- Leis, O., Eguara, A., Lopez-Arribillaga, E., Alberdi, M. J., Hernandez-Garcia, S., Elorriaga, K., et al. (2012). Sox2 expression in breast tumours and activation in breast cancer stem cells. *Oncogene* 31, 1354–1365. doi: 10.1038/onc.2011.338
- Li, H., Jiang, Y., Rajpurkar, A., Dunbar, J. C., and Dhabuwala, C. B. (1999). Cocaine induced apoptosis in rat testes. *J. Urol.* 162, 213–216. doi: 10.1097/00005392-199907000-00070
- Maze, I., Covington, H. E. III, Dietz, D. M., LaPlant, Q., Renthal, W., Russo, S. J., et al. (2010). Essential role of the histone methyltransferase G9a in cocaine-induced plasticity. *Science* 327, 213–216. doi: 10.1126/science.1179438
- Miller, J. L., and Grant, P. A. (2013). The role of DNA methylation and histone modifications in transcriptional regulation in humans. *Subcell. Biochem.* 61, 289–317. doi: 10.1007/978-94-007-4525-4_13
- Myrick, D. A., Christopher, M. A., Scott, A. M., Simon, A. K., Donlin-Asp, P. G., Kelly, W. G., et al. (2017). KDM1A/LSD1 regulates the differentiation and maintenance of spermatogonia in mice. *PLoS One* 12:e0177473. doi: 10.1371/journal.pone.0177473
- National Research Council (US) Committee on Guidelines for the Use of Animals in Neuroscience and Behavioral Research (2003). *Guidelines for the Care and Use of Mammals in Neuroscience and Behavioral Research*. Washington, DC: National Academies Press (US). Available online at: <https://www.ncbi.nlm.nih.gov/books/NBK43327/>
- Rajender, S., Avery, K., and Agarwal, A. (2011). Epigenetics, spermatogenesis and male infertility. *Mutat. Res.* 727, 62–71.
- Richardson, B. P., Turkalj, I., and Fluckieger, E. (1984). “Bromocriptine,” in *Safety Testing of New Drugs: Laboratory Predictions and Clinical Performance*, eds D. R. Laurence, A. E. M. McLean, and M. Weatherall, (London: Academic Press), 19–63.

- Rodriguez, M. C., Sanchez-Yague, J., and Paniagua, R. (1992). Effects of cocaine on testicular structure in the rat. *Reprod. Toxicol.* 6, 51–55. doi: 10.1016/0890-6238(92)90020-t
- Rubi, B., and Maechler, P. (2010). Minireview: new roles for peripheral dopamine on metabolic control and tumor growth: let's seek the balance. *Endocrinology* 151, 5570–5581. doi: 10.1210/en.2010-0745
- Shirakata, Y., Hiradate, Y., Inoue, H., Sato, E., and Tanemura, K. (2014). Histone h4 modification during mouse spermatogenesis. *J. Reprod. Dev.* 60, 383–387. doi: 10.1262/jrd.2014-018
- Steilmann, C., Paradowska, A., Bartkuhn, M., Vieweg, M., Schuppe, H. C., Bergmann, M., et al. (2011). Presence of histone H3 acetylated at lysine 9 in male germ cells and its distribution pattern in the genome of human spermatozoa. *Reprod. Fertil. Dev.* 23, 997–1011. doi: 10.1071/RD10197
- Tachibana, M., Nozaki, M., Takeda, N., and Shinkai, Y. (2007). Functional dynamics of H3K9 methylation during meiotic prophase progression. *EMBO J.* 26, 3346–3359. doi: 10.1038/sj.emboj.7601767
- Vassoler, F. M., White, S. L., Schmidt, H. D., Sadri-Vakili, G., and Pierce, R. C. (2013). Epigenetic inheritance of a cocaine-resistance phenotype. *Nat. Neurosci.* 16, 42–47. doi: 10.1038/nn.3280
- White, S. L., Vassoler, F. M., Schmidt, H. D., Pierce, R. C., and Wimmer, M. E. (2016). Enhanced anxiety in the male offspring of sires that self-administered cocaine. *Addict. Biol.* 21, 802–810. doi: 10.1111/adb.12258
- Whyte, W. A., Bilodeau, S., Orlando, D. A., Hoke, H. A., Frampton, G. M., Foster, C. T., et al. (2012). Enhancer decommissioning by LSD1 during embryonic stem cell differentiation. *Nature* 482, 221–225. doi: 10.1038/nature10805
- Williams, G. V., and Castner, S. A. (2006). Under the curve: critical issues for elucidating D1 receptor function in working memory. *Neuroscience* 139, 263–276. doi: 10.1016/j.neuroscience.2005.09.028
- Wimmer, M. E., Briand, L. A., Fant, B., Guercio, L. A., Arreola, A. C., Schmidt, H. D., et al. (2017). Paternal cocaine taking elicits epigenetic remodeling and memory deficits in male progeny. *Mol. Psychiatry* 22, 1641–1650. doi: 10.1038/mp.2017.8
- Yamauchi, K., Takaura, Y., Noto, T., Saegusa, T., Nakatsuji, S., Ohishi, Y., et al. (2000). Collaborative work to evaluate toxicity on male reproductive organs by repeated dose studies in rats 7). Effects of reserpine in 2- and 4-weeks studies. *J. Toxicol. Sci.* 25, 79–85. doi: 10.2131/jts.25.specialissue_79
- Zieher, L. M., Debeljuk, L., Iturriza, F., and Mancini, R. E. (1971). Biogenic amine concentration in testes of rats at different ages. *Endocrinology* 88, 351–354. doi: 10.1210/endo-88-2-351

Conflict of Interest: The authors declare that the research was conducted in the absence of any commercial or financial relationships that could be construed as a potential conflict of interest.

Copyright © 2020 González, Gancedo, Janeir Garazatua, Roldán, Vitullo and González. This is an open-access article distributed under the terms of the Creative Commons Attribution License (CC BY). The use, distribution or reproduction in other forums is permitted, provided the original author(s) and the copyright owner(s) are credited and that the original publication in this journal is cited, in accordance with accepted academic practice. No use, distribution or reproduction is permitted which does not comply with these terms.



ZNF143 in Chromatin Looping and Gene Regulation

Bingyu Ye^{1,2,3,4,5,6†}, Ganggang Yang^{1,2,3,4,5,6†}, Yuanmeng Li⁴, Chunyan Zhang^{1,2,3,4,5,6*}, Qiwen Wang^{1,2,3,4,5,6*} and Guoying Yu^{1,2,3,4,5,6*}

¹ State Key Laboratory of Cell Differentiation and Regulation, Henan Normal University, Xinxiang, China, ² Henan International Joint Laboratory of Pulmonary Fibrosis, Henan Normal University, Xinxiang, China, ³ Henan Center for Outstanding Overseas Scientists of Pulmonary Fibrosis, Henan Normal University, Xinxiang, China, ⁴ College of Life Sciences, Henan Normal University, Xinxiang, China, ⁵ Institute of Biomedical Science, Henan Normal University, Xinxiang, China, ⁶ Overseas Expertise Introduction Center for Discipline Innovation of Pulmonary Fibrosis (111 Project), Henan Normal University, Xinxiang, China

OPEN ACCESS

Edited by:

Huiming Zhang,
Shanghai Institutes for Biological
Sciences (CAS), China

Reviewed by:

Hye Jin You,
National Cancer Center, South Korea
Dag H. Yasui,
University of California, Davis,
United States

*Correspondence:

Chunyan Zhang
zcy1119sdc@163.com
Qiwen Wang
wangqiwen@htu.edu.cn
Guoying Yu
guoyingyu@htu.edu.cn

[†] These authors have contributed
equally to this work

Specialty section:

This article was submitted to
Epigenomics and Epigenetics,
a section of the journal
Frontiers in Genetics

Received: 25 December 2019

Accepted: 20 March 2020

Published: 07 April 2020

Citation:

Ye B, Yang G, Li Y, Zhang C,
Wang Q and Yu G (2020) ZNF143
in Chromatin Looping and Gene
Regulation. *Front. Genet.* 11:338.
doi: 10.3389/fgene.2020.00338

ZNF143, a human homolog of the transcriptional activator Staf, is a C2H2-type protein consisting of seven zinc finger domains. As a transcription factor (TF), ZNF143 is sequence specifically binding to chromatin and activates the expression of protein-coding and non-coding genes on a genome scale. Although it is ubiquitous expressed, its expression in cancer cells and tissues is usually higher than that in normal cells and tissues. Therefore, abnormal expression of ZNF143 is related to cancer cell survival, proliferation, differentiation, migration, and invasion, suggesting that new small molecules can be designed by targeting ZNF143 as it may be a good potential biomarker and therapeutic target for related cancers. However, the mechanism on how ZNF143 regulates its targeting gene remains unclear. Recently, with the development of chromatin conformation capture (3C) and its derivatives, and high-throughput sequencing technology, new findings have been obtained in the study of ZNF143. Pioneering studies have showed that ZNF143 binds directly to promoters and contributes to chromatin interactions connecting promoters to distal regulatory elements, such as enhancers. Further, it has proved that ZNF143 is involved in CCCTC-binding factor (CTCF) in establishing the conserved chromatin loops by cooperating with cohesin and other partners. These results indicate that ZNF143 is a key loop formation factor. In addition, we report ZNF143 is dynamically bound to chromatin during the cell cycle demonstrated that it is a potential mitotic bookmarking factor. It may be associated with CTCF for mitosis-to-G1 phase transition and chromatin loop re-establishment in early G1 phase. In the future, researchers could further clarify the fine mechanism of ZNF143 in mediating chromatin loops with the help of CUT&RUN (CUT&Tag) and Cut-C technology. Thus, in this review, we summarize the research progress of TF ZNF143 in detail and also predict the potential functions of ZNF143 in cell fate and identity based on our recent discoveries.

Keywords: transcription factor, ZNF143, biomarker, chromatin organization, loop

INTRODUCTION

Schuster et al. (1995) found a transcription factor (TF), which can be bound specifically to the promoter of selenocysteine tRNA in *Xenopus* oocytes and named it Staf (selenocysteine tRNA gene transcription activating factor). In the same year, Tommerup and Vissing (1995) reported zinc finger protein 143 (ZNF143), a human homolog of the transcriptional activator Staf, was located on the human 11th chromosome, 11p15.3–15.4. Subsequently, Adachi et al. (1998) isolated and characterized m-Staf from mouse mammary gland, which is consistent with human ZNF143. ZNF143 is a member of the Kruppel family and is a widely expressed transcriptional activation factor that regulates gene expression associated with cell cycle and DNA replication (Izumi et al., 2010). Therefore, it is widely involved in a variety of cellular and pathogenic processes, such as cell survival, growth, proliferation, etc. (Table 1). However, the molecular mechanism of ZNF143 in regulating gene expression remains elusive.

In recent years, studies have revealed that ZNF143 not only exists in most cancer cells but is also necessary for the normal development of tissues (Izumi et al., 2011; Halbig et al., 2012;

Kawatsu et al., 2014; Paek et al., 2014; Wei et al., 2016; Paek et al., 2017). Genome-wide analyses have shown that TF ZNF143 with sequence binding specificity is usually bound to the promoter of its regulatory gene and promotes the formation of chromatin loop by interacting with other chromatin structure and organization factors, such as CCCTC-binding factor (CTCF) and cohesin (Heidari et al., 2014; Bailey et al., 2015; Ye et al., 2016; Yang et al., 2017; Mourad and Cuvier, 2018; Wen et al., 2018). In summary, as a key TF, ZNF143 plays a critical role in chromatin loop formation and gene regulation (Table 2), illustrating great importance in the study of its regulatory mechanism.

THE STRUCTURAL FEATURES OF ZNF143

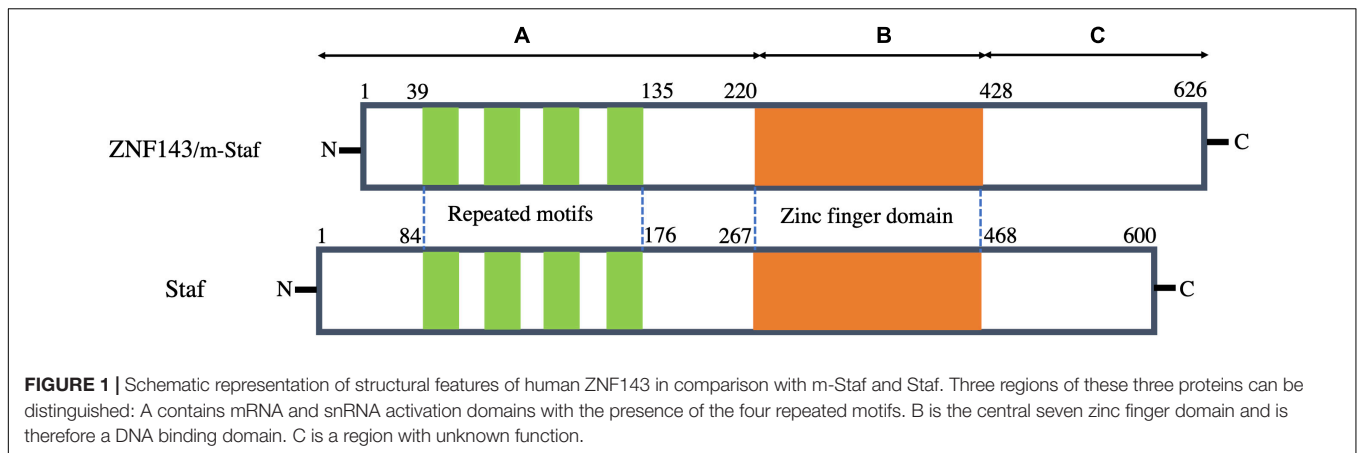
The amino acid sequence of human ZNF143 is highly homologous to both m-Staf and Staf. Among its sequence, 97.1 and 84% residues are identical to those of m-Staf and Staf, respectively (Schuster et al., 1995; Adachi et al., 1998; Myslinski et al., 1998). Structurally, these proteins consist of three regions (A, B, and C) (Figure 1). Analysis of the three regions indicates that the central region B (residues 220–428 in ZNF143 and m-Staf, residues 267–468 in Staf) encompasses seven tandemly repeated zinc fingers of the C2H2 type, is highly basic, while the regions A (residues 1–219 in ZNF143 and m-Staf, residues 1–266 in Staf) encodes four repeated motifs and C (residues

TABLE 1 | The role of ZNF143 in cancer progression.

ZNF143 status	Cancer type	Association	References
Knockdown	Human prostate cancer PC3	Induce cell apoptosis	Izumi et al., 2010
	Breast carcinoma	Increase cellular motility	Paek et al., 2017
	Colon cancer (HCT116)	Increase cell migration and invasion	Paek et al., 2014
	HeLa-S3	Reduce cell proliferation	Ngondo-Mbongo et al., 2013
	Breast cancer	Better cell survival	Paek et al., 2019
	HeLa	Reduce cell proliferation, cell-cycle progression, and cell viability	Parker et al., 2014
Overexpression	Colon cancer	Increase cell plasticity	Verma et al., 2019
	PC3 prostate cancer cell lines	Increase cell division	Izumi et al., 2011
	Gastric cancer(GC)	Enhance GC migration	Wei et al., 2016
	HepG2 and HeLa	Increase cell survival and differentiation	Grossman et al., 2014
Positively expression	Lung cancer	Increase cell growth	Kawatsu et al., 2014
	Lung adenocarcinoma	With highly invasive and proliferation	Kawatsu et al., 2014
	Ovarian tumors and Low-grade ovarian cancers	Relate to cancer invasion, metastasis formation	Sadlecki et al., 2019

TABLE 2 | ZNF143 plays a critical role in chromatin interaction.

Cell type	Detection method	Interaction factor	References
GM12878, K562, HeLaS3	Carbon-copy chromatin conformation capture (5C), 3C, ChIP-seq	Cohesin (SMC3), CTCF	Bailey et al., 2015
GM12878, K562	ChIA-PET, ChIP-seq, RNA-seq	Cohesin (RAD21), CTCF	Heidari et al., 2014
GM12878, K562	ChIA-PET, ChIP-seq	Cohesin (RAD21 and SMC3), CTCF	Ye et al., 2016
Kc167, GM12878	Hi-C, ChIP-seq	Cohesin (RAD21), CTCF	Mourad and Cuvier, 2018
HEK293T	Hi-C	Cohesin (RAD21), CTCF	Wen et al., 2018
HeLa-S3, HEK293, K562, HPB-ALL, NIH3T3, mESC, MEF	ChIP-Seq, RNA-seq	Notch1, THAP11	Ngondo-Mbongo et al., 2013
293T/17, HeLa, SW620, T98G	ChIP-Seq	THAP11, HCF-1	Parker et al., 2014; Vinckeivicius et al., 2015
Mouse ES	ChIP	Oct4	Chen et al., 2008
Human TLL	RNA-microarray, ChIP-Seq	Notch1, RBPJ	Wang et al., 2011
HeLa	RNA-microarray, ChIP-Seq	HCF-1, THAP11, YY1, GABP	Michaud et al., 2013



429–626 in ZNF143 and m-Staf, residues 469–600 in Staf) are acidic (**Figure 1**). The central region of seven zinc fingers domain is the DNA binding domain. Outside of the central domain, N-domain (region A) is the activation domain both for mRNA and snRNA, and the characteristic features of this domain of these three proteins are very similar. The function of C-domain (region C) is unclear (Myslinski et al., 1998). Strikingly, the four repeated motifs can be observed between residues 39 and 135 in region A of ZNF143/m-Staf (residues 84 and 176 in region A of Staf) (**Figure 1**). Each repeat motif contains 15 amino acids and the distance between them contains 10–12 amino acids (Schuster et al., 1995).

As a TF, it is noted that the tandemly repeated zinc finger domain (DNA binding domain) and the element of repeated motifs (activation domain) are especially well conserved among these three proteins (Myslinski et al., 1998). It is reported that this TF possesses the capacity to bind over 2000 promoter regions of both mRNA and small nuclear RNA (snRNA) genes (Myslinski et al., 1998, 2006). Recently, Ngondo-Mbongo et al. (2013) have found that ZNF143 has two main DNA binding motifs of high affinity, namely, SBS1 (GTTATGGAATTCCCATTATGCACCGCG) and SBS2 (AAACTACAATTCCCATTATGCACCGCG). Both of them are closely related to its specific binding on the chromatin, and thus initiate gene expression and regulation.

THE FUNCTION OF ZNF143

Regulating Cell-Cycle Progression

TF ZNF143 regulates gene expression associated with cell cycle. Many studies utilize knockdown or overexpression methods to evaluate the effect of ZNF143 on cancer cell progression. For example, Izumi et al. (2010) have reported that ZNF143 is associated with cell cycle and cell proliferation, whereas ZNF143 knockdown causes human prostate cancer PC3 cells to stagnate during G2/M and is accompanied with apoptosis. By establishing two forced expression of ZNF143 PC3 cancer cell lines, they found that overexpress genes strongly associated with cell cycle and cell division

(Izumi et al., 2011). ZNF143 knockdown induces increased breast cancer motility, which indicates that ZNF143 expression contributes to breast cancer progression (Paek et al., 2017). In addition, low ZNF143 expression exhibits better cell survival through an autophagic process by regulating the p53–Beclin1 axis in breast cancer cells (Paek et al., 2019). ZNF143 is essential and sufficient for Skp2 promoter activity and ZNF143 silencing inhibits cell proliferation; however, ectopic ZNF143 can rescue Skp2 expression (Hernandez-Negrete et al., 2011). Overexpression of ZNF143 enhances transaldolase promoter activity in HepG2 and HeLa cells and ZNF143 plays a key role in controlling cell survival and differentiation (Grossman et al., 2014). Simultaneously, other researchers have reported that THAP11/ZNF143/HCF-1 complex is an indispensable component of the transcriptional regulatory network and disruption of this complex leads to reduced cell proliferation, cell-cycle progression, and cell viability (Parker et al., 2014). Ngondo-Mbongo et al. (2013) have also showed that ZNF143, ICN1, and THAP11 play a pivotal role in modulating cell proliferation of rapidly dividing cells. Myslinski et al. (2007) have found that human BUB1B gene mediates the activity of spindle checkpoints to ensure chromosomal stability and euploidy, requires ZNF143 binding.

Regulating Embryonic Development and Maintaining Stem Cell Identity

As a key TF, ZNF143 has a critical function in regulating embryonic development. Halbig et al. (2012) have found that ZNF143 significantly changes zebrafish embryonic phenotypes. Therefore, ZNF143 is necessary for the normal development of zebrafish embryos. The identification and characterization of paralogous genes is also critical for understanding gene function. In the functional study of ZNF143, Huning and Kunkel (2020) have found that *znf143a*, a novel paralog of *znf143*, encodes a strong transcriptional activator protein and performs a similar role in the normal development of zebrafish embryos but expressed at a different level during early development. In mouse embryonic stem (ES) cells, ZNF143 regulates Nanog by regulating the binding of Oct4, and ZNF143 is also critical for maintaining human ES cell identity (Chen et al., 2008).

Potential Drug Design Target

TF ZNF143 is a potential drug design target to treat solid cancers. After cisplatin treatment, the binding activity of ZNF143 and MRP S11 significantly increases. This indicates that ZNF143 is involved in response to DNA damage (Ishiguchi et al., 2004; Torigoe et al., 2005; Wakasugi et al., 2007). P73 promotes ZNF143 binding with cisplatin-modified DNA, indicating that ZNF143 can regulate the transcription of DNA repair genes (Wakasugi et al., 2007). ZNF143 can also mediate cell survival by upregulating glutathione peroxidase (GPX1) activity. Thus, ZNF143 interference can increase drug sensitivity to cisplatin treatment of mitochondrial dysfunction (Lu et al., 2012). GAIP-interacting protein, C-terminus (GIPC) induces ZNF143 expression by participating in IGF-1 signal transduction to regulate reactive oxygen products (Paek and You, 2011). ZNF143 is also involved in the migration and invasion of colon cancer cells through a ZEB1-E-cadherin-linked pathway (Paek et al., 2014). The expression levels of ZNF143 and IL-8 are inversely correlated with three-dimensionally grown spheroids and colon cancer tissues (Verma et al., 2019). ZNF143 is accompanied with an increase in MIB-1 index in patients with lung adenocarcinoma, leading to high cell proliferation activity and poor prognostic treatment (Kawatsu et al., 2014). Wei et al. (2016) have found that ZNF143 expression can enhance the metastasis of gastric cancer cells, indicating that ZNF143 can be a drug target for the treatment of gastric cancer. The reduction in ZNF143 expression eventually leads to the cobaltamine transport protein not effectively transporting cobalamin (Pupavac et al., 2016). The expression patterns of ZNF143 and ZNF281 in serous borderline ovarian tumors (SBOTs) and low-grade epithelial ovarian carcinomas (EOCs) play a key role in cancer invasion, metastasis formation, and chemotherapy resistance (Sadlecki et al., 2019). ZNF143 is an upstream regulator to increase the expression of the RNA binding protein TARBP2 in breast and lung cancers (Fish et al., 2019). Thus, how to effectively design small molecule drugs to target ZNF143 is imminent. Fortunately, Haibara et al. (2017) have found that new small molecules YPC-21661 and YPC-22026 can reduce the expression of their target genes RAD51, PLK1, and Survivin by inhibiting the binding of ZNF143 to their promoters. In the future, it is believed that more and more molecule drugs will be exploited by targeting ZNF143 to treat related cancers.

ZNF143 REGULATES GENE EXPRESSION AND ITS MECHANISM

ZNF143 Participates in the Regulation of Coding and Non-coding Genes

As an important TF, ZNF143 regulates the expression of various genes. During transcription activation, Schuster et al. (1998) have found that ZNF143 activation domains bound by mRNA and snRNA are different. Myslinski et al. (1998) first have found ZNF143 can activate the transcription from RNA polymerase II TATA box-containing mRNA promoters. For example, Kubota

et al. (2000) have reported that ZNF143 is the key TF upregulating the molecular chaperone coding gene Cct α transcription through binding with the two activation elements (CAE1 and CAE2). Mach et al. (2002) have also showed that ZNF143 stimulates transcription of the human interferon regulatory factor-3 (IRF-3) gene by binding to *SphI* postoctamer homology (SPH) elements *in vitro* and in transfected cells. ZNF143 plays an important role in the transcription of neuronal nitric-oxide synthase (nNOS) exon 1, the mutation of the binding site of ZNF143 leads to a significant reduction in the activity of this exon (Saur et al., 2002). Barski et al. (2004) use ChIP as well as deletion/mutation analysis reveal that the aldehyde reductase is significantly enhanced by transcription activation after binding to ZNF143. Di Leva et al. (2004) have found that ZNF143, together with CAAT factors, regulates human synaptobrevin-like 1 (SYP-like 1) through binding to the SYBL1 promoter in HeLa cells. Gerard et al. (2007) have reported that ZNF143 binds to the promoter of mitochondrial TF A (Tfam) to regulate transcription initiation and replication of mitochondrial DNA in consistent with Sp1, NRF-1, and NRF-2. ZNF143 binds with the -305/-107 of the BUB1B promoter to regulate BUB1B expression to maintain chromosomal stability and euploidy (Myslinski et al., 2007). Gonzalez et al. (2017) have reported that ZNF143, specifically binds to the 8-bp sequence (CCCAGCAG), ~100 bases upstream of the C/EBP α transcription start site (TSS), plays an important role in the expression of C/EBP α in myeloid cells.

ZNF143 acts as a transcription-activated factor under the joint action of RNA polymerase III (Schaub et al., 1997). The snRNA and snRNA-type genes require the binding of ZNF143 during transcription, such as human U4C, U6, Y4, 7SK; mouse U6 RNAs and *Xenopus* U1b1, U2, U5, MRP. However, the binding of ZNF143 to snRNA occurs on a distal sequence element (DSE) (Schaub et al., 1997). By comparing ZNF143 recognition sequence of human U6 snRNA and selenocysteine tRNA, Schaub et al. have found that there are only 47% consistent in sequences. In the seven zinc fingers of ZNF143 recognition sequence, the first zinc finger is necessary for selenocysteine tRNA promoter identification, whereas U6 snRNA is not. The seventh zinc finger is essential for the binding activity of them. The flexibility binding results in differences in transcription activation mechanisms (Schaub et al., 1999a). U6 snRNA transcription activation requires ZNF143-DNA-Oct-1 complex, whereas selenocysteine tRNA requires ZNF143-DNA complex (Schaub et al., 1999b). Schaub et al. (2000) have found that zinc fingers 3-6 are the minimum zinc finger regions.

Self-Regulation of ZNF143

To maintain stable ZNF143 expression at normal levels, the transcription feedback regulation mechanism is the simplest and most direct means. ZNF143 selectively adjusts reverse expression by using a low affinity binding site (TSS2) located downstream of the TSS. When ZNF143 expression is higher than normal, transcripts containing longer 5'-UTR (few translation products) are produced by TSS2 transcription. In addition, when ZNF143 levels are lower than normal, the canonical TSS1 binding site is used to express transcripts

containing shorter 5'-UTR (many translation products). This transcriptional auto-regulatory mechanism regulates ZNF143 expression by the conversion of the TSS switch, which plays an important role in cell proliferation and growth (Ngondo and Carbon, 2004). Given that ZNF143 is closely related to many biological processes, its expression must be strictly regulated. Ngondo et al. have found that ZNF143 transcripts have three different lengths of 3'-UTR, with the longer 3'-UTR isoform containing variable polyadenylation sites, miRNA target sites, or AU-rich element (ARE). Thus, it tends to post-transcriptional regulation. The longest 3'-UTR isoform contains an unstabilizing ARE and is targeted by mir-590-3p. These results emphasize that ZNF143 post-transcriptional regulation depends on the long 3'-UTR isoform (Ngondo and Carbon, 2014).

ZNF143 Is a Chromatin-Looping Factor

Myslinski et al. have predicted the whole genome binding sites of ZNF143 through computer simulation (*in silico*) and biochemical methods. They speculated that at least 2500

ZNF143-binding sites are distributed in 2000 promoter regions throughout the mammalian genome. Further research has found that the presence of ZNF143-binding site alone can initiate the expression of a luciferase reporter gene, suggesting that ZNF143 itself exhibits the ability to recruit the transcription machinery (Myslinski et al., 2006). Recently, Wang et al. have reported the co-localization of RBPJ/Notch1/ZNF143, in which ZNF143 can bind with 40% of the Notch1 sites, and RBPJ shows high promoter binding preference by embedding in the ZNF143 motifs. These results may indicate a dynamic exchange of RBPJ/Notch1 and ZNF143 complexes through competition in the binding sites (Wang et al., 2011). Ngondo-Mbongo et al. (2013) have revealed that ZNF143, THAP11, and Notch1 regulate the common target genes through the mutually exclusive occupation of overlapping binding sites. Michaud et al. (2013) have found that HCF-1 is bound with 5400 CpG island promoters. HCF-1, ZNF143, and THAP11 exhibit co-localization, with HCF-1 in collaboration with ZNF143 and THAP11 plays an important role in the transcriptional regulation of HeLa cells. Parker et al. have found that HCF-1, as

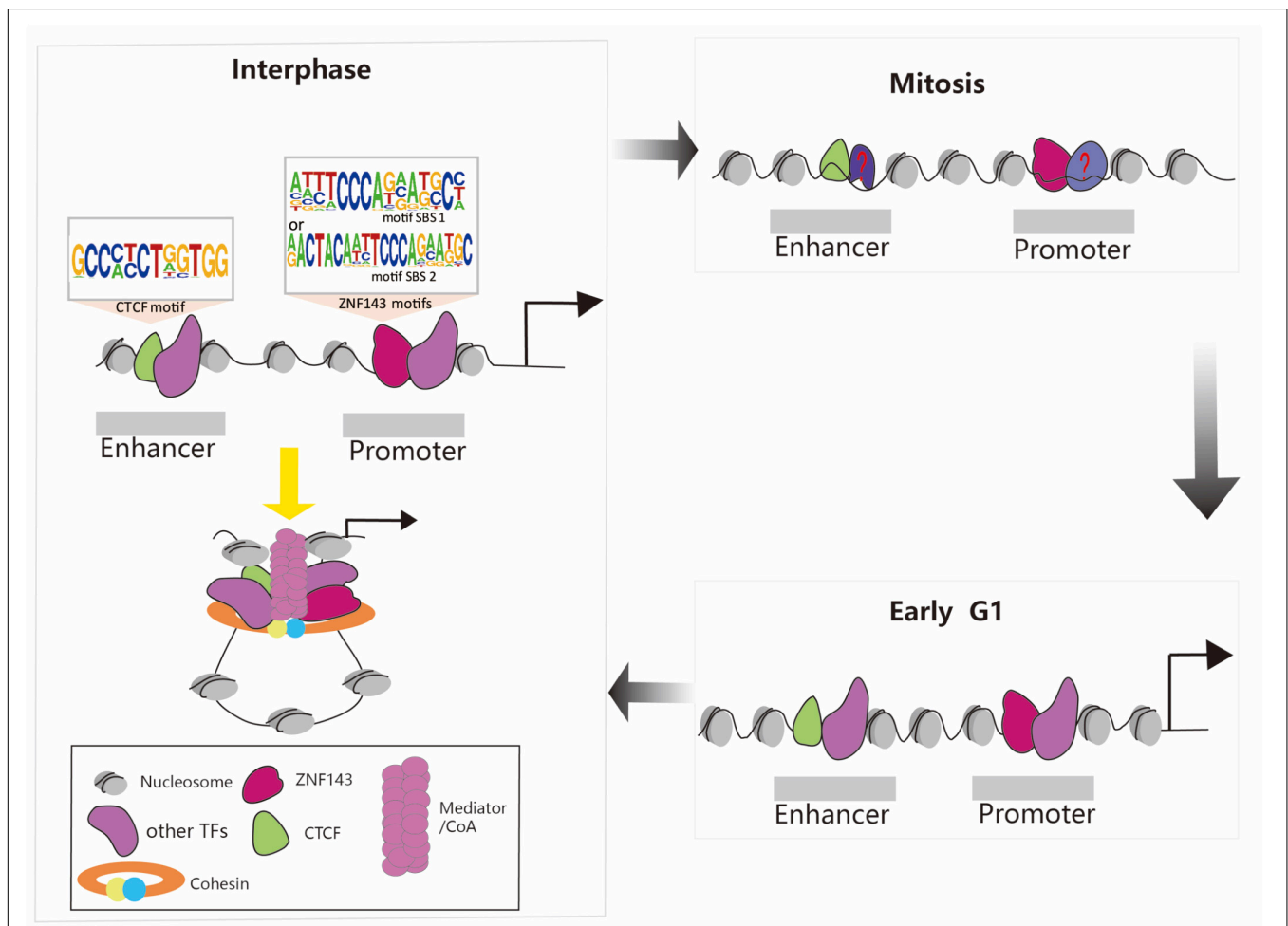


FIGURE 2 | Schematic representation of chromatin loop formation mediated by ZNF143, CTCF, cohesin, and other TFs during the cell cycle. ZNF143 is a potential mitotic bookmarking factor helps to re-establish chromatin loops in early G1.

a coregulator of the TF E2F proteins, is not directly collected in the promoter region but is mediated by ZNF143 and THAP11. HCF-1/ZNF143/THAP11 as a complex that occupies specific sites of chromatin co-regulates the expression of cell proliferation genes (Parker et al., 2014). However, how DNA sequences guide the THAP11/ZNF143/HCF-1 complex to chromatin remains in dispute. Vinckevicius et al. (2015) have explicitly proposed that ACTACA, as a joint submotif of ZNF143 and THAP11, guides THAP11 and HCF-1 to ZNF143-occupied loci and emphasized the importance of the position, spacing, and direction relative to the ZNF143 core motif.

TF ZNF143 can interact with other transcriptional regulators in mediating chromatin loop formation. Chromatin interactions between promoters and long-region regulatory elements can determine the expression level of a gene (Fraser, 2006; Fraser and Bickmore, 2007). In recent years, with the development of high-throughput sequencing and chromatin conformation capture technologies (3C, chromatin conformation capture; Hi-C, chromatin conformation capture using high throughput sequencing; ChIA-PET, chromatin interaction analysis by paired-end tag sequencing) (Dekker et al., 2002; Fullwood et al., 2009; Lieberman-Aiden et al., 2009), increasing evidence indicates that the interaction between genomic regulatory elements plays an important role in regulating gene expression. Heidari et al. (2014) have discovered that ZNF143 plays an important role in mediated distal chromatin interactions. Bailey et al. (2015) have found that ZNF143, as a novel and key chromatin-looping factor, with sequence specificity dependency at promoters and links the distal regulatory elements together, playing an important role in the establishment of the genomic organization. ZNF143 binds to the PMM2 promoter could establish a functional chromatin loop enabling interaction between the promoter and distal regulatory elements, which allows specific spatiotemporal regulation of PMM2 (Cabezas et al., 2017). ZNF143 knockdown mainly eliminates or destabilizes chromatin loops (Wen et al., 2018). We also found that ZNF143 was involved in the CTCF-mediated chromatin interactions by cooperating with cohesin (Ye et al., 2016). Other researchers have showed that ZNF143 interacts with other regulators are also important for chromatin domain formation. For example, Mourad and Cuvier (2006) have revealed that the formation of 3D chromatin domains is affected by positive driving factors CTCF, cohesin, ZNF143, polycomb proteins, and negative driving factors P300, RXRA, BCL11A, ELK1. CTCF binding sites are not only closely associated with topologically associating domain (TAD) boundaries, but also interact with ZNF143 and Yin Yang (YY)1 (Hong and Kim, 2017).

CONCLUSION AND PROSPECTS

ZNF143 can bind with multi-species, multi-type coding and non-coding genes (Schuster et al., 1995; Schaub et al., 1997; Myslinski et al., 1998). However, ZNF143 binding and co-initiative transcription differs due to the diversity of promoter structures. Although the promoter structure of H1 RNA, the

RNA component of the human nuclear RNase P, is similar to that of vertebrate snRNA, H1 RNA's promoter is distributed within 100 bp of the 5' flanking sequence and presents a highly compact structure to initiate transcription (Myslinski et al., 2001). ZNF143 binding with U6 found in zebrafish are located upstream of the TATA box and downstream of proximal sequence element (PSE), unlike the U6 of other species (Halbig et al., 2008). The promoter of SCARNA2 is contained within 161 bp upstream of TSS due to its special transcription (different from SCARNA), whereas ZNF143 is the basic regulator (Gerard et al., 2010).

As a general TF, ZNF143 participates in numerous cellular biological activities. Using comparative genomic analysis to identify the distribution of ZNF143 target genes, Myslinski et al. (2006) have found that DNA binding and TFs account for 23%, protein synthesis/degradation/modification account for 21%, and DNA replication/cell cycle/cell growth/differentiation/apoptosis account for 13%. Anno et al. have also found that ZNF143 *per se* exhibits an inherently bidirectional transcription activity. Thus, ZNF143 has the ability to control the expression of divergent protein-protein and protein-non-coding RNA gene pairs (Anno et al., 2011). ZNF143 is expressed differently in various tissues. It is highly expressed in the lung, ovary and thymus, but weakly expressed in the brain, liver, and kidney (Grossman et al., 2014). ZNF143 is highly expressed in many solid tumors, and it is involved in cisplatin resistance because cisplatin induced ZNF143 binds to cisplatin-modified DNA (Wakasugi et al., 2007; Paek and You, 2011; Lu et al., 2012). Thus, novel small molecules can be designed for ZNF143 to enhance the sensitivity of cisplatin chemotherapy (Haibara et al., 2017). ZNF143 is not only indispensable for the embryonic development of zebrafish but also necessary for ES cell identity and self-renewal capability of ES cell (Chen et al., 2008; Halbig et al., 2012). What is more, histone methylation in the ZNF143 binding sites is usually related to transcription regulation. Yang et al. (2019) have found that both active (H3K4me1, H3K4me3, and H3K27ac) and suppressive (H3K27me3) histone marks can modulate ZNF143 binding, which in turn, regulate gene expression. However, how to develop new and convenient detection systems to study the function of ZNF143 is still a big challenge. Recently, Sathyan et al. (2019) have developed an improved auxin-inducible degron system to study TF function. After rapidly depleting the ZNF143 TF, transcriptional profiling indicates that ZNF143 activates transcription in cis and regulates promoter-proximal paused RNA polymerase density.

CTCF, cohesion, and ZNF143 are three major regulators involved in the establishment and maintenance of long-range chromatin interactions. In mammalian cells, TAD-free analysis indicates that the blocking effects of CTCF, cohesin, and ZNF143 depend on the distance between loci because each protein may participate at different scales of chromatin organization (Mourad and Cuvier, 2018). CTCF and cohesin are the key factors in organizing the mammalian genome to form TADs and loops, and the CTCF loops are formed as a result of cohesin-dependent loop extrusion (Dixon et al., 2012; Nor et al., 2012; Sanborn et al., 2015; Fudenberg et al., 2016; Goloborodko et al., 2016;

Busslinger et al., 2017; Nuebler et al., 2018). ZNF143 is not only involved in CTCF/cohesin-mediated chromatin interactions, but also can bind directly to the promoter and connect it to distal regulatory elements (such as enhancer) to form chromatin loops (Heidari et al., 2014; Bailey et al., 2015; Ye et al., 2016). The recurrent C→T conversion at the ZNF143 locus influences the chromatin loop formation and alters distal gene expression in breast cancer (Yang et al., 2018). Lin et al. (2017) have reported a new epigenetic feature called sparse conserved under-methylated CpGs (scUMCs) is involved in cell-specific regulation of long-range chromatin interaction mediated by chromatin-looping factors (CTCF, cohesin, and ZNF143), providing a new direction in the research of the relationship between DNA methylation and chromatin organization. Recent technical developments allow more accurately identify where TFs bind to DNA. Skene et al. have showed that their new *in situ* methods, such as cleavage under targets and release using nuclease (CUT&RUN) and cleavage under targets and tagmentation (CUT&Tag), will be viewed as a cost-effective and versatile alternative to ChIP because of low backgrounds, which requiring only ~1/10th the sequencing depth as ChIP (Skene and Henikoff, 2017; Skene et al., 2018; Kaya-Okur et al., 2019; Meers et al., 2019). Based on these methods, Shimbo et al. (2019) have developed cleavage under tethered nuclease for conformational capture (Cut-C) technology to identify chromatin interactions mediated by a protein of interest along with the genome-wide distribution of the target proteins. Thus, using these latest technologies, we may be clearly captured the accuracy of chromatin loops mediated by ZNF143 in a genome-wide scale.

During mitosis, transcription is globally shut down, chromatin condenses, the nuclear envelope is disassembled, and most TFs are stripped off the mitotic chromosomes. How do the new daughter cells faithfully re-establish the cell-type specific transcription program? Recent discoveries that a select set of TFs remain associated with mitotic chromosomes suggest a phenomenon termed mitotic bookmarking (Huang and Wang, 2017). For example, many studies have reported that CTCF is still partially retained in mitotic chromosomes and chromatin structure dynamics during the mitosis-to-G1 phase transition (Burke et al., 2005; Yan et al., 2013; Shen et al., 2015; Teves et al., 2016; Oomen et al., 2019; Palozola et al., 2019; Zhang et al., 2019). Thus, the presence of CTCF during mitosis may function as candidate mitotic bookmarking protein. This mechanism plays a potential and critical role in

maintaining cell identity and cell destiny. Meanwhile, ZNF143 can interact with CTCF and mediate the formation of the chromatin loops. We recently discovered that ZNF143 was still partially bound to the chromosome during mitosis and 80% of the retained regions preferentially localized to promoters, supporting that it functioned mainly through promoters (Ye et al., 2020). Thus, the presence of CTCF and ZNF143 during mitosis may be crucial to recruit other regulatory factors to bind to chromosomes and re-establish chromatin loops in early G1 phase (Figure 2). Therefore, further studies on ZNF143 are necessary to help reveal its regulatory mechanism during the cell cycle.

As a key TF, the role of ZNF143 in cancer progression through transcriptional regulation of genes related to DNA replication and cell cycle (Izumi et al., 2010). Furthermore, Song et al. have showed that miR-590-3p could negatively modulate the expression of ZNF143 via binding to the ZNF143 3'-UTR and ZNF143 can directly activate FAM224A expression through binding to its promoter, forming the A1CF-FAM224A-miR-590-3p-ZNF143 positive feedback loop. This loop plays a critical role in regulating the malignant progression of glioma cells, providing a novel molecular target for glioma therapy (Song et al., 2019). In recent years, with the technology and bioinformatics analysis development, the molecular mechanism of ZNF143-mediated gene transcriptional regulation has been largely exploited. Chromatin looping between promoters and distal regulatory elements depends on DNA binding by ZNF143 and other partners. In the future, how to comprehensively analyze the mechanism of ZNF143 in mediating gene expression of different cell types and discover the novel and potential functions of ZNF143 remains a considerable challenge.

AUTHOR CONTRIBUTIONS

BY, GaY, and YL drafted the manuscript. CZ, QW, and GuY critically revised the manuscript.

FUNDING

This work was supported by Postdoctoral Research Grant in Henan Province (001803040), the Key Scientific Research Projects of Henan Higher Education (18A180019).

REFERENCES

- Adachi, K., Saito, H., Tanaka, T., and Oka, T. (1998). Molecular cloning and characterization of the murine staf cDNA encoding a transcription activating factor for the selenocysteine tRNA gene in mouse mammary gland. *J. Biol. Chem.* 273, 8598–8606. doi: 10.1074/jbc.273.15.8598
- Anno, Y. N., Myslinski, E., Ngondo-Mbongo, R. P., Krol, A., Poch, O., Lecompte, O., et al. (2011). Genome-wide evidence for an essential role of the human Staf/ZNF143 transcription factor in bidirectional transcription. *Nucleic Acids Res.* 39, 3116–3127. doi: 10.1093/nar/gkq1301
- Bailey, S. D., Zhang, X., Desai, K., Aid, M., Corradin, O., Cowper-Sal Lari, R., et al. (2015). ZNF143 provides sequence specificity to secure chromatin interactions at gene promoters. *Nat. Commun.* 2:6186.
- Barski, O. A., Papusha, V. Z., Kunkel, G. R., and Gabbay, K. H. (2004). Regulation of aldehyde reductase expression by STAF and CHOP. *Genomics* 83, 119–129. doi: 10.1016/s0888-7543(03)00213-1
- Burke, L. J., Zhang, R., Bartkuhn, M., Tiwari, V. K., Tavoosidana, G., Kurukuti, S., et al. (2005). CTCF binding and higher order chromatin structure of the H19 locus are maintained in mitotic chromatin. *EMBO J.* 24, 3291–3300. doi: 10.1038/sj.emboj.7600793
- Busslinger, G. A., Stocsits, R. R., van der Lelij, P., Axelsson, E., Tedeschi, A., Galjart, N., et al. (2017). Cohesin is positioned in mammalian genomes by transcription, CTCF and Wapl. *Nature* 544, 503–507. doi: 10.1038/nature22063
- Cabezas, O. R., Flanagan, S. E., Stanesco, H., García-Martínez, E., Caswell, R., Lango-Allen, H., et al. (2017). Polycystic kidney disease with hyperinsulinemic

- hypoglycemia caused by a promoter mutation in phosphomannomutase 2. *J. Am. Soc. Nephrol.* 28, 2529–2539.
- Chen, X., Fang, F., Liou, Y. C., and Ng, H. H. (2008). Zfp143 regulates Nanog through modulation of Oct4 binding. *Stem Cells* 26, 2759–2767. doi: 10.1634/stemcells.2008-0398
- Dekker, J., Rippe, K., Dekker, M., and Kleckner, N. (2002). Capturing chromosome conformation. *Science* 295, 1306–1311. doi: 10.1126/science.1067799
- Di Leva, F., Ferrante, M. I., Demarchi, F., Caravelli, A., Matarazzo, M. R., Giacca, M., et al. (2004). Human synaptobrevin-like 1 gene basal transcription is regulated through the interaction of selenocysteine tRNA gene transcription activating factor-zinc finger 143 factors with evolutionary conserved cis-elements. *J. Biol. Chem.* 279, 7734–7739. doi: 10.1074/jbc.m308140200
- Dixon, J. R., Selvaraj, S., Yue, F., Kim, A., Li, Y., Shen, Y., et al. (2012). Topological domains in mammalian genomes identified by analysis of chromatin interactions. *Nature* 485, 376–380. doi: 10.1038/nature11082
- Fish, L., Navickas, A., Culbertson, B., Xu, Y., Nguyen, H. C. B., Zhang, S., et al. (2019). Nuclear TARBP2 drives oncogenic dysregulation of RNA splicing and decay. *Mol. Cell* 75, 967–981.
- Fraser, P. (2006). Transcriptional control thrown for a loop. *Curr. Opin. Genet. Dev.* 16, 490–495. doi: 10.1016/j.gde.2006.08.002
- Fraser, P., and Bickmore, W. (2007). Nuclear organization of the genome and the potential for gene regulation. *Nature* 447, 413–417. doi: 10.1038/nature05916
- Fudenberg, G., Imakaev, M., Lu, C., Goloborodko, A., Abdennur, N., and Mirny, L. A. (2016). Formation of chromosomal domains by loop extrusion. *Cell Rep.* 15, 2038–2049. doi: 10.1016/j.celrep.2016.04.085
- Fullwood, M. J., Liu, M., Pan, Y. F., Liu, J., Xu, H., Mohamed, Y. B., et al. (2009). An oestrogen-receptor- α -bound human chromatin interactome. *Nature* 462, 58–64.
- Gerard, M. A., Krol, A., and Carbon, P. (2007). Transcription factor hStaf/ZNF143 is required for expression of the human TFAM gene. *Gene* 401, 145–153. doi: 10.1016/j.gene.2007.07.011
- Gerard, M. A., Myslinski, E., Chylak, N., Baudrey, S., Krol, A., and Carbon, P. (2010). The scaRNA2 is produced by an independent transcription unit and its processing is directed by the encoding region. *Nucleic Acids Res.* 38, 370–381. doi: 10.1093/nar/gkp988
- Goloborodko, A., Marko, J. F., and Mirny, L. A. (2016). Chromosome compaction by active loop extrusion. *Biophys. J.* 110, 2162–2168. doi: 10.1016/j.bpj.2016.02.041
- Gonzalez, D., Luyten, A., Bartholdy, B., Zhou, Q., Kardosova, M., Ebralidze, A., et al. (2017). ZNF143 protein is an important regulator of the myeloid transcription factor C/EBP α . *J. Biol. Chem.* 292, 18924–18936. doi: 10.1074/jbc.m117.811109
- Grossman, C. E., Qian, Y., Banki, K., and Perl, A. (2014). ZNF143 mediates basal and tissue-specific expression of human transaldolase. *J. Biol. Chem.* 279, 12190–12205. doi: 10.1074/jbc.m307039200
- Haibara, H., Yamazaki, R., Nishiyama, Y., Ono, M., Kobayashi, T., Hokkyo-Itagaki, A., et al. (2017). YPC-21661 and YPC-22026, novel small molecules, inhibit ZNF143 activity *in vitro* and *in vivo*. *Cancer Sci.* 108, 1042–1048. doi: 10.1111/cas.13199
- Halbig, K. M., Lekven, A. C., and Kunkel, G. R. (2008). Zebrafish U6 small nuclear RNA gene promoters contain a SPH element in an unusual location. *Gene* 421, 89–94. doi: 10.1016/j.gene.2008.06.019
- Halbig, K. M., Lekven, A. C., and Kunkel, G. R. (2012). The transcriptional activator ZNF143 is essential for normal development in zebrafish. *BMC Mol. Biol.* 13:3. doi: 10.1186/1471-2199-13-3
- Heidari, N., Phanstiel, D. H., He, C., Grubert, F., Jahanbani, F., Kasowski, M., et al. (2014). Genome-wide map of regulatory interactions in the human genome. *Genome Res.* 24, 1905–1917. doi: 10.1101/gr.176586.114
- Hernandez-Negrete, I., Sala-Newby, G. B., Perl, A., Kunkel, G. R., Newby, A. C., and Bond, M. (2011). Adhesion-dependent Skp2 transcription requires selenocysteine tRNA gene transcription-activating factor (STAF). *Biochem. J.* 436, 133–143. doi: 10.1042/bj20101798
- Hong, S., and Kim, D. (2017). Computational characterization of chromatin domain boundary-associated genomic elements. *Nucleic Acids Res.* 45, 10403–10414. doi: 10.1093/nar/gkx738
- Huang, X., and Wang, J. (2017). Mitotic bookmarking: maintaining the stem cell identity during mitosis. *Cell Stem Cell* 20, 741–742. doi: 10.1016/j.stem.2017.05.002
- Huning, L., and Kunkel, G. R. (2020). Two paralogous znf143 genes in zebrafish encode transcriptional activator proteins with similar functions but expressed at different levels during early development. *BMC Mol. Cell Biol.* 21:3. doi: 10.1186/s12860-020-0247-7
- Ishiguchi, H., Izumi, H., Torigoe, T., Yoshida, Y., Kubota, H., Tsuji, S., et al. (2004). ZNF143 activates gene expression in response to DNA damage and binds to cisplatin-modified DNA. *Int. J. Cancer.* 111, 900–909. doi: 10.1002/ijc.20358
- Izumi, H., Wakasugi, T., Shimajiri, S., Tanimoto, A., Sasaguri, Y., Kashiwagi, E., et al. (2010). Role of ZNF143 in tumor growth through transcriptional regulation of DNA replication and cell-cycle-associated genes. *Cancer Sci.* 101, 2538–2545. doi: 10.1111/j.1349-7006.2010.01725.x
- Izumi, H., Yasuniwa, Y., Akiyama, M., Yamaguchi, T., Kuma, A., Kitamura, N., et al. (2011). Forced expression of ZNF143 restrains cancer cell growth. *Cancers* 3, 3909–3920. doi: 10.3390/cancers3043909
- Kawatsu, Y., Kitada, S., Uramoto, H., Zhi, L., Takeda, T., Kimura, T., et al. (2014). The combination of strong expression of ZNF143 and high MIB-1 labelling index independently predicts shorter disease-specific survival in lung adenocarcinoma. *Br. J. Cancer* 110, 2583–2592. doi: 10.1038/bjc.2014.202
- Kaya-Okur, H. S., Wu, S. J., Codomo, C. A., Pledger, E. S., Bryson, T. D., Henikoff, J. G., et al. (2019). CUT&Tag for efficient epigenomic profiling of small samples and single cells. *Nat. Commun.* 10:1930.
- Kubota, H., Yokota, S., Yanagi, H., and Yura, T. (2000). Transcriptional regulation of the mouse cytosolic chaperonin subunit gene Ccta/t-complex polypeptide 1 by selenocysteine tRNA gene transcription activating factor family zinc finger proteins. *J. Biol. Chem.* 275, 28641–28648. doi: 10.1074/jbc.m005009200
- Lieberman-Aiden, E., van Berkum, N. L., Williams, L., Imakaev, M., Ragoczy, T., Telling, A., et al. (2009). Comprehensive mapping of long-range interactions reveals folding principles of the human genome. *Science* 326, 289–293. doi: 10.1126/science.1181369
- Lin, X., Su, J., Chen, K., Rodriguez, B., and Li, W. (2017). Sparse conserved under-methylated CpGs are associated with high-order chromatin structure. *Genome Biol.* 18:163.
- Lu, W., Chen, Z., Zhang, H., Wang, Y., Luo, Y., and Huang, P. (2012). ZNF143 transcription factor mediates cell survival through upregulation of the GPX1 activity in the mitochondrial respiratory dysfunction. *Cell Death Dis.* 3:e422. doi: 10.1038/cddis.2012.156
- Mach, C. M., Hargrove, B. W., and Kunkel, G. R. (2002). The Small RNA gene activator protein, SphI postoctamer homology-binding factor/selenocysteine tRNA gene transcription activating factor, stimulates transcription of the human interferon regulatory factor-3 gene. *J. Biol. Chem.* 277, 4853–4858. doi: 10.1074/jbc.m108308200
- Meers, M. P., Bryson, T. D., Henikoff, J. G., and Henikoff, S. (2019). Improved CUT&RUN chromatin profiling tools. *eLife* 8:e46314.
- Michaud, J., Praz, V., James Faresse, N., Inbaptiste, C. K., Tyagi, S., Schütz, F., et al. (2013). HCFC1 is a common component of active human CpG-island promoters and coincides with ZNF143, THAP11, YY1, and GABP transcription factor occupancy. *Genome Res.* 23, 907–916. doi: 10.1101/gr.150078.112
- Mourad, R., and Cuvier, O. (2006). Computational identification of genomic features that influence 3D chromatin domain formation. *PLoS Comput. Biol.* 12:e1004908. doi: 10.1371/journal.pcbi.1004908
- Mourad, R., and Cuvier, O. (2018). TAD-free analysis of architectural proteins and insulators. *Nucleic Acids Res.* 46:e27. doi: 10.1093/nar/gkx1246
- Myslinski, E., Amé, J. C., Krol, A., and Carbon, P. (2001). An unusually compact external promoter for RNA polymerase III transcription of the human H1RNA gene. *Nucleic Acids Res.* 29, 2502–2509. doi: 10.1093/nar/29.12.2502
- Myslinski, E., Gerard, M. A., Krol, A., and Carbon, P. (2006). A genome scale location analysis of human Staf/ZNF143-binding sites suggests a widespread role for human Staf/ZNF143 in mammalian promoters. *J. Biol. Chem.* 281, 39953–39962. doi: 10.1074/jbc.m608507200
- Myslinski, E., Gerard, M. A., Krol, A., and Carbon, P. (2007). Transcription of the human cell cycle regulated BUB1B gene requires hStaf/ZNF143. *Nucleic Acids Res.* 35, 3453–3464. doi: 10.1093/nar/gkm239
- Myslinski, E., Krol, A., and Carbon, P. (1998). ZNF76 and ZNF143 are two human homologs of the transcriptional activator Staf. *J. Biol. Chem.* 273, 21998–22006. doi: 10.1074/jbc.273.34.21998
- Ngondo, R. P., and Carbon, P. (2004). Transcription factor abundance controlled by an auto-regulatory mechanism involving a transcription start site switch. *Nucleic Acids Res.* 42, 2171–2184. doi: 10.1093/nar/gkt1136

- Ngondo, R. P., and Carbon, P. (2014). ZNF143 is regulated through alternative 3'UTR isoforms. *Biochimie* 104, 137–146. doi: 10.1016/j.biochi.2014.06.008
- Ngondo-Mbongo, R. P., Myslinski, E., Aster, J. C., and Carbon, P. (2013). Modulation of gene expression via overlapping binding sites exerted by ZNF143, Notch1 and THAP11. *Nucleic Acids Res.* 41, 4000–4014. doi: 10.1093/nar/gkt088
- Nor, E. P., Lajoie, B. R., Schulz, E. G., Giorgetti, L., Okamoto, I., Servant, N., et al. (2012). Spatial partitioning of the regulatory landscape of the X-inactivation centre. *Nature* 485, 381–385. doi: 10.1038/nature11049
- Nuebler, J., Fudenberg, G., Imakaev, M., Abdennur, N., and Mirny, L. A. (2018). Chromatin organization by an interplay of loop extrusion and compartmental segregation. *Proc. Natl. Acad. Sci. U.S.A.* 115, E6697–E6706.
- Oomen, M. E., Hansen, A. S., Liu, Y., Darzacq, X., and Dekker, J. (2019). CTCF sites display cell cycle-dependent dynamics in factor binding and nucleosome positioning. *Genome Res.* 29, 236–249. doi: 10.1101/gr.241547.118
- Paek, A. R., Lee, C. H., and You, H. J. (2014). A role of zinc-finger protein 143 for cancer cell migration and invasion through ZEB1 and E-cadherin in colon cancer cells. *Mol. Carcinog.* 53, E161–E168.
- Paek, A. R., Mun, J. Y., Hong, K. M., Lee, J., Hong, D. W., and You, H. J. (2017). Zinc finger protein 143 expression is closely related to tumor malignancy via regulating cell motility in breast cancer. *BMB Rep.* 50, 621–627. doi: 10.5483/bmbrep.2017.50.12.177
- Paek, A. R., Mun, J. Y., Jo, M. J., Choi, H., Lee, Y. J., Cheong, H., et al. (2019). The role of ZNF143 in breast cancer cell survival through the NAD(P)H quinone dehydrogenase 1 (-) 53 (-) beclin1 axis under metabolic stress. *Cells* 8:E296.
- Paek, A. R., and You, H. J. (2011). GAIP-interacting protein, C-terminus is involved in the induction of zinc-finger protein 143 in response to insulin-like growth factor-1 in colon cancer cells. *Mol. Cells* 32, 415–419. doi: 10.1007/s10059-011-0078-7
- Palozola, K. C., Lerner, J., and Zaret, K. S. (2019). A changing paradigm of transcriptional memory propagation through mitosis. *Nat. Rev. Mol. Cell. Biol.* 20, 55–64. doi: 10.1038/s41580-018-0077-z
- Parker, J. B., Yin, H., Vinckevicius, A., and Chakravarti, D. (2014). Host cell factor-1 recruitment to E2F-bound and cell-cycle-control genes is mediated by THAP11 and ZNF143. *Cell Rep.* 9, 967–982. doi: 10.1016/j.celrep.2014.09.051
- Pupavac, M., Watkins, D., Petrella, F., Fahiminiya, S., Janer, A., Cheung, W., et al. (2016). Inborn error of cobalamin metabolism associated with the intracellular accumulation of transcobalamin-bound cobalamin and mutations in ZNF143, which codes for a transcriptional activator. *Hum. Mutat.* 37, 976–982. doi: 10.1002/humu.23037
- Sadlecki, P., Grabiec, M., Grzanka, D., Jozwicki, J., Antosik, P., and Walentowicz-Sadlecka, M. (2019). Expression of zinc finger transcription factors (ZNF143 and ZNF281) in serous borderline ovarian tumors and low-grade ovarian cancers. *J. Ovarian Res.* 12:23.
- Sanborn, A. L., Rao, S. S., Huang, S. C., Durand, N. C., Huntley, M. H., Jewett, A. I., et al. (2015). Chromatin extrusion explains key features of loop and domain formation in wild-type and engineered genomes. *Proc. Natl. Acad. Sci. U.S.A.* 112, E6456–E6465.
- Sathyan, K. M., McKenna, B. D., Anderson, W. D., Duarte, F. M., Core, L., and Guertin, M. J. (2019). An improved auxin-inducible degron system preserves native protein levels and enables rapid and specific protein depletion. *Genes Dev.* 33, 1441–1455. doi: 10.1101/gad.328237.119
- Saur, D., Seidler, B., Paehge, H., Schusdziarra, V., and Allescher, H. D. (2002). Complex regulation of human neuronal nitric-oxide synthase exon 1c gene transcription. Essential role of Sp and ZNF family members of transcription factors. *J. Biol. Chem.* 277, 25798–25814. doi: 10.1074/jbc.m109802200
- Schaub, M., Krol, A., and Carbon, P. (1999a). Flexible zinc finger requirement for binding of the transcriptional activator staf to U6 small nuclear RNA and tRNA(Sec) promoters. *J. Biol. Chem.* 274, 24241–24249. doi: 10.1074/jbc.274.34.24241
- Schaub, M., Krol, A., and Carbon, P. (2000). Structural organization of Staf-DNA complexes. *Nucleic Acids Res.* 28, 2114–2121. doi: 10.1093/nar/28.10.2114
- Schaub, M., Myslinski, E., Krol, A., and Carbon, P. (1999b). Maximization of selenocysteine tRNA and U6 small nuclear RNA transcriptional activation achieved by flexible utilization of a Staf zinc finger. *J. Biol. Chem.* 274, 25042–25050. doi: 10.1074/jbc.274.35.25042
- Schaub, M., Myslinski, E., Schuster, C., Krol, A., and Carbon, P. (1997). Staf, a promiscuous activator for enhanced transcription by RNA polymerases II and III. *EMBO J.* 16, 173–181. doi: 10.1093/emboj/16.1.173
- Schuster, C., Krol, A., and Carbon, P. (1998). Two distinct domains in Staf to selectively activate small nuclear RNA-type and mRNA promoters. *Mol. Cell Biol.* 18, 2650–2658. doi: 10.1128/mcb.18.5.2650
- Schuster, C., Myslinski, E., Krol, A., and Carbon, P. (1995). Staf, a novel zinc finger protein that activates the RNA polymerase III promoter of the selenocysteine tRNA gene. *EMBO J.* 14, 3777–3787. doi: 10.1002/j.1460-2075.1995.tb00047.x
- Shen, W. L., Wang, D., Ye, B. Y., Shi, M. L., Zhang, Y., and Zhao, Z. H. (2015). A possible role of Drosophila CTCF in mitotic bookmarking and maintaining chromatin domains during the cell cycle. *Biol. Res.* 48:27.
- Shimbo, T., Kawamura, M., Wijaya, E., Takaki, E., Kaneda, Y., and Tamai, K. (2019). Cut-C: cleavage under tethered nuclease for conformational capture. *BMC Genomics* 20:614. doi: 10.1186/s12864-019-5989-2
- Skene, P. J., Henikoff, J. G., and Henikoff, S. (2018). Targeted in situ genome-wide profiling with high efficiency for low cell numbers. *Nat. Protoc.* 13, 1006–1019. doi: 10.1038/nprot.2018.015
- Skene, P. J., and Henikoff, S. (2017). An efficient targeted nuclease strategy for high-resolution mapping of DNA binding sites. *eLife* 6:e21856.
- Song, Y., Shao, L., Xue, Y., Xuelei, R., Xiaobai, L., Chunqing, Y., et al. (2019). Inhibition of the aberrant A1CF-FAM224A- miR-590-3p-ZNF143 positive feedback loop attenuated malignant biological behaviors of glioma cells. *J. Exp. Clin. Cancer Res.* 38:248.
- Teves, S. S., An, L., Hansen, A. S., Xie, L., Darzacq, X., and Tjian, R. (2016). A dynamic mode of mitotic bookmarking by transcription factors. *eLife* 5:e22280.
- Tommerup, N., and Vissing, H. (1995). Isolation and fine mapping of 16 novel human zinc finger-encoding cDNAs identify putative candidate genes for developmental and malignant disorders. *Genomics* 27, 259–264. doi: 10.1006/geno.1995.1040
- Torigoe, T., Izumi, H., Ishiguchi, H., Yoshida, Y., Tanabe, M., Yoshida, T., et al. (2005). Cisplatin resistance and transcription factors. *Curr. Med. Chem. Anticancer Agents* 5, 15–27.
- Verma, V., Paek, A. R., Choi, B. K., Hong, E. K., and You, H. J. (2019). Loss of zinc-finger protein 143 contributes to tumour progression by interleukin-8-CXCR axis in colon cancer. *J. Cell. Mol. Med.* 23, 4043–4053. doi: 10.1111/jcmm.14290
- Vinckevicius, A., Parker, J. B., and Chakravarti, D. (2015). Genomic determinants of THAP11/ZNF143/HCFC1 complex recruitment to chromatin. *Mol. Cell Biol.* 35, 4135–4146. doi: 10.1128/mcb.00477-15
- Wakasugi, T., Izumi, H., Uchiumi, T., Suzuki, H., Arao, T., Nishio, K., et al. (2007). ZNF143 interacts with p73 and is involved in cisplatin resistance through the transcriptional regulation of DNA repair genes. *Oncogene* 26, 5194–5203. doi: 10.1038/sj.onc.1210326
- Wang, H., Zou, J., Zhao, B., Eric, J., Todd, A., Hoifung, W., et al. (2011). Genome-wide analysis reveals conserved and divergent features of Notch1/RBPJ binding in human and murine T-lymphoblastic leukemia cells. *Proc. Natl. Acad. Sci. U.S.A.* 108, 14908–14913. doi: 10.1073/pnas.1109023108
- Wei, S., Wang, L., Zhang, L., Li, B., Li, Z., Zhang, Q., et al. (2016). ZNF143 enhances metastasis of gastric cancer by promoting the process of EMT through PI3K/AKT signaling pathway. *Tumour Biol.* 37, 12813–12821. doi: 10.1007/s13277-016-5239-z
- Wen, Z., Huang, Z. T., Zhang, R., and Peng, C. (2018). ZNF143 is a regulator of chromatin loop. *Cell. Biol. Toxicol.* 34, 471–478. doi: 10.1007/s10565-018-9443-z
- Yan, J., Enge, M., Whittington, T., Dave, K., Liu, J., Sur, I., et al. (2013). Transcription factor binding in human cells occurs in dense clusters formed around cohesin anchor sites. *Cell* 154, 801–813. doi: 10.1016/j.cell.2013.07.034
- Yang, J., Wei, X., Tufan, T., Kusc, C., Unlu, H., Farooq, S., et al. (2018). Recurrent mutations at estrogen receptor binding sites alter chromatin topology and distal gene expression in breast cancer. *Genome Biol.* 19:190.
- Yang, X., Bam, M., Nagarkatti, P. S., and Nagarkatti, M. (2019). Cannabidiol regulates gene expression in encephalitogenic T cells using histone methylation and noncoding rna during experimental autoimmune encephalomyelitis. *Sci. Rep.* 9:15780.
- Yang, Y., Zhang, R. C., Singh, S., and Ma, J. (2017). Exploiting sequence-based features for predicting enhancer-promoter interactions. *Bioinformatics* 33, i252–i260. doi: 10.1093/bioinformatics/btx257

- Ye, B. Y., Shen, W. L., Wang, D., Li, P., Zhang, Z., Shi, M. L., et al. (2016). ZNF143 is involved in CTCF-mediated chromatin interactions by cooperation with cohesin and other partners. *Mol. Biol.* 50, 496–503.
- Ye, B. Y., Shen, W. L., and Zhao, Z. H. (2020). ZNF143 is dynamically bound to a subset of its interphase sites during mitosis. *Biochem. Biophys. Res. Commun.* 523, 293–298. doi: 10.1016/j.bbrc.2019.12.031
- Zhang, H., Emerson, D. J., Gilgenast, T. G., Titus, K. R., Lan, Y., Huang, P., et al. (2019). Chromatin structure dynamics during the mitosis-to-G1 phase transition. *Nature* 576, 158–162. doi: 10.1038/s41586-019-1778-y

Conflict of Interest: The authors declare that the research was conducted in the absence of any commercial or financial relationships that could be construed as a potential conflict of interest.

Copyright © 2020 Ye, Yang, Li, Zhang, Wang and Yu. This is an open-access article distributed under the terms of the Creative Commons Attribution License (CC BY). The use, distribution or reproduction in other forums is permitted, provided the original author(s) and the copyright owner(s) are credited and that the original publication in this journal is cited, in accordance with accepted academic practice. No use, distribution or reproduction is permitted which does not comply with these terms.



Functional Implications of Active N⁶-Methyladenosine in Plants

Hongxiang Zheng^{1†}, Simin Li^{1†}, Xiansheng Zhang^{2*} and Na Sui^{1*}

¹ Shandong Provincial Key Laboratory of Plant Stress, College of Life Sciences, Shandong Normal University, Jinan, China,

² State Key Laboratory of Crop Biology, College of Life Sciences, Shandong Agricultural University, Tai'an, China

OPEN ACCESS

Edited by:

Kai Tang,
Purdue University, United States

Reviewed by:

Thierry Lagrange,
UMR 5096 Laboratoire Génome et
Développement des Plantes, France
Ye Fu,
Harvard University, United States

Peter Dedon,
Massachusetts Institute
of Technology, United States

*Correspondence:

Xiansheng Zhang
zhangxs@sdau.edu.cn
Na Sui
suina@sdu.edu.cn;
suina800101@163.com

[†] These authors have contributed
equally to this work

Specialty section:

This article was submitted to
Epigenomics and Epigenetics,
a section of the journal
Frontiers in Cell and Developmental
Biology

Received: 06 January 2020

Accepted: 03 April 2020

Published: 29 April 2020

Citation:

Zheng H, Li S, Zhang X and Sui N
(2020) Functional Implications
of Active N⁶-Methyladenosine
in Plants. *Front. Cell Dev. Biol.* 8:291.
doi: 10.3389/fcell.2020.00291

N⁶-methyladenosine (m⁶A) is the most common type of eukaryotic mRNA modification and has been found in many organisms, including mammals, and plants. It has important regulatory effects on RNA splicing, export, stability, and translation. The abundance of m⁶A on RNA depends on the dynamic regulation between methyltransferase (“writer”) and demethylase (“eraser”), and m⁶A binding protein (“reader”) exerts more specific regulatory function by binding m⁶A modification sites on RNA. Progress in research has revealed important functions of m⁶A modification in plants. In this review, we systematically summarize the latest advances in research on the composition and mechanism of action of the m⁶A system in plants. We emphasize the function of m⁶A modification on RNA fate, plant development, and stress resistance. Finally, we discuss the outstanding questions and opportunities exist for future research on m⁶A modification in plant.

Keywords: N⁶-methyladenosine, functional implications, plant, RNA function, stress response

INTRODUCTION

More than 150 RNA modifications have been identified as post-transcriptional regulatory markers in a variety of RNA species, including messenger RNA (mRNA), transfer RNA (tRNA), ribosomal RNA (rRNA), small non-coding RNA (snRNA), and long non-coding RNA (lncRNA), RNA methylation is one of the post-transcriptional modifications of RNA, and N⁶-methyladenosine (m⁶A) is the most common type of RNA methylation modification, accounting for more than 80% of RNA methylation modifications in organism. Current study suggests that the m⁶A modification plays an important role in RNA fate, such as RNA splicing (Liu et al., 2015, 2017; Haussmann et al., 2016; Lence et al., 2016; Xiao et al., 2016; Pendleton et al., 2017), RNA stability (Wang et al., 2014; Du et al., 2016; Mishima and Tomari, 2016; Huang et al., 2018), RNA export (Roundtree et al., 2017; Edens et al., 2019), 3' untranslated region (UTR) processing (Ke et al., 2015; Bartosovic et al., 2017; Wei et al., 2018; Yue et al., 2018), translation (Zhou et al., 2015; Choi et al., 2016; Li et al., 2017; Shi et al., 2017), and miRNA processing (Alarcón et al., 2015a,b; Bhat et al., 2019). Although the presence of m⁶A was detected in mammals (Desrosiers et al., 1974; Wei et al., 1975; Schibler et al., 1977) and plants (Kennedy and Lane, 1979; Nichols, 1979) in the 1970s, it had not received much attention because it was considered to be “static” due to the method of detecting m⁶A sites. However, the discovery of the first m⁶A demethylase fat mass and obesity-associated protein (FTO) was an exciting development (Jia et al., 2011), as it demonstrated that the m⁶A modification process is dynamic and reversible in the cell. Subsequently, the methyl-RNA immunoprecipitation combined with RNA sequencing (MeRIP-Seq) method was established for identifying m⁶A modifications on mRNA in the transcriptome (Dominissini et al., 2012; Meyer et al., 2012). This method relies on the highly specific antibody of m⁶A to precipitate m⁶A and then

involves high-throughput sequencing to reveal methylated transcripts (Dominissini et al., 2012; Meyer et al., 2012). This method revealed that the m⁶A site is not uniformly distributed over the mRNA: only some mRNAs have m⁶A sites, most of which are located near the stop codon and the 3' UTR (Dominissini et al., 2012; Meyer et al., 2012). At the same time, m⁶A is highly dynamic, and the level of m⁶A varies greatly depending on the developmental stage (Dominissini et al., 2012; Meyer et al., 2012). These findings suggested that m⁶A modification may affect the fate and function of mRNA in cells. As more m⁶A-related enzymes are identified, the important biological functions played by m⁶A modification are being gradually unveiled. Although the study of m⁶A functions was mainly in animal systems, current studies shows that m⁶A modification also plays important role in regulating plant development (Zhong et al., 2008; Bodi et al., 2012; Shen et al., 2016; Hofmann, 2017; Růžicka et al., 2017; Anderson et al., 2018; Arribas-Hernández et al., 2018; Chen et al., 2018; Scutenaire et al., 2018; Wei et al., 2018; Zhang et al., 2019; Zhou et al., 2019; Luo et al., 2020) and stress resistance (Martínez-Pérez et al., 2017; Anderson et al., 2018; Li et al., 2018; Miao et al., 2020).

Writers, erasers, readers are the core components of the m⁶A regulatory system. The writers and erasers are responsible for adding or removing m⁶A to the conserved sequence "RRACH" (where R = A/G, A is the modified m⁶A site, and H = A/C/U) (Dominissini et al., 2012; Schwartz et al., 2013; Li et al., 2014; Luo et al., 2014; Lence et al., 2016; Shen et al., 2016; Parker et al., 2020), respectively. The readers are responsible for binding m⁶A sites and play specific regulatory roles for modified-RNA. Writers, erasers, and readers form the basis of a complex regulatory network under the guidance of m⁶A modification. However, not all RNAs containing the "RRACH" sequence will have m⁶A added to them (Dominissini et al., 2012; Li et al., 2014). It is unclear how the writers and erasers selectively add or remove m⁶A on RNA sequences. Therefore, the discovery and functional studies of more m⁶A-related enzymes can help us to understand the mechanism of m⁶A regulation.

THE MAIN COMPONENTS OF THE m⁶A SYSTEM: WRITERS, ERASERS, AND READERS

Studies on m⁶A enzymes or novel functions have mainly focused on animal systems, while there have been few studies in plants, especially in crops. In mammals, m⁶A is produced by a methyltransferase complex consisting of MTase complex comprising methyltransferase-like 3 (METTL3) (Bokar et al., 1994), wilms' tumor 1-associating protein (WTAP) (Agarwala et al., 2012), and methyltransferase-like 14 (METTL14) (Liu et al., 2014) and is removed by the action of the demethylases FTO (Jia et al., 2011) and α -ketoglutarate-dependent dioxygenase alkB homolog 5 (ALKBH5) (Zheng et al., 2013). This modification process is dynamic and reversible in the cell. The reader plays a specific regulatory role by recognizing the m⁶A modification site, which mainly includes the YTH (YT512-BHomology) domain-containing proteins YTHDC1/2 (DC1/2) (Bailey et al., 2017;

Hsu et al., 2017; Roundtree et al., 2017; Zhang et al., 2010) and YTHDF1/2/3 (DF1/2/3) (Dominissini et al., 2012; Wang et al., 2014, 2015; Zhou et al., 2015; Shi et al., 2017), HNRNPA2B1 (Agarwala et al., 2012), and eukaryotic initiation factor 3 (eIF3) (Meyer et al., 2015). However, it should be emphasized that the core enzymes in the m⁶A system are highly conserved among different species, so studying the regulatory patterns of m⁶A in animals should also help us to explore its regulation in plants.

WRITERS

In *Arabidopsis*, the METTL3 homolog MTA (At4g10760) is highly expressed in seeds, pollen microspores, and meristems. In loss-of-function mutants of T-DNA insertion, an embryonic lethal phenotype and m⁶A completion loss occur (Craigon et al., 2004). This is consistent with the phenomenon of METTL3 mutation in animals and yeast (Geula et al., 2015). Yeast two-hybrid assay and co-immunoprecipitation experiments showed that MTA protein interacts with the protein encoded by FIP37 (At3g54170) *in vitro* and *in vivo* (Zhong et al., 2008). FIP37 is a homolog of the selective cleavage protein WTAP in human and *Drosophila*. FIP37 expression patterns are similar to those of MTA. In addition, disruption of FIP37 by T-DNA insertion also results in an embryonic lethal phenotype with developmental arrest at the globular stage (Vespa et al., 2004; Růžicka et al., 2017). MTB is a homolog of human METTL14, which has also been shown to be a part of the m⁶A methyltransferase complex (Liu et al., 2014). Experiments on RNA interference (RNAi) lines with inducible knockdown of MTB have shown that such knockdown leads to a nearly 50% reduction in m⁶A levels (Růžicka et al., 2017). In addition, using the method of tandem affinity purification (TAP), VIRILIZER (KIAA1429 human homologous protein) (Schwartz et al., 2014) and E3 ubiquitin ligase HAKAI (HAKAI human homologous protein) were also found to be components of the *Arabidopsis* methyltransferase complex (Růžicka et al., 2017). Inhibition of the expression of VIRILIZER and HAKAI resulted in a decrease in the level of m⁶A in *Arabidopsis* mRNA (Růžicka et al., 2017). MTA, MTB, FIP37, VIRILIZER, and HAKAI are considered to be the main components of the m⁶A methyltransferase complexes in *Arabidopsis* system (Figure 1). In addition, the writers in the m⁶A system have also been reported in other plants. Knockout of OsFIP or OsMTA2 in rice significantly reduced the level of m⁶A, while no effect on total m⁶A levels was observed in the OsMTA1, OsMTA3, and OsMTA4 knockout lines (Zhang et al., 2019). This suggested that OsMTA2 and OsFIP are the main components of the m⁶A methyltransferase complex in rice (Zhang et al., 2019).

ERASERS

ALKBH9B (At2g17970) and ALKBH10B (At4g02940) have been shown to be active m⁶A demethylases concerning *Arabidopsis* system (Duan et al., 2017; Martínez-Pérez et al., 2017). ALKBH9B was the first m⁶A demethylase reported from *Arabidopsis*, which enables ssRNA to demethylate m⁶A

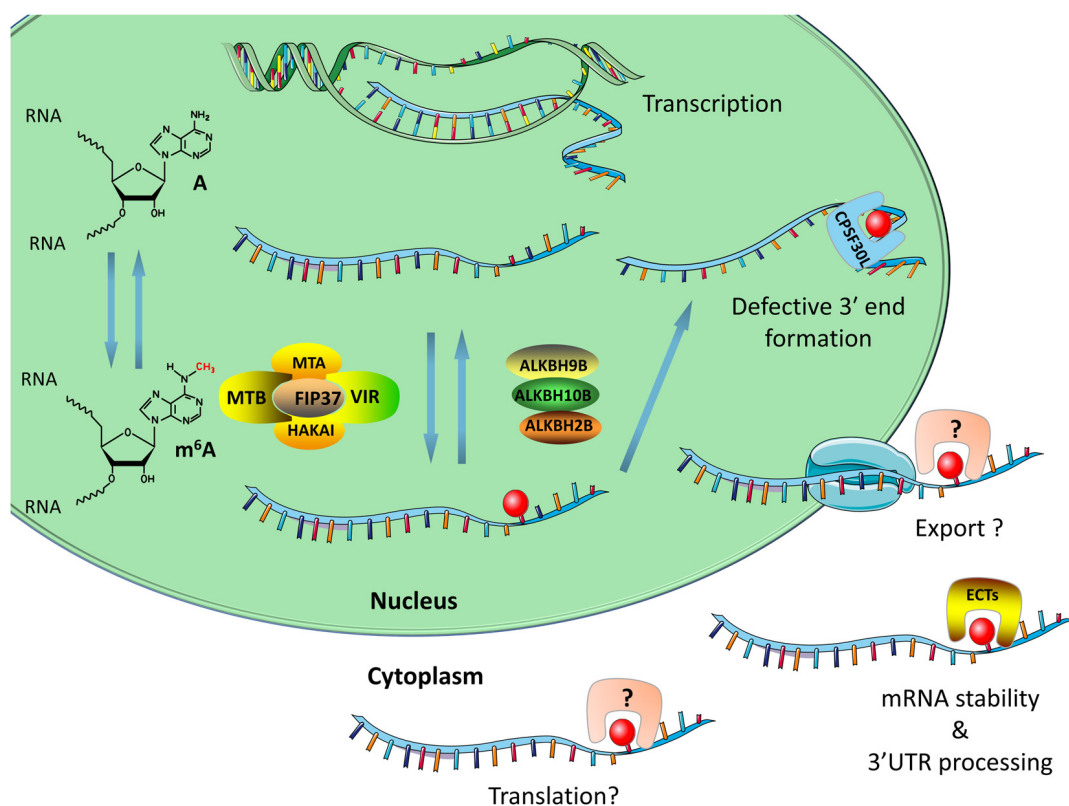


FIGURE 1 | The main components of the m⁶A system in plants include writers, erasers, and readers. The writers consist of MTA, FIP37, MTB, HAKAI, and VIRILIZER. The demethylases are mainly ALKBH2, ALKBH9B, and ALKBH10B. The m⁶A binding proteins are mainly ECT family proteins and CPSF30, both of which contain a YTH domain. The writers and erasers are responsible for adding or removing m⁶A site on RNA. The readers interact with m⁶A-modified RNA and regulate RNA splicing, RNA stability, and 3'UTR processing. This figure was created using smart Servier Medical Art (<https://smart.servier.com/>).

in vitro. Moreover, ALKBH9B has a positive effect on viral abundance in plant cells. These findings indicate that methylation status plays an important role in regulating viral infection in *Arabidopsis* (Martínez-Pérez et al., 2017). Duan et al. (2017) also demonstrated that ALKBH10B-mediated demethylation of mRNA m⁶A affects the mRNA stability of key flowering time regulators, thereby affecting flower turnover. *In vitro* experiments and those involving transient transformation of tobacco showed that tomato SLALKBH2 can effectively remove m⁶A modification and reduce the m⁶A level *in vitro* and *in vivo* (Zhou et al., 2019). This indicates that tomato SLALKBH2 has m⁶A demethylation activity (Zhou et al., 2019).

READERS

The member of the ECT family containing the YTH domain is the most important m⁶A binding protein in plants (Anderson et al., 2018; Arribas-Hernández et al., 2018; Scutenaire et al., 2018). Scutenaire showed that ECT2 binds to m⁶A via a tri-tryptophan pocket, and if these amino acids are mutated, ECT2 loses its m⁶A binding ability (Scutenaire et al., 2018). They also showed that *ect* mutants share phenotypes (defective trichomes) with *mta* mutants and FIP37-overexpressing transgenic lines, and

the morphological changes in the *ect* mutant are the result of higher cell ploidy caused by intranuclear replication (Scutenaire et al., 2018), this result was consistent with the phenomenon observed by Arribas-Hernández et al. (2018). In addition, ECT2 improves the stability of m⁶A methylated RNAs transcribed from genes involved in trichome morphogenesis (Wei et al., 2018). This observation contrasts to the reported decrease in stability of RNAs caused by the binding of YTHDF proteins to this mark in animal systems (Du et al., 2016). However, a previous study by Shen in *Arabidopsis* found that m⁶A destabilizes a few transcripts in undifferentiated tissues (Shen et al., 2016). Thus, the mechanisms by which m⁶A regulates transcript stability have still not been completely clarified in any organism. In a study focused more on the morphological aspects of ECT proteins, including ECT2/3 and 4, it was shown that these proteins are intrinsically important for proper leaf morphogenesis, including trichome branching (Arribas-Hernández et al., 2018).

As described in a recent report, sequence analysis of m⁶A methyltransferase in 22 plants using *Arabidopsis* as a model plant revealed that, in higher plants, the number of m⁶A writers is greater than that in lower plants (Yue et al., 2019). This suggests that higher plants may require more precise mechanisms regulating m⁶A modification to cope with complex and variable environments (Yue et al., 2019).

Summarizing recent research, we can find that the key component genes of the m⁶A system are mainly concentrated in meristems and reproductive organs, and lower expression in tissues that stop differentiation and mature (Zhong et al., 2008; Hofmann, 2017; Růžicka et al., 2017; Zhang et al., 2019; Zhou et al., 2019). This suggests that m⁶A modifications are more likely to occur on actively transcribed genes. Besides, m⁶A modifications are detected on mRNA, rRNA, tRNA, and sn(o)RNA in plant system (Li et al., 2014; Luo et al., 2014; Wan et al., 2015; Anderson et al., 2018; Parker et al., 2020).

EFFECT OF m⁶A MODIFICATION ON RNA FUNCTION

The above main components of the m⁶A system above regulate the fate of RNA, by adding, removing, and binding m⁶A site on RNA. In mammals, m⁶A modification plays an important role in the regulation of RNA splicing (Liu et al., 2015, 2017; Haussmann et al., 2016; Lence et al., 2016; Xiao et al., 2016; Pendleton et al., 2017), RNA stability (Wang et al., 2014; Du et al., 2016; Mishima and Tomari, 2016; Huang et al., 2018), RNA export (Roundtree et al., 2017; Edens et al., 2019), 3' UTR processing (Ke et al., 2015; Bartosovic et al., 2017; Wei et al., 2018; Yue et al., 2018), translation (Zhou et al., 2015; Choi et al., 2016; Li et al., 2017; Shi et al., 2017), and miRNA processing (Alarcón et al., 2015a,b; Bhat et al., 2019). On the contrary, much less is known about the function of m⁶A modification regulation of RNA on plant. Our understanding of how the m⁶A regulated RNA fate is limited to it's an mRNA stabilizing (Shen et al., 2016; Hofmann, 2017; Wei et al., 2018) or 3' UTR processing at specific genomic loci (Pontier et al., 2019) mark. The roles in regulating plant RNA export, RNA splicing, and translation remain unexplored. In addition, research on the effect of m⁶A modification on RNA has mainly focused on genetic interference, and there is no way to accurately predict the effect of m⁶A modification on RNA at the transcriptome-wide level. Only one or some of the effects of RNA due to changes in m⁶A modification can be identified.

3' UTR PROCESSING

In animal systems, m⁶A modification has been widely reported to regulate mRNA processing including RNA splicing (Liu et al., 2015, 2017; Haussmann et al., 2016; Lence et al., 2016; Xiao et al., 2016; Pendleton et al., 2017) and 3' UTR processing (Ke et al., 2015; Bartosovic et al., 2017; Yue et al., 2018). For example, in *Drosophila*, m⁶A modification regulates the sex selection process by regulating alternative splicing of the sex determination factor Sex lethal (Sxl) pre-mRNA (Haussmann et al., 2016; Lence et al., 2016); In animal cells, METTL16 regulates the SAM synthetase gene *MAT2A* splicing process by regulating the m⁶A modification on *MAT2A* mRNA, thereby regulating regulate SAM homeostasis (Pendleton et al., 2017). YTH domain-containing protein YTHDC1 regulates the cleavage process by recognizing m⁶A on mRNA and recruiting the SR protein to its corresponding binding site (Xiao et al., 2016).

Therefore, m⁶A is also considered to be a post-transcriptional regulator of mRNA splicing in animal systems.

In *Arabidopsis*, the methyltransferase VIRILIZER was found to be co-localized with the splicing factor SR34, but no abnormally spliced transcript was detected in the root of VIRILIZER mutant (Růžicka et al., 2017). This suggests that m⁶A is not involved in large-scale splicing regulation of plant transcripts, which appears to contrast with the findings reported from animals (Xiao et al., 2016). Alternatively, variable splicing regulated by m⁶A occurs only on specific transcripts or specific tissues, but the level of this is below the limit of detection of the method used for analyzing it.

In mammals, m⁶A modification regulates alternative poly(A) sites (APA) during 3' UTR processing (Ke et al., 2015; Bartosovic et al., 2017; Yue et al., 2018). Research by Ke et al. (2015) shows that higher m⁶A modification in the last exon may affect the usage of APA, while Bartosovic et al. (2017) further shows that m⁶A modification in the last exon regulates 3' UTR length by regulating APA. A similar situation was found in plant systems. A recent study showed that the loss of methylation enzyme function of FIP37 resulted in a decrease in m⁶A modification (Shen et al., 2016) and the pair of spatially adjacent two genes (such as the pair AT4G30570/580 or AT1G71330/340) to form chimeric mRNA (Pontier et al., 2019). The m⁶A modification can assist in the polyadenylation of the first gene mRNA, thereby limiting mis-splicing to form chimeric mRNA (Pontier et al., 2019). However, this process requires the assistance of F30L, which is a protein comprising the typical m⁶A recognition protein domain YTH (Figure 1; Pontier et al., 2019). This suggested that the m-ASP (m⁶A-assisted polyadenylation) pathway ensures transcriptome integrity at rearranged genomic loci in plants (Pontier et al., 2019).

mRNA STABILITY

How does m⁶A modification work in plant systems? The most recent report on this issue describes that m⁶A regulates plant growth and development by affecting mRNA stability. The lack of the *Arabidopsis* methyltransferase FIP37 results in reduced m⁶A modification on the mRNA encoded by SAM proliferation-related genes [WUSCHEL (WUS) and SHOOTMERISTEMLESS (STM)], and enhances its stability (Shen et al., 2016). Excessive accumulation of WUS and STM mRNA causes excessive proliferation of SAM (Shen et al., 2016). However, Duan et al. (2017) obtained results that differ from these findings. Specifically, in the functional deletion mutant of *Arabidopsis* demethylase ALKBH10B, m⁶A modification on the mRNA encoded by key genes regulating FT, SPL3, and SPL9 was increased, which reduced its stability, accelerated its degradation, and produced a delayed flowering phenotype (Hofmann, 2017). In addition, studies on the m⁶A reader ECT2 in plants have indicated that it plays an important role in regulating 3' UTR processing in the nucleus and promoting mRNA stabilization in the cytoplasm (Figure 1; Wei et al., 2018). Loss of function of ECT2 accelerates the degradation of three ECT2-binding mRNAs involved in morphogenesis of the trichome, thereby affecting the branching of the trichome (Wei et al., 2018).

Although m⁶A modification may stabilize mRNA in plants, no consensus on this issue has yet been reached. In addition, after the modification of methylation of mRNA, m⁶A binding protein also plays an important role. Moreover, studies on the stability of mRNA by m⁶A modification have mostly focused on a single mRNA, and cannot explain the effect of m⁶A modification on mRNA stability across the transcriptome. In summary, m⁶A may have different effects on mRNA stability in different tissues or organs. It should be emphasized that m⁶A readers may play precise and complex regulatory roles by recognizing changes in m⁶A modification on mRNA.

PLANT GROWTH AND DEVELOPMENT

The mechanism of how m⁶A modification regulates the fate of plant RNA is still unclear. Previous studies have shown that the loss of function of any key component in the m⁶A system of writers, erasers, or readers can cause disorders in the m⁶A regulatory system, leading to abnormal growth and development (Figure 2). The lack or reduction of m⁶A writers, including MTA (Zhong et al., 2008; Anderson et al., 2018), MTB, FIP37 (Vespa et al., 2004), Virilizer (Růžicka et al., 2017), and HAKAI (Růžicka et al., 2017), results in a significant reduction in the overall level of m⁶A. This causes phenotypes including embryonic lethality, epidermal hair development abnormality, defective leaf sprouting, and excessive proliferation of vegetative shoot apical meristem. Moreover, loss of function of the eraser ALKBH10B results in leaf dysplasia and a delayed flowering phenotype in *Arabidopsis* (Hofmann, 2017). Several studies on m⁶A reader ECT family members have also comprehensively demonstrated the role of ECT protein in regulating *Arabidopsis* leaf and epidermal hair development (Arribas-Hernández et al., 2018; Scutenaire et al., 2018; Wei et al., 2018).

In addition, the role of m⁶A modification in regulating the growth and development of other plants has also begun to be discovered. In rice, the m⁶A writer OsFIP regulates the development of pollen microspores by directly mediating the addition of m⁶A to a group of threonine proteases and NTPase mRNA, and regulates its expression and splicing (Zhang et al., 2019). In addition, the complete loss of function of OsFIP leads to a decrease in the level of m⁶A modification and early degeneration of microspores at the vacuolated pollen stage (Zhang et al., 2019).

Summarizing current studies, we find that the core component of m⁶A in plant is mainly expressed in meristems, but at low levels in mature tissues and leaves. This suggests that the main regulatory mechanisms of m⁶A acting on plant growth and development are achieved by adding, removing, or recognizing m⁶A sites on transcripts that are particularly important for the growth and development of the above-mentioned organs and tissues. In addition, the use of genetic interference methods to study the function of m⁶A modification will lead to changes in the overall level of m⁶A modification, and produce unpredictable effects, we need a useful tool to exploring the functions of specific site m⁶A modifications on RNA.

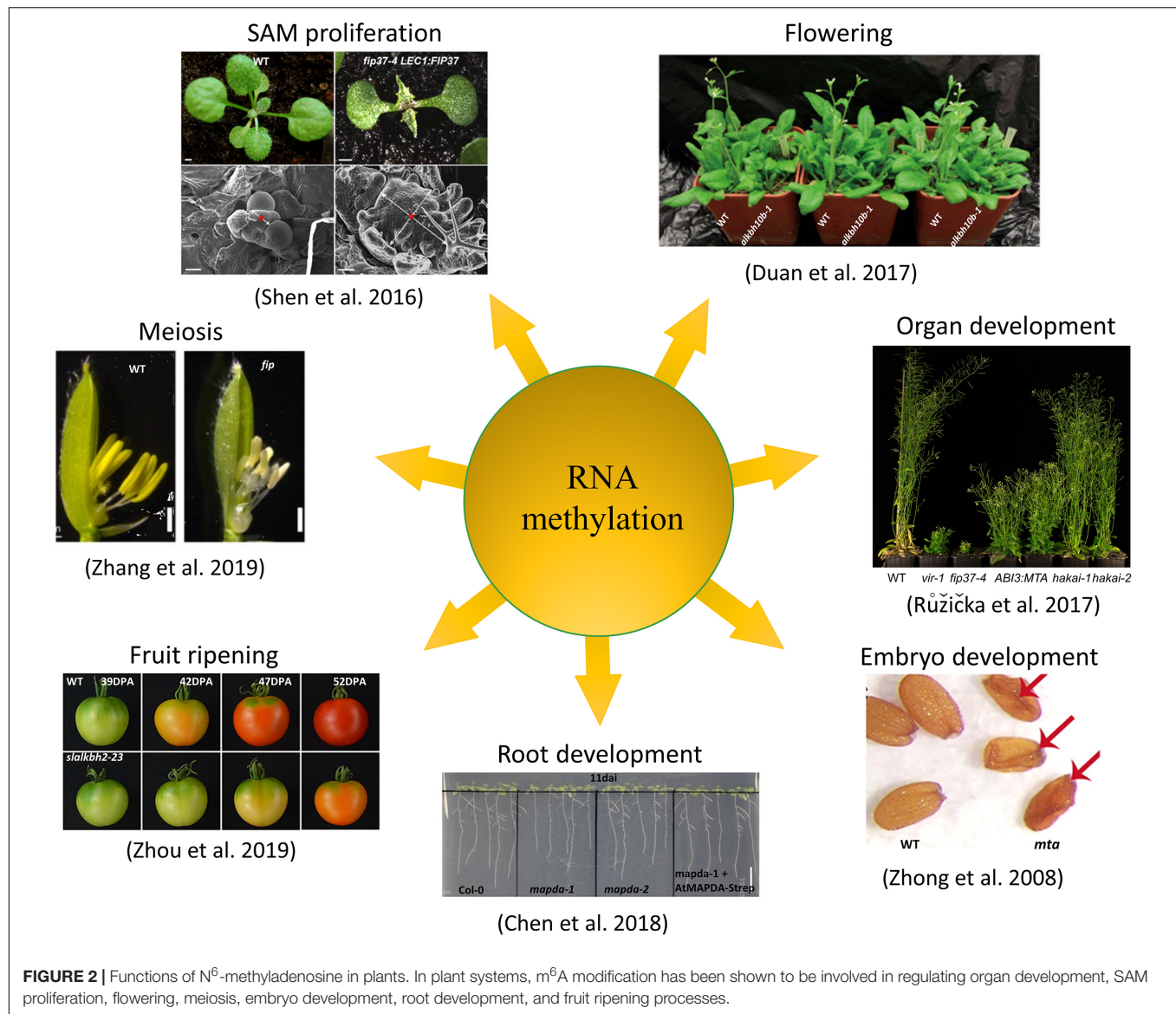
FUNCTION IN BIOTIC STRESS ADAPTATION

Plants have evolved a series of regulatory mechanisms in response to viral infections. These include sRNA (silencing based on small RNA) (Llave, 2010; Pumplin and Voinnet, 2013; Sharma et al., 2013), DNA methylation (Tirnaz and Batley, 2019), and RNA methylation (Martínez-Pérez et al., 2017). In animal systems, m⁶A modification has been reported to play an important role in regulating viral replication and the viral life cycle (Gokhale et al., 2016; Kennedy et al., 2016; Lichinchi et al., 2016a,b; Tirumuru et al., 2016). However, in plants, with the exception of the smaller group of DNA viruses, most viruses are RNA viruses. RNA viruses are hardly affected by DNA methylation because they do not have DNA during replication. As a widespread modification on RNA, m⁶A modification may have great potential in regulating plant anti-RNA virus infection.

In the *Arabidopsis* T-DNA insertion mutant of *alkbh9b*, the overall m⁶A level of viral RNA was found to be increased, and relative to the decrease in viral accumulation in the wild type, its resistance to alfalfa mosaic virus (AMV) was enhanced (Martínez-Pérez et al., 2017). It should be emphasized that ALKBH9B does not exhibit the ability to regulate cucumber mosaic virus (CMV) infection. This may be due to the fact that ALKBH9B can interact with the coat protein (CP) of AMV, but not with that of CMV (Martínez-Pérez et al., 2017). In addition, in tobacco, the level of m⁶A modification in tobacco is significantly reduced after infection with TMV (Li et al., 2018). This study suggests that m⁶A modification may represent a host regulatory mechanism for plants to respond to viral infections. Interestingly, in the genome of several single-stranded RNA plant viruses, ALKB containing a conserved domain has been identified (Bratlie and Drabløs, 2005; Van Den Born et al., 2008). This suggests that some plant viruses have evolved mechanisms to respond to host m⁶A system regulation.

ABIOTIC STRESS PROCESS

In responding to environmental stress, m⁶A modification exhibits high sensitivity and complexity in the regulation of responses to heat stress, salt stress, and drought stress. Under salt stress, the m⁶A system enhances the stability of transcripts by adding m⁶A sites to salt-tolerant transcripts to regulate the salt tolerance process in *Arabidopsis* (Anderson et al., 2018). Under drought stress, the expression levels of the maize writer and reader members of the ALKBH10 family and ECT2 family were found to be increased, and the overall level of m⁶A modification in cells was decreased (Miao et al., 2020). In addition, in different genotypes of maize, m⁶A modifications were shown to be concentrated on different transcripts. This suggests that m⁶A modification is involved in the regulation of maize drought resistance and that there are different regulatory mechanisms in different genotypes of maize (Miao et al., 2020). Under heat stress conditions, the *Arabidopsis* reader ECT2 was found to respond to heat stress and relocate to stress granules (SGs) in the cell (Scutenaire et al., 2018; Wei et al., 2018). This process



may result in the mRNA that binds to ECT2 relocalizing to stress particles under heat stress. Existing research suggests that the reader regulation of RNA is more direct and rapid than that by adding or erasing m⁶A sites on RNA, which relies on a writer and eraser. Regulation by a reader can be based on m⁶A modification on the original mRNA, and it can rapidly regulate the stress signal, especially in regulating short-term stress.

CONCLUSION AND PERSPECTIVES

At present, most m⁶A modification maps in plant systems was drawn by the m⁶A-seq method. However, there are some limitations to this approach, such as the need for a large number of samples, high requirements for antibody quality, and inability to accurately locate the position of m⁶A modifications on RNA. Although some improvements have been made to the resolution

of m⁶A-seq, including m⁶A individual-nucleotide-resolution cross-linking and immunoprecipitation (miCLIP) (Linder et al., 2015), photo-crosslinking-assisted m⁶A-seq (PA-m⁶A-seq) (Chen et al., 2015), and m⁶A-cross-linking immunoprecipitation (m⁶A-CLIP) (Ke et al., 2015), but these improved methods still have not yet been tested in plants. In addition, m⁶A modifications are mainly concentrated in meristematic and reproductive organs, suggesting that m⁶A modifications are more likely to occur on actively transcribed genes. The sample size of these sites is often small, and the m⁶A-seq methods cannot accurately detect m⁶A modifications in tissues or cells and perform biological duplication. Therefore, for the development of new m⁶A detection methods, especially to reduce the sample size and improve detection accuracy, accurate identification of m⁶A modification at the cellular level is necessary.

Compared with detection methods based on NGS or PCR amplification, the technology of direct detection of m⁶A

modification on RNA, including single-molecule real-time (SMRT) (Vilfan et al., 2013) and single-molecule nanoporous sequencing has great potential. Because PCR amplification is not required, direct detection-based methods do not produce base mismatches and PCR bias, and have the potential to detect multiple types of RNA modification at the same time. And only a lower sample starting amount is required. Ayub et al. have used α -hemolysin (α HL) nanopore sequencing to distinguish between modified and unmodified bases in RNA, including m⁶A and 5-methylcytosine (m⁵C) (Ayub and Bayley, 2012). Especially in recent years, nanopore sequencing technology has developed rapidly. Garalde et al. have developed a method for highly parallel direct RNA sequencing on Highly parallel direct RNA sequencing on an array of nanopores (Garalde et al., 2018). Parker et al. used nanopore sequencing technology to map the m⁶A modification in *Arabidopsis thaliana*, and revealed the complexity of m⁶A dynamic modification during mRNA processing (Parker et al., 2020). Therefore, we believe that nanopore sequencing is very suitable for studying small molecule samples and has the potential to accelerate the study of biological functions of modifications on RNA.

The m⁶A enzyme plays a fundamental role in the m⁶A regulatory system. However, the number of m⁶A enzymes found to date in plants is small relative to the number in animals, and no homolog of the major demethylase FTO in animals has been found. Only one demethylase of the ALKBH family was discovered (Hofmann, 2017; Martínez-Pérez et al., 2017; Zhou et al., 2019), and it is unclear whether ALKBH family protein can complete the removal of the m⁶A site on the mRNA. Therefore, it is also very important to find more key components of the m⁶A system in plants. In addition, it is not clear how writers and erasers selectively add or remove m⁶A on RNA, which may be related to the special secondary structure of RNA. Cryo-electron microscopy and molecular imaging may help to explore the process of m⁶A selective modification.

The main way to explore the function of m⁶A modification is still through genetic interference. However, the impact of

adding or removing any key component of the m⁶A system on plants may be far more than we are concerned about. Therefore, the development of RNA methylation without changing the nucleotide sequence and the overall m⁶A modification level may be a major development regarding m⁶A for exploring the m⁶A function in the future. The CRISPR–Cas9 technology is rapidly evolving and has enabled accurate genome editing, including targeted DNA cleavage, repair, direct base editing, and site-specific epigenome editing. Recently, researchers have used a similar method to fuse m⁶A writers or erasers with Cas protein, and under the guidance of sgRNA and PAMer, edit the m⁶A modification on specific mRNA in the cell (Wei and He, 2019). This method of editing m⁶A did not change the nucleotide sequence and the overall m⁶A modification level (Wei and He, 2019). This method provides a new tool for studying the biological function of m⁶A modification and makes it possible to edit m⁶A at a specific site to improve crop quality.

AUTHOR CONTRIBUTIONS

HZ and SL prepared the manuscript. NS and XZ conceptualized the idea and revised the manuscript. All authors read and approved the final manuscript.

FUNDING

We are grateful for financial support from the National Natural Science Research Foundation of China (31871538 and U1906204), the National Key R&D Program of China (2018YFD1000700 and 2018YFD1000704), Shandong Province Key Research and Development Program (2019GSF107079), the Development Plan for Youth Innovation Team of Shandong Provincial (2019KJE012), and the Opening Foundation of Shandong Key Laboratory of Crop Genetic Improvement, Ecology and Physiology (SDKL2018008-3).

REFERENCES

- Agarwala, S. D., Blitzblau, H. G., Hochwagen, A., and Fink, G. R. (2012). RNA methylation by the MIS complex regulates a cell fate decision in yeast. *PLoS Genet.* 8:e1002732. doi: 10.1371/journal.pgen.1002732
- Alarcón, C. R., Goodarzi, H., Lee, H., Liu, X., Tavazoie, S., and Tavazoie, S. F. (2015a). HNRNPA2B1 is a mediator of m⁶A-dependent nuclear RNA processing events. *Cell* 162, 1299–1308. doi: 10.1016/j.cell.2015.08.011
- Alarcón, C. R., Lee, H., Goodarzi, H., Halberg, N., and Tavazoie, S. F. (2015b). N⁶-methyladenosine marks primary microRNAs for processing. *Nature* 519, 482–425. doi: 10.1038/nature14281
- Anderson, S. J., Kramer, M. C., Gosai, S. J., Yu, X., Vandivier, L. E., Nelson, A. D. L., et al. (2018). N⁶-methyladenosine inhibits local ribonucleolytic cleavage to stabilize mRNAs in *Arabidopsis*. *Cell Rep.* 25, 1146.e3–1157.e3. doi: 10.1016/j.celrep.2018.10.020
- Arribas-Hernández, L., Bressendorff, S., Hansen, M. H., Poulsen, C., Erdmann, S., and Brodersen, P. (2018). An m⁶A-YTH module controls developmental timing and morphogenesis in *Arabidopsis*. *Plant Cell* 30, 952–976. doi: 10.1105/tpc.17.00833
- Ayub, M., and Bayley, H. (2012). Individual RNA base recognition in immobilized oligonucleotides using a protein nanopore. *Nano Lett.* 12, 5637–5643. doi: 10.1021/nl3027873
- Bailey, A. S., Batista, P. J., Gold, R. S., Chen, Y. G., de Rooij, D. G., Chang, H. Y., et al. (2017). The conserved RNA helicase YTHDC2 regulates the transition from proliferation to differentiation in the germline. *eLife* 6:e26116. doi: 10.7554/eLife.26116
- Bartosovic, M., Molares, H. C., Gregorova, P., Hrossova, D., Kudla, G., and Vanacova, S. (2017). N⁶-methyladenosine demethylase FTO targets pre-mRNAs and regulates alternative splicing and 3'-end processing. *Nucleic Acids Res.* 45, 11356–11370. doi: 10.1093/nar/gkx778
- Bhat, S. S., Bielewicz, D., Grzelak, N., Gulanicz, T., Bodi, Z., Szewc, L., et al. (2019). mRNA adenosine methylase (MTA) deposits m⁶A on pri-miRNAs to modulate miRNA biogenesis in *Arabidopsis thaliana*. *bioRxiv* [Preprint]. doi: 10.1101/557900
- Bodi, Z., Zhong, S., Mehra, S., Song, J., Li, H., Graham, N., et al. (2012). Adenosine methylation in *Arabidopsis* mRNA is associated with the 3' end and reduced levels cause developmental defects. *Front. Plant Sci.* 3:48. doi: 10.3389/fpls.2012.00048

- Bokar, J. A., Rath-Shambaugh, M. E., Ludwiczak, R., Narayan, P., and Rottman, F. (1994). Characterization and partial purification of mRNA N⁶-adenosine methyltransferase from HeLa cell nuclei. Internal mRNA methylation requires a multisubunit complex. *J. Biol. Chem.* 269, 17697–17704.
- Bratlie, M. S., and Drablos, F. (2005). Bioinformatic mapping of AlkB homology domains in viruses. *BMC Genomics* 6:1. doi: 10.1186/1471-2164-6-1
- Chen, K., Lu, Z., Wang, X., Fu, Y., Luo, G. Z., Liu, N., et al. (2015). High-resolution N⁶-methyladenosine (m⁶A) map using photo-crosslinking-assisted m⁶A sequencing. *Angew. Chem. Int. Ed.* 54, 1587–1590. doi: 10.1002/anie.201410647
- Chen, M., Urs, M. J., Sánchez-González, I., Olayioye, M. A., Herde, M., and Witte, C.-P. (2018). m⁶A RNA degradation products are catabolized by an evolutionarily conserved N⁶-Methyl-AMP deaminase in plant and mammalian cells. *Plant Cell* 30, 1511–1522. doi: 10.1105/tpc.18.00236
- Choi, J., Jeong, K.-W., Demirci, H., Chen, J., Petrov, A., Prabhakar, A., et al. (2016). N⁶-methyladenosine in mRNA disrupts tRNA selection and translation-elongation dynamics. *Nat. Struct. Mol. Biol.* 23, 110–115.
- Craigon, D. J., James, N., Okyere, J., Higgins, J., Jotham, J., and May, S. (2004). NASCArrays: a repository for microarray data generated by NASC's transcriptomics service. *Nucleic Acids Res.* 32, D575–D577. doi: 10.1093/nar/gkh133
- Desrosiers, R., Friderici, K., and Rottman, F. (1974). Identification of methylated nucleosides in messenger RNA from novikoff hepatoma cells. *Proc. Natl. Acad. Sci.* 71, 3971–3975. doi: 10.1073/pnas.71.10.3971
- Dominissini, D., Moshitch-Moshkovitz, S., Schwartz, S., Salmon-Divon, M., Ungar, L., Osenberg, S., et al. (2012). Topology of the human and mouse m⁶A RNA methylomes revealed by m⁶A-seq. *Nature* 485, 201. doi: 10.1038/nature11112
- Du, H., Zhao, Y., He, J., Zhang, Y., Xi, H., Liu, M., et al. (2016). YTHDF2 destabilizes m⁶A-containing RNA through direct recruitment of the CCR4–NOT deadenylase complex. *Nat. Commun.* 7, 121–126. doi: 10.1038/ncomms12626
- Duan, H.-C., Wei, L.-H., Zhang, C., Wang, Y., Chen, L., Lu, Z., et al. (2017). ALKBH10B is an RNA N⁶-methyladenosine demethylase affecting *Arabidopsis* floral transition. *Plant Cell* 29, 2995–3011. doi: 10.1105/tpc.16.00912
- Edens, B. M., Vissers, C., Su, J., Arumugam, S., Xu, Z., Shi, H., et al. (2019). FMRP modulates neural differentiation through m⁶A-Dependent mRNA Nuclear Export. *Cell Rep.* 28, 845–854. doi: 10.1016/j.celrep.2019.06.072
- Garalde, D. R., Snell, E. A., Jachimowicz, D., Sipos, B., Lloyd, J. H., Bruce, M., et al. (2018). Highly parallel direct RNA sequencing on an array of nanopores. *Nat. Methods* 15:201. doi: 10.1038/nmeth.4577
- Geula, S., Moshitch-Moshkovitz, S., Dominissini, D., Mansour, A. A., Kol, N., Salmon-Divon, M., et al. (2015). m⁶A mRNA methylation facilitates resolution of naïve pluripotency toward differentiation. *Science* 347, 1002–1006. doi: 10.1126/science.1261417
- Gokhale, N. S., McIntyre, A. B., McFadden, M. J., Roder, A. E., Kennedy, E. M., Gandara, J. A., et al. (2016). N⁶-methyladenosine in Flaviviridae viral RNA genomes regulates infection. *Cell Host Microb.* 20, 654–665. doi: 10.1016/j.chom.2016.09.015
- Hausmann, I. U., Bodi, Z., Sanchez-Moran, E., Mongan, N. P., Archer, N., Fray, R. G., et al. (2016). m⁶A potentiates Sxl alternative pre-mRNA splicing for robust *Drosophila* sex determination. *Nature* 540, 301–304. doi: 10.1038/nature20577
- Hofmann, N. R. (2017). Epitranscriptomics and flowering: mRNA methylation/demethylation regulates flowering time. *Plant Cell* 29, 2949–2950. doi: 10.1105/tpc.17.00929
- Hsu, P. J., Zhu, Y., Ma, H., Guo, Y., Shi, X., Liu, Y., et al. (2017). Ythdc2 is an N⁶-methyladenosine binding protein that regulates mammalian spermatogenesis. *Cell Res.* 27, 1115–1127. doi: 10.1038/cr.2017.99
- Huang, H., Weng, H., Sun, W., Qin, X., Shi, H., Wu, H., et al. (2018). Recognition of RNA N⁶-methyladenosine by IGF2BP proteins enhances mRNA stability and translation. *Nat. Cell Biol.* 20, 285–295. doi: 10.1038/s41556-018-0045-z
- Jia, G., Fu, Y., Zhao, X., Dai, Q., Zheng, G., Yang, Y., et al. (2011). N⁶-methyladenosine in nuclear RNA is a major substrate of the obesity-associated FTO. *Nat. Chem. Biol.* 7, 885–887. doi: 10.1038/nchembio.687
- Ke, S., Alemu, E. A., Mertens, C., Gantman, E. C., Fak, J. J., Mele, A., et al. (2015). A majority of m⁶A residues are in the last exons, allowing the potential for 3' UTR regulation. *Genes Dev.* 29, 2037–2053. doi: 10.1101/gad.269415.115
- Kennedy, E. M., Bogerd, H. P., Kornepati, A. V., Kang, D., Ghoshal, D., Marshall, J. B., et al. (2016). Posttranscriptional m⁶A editing of HIV-1 mRNAs enhances viral gene expression. *Cell Host Microbe* 19, 675–685. doi: 10.1016/j.chom.2016.04.002
- Kennedy, T. D., and Lane, B. G. (1979). Wheat embryo ribonucleates. XIII. Methyl-substituted nucleoside constituents and 5'-terminal dinucleotide sequences in bulk poly(A)-rich RNA from imbibing wheat embryos. *Can. J. Biochem.* 57, 927–931. doi: 10.1139/o79-112
- Lence, T., Akhtar, J., Bayer, M., Schmid, K., Spindler, L., Ho, C. H., et al. (2016). m⁶A modulates neuronal functions and sex determination in *Drosophila*. *Nature* 540, 242–247. doi: 10.1038/nature20568
- Li, A., Chen, Y.-S., Ping, X.-L., Yang, X., Xiao, W., Yang, Y., et al. (2017). Cytoplasmic m⁶A reader YTHDF3 promotes mRNA translation. *Cell Res.* 27, 444–447. doi: 10.1038/cr.2017.10
- Li, Y., Wang, X., Li, C., Hu, S., Yu, J., and Song, S. (2014). Transcriptome-wide N⁶-methyladenosine profiling of rice callus and leaf reveals the presence of tissue-specific competitors involved in selective mRNA modification. *RNA Biol.* 11, 1180–1188. doi: 10.4161/rna.36281
- Li, Z., Shi, J., Yu, L., Zhao, X., Ran, L., Hu, D., et al. (2018). N⁶-methyl-adenosine level in *Nicotiana tabacum* is associated with tobacco mosaic virus. *Virol. J.* 15:87. doi: 10.1186/s12985-018-0997-4
- Lichinchi, G., Gao, S., Saletore, Y., Gonzalez, G. M., Bansal, V., Wang, Y., et al. (2016a). Dynamics of the human and viral m⁶A RNA methylomes during HIV-1 infection of T cells. *Nat. Microbiol.* 1:16011. doi: 10.1038/nmicrobiol.2016.11
- Lichinchi, G., Zhao, B. S., Wu, Y., Lu, Z., Qin, Y., He, C., et al. (2016b). Dynamics of human and viral RNA methylation during Zika virus infection. *Cell Host Microbe* 20, 666–673. doi: 10.1016/j.chom.2016.10.002
- Linder, B., Grozhik, A. V., Olarerin-George, A. O., Meydan, C., Mason, C. E., and Jaffrey, S. R. (2015). Single-nucleotide-resolution mapping of m⁶A and m⁶Am throughout the transcriptome. *Nat. Methods* 12, 767–772. doi: 10.1038/nmeth.3453
- Liu, J., Yue, Y., Han, D., Wang, X., Fu, Y., Zhang, L., et al. (2014). A METTL3–METTL14 complex mediates mammalian nuclear RNA N⁶-adenosine methylation. *Nat. Chem. Biol.* 10, 93–95. doi: 10.1038/nchembio.1432
- Liu, N., Dai, Q., Zheng, G., He, C., Parisien, M., and Pan, T. (2015). N⁶-methyladenosine-dependent RNA structural switches regulate RNA-protein interactions. *Nature* 518, 560–564. doi: 10.1038/nature14234
- Liu, N., Zhou, K. I., Parisien, M., Dai, Q., Diatchenko, L., and Pan, T. (2017). N⁶-methyladenosine alters RNA structure to regulate binding of a low-complexity protein. *Nucleic Acids Res.* 45, 6051–6063. doi: 10.1093/nar/gkx141
- Llave, C. (2010). Virus-derived small interfering RNAs at the core of plant–virus interactions. *Trends Plant Sci.* 15, 701–707. doi: 10.1016/j.tplants.2010.09.001
- Luo, G.-Z., MacQueen, A., Zheng, G., Duan, H., Dore, L. C., Lu, Z., et al. (2014). Unique features of the m⁶A methylome in *Arabidopsis thaliana*. *Nat. Commun.* 5:5630. doi: 10.1038/ncomms5630
- Luo, J., Wang, Y., Wang, M., Zhang, L., Peng, H., Zhou, Y., et al. (2020). Natural variation in RNA m⁶A methylation and its relationship with translational status. *Plant Physiol.* 182, 332–344. doi: 10.1104/pp.19.00987
- Martínez-Pérez, M., Aparicio, F., López-Gresa, M. P., Bellés, J. M., Sánchez-Navarro, J. A., and Pallás, V. (2017). *Arabidopsis* m⁶A demethylase activity modulates viral infection of a plant virus and the m⁶A abundance in its genomic RNAs. *Proc. Natl. Acad. Sci. U.S.A.* 114:10755. doi: 10.1073/pnas.1703139114
- Meyer, K. D., Patil, D. P., Zhou, J., Zinoviev, A., Skabkin, M. A., Elemento, O., et al. (2015). 5' UTR m⁶A promotes cap-independent translation. *Cell* 163, 999–1010. doi: 10.1016/j.cell.2015.10.012
- Meyer, K. D., Saletore, Y., Zumbo, P., Elemento, O., Mason, C. E., and Jaffrey, S. R. (2012). Comprehensive analysis of mRNA methylation reveals enrichment in 3' UTRs and near stop codons. *Cell* 149, 1635–1646. doi: 10.1016/j.cell.2012.05.003
- Miao, Z., Zhang, T., Qi, Y., Song, J., Han, Z., and Ma, C. (2020). Evolution of the RNA N⁶-methyladenosine methylome mediated by genomic duplication. *Plant Physiol.* 182, 345–360. doi: 10.1104/pp.19.00323

- Mishima, Y., and Tomari, Y. (2016). Codon usage and 3' UTR length determine maternal mRNA stability in zebrafish. *Mol. Cell* 61, 874–885. doi: 10.1016/j.molcel.2016.02.027
- Nichols, J. (1979). N⁶-methyladenosine in maize poly (A)-containing RNA. *Plant Sci. Lett.* 15, 357–361. doi: 10.1016/0304-4211(79)90141-X
- Parker, M. T., Knop, K., Sherwood, A. V., Schurch, N. J., Mackinnon, K., Gould, P. D., et al. (2020). Nanopore direct RNA sequencing maps the complexity of *Arabidopsis* mRNA processing and m⁶A modification. *eLife* 9:e49658. doi: 10.7554/eLife.49658
- Pendleton, K. E., Chen, B., Liu, K., Hunter, O. V., Xie, Y., Tu, B. P., et al. (2017). The U6 snRNA m⁶A methyltransferase METTL16 regulates SAM synthetase intron retention. *Cell* 169, 824–835. doi: 10.1016/j.cell.2017.05.003
- Pontier, D., Picart, C., El Baidouri, M., Roudier, F., Xu, T., Lahmy, S., et al. (2019). The m⁶A pathway protects the transcriptome integrity by restricting RNA chimera formation in plants. *Life Sci. Alliance* 2:e201900393. doi: 10.26508/lisa.201900393
- Pumplin, N., and Voinnet, O. (2013). RNA silencing suppression by plant pathogens: defence, counter-defence and counter-counter-defence. *Nat. Rev. Microbiol.* 11, 745–760. doi: 10.1038/nrmicro3120
- Roundtree, I. A., Luo, G.-Z., Zhang, Z., Wang, X., Zhou, T., Cui, Y., et al. (2017). YTHDC1 mediates nuclear export of N⁶-methyladenosine methylated mRNAs. *eLife* 6:e31311. doi: 10.7554/eLife.31311
- Růžicka, K., Zhang, M., Campilho, A., Bodi, Z., Kashif, M., Saleh, M., et al. (2017). Identification of factors required for m⁶A mRNA methylation in *Arabidopsis* reveals a role for the conserved E3 ubiquitin ligase HAKAI. *New Phytol.* 215, 157–172. doi: 10.1111/nph.14586
- Schibler, U., Kelley, D. E., and Perry, R. P. (1977). Comparison of methylated sequences in messenger RNA and heterogeneous nuclear RNA from mouse L cells. *J. Mol. Biol.* 115, 695–714. doi: 10.1016/0022-2836(77)90110-3
- Schwartz, S., Agarwala, S. D., Mumbach, M. R., Jovanovic, M., Mertins, P., Shishkin, A., et al. (2013). High-resolution mapping reveals a conserved, widespread, dynamic mRNA methylation program in yeast meiosis. *Cell* 155, 1409–1421. doi: 10.1016/j.cell.2013.10.047
- Schwartz, S., Mumbach, M. R., Jovanovic, M., Wang, T., Maciag, K., Bushkin, G. G., et al. (2014). Perturbation of m⁶A writers reveals two distinct classes of mRNA methylation at internal and 5' sites. *Cell Rep.* 8, 284–296. doi: 10.1016/j.celrep.2014.05.048
- Scutenaire, J., Deragon, J.-M., Jean, V., Benhamed, M., Raynaud, C., Favory, J.-J., et al. (2018). The YTH domain protein ECT2 is an m⁶A Reader required for normal trichome branching in *Arabidopsis*. *Plant Cell* 30, 986–1005. doi: 10.1105/tpc.17.00854
- Sharma, N., Sahu, P. P., Puranik, S., and Prasad, M. (2013). Recent advances in plant-virus interaction with emphasis on small interfering RNAs (siRNAs). *Mol. Biotechnol.* 55, 63–77. doi: 10.1007/s12033-012-9615-7
- Shen, L., Liang, Z., Gu, X., Chen, Y., Teo, Z. W. N., Hou, X., et al. (2016). N⁶-methyladenosine RNA modification regulates shoot stem cell fate in *Arabidopsis*. *Dev. Cell* 38, 186–200. doi: 10.1016/j.devcel.2016.06.008
- Shi, H., Wang, X., Lu, Z., Zhao, B. S., Ma, H., Hsu, P. J., et al. (2017). YTHDF3 facilitates translation and decay of N⁶-methyladenosine-modified RNA. *Cell Res.* 27, 315–328. doi: 10.1038/cr.2017.15
- Tirnaz, S., and Batley, J. (2019). DNA methylation: toward crop disease resistance improvement. *Trends Plant Sci.* 24, 1137–1150. doi: 10.1016/j.tplants.2019.08.007
- Tirumuru, N., Zhao, B. S., Lu, W., Lu, Z., He, C., and Wu, L. (2016). N⁶-methyladenosine of HIV-1 RNA regulates viral infection and HIV-1 Gag protein expression. *eLife* 5:e15528. doi: 10.7554/eLife.15528
- Van den Born, E., Omelchenko, M. V., Bekkelund, A., Leihne, V., Koonin, E. V., Dolja, V. V., et al. (2008). Viral AlkB proteins repair RNA damage by oxidative demethylation. *Nucleic Acids Res.* 36, 5451–5461. doi: 10.1093/nar/gkn519
- Vespa, L., Vachon, G., Berger, F., Perazza, D., Faure, J.-D., and Herzog, M. (2004). The immunophilin-interacting protein AtFIP37 from *Arabidopsis* is essential for plant development and is involved in trichome endoreduplication. *Plant Physiol.* 134, 1283–1292. doi: 10.1104/pp.103.028050
- Vilfan, I. D., Tsai, Y.-C., Clark, T. A., Wegener, J., Dai, Q., Yi, C., et al. (2013). Analysis of RNA base modification and structural rearrangement by single-molecule real-time detection of reverse transcription. *J. Nanobiotechnol.* 11:8. doi: 10.1186/1477-3155-11-8
- Wan, Y., Tang, K., Zhang, D., Xie, S., Zhu, X., Wang, Z., et al. (2015). Transcriptome-wide high-throughput deep m⁶A-seq reveals unique differential m⁶A methylation patterns between three organs in *Arabidopsis thaliana*. *Genome Biol.* 16:272. doi: 10.1186/s13059-015-0839-2
- Wang, X., Lu, Z., Gomez, A., Hon, G. C., Yue, Y., Han, D., et al. (2014). N⁶-methyladenosine-dependent regulation of messenger RNA stability. *Nature* 505, 117–120. doi: 10.1038/nature12730
- Wang, X., Zhao, B. S., Roundtree, I. A., Lu, Z., Han, D., Ma, H., et al. (2015). N⁶-methyladenosine modulates messenger RNA translation efficiency. *Cell* 161, 1388–1399. doi: 10.1016/j.cell.2015.05.014
- Wei, C.-M., Gershowitz, A., and Moss, B. (1975). Methylated nucleotides block 5' terminus of HeLa cell messenger RNA. *Cell* 4, 379–386. doi: 10.1016/0092-8674(75)90158-0
- Wei, J., and He, C. (2019). Site-specific m⁶A editing. *Nat. Chem. Biol.* 15, 848–849. doi: 10.1038/s41589-019-0349-8
- Wei, L.-H., Song, P., Wang, Y., Lu, Z., Tang, Q., Yu, Q., et al. (2018). The m⁶A Reader ECT2 controls trichome morphology by affecting mRNA stability in *Arabidopsis*. *Plant Cell* 30, 968–985. doi: 10.1105/tpc.17.00934
- Xiao, W., Adhikari, S., Dahal, U., Chen, Y.-S., Hao, Y.-J., Sun, B.-F., et al. (2016). Nuclear m⁶A reader YTHDC1 regulates mRNA splicing. *Mol. Cell* 61, 507–519. doi: 10.1016/j.molcel.2016.01.012
- Yue, H., Nie, X., Yan, Z., and Weining, S. (2019). N⁶-methyladenosine regulatory machinery in plants: composition, function and evolution. *Plant Biotechnol. J.* 17, 1194–1208. doi: 10.1111/pbi.13149
- Yue, Y., Liu, J., Cui, X., Cao, J., Luo, G., Zhang, Z., et al. (2018). VIRMA mediates preferential m⁶A mRNA methylation in 3' UTR and near stop codon and associates with alternative polyadenylation. *Cell Discovery* 4, 1–17.
- Zhang, F., Zhang, Y.-C., Liao, J.-Y., Yu, Y., Zhou, Y.-F., Feng, Y.-Z., et al. (2019). The subunit of RNA N⁶-methyladenosine methyltransferase OsFIP regulates early degeneration of microspores in rice. *PLoS Genet.* 15:e1008120. doi: 10.1371/journal.pgen.1008120
- Zhang, Z., Theler, D., Kaminska, K. H., Hiller, M., de la Grange, P., Pudimat, R., et al. (2010). The YTH domain is a novel RNA binding domain. *J. Biol. Chem.* 285, 14701–14710. doi: 10.1074/jbc.M110.104711
- Zheng, G., Dahl, J. A., Niu, Y., Fedorcsak, P., Huang, C.-M., Li, C. J., et al. (2013). ALKBH5 is a mammalian RNA demethylase that impacts RNA metabolism and mouse fertility. *Mol. Cell* 49, 18–29. doi: 10.1016/j.molcel.2012.10.015
- Zhong, S., Li, H., Bodi, Z., Button, J., Vespa, L., Herzog, M., et al. (2008). MTA is an *Arabidopsis* messenger RNA adenosine methylase and interacts with a homolog of a sex-specific splicing factor. *Plant Cell* 20, 1278–1288. doi: 10.1105/tpc.108.058883
- Zhou, J., Wan, J., Gao, X., Zhang, X., Jaffrey, S. R., and Qian, S.-B. (2015). Dynamic m⁶A mRNA methylation directs translational control of heat shock response. *Nature* 526, 591–594.
- Zhou, L., Tian, S., and Qin, G. (2019). RNA methylomes reveal the m⁶A-mediated regulation of DNA demethylase gene SIDML2 in tomato fruit ripening. *Genome Biol.* 20:156. doi: 10.1186/s13059-019-1771-7

Conflict of Interest: The authors declare that the research was conducted in the absence of any commercial or financial relationships that could be construed as a potential conflict of interest.

Copyright © 2020 Zheng, Li, Zhang and Sui. This is an open-access article distributed under the terms of the Creative Commons Attribution License (CC BY). The use, distribution or reproduction in other forums is permitted, provided the original author(s) and the copyright owner(s) are credited and that the original publication in this journal is cited, in accordance with accepted academic practice. No use, distribution or reproduction is permitted which does not comply with these terms.



The Crosstalk Between Epigenetic Mechanisms and Alternative RNA Processing Regulation

Jian Zhang^{1,2}, Yi-Zhe Zhang^{1,2}, Jing Jiang³ and Cheng-Guo Duan^{1,3*}

¹ Shanghai Center for Plant Stress Biology, CAS Center for Excellence in Molecular Plant Sciences, Chinese Academy of Sciences, Shanghai, China, ² University of Chinese Academy of Sciences, Beijing, China, ³ State Key Laboratory of Crop Stress Adaptation and Improvement, School of Life Sciences, Henan University, Kaifeng, China

OPEN ACCESS

Edited by:

Mojgan Rastegar,
University of Manitoba, Canada

Reviewed by:

Martin Crespi,
UMR 9213 Institut des Sciences des
Plantes de Paris Saclay (IPS2), France
Paolo Provero,
University of Turin, Italy

*Correspondence:

Cheng-Guo Duan
cgduan@psc.ac.cn

Specialty section:

This article was submitted to
Epigenomics and Epigenetics,
a section of the journal
Frontiers in Genetics

Received: 02 May 2020

Accepted: 05 August 2020

Published: 20 August 2020

Citation:

Zhang J, Zhang Y-Z, Jiang J and
Duan C-G (2020) The Crosstalk
Between Epigenetic Mechanisms
and Alternative RNA Processing
Regulation. *Front. Genet.* 11:998.
doi: 10.3389/fgene.2020.00998

As a co-transcriptional process, RNA processing, including alternative splicing and alternative polyadenylation, is crucial for the generation of multiple mRNA isoforms. RNA processing mechanisms are widespread across all higher eukaryotes and play critical roles in cell differentiation, organ development and disease response. Recently, significant progresses have been made in understanding the mechanism of RNA processing. RNA processing is regulated by *trans*-acting factors such as splicing factors, RNA-binding proteins and *cis*-sequences in pre-mRNA, and increasing evidence suggests that epigenetic mechanisms, which are important for the dynamic regulation and state of specific chromatic regions, are also involved in co-transcriptional RNA processing. In contrast, recent studies also suggest that alternative RNA processing also has a feedback regulation on epigenetic mechanisms. In this review, we discuss recent studies and summarize the current knowledge on the epigenetic regulation of alternative RNA processing. In addition, a feedback regulation of RNA processing on epigenetic regulators is also discussed.

Keywords: RNA processing, alternative splicing, alternative polyadenylation, epigenetics, DNA methylation, histone modifications

INTRODUCTION

Messenger RNA production is a fantastically complex process in eukaryotes, including transcription of mRNA precursors followed by capping, splicing, and polyadenylation. Alternative RNA processing, including splicing and polyadenylation (AS/APA), leads to the formation of distinct mRNA isoforms and explains how massive proteomic complexity can be accomplished with the relatively few genes in higher eukaryotes (Elkon et al., 2013; Tian and Manley, 2016). AS/APA are mechanisms widespread across all eukaryotic species, from yeast to humans and plants. Recent advances based on a vast amount of high-throughput sequencing data indicate that nearly 95% of multi-exon mammalian genes undergo alternative splicing (Pan et al., 2008; Barash et al., 2010) and more than 70% of mammalian genes express APA isoforms (Derti et al., 2012; Hoque et al., 2013). AS/APA have gained renewed and expanded consideration as crucial regulators of gene expression and contribute to development and cellular differentiation and proliferation, neuron activation and other biological processes (Hong et al., 2018; Xu and Zhang, 2018; Fan et al., 2018; Yoshimi et al., 2019).

Traditionally, alternative RNA processing has been thought to be predominantly controlled by both *cis*-regulatory sequences and *trans*-acting factors. In AS regulation, *cis*-regulatory sequences include splicing enhancers and silencers, typically 10 nt in length, the impact of which depends on their location and their preferential splice sites (Cáceres and Kornblihtt, 2002; Cooper et al., 2009). *Trans*-acting factors activate, whereas other factors inhibit, the use of splice sites, by binding to splicing enhancers and silencers (Jelen et al., 2007; Han et al., 2010). Similar to AS, the combined effects of multiple *trans*-acting factors and *cis* elements clearly determine the likelihood of diverse poly(A) site usage (Movassat et al., 2016; Tian and Manley, 2016).

Despite the wide acceptance that these *cis*-regulatory sequences and *trans*-acting factors regulate alternative RNA processing, AS and APA are more complicated processes in co-transcriptional events than originally anticipated. Here, we review the implications of the recently exposed roles of epigenetic mechanisms, such as DNA methylation, histone modifications, histone variants, and some non-coding RNA (ncRNA) in alternative RNA processing regulation. A feedback of alternative RNA processing on epigenetic regulation was also discussed.

CHROMATIN-BASED REGULATION OF ALTERNATIVE RNA PROCESSING

DNA Methylation and Alternative RNA Processing

DNA methylation, resulting in 5' methylation of cytosine (5mC), is a conserved and heritable DNA modification that affects gene expression in a genome-wide manner (Li and Zhang, 2014). The impact of DNA methylation on gene expression varies depending on its genomic contexts. The role of promoter DNA methylation in gene expression has been well investigated, which is widely believed to cause transcriptional inhibition of downstream genes (Law and Jacobsen, 2010). Interestingly, recent studies in model plant *Arabidopsis* revealed that two SU(VAR)3-9 homologs, SUVH1 and SUVH3, bind to methylated DNA and recruit the DNAP1 proteins to enhance proximal gene expression, thereby counteracting the repressive effects of transposon insertion near genes (Harris et al., 2018; Xiao et al., 2019; Zhao et al., 2019). Compared to DNA methylation in promoter regions, the function of genic DNA methylation remains elusive (Ball et al., 2009). During the last decade, several studies indicate that genic DNA methylation has a positive effect on the expression of associated genes and prevents spurious transcription initiation, and it is present within a number of cancer-related genes and has been regarded as a hallmark of human cancer (Baylin and Jones, 2011; Yang et al., 2014; Neri et al., 2017).

Recent studies reveal a strong correlation between DNA methylation and alternative splicing. Yang et al. (2014) showed that gene body DNA demethylation mediated by DNA methyltransferase inhibitor 5-aza-2'-deoxycytidine results in reduced efficiencies of transcription elongation or splicing. In human cells, Shukla et al. (2011) reported that a DNA-binding protein, called CCCTC-binding factor (CTCF), can promote

inclusion of weak upstream exons by mediating local RNA polymerase II pausing. In this case, DNA methylation inhibits CTCF binding to *CD45* exon 5, which enables Pol II to transcribe more rapidly, giving rise to an exon 5 exclusion (Ong and Corces, 2014). More recently, Nanavaty et al. (2020) further revealed that CTCF is a bifunctional regulator which influences both alternative splicing and alternative polyadenylation. Removal of DNA methylation enables CTCF binding and recruitment of the cohesin complex, which in turn form chromatin loops to promote proximal polyadenylation site usage. These works clearly demonstrate that DNA methylation has an important participation in RNA processing regulation. While, limited information is currently available regarding how DNA binding proteins disturb the elongation of Pol II. It reminded us that there maybe are other factors influencing Pol II elongation in CTCF-mediated AS regulation, like the cohesin complex.

Unlike CTCF protein which binds to unmethylated DNA, a growing number of studies have shown that the methyl cytosine-guanine dinucleotide (CpG) binding protein 2 (MeCP2) binds to methylated regions to influence AS. MeCP2 is the earliest reported multifunctional protein that contains both methyl-CpG-binding domains and transcriptional repressor domains (Nan et al., 1997). Acting as a chromatin adaptor, MeCP2 is attracted to 5mC on alternative exons, triggering its interaction with histone deacetylases (HDACs), which modulate alternative splicing (Maunakea et al., 2013). As we delve deeper into the function of MeCP2, it is becoming clear that MeCP2 recruiting splicing factors to regulate mRNA splicing is also a nearly ubiquitous mechanism in animals (Cheng et al., 2017; Wong et al., 2017).

In plants, the available information regarding whether gene body DNA methylation affects AS and the extent of this mediation is currently limited. The first study of DNA methylation-related functions in splicing was reported in maize (Regulski et al., 2013). More recently, the cytosine methyltransferase OsMET1 was found to affect global AS events in rice, in which a total of 6319 more events were identified with the *met1* mutant compared with those associated with the wild-type strain (Wang et al., 2016). However, deeper research combining DNA methylation and AS/APA in plant is lacking. Whether it has the similar regulatory mechanism with mammals needs to be further elucidated.

Histone Modification-Mediated Regulation of Alternative RNA Processing

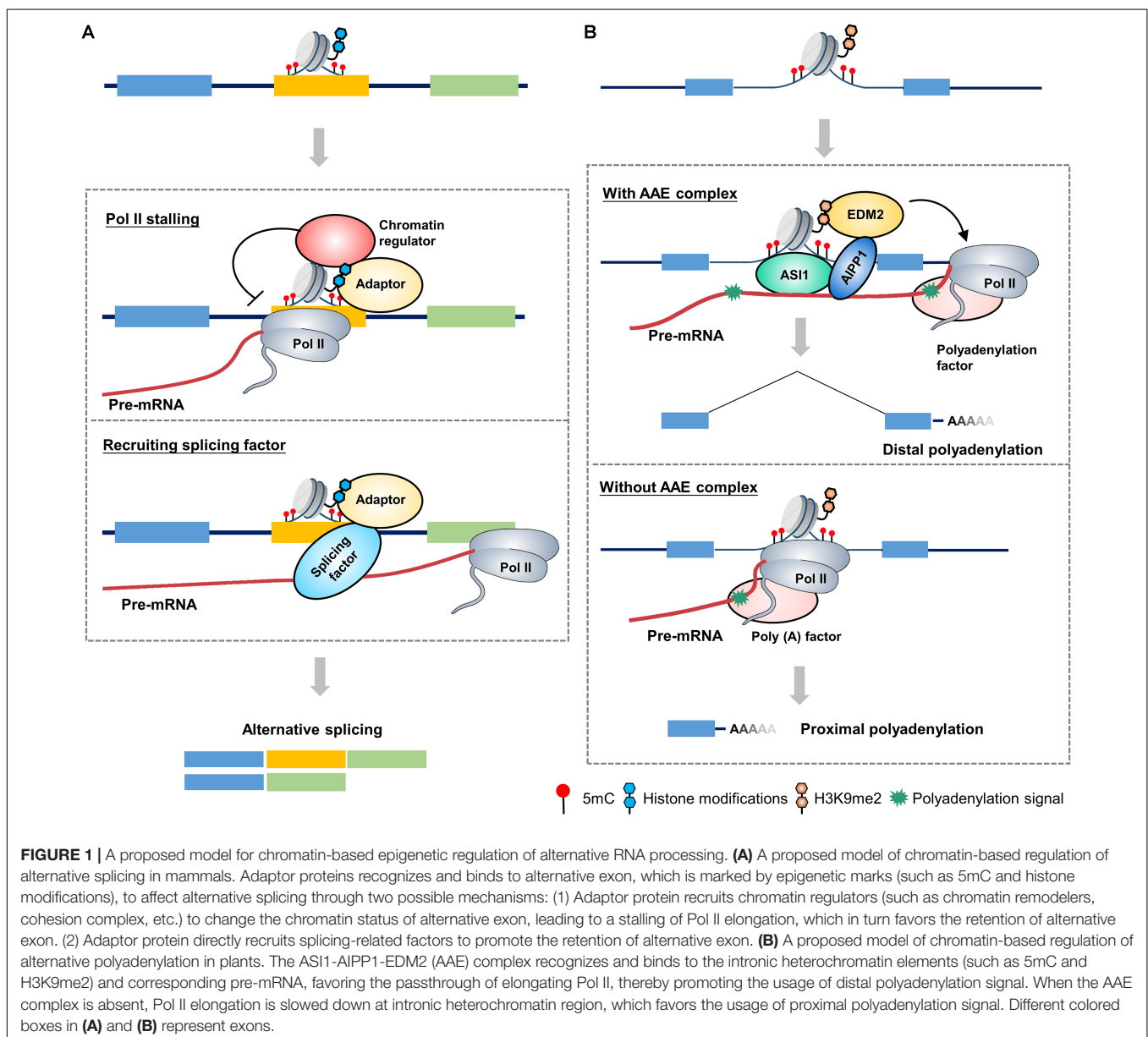
Chromatin structure is dominated by nucleosome density and positioning, as well as by histone modifications and DNA methylation (Duan et al., 2018). In contrast to DNA methylation, more than 50 diverse modifications have been identified on histone tails. Different modifications are linked with distinct functions, such as transcriptional activation or inhibition (Henikoff and Shilatifard, 2011). Recent reports indicate that histone modifications are also involved in the regulation of RNA processing. In fact, the involvement of histone modification in regulation of RNA processing was found earlier

than DNA methylation (Luco et al., 2010). Similar to DNA methylation, absence of histone marks results in chromatin structure changes, immediately affecting Pol II elongation and alternative RNA processing.

Histone H3 lysine 36 trimethylation (H3K36me3) mark is an active mark and is abundant in actively transcribed gene bodies (Liu et al., 2010). It has been shown that dysfunction of SETD2, an H3K36me3 methyltransferase, induced changes in 186 AS events (Yuan et al., 2017). In humans, the MORF-related gene on chromosome 15 (MRG15) is a well-established model system to study the interplay between histone modifications and the splicing machinery. The H3K36me3 mark influences splicing by impacting the recruitment of splicing regulators through a chromatin-binding protein, that is, MRG15. In this mechanism, the H3K36me3 mark serves as anchors for MRG15 binding,

which in turn recruits the splicing regulator polypyrimidine tract-binding (PTB) to pre-mRNA (Figure 1A). The H3K36me3–MRG15–PTB complex forms a chromatin-splicing adaptor system regulating numerous splicing events, including FGFR2 splicing, which is essential for tumor growth and invasion of lung cancer (Sanidas et al., 2014; Naftelberg et al., 2015).

In contrast to the H3K36me3–MRG15–PTB complex which favors exclusion of alternative exons, diverse histone modifications can lead to a diametrically opposite splicing pattern. Heterochromatin protein 1 (HP1), which has three isoforms in humans, HP1 α , HP1 β , and HP1 γ , binds directly to histone H3 lysine 9 trimethylation (H3K9me3; Bannister et al., 2001). A previous study indicated that HP1 γ forms an additional link with chromatin, binding to the coding region where it associates with pre-mRNA and favoring its transient retention



on chromatin. The modification to the chromatin structures of the *CD44* gene slows the elongation rate of Pol II, which in turn facilitates the recruitment of splicing factors such as U2AF65 and PRP8 to alternative exons, resulting in the inclusion of alternative exons (Saint-André et al., 2011; Yearim et al., 2015). Unsurprisingly, diverse adaptor proteins at H3K9me3 lead to distinct splicing patterns. HP1 α and HP1 β bind to methylated alternative exons and recruit the splicing factor serine/arginine-rich splicing factor 3 (SRSF3), thus enhancing the role of as a splicing silencer and reducing the number of induced alternative exons (Yearim et al., 2015).

In plants, *Arabidopsis* encodes two homologs of human MRG15, MRG1 and MRG2, which bind to H3K4me3/H3K36me3-modifying histone marks and trigger temperature-induced flowering via the florigen gene *FT* (Bu et al., 2014). However, it seems like that MRG1/2 have diversified from their animal homologs during evolution, yet they still maintain their conserved H3K36me3-binding molecular function (Xu et al., 2014; An et al., 2020; Guo et al., 2020). Recently, a protein complex in *Arabidopsis*, called anti-silencing 1 (ASI1)-ASI1 immunoprecipitated protein 1 (AIPP1)-enhanced downy mildew 2 (EDM2) (AAE) complex, was identified targeting genic heterochromatic elements to regulate APA (Duan et al., 2017). In this complex, ASI1, also named IBM2 and SG1 (Saze et al., 2013; Coustham et al., 2014), is a plant-specific chromatin regulator which bears chromatin- and RNA-binding capacity through its bromo-adjacent homology (BAH) and RNA recognition motif (RRM) domains, respectively (Wang et al., 2013). EDM2 is a multifunctional chromatin regulator containing two and half plant homeodomains (PHDs). Its PHD fingers have the binding capacity of H3K9me2 and other histone modifications (Lei et al., 2014). ASI1 and EDM2 associate *in vivo* through an RRM motif-containing bridge protein AIPP1 (also named EDM3; Duan et al., 2017). The AAE complex can bind to intronic heterochromatin, most of which come from insertions of epigenetically silenced transposable and repetitive elements, promoting the usage of distal polyadenylation site (Figure 1B). Dysfunctions of the AAE complex lead to ectopic accumulations of proximally polyadenylated short transcripts. Thus, the AAE complex is indispensable for the generation of full-length transcripts of genic heterochromatin-containing genes. Regarding the underlying mechanism, recent report indicates that EDM2 and AIPP1 mutations can slow down Pol II elongation rate at proximal polyadenylation site, leading to a promotion of proximal polyadenylation site usage (Lai et al., 2019). AAE complex-mediated polyadenylation regulation plays an important role in multiple biological processes, including modulating plant immunity by targeting innate immunity receptor gene *RPP7* (Tsuchiya and Eulgem, 2013), epigenome regulation by targeting histone H3K9me2 demethylase gene *IBM1*, and T-DNA suppression (Saze et al., 2013; Wang et al., 2013). Similar mechanism may also exist in other plants, like bamboo and oil palm (Wang et al., 2017). For example, in oil palm, loss of *Karma* transposon methylation leads to ectopic splicing of the homeotic gene *DEFICIENS*, which accounts for the mantled soma clonal variant phenotype of oil palm (Ong-Abdullah et al., 2015). Interestingly, recent study indicates that

FPA, a flowering time regulator in *Arabidopsis*, can antagonize ASI1 in the selection of polyadenylation site. In the double mutant of *asi1* and *fpa*, the polyadenylation pattern phenocopies *fpa* but not *asi1*. While, this antagonistic control only occurs in specific target genes, indicating a complex regulation of AAE complex-mediated polyadenylation (Deremetz et al., 2019).

Histone Variants and Chromatin-Remodeling Factors

Nucleosome, consisting of 147-bp double-stranded DNA and a single histone octamer, is the basic unit of chromatin. Histone variants, which are transcribed from separate genes, have been shown playing key roles in the regulation of chromatin features. This finding reminds us that histone variants may also regulate co-transcriptional RNA processing. In mammals, five somatic H1 variants (H1.1 to H1.5) have been identified (Happel and Doenecke, 2009). More recently, Glaich et al. (2019) reported that H1.5 deposition is observed at the splicing sites of the short exons in human lung fibroblasts (IMR90 cells), and Pol II on H1.5-marked exons exhibits greater stalling than it does on unmarked exons. Deletion of H1.5 affects the inclusion of short exons with relatively long introns and reduces Pol II occupancy on these exons (Glaich et al., 2019). This finding clearly indicates that the linker histones participate in the regulation of alternative RNA processing, which has not been previously demonstrated (Glaich et al., 2019).

In addition to histone variants, chromatin remodeling factors also affect chromosome segregation and transcription (Clapier and Cairns, 2009). During the last two decades, a growing number of studies have indicated that chromatin remodeling factors also play a role in alternative splicing. Brahma (BRM), the core adenosine triphosphatase (ATPase) subunit of the switch/sucrose nonfermenting (SWI/SNF) chromatin-remodeling complex, was firstly shown to facilitate the inclusion of alternative exons by interacting with Pol II to induce its stalling (Figure 1A; Batsché et al., 2006; Jancewicz et al., 2019). Actually, chromatin remodeler mediated-regulation of AS is an evolutionarily conserved mechanism across most species, such as in maize. ZmCHB101, a SWI3D protein, has been shown controlling AS by altering chromatin status and transcriptional elongation rates under osmotic stress (Yu et al., 2019), although the mechanism by which chromatin remodeling factors interact with Pol II transcription to impact mRNA processing machinery remains unclear.

NON-CODING RNAs AND ALTERNATIVE RNA PROCESSING

In addition to the identification of many alternative RNA processing events based on chromatin level, an interesting finding suggests that ncRNAs may play a key role in RNA processing regulation (Kishore and Stamm, 2006). Generally, ncRNAs are divided into two groups according to their size: small ncRNAs (< 200 bp), including rRNA, microRNA (miRNA), small nuclear RNA (snRNA), small nucleolar RNA (snoRNA), small interfering RNA (siRNA), and piwi interacting RNA (piRNA); long ncRNAs

(> 200 bp, lncRNA; Bartel, 2009). ncRNAs are now commonly believed to have a variety of biological functions, and it is possible that certain ncRNAs catalyze some steps of the splicing reaction (Cech and Steitz, 2014).

snoRNAs

It is assumed that most snoRNAs, nearly 70 nt in length, are derived from excised introns through exonucleolytic processing (Watkins and Bohnsack, 2012). There are hundreds of different snoRNAs in vertebrates and have even been found in archaea (Terns and Terns, 2002). The first evidence of the participation of snoRNA in AS was snoRNA HBII-52, which regulates the serotonin receptor 2C and is associated with the congenital disease Prader–Willi syndrome (PWS). HBII-52 regulates AS of 5-HT_{2C}R by binding to a silencing element in exon Vb. PWS patients do not express HBII-52. They have different 5-HT_{2C}R messenger RNA (mRNA) isoforms than healthy individuals (Kishore and Stamm, 2006). Recently, a class of intronic lncRNAs named snoRNA-related lncRNAs (sno-lncRNAs) was identified in humans. The sno-lncRNAs generated from the PWS region associate strongly with Fox family splicing regulators, altering serotonin receptor 5-HT_{2C}R splicing (**Figure 2A**). In patients with PWS, the expression of some specific sno-lncRNAs is downregulated. As a result, these patients have different 5-HT_{2C}R mRNA isoforms than healthy individuals, which have been identified during early embryonic development and adulthood (Yin et al., 2012).

Almost all eukaryotic pre-mRNAs and many ncRNAs are subject to cleavage/polyadenylation at the 3' end, which takes place in macromolecular machinery called the mRNA 3'-processing complex (Tian and Manley, 2016). It has been shown that snoRNAs, which are classified as *trans*-acting RNAs, directly interact with Fip1, a component of the cleavage and polyadenylation specificity factor (CPSF) complex. Small Nucleolar RNA C/D Box 50A (SNORD50A), a U/A-rich C/D-box snoRNA, inhibits mRNA 3' processing by disturbing the Fip1-poly(A) site (PAS) interaction (**Figure 2B**). SNORD50A depletion leads to more frequent binding of Fip1 to PAS and increases the 3' processing of target mRNAs containing U-rich sequences (Huang et al., 2017; Shi et al., 2017). Taken together, these studies strongly suggest that snoRNA is an important regulator of polyadenylation for specific genes by serving as an antagonistic RNA. An important question remains for future studies to address: how do ncRNAs bind to neighboring sequences and regulate the interactions between the core mRNA processing factors and processing sites?

lncRNAs

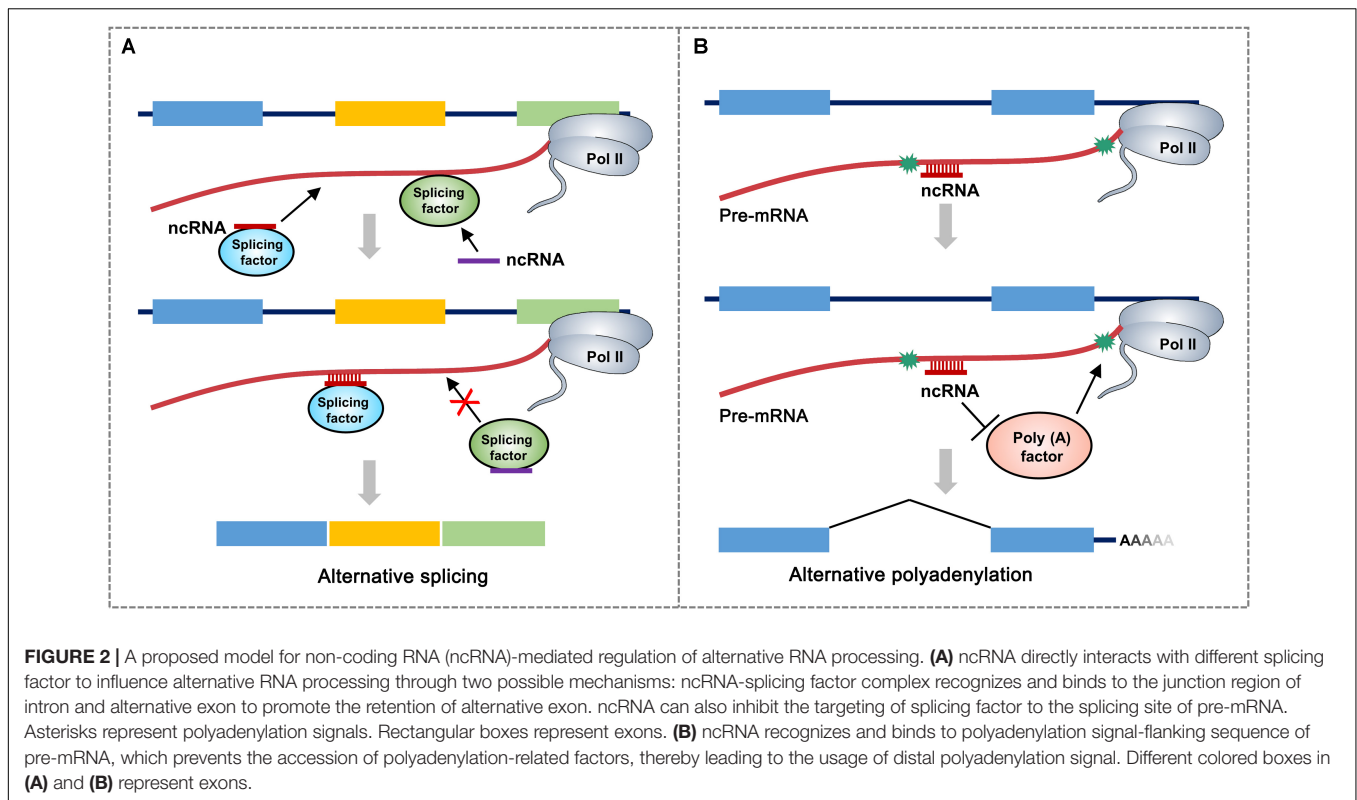
Recently, lncRNAs have received increasing attention. In human, Metastasis-associated lung adenocarcinoma transcript 1 (Malat1) is the most widely studied lncRNA. Malat1 was first identified in human non-small cell lung cancer (NSCLC; Ji et al., 2003). A number of serine/arginine-rich (SR) proteins, including SRSF1, SRSF2, and SRSF3, associate with Malat1. Absence of Malat1 affects the localization of some splicing factors in the HeLa cell line and leads to changes AS pattern (Blencowe, 2006). However, the loss of Malat1 in normal mice rarely causes global changes

in splicing factor levels and results only in the dysregulation of small mRNAs (Zhang et al., 2012). Meanwhile, deletion of Malat1 in mammary carcinoma mice leads to many AS events in genes essential for cell differentiation and tumorigenesis (Arun et al., 2016). It can therefore be proposed that Malat1 regulates AS in specific cells and tissues under particular conditions. In human cells, the lncRNA Gomafu, which is dynamically regulated by neuronal activation, directly binds to the splicing factors QKI and SRSF1 and inhibits their association with the schizophrenia disease-related gene transcripts, thereby affecting alternative splicing (Barry et al., 2014). In *Arabidopsis*, an lncRNA called alternative splicing competitor (ASCO) binds to the highly conserved spliceosome component PRP8a, thereby impairing the recognition of specific flagellin-related transcripts by PRP8a (Rigo et al., 2020). Actually, it has been shown that ASCO can bind to multiple splicing factors, indicating that lncRNAs may integrate a dynamic network to modulate transcriptome reprogramming, including alternative splicing.

In addition to the evidence we discussed above, some ncRNAs are directly or indirectly involved in RNA processing. It has been shown that piRNAs and piRNA biogenesis components affect mRNA splicing of P-transposable element transcripts *in vivo*, resulting in the production of a non-transposase-encoding mature mRNA isoform in *Drosophila* germ cells (Teixeira et al., 2017). In plants, there is a special family of ncRNAs that can confer *de novo* DNA methylation through the RNA-directed DNA methylation (RdDM) pathway, and thereby inducing global AS/APA events (Matzke and Mosher, 2014; Wang and Chekanova, 2016). As the non-coding transcriptome, ncRNAs are important components of the eukaryotic genome. There may be a large number of mechanisms by which ncRNAs enhance the plasticity of the proteome by interacting with mRNA-processing machinery. A deep understanding of this mechanism will open up broad prospects for gene therapy of various diseases, including cancer, and the application of biotechnology in agricultural and human health fields.

EPIGENETIC REGULATION AND ALTERNATIVE RNA PROCESSING-MEDIATED STRESS RESPONSE IN PLANTS

Unlike animals, plants display a high degree of plasticity during growth and development. In plants, to overcome the constant challenge from a rapidly changing environment, specific adaptation mechanisms have been evolved, among which alternative RNA processing is an important strategy (Chaudhary et al., 2019). Recent work has indicated that the role of epigenetic modifications in regulating AS/APA under stress is emerging (Jabre et al., 2019). Temperature is one of the environmental signals that strongly affects plant development. An recent study indicated that temperature variation is memorized by chromatin via H3K36me3 modification, resulting in a specific splicing pattern, which enables a feasible adaptation to stress conditions (Pajoro et al., 2017). Another study showed that genes which are



quickly activated under cold stress and differentially expressed at the splicing level, were found to be modified by H3K27me3 in non-stress conditions (Vyse et al., 2020). These reports suggest a dynamic regulation of temperature stress-responsive genes by alternative RNA processing and histone modification. In *Arabidopsis*, the Nuclear speckle RNA binding proteins (NSRs) have been known as regulators of AS functioning in auxin-associated developmental processes such as lateral root formation (Bazin et al., 2018). These proteins were shown to interact with specific alternatively spliced mRNA targets and at least with one structured lncRNA named ASCO (Bardou et al., 2014). The specific interaction of NSR with the ASCO is able to modulate AS patterns of a subset of NSR target genes, thereby impacting auxin response (Bazin et al., 2018). In other plants, specific association between epigenetic regulators and RNA processing factors under stress conditions has also been found. A maize SWI3D protein, ZmCHB101, has been found to impact alternative splicing contexts of a subset of osmotic stress-responsive genes on genome-wide level (Yu et al., 2019). In turn, alternative RNA processing of pivotal regulatory genes confers plants quick response to the changing climate conditions through alteration of reversible epigenetic marks. While, most of the current researches only focus on one aspect of how plants respond to changeable environment. That means, alternative RNA processing impacts the transcriptome of responsive genes or environment change leads to dynamic alterations of diverse epigenetic modifications (Rataj and Simpson, 2014; Calixto et al., 2018; Li et al., 2018). The mechanistic insights into the detailed interplay between epigenetic regulation and AS/APA in changing environment

remains largely limited. In addition, the complicated regulatory mechanisms controlling mRNA isoform ratios in a tissue- or condition-specific manner still remain unclear.

FEEDBACK REGULATION OF RNA PROCESSING ON EPIGENETIC MECHANISMS

On the one hand, the evidence above supports a notion that chromatin- and ncRNA-based epigenetic mechanisms have a huge impact on the patterns of alternative RNA processing. On the other hand, alteration of RNA processing pattern can also exert an important influence on epigenetic regulation pathways. In agreement with the notion that the majority of protein-coding genes show alternative processing (Elkon et al., 2013; Naftelberg et al., 2015), a number of epigenetic modifier-encoding genes are subjected to RNA processing regulation. As mentioned above, one classic feedback case is *IBM1*, a major H3K9me2 demethylase-encoding gene in *Arabidopsis*. *IBM1* is a target of the AAE complex which binds to its intronic repetitive sequence region to promote the generation of functional full-length transcript (Saze et al., 2008; Wang et al., 2013). In one aspect, epigenetic regulators required for the formation of intronic heterochromatin facilitates AAE complex targeting. In line with this notion, mutations of DNA methyltransferases MET1, CMT3 and histone H3K9me2 methyltransferase KYP (SUVH4) phenocopy the phenotype observed in the *aae* mutants, resulting in great reduction of

functional *IBM1* transcript (Rigal et al., 2012; Duan et al., 2017). In another aspect, reduced expression of *IBM1* protein causes an increase of genome-wide H3K9me2 level, which in turn causes genic CHG hypermethylation through recruiting more CMT3 DNA methyltransferase (Duan et al., 2017). Thus, *IBM1*-AAE interaction implies an interdependency between epigenetic regulation and alternative polyadenylation. Intriguingly, DNA and H3K9me2 methylation levels in *IBM1* intronic heterochromatin region were not obviously changed by the dysfunction of the AAE complex (Duan et al., 2017). One possible explanation is that the AAE complex may have a direct participation in the regulation of the epigenetic status of intronic heterochromatin.

Another example is the BAF complex, including at-rich interactive domain-containing protein 1A (*ARID1A*), which is an evolutionarily conserved chromatin-remodeling factor (Narayanan et al., 2015). A recent study indicated that EWS–friend leukemia integration 1 (*FLI1*), a well-established ES oncoprotein, plays a precise role in chromatin regulation by interacting with the BAF complex (Boulay et al., 2017). In addition to modulating chromatin organization, EWS–*FLI1* also alters the splicing of many mRNA isoforms (Selvanathan et al., 2015). Surprisingly, EWS–*FLI1* leads to preferential splicing of *ARID1A*-L, promoting ES growth, and *ARID1A*-L reciprocally facilitates EWS–*FLI1* protein stability to maintain the expression of *ARID1A*-L. The *ARID1A*-L isoform is essential for the splicing event, and a reduction in both *ARID1A* isoforms leads to EWS–*FLI1* degradation and cell death. The loss of *ARID1A*-L has been demonstrated as an explanation of its ability to stabilize EWS–*FLI1* (Selvanathan et al., 2019). In this EWS–*FLI1*-*ARID1A* system, chromatin remodeling and alternative splicing are both indispensable. Future efforts should be directed at finding interacting components of epigenetic regulation and AS/APA.

In addition, alternative RNA processing events can also lead to the formation of ncRNAs (Memczak et al., 2013). More recently, Ma et al. reported microRNA-mediated phased small interfering RNA (phasiRNA) generation from long non-coding genes coupled with alternative splicing/polyadenylation in litchi (Ma et al., 2018). An miR482/2118-targeted locus generates four primary transcript isoforms through AS/APA, and diverse phasiRNAs generated from these isoforms appeared to target long terminal repeat (LTR) retrotransposons and other unrelated genes. This study raised the intriguing possibility of cross talk between ncRNAs and AS/APA components. In addition, the diverse alternative mRNA processing-mediated protein variants thus generated immediately affect the properties of proteins, resulting in dysfunction of epigenetic regulators, including chromatin modification enzymes and remodeling factors (Lei et al., 2014; Rusconi et al., 2017; Jancewicz et al., 2019).

CONCLUSION

Epigenetic modifications are dynamically regulated by different catalytic enzymes and reader proteins. This feature makes epigenetic mechanisms suitable for multiple biological processes, ranging from cell differentiation, development and environmental stress responses. RNA processing, a

widespread mechanism of gene expression in eukaryotic cells, also play vital roles in multiple biological processes. During the last two decades, a great deal of efforts has been made in the crosstalk between epigenetic mechanisms and alternative RNA processing. As shown in **Figure 1**, chromatin modification, such as DNA methylation and histone modifications can inhibit or reinforce the binding of diverse adaptors. These chromatin adaptors induce alternative RNA processing through changing chromatin structure by collaborating with certain chromatin remodelers or the cohesion complex, or directly recruiting RNA processing factors to distinct splicing/polyadenylation site. Most of the current researches have focused on chromatin-based global changes of alternative RNA processing. In fact, it's a precise mechanism that is dynamically regulated under diverse conditions, such as during development and environmental stresses.

Different from the chromatin-based alternative RNA processing, ncRNA impact AS/APA on RNA level, mainly by disturbing the binding of RNA processing factors (**Figure 2**). They can bind to splicing/polyadenylation sites and inhibit the targeting of other RNA binding protein. Study on ncRNA-mediated regulation of alternative RNA processing is a promising field, particularly in the field of pharmaceutical research including RNA interference drugs. It may be a very effective method to treat many human diseases, which are caused by inaccurate splicing or polyadenylation, by covering false splicing/polyadenylation site. Therefore, it is important to find more cases of ncRNA-mediated regulation of RNA processing. In addition, deciphering the physiological relevance of the crosstalk between epigenetic regulation and alternative processing is also important toward understanding normal tissue homeostasis and transition to disease.

Study on the interplay between epigenetic regulation and alternative RNA processing is a novel field which is still at an early stage. In addition to the important researches described above, there are still some outstanding questions regarding the underlying mechanism of alternative RNA processing due to the space constraints not discussed in this review, such as the identification of conserved factors involved in such regulation, a comparison of epigenetic regulation in RNA processing between animals and plants, and the precise epigenetic mechanisms of tissue- and environment-specific AS/APA events. Addressing the remaining questions will undoubtedly expand our understanding of the chromatin codes in the regulation alternative RNA processing.

AUTHOR CONTRIBUTIONS

JZ and C-GD designed this review. JZ and Y-ZZ wrote the draft. JJ and C-GD edited it. All authors contributed to the article and approved the submitted version.

FUNDING

The work of C-GD was supported by Chinese Academy of Sciences and the Strategic Priority Research Program of the Chinese Academy of Sciences (XDB27040203).

REFERENCES

- An, Z., Yin, L., Liu, Y., Peng, M., Shen, W. H., and Dong, A. (2020). The histone methylation readers MRG1/MRG2 and the histone chaperones NRP1/NRP2 associate in fine-tuning *Arabidopsis* flowering time. *Plant J.* 1, 1–15. doi: 10.1111/tjp.14780
- Arun, G., Diermeier, S., Akerman, M., Chang, K. C., Wilkinson, J. E., Hearn, S., et al. (2016). Differentiation of mammary tumors and reduction in metastasis upon Malat1 lncRNA loss. *Genes Dev.* 30, 34–51. doi: 10.1101/gad.270959.115
- Ball, M. P., Li, J. B., Gao, Y., Lee, J. H., Leproust, E. M., Park, I. H., et al. (2009). Targeted and genome-scale strategies reveal gene-body methylation signatures in human cells. *Nat. Biotechnol.* 27, 361–368. doi: 10.1038/nbt.1533
- Bannister, A. J., Zegerman, P., Partridge, J. F., Miska, E. A., Thomas, J. O., Allshire, R. C., et al. (2001). Selective recognition of methylated lysine 9 on histone H3 by the HP1 chromo domain. *Nature* 410, 120–124. doi: 10.1038/35065138
- Barash, Y., Calarco, J. A., Gao, W., Pan, Q., Wang, X., Shai, O., et al. (2010). Deciphering the splicing code. *Nature* 465, 53–59. doi: 10.1038/nature09000
- Bardou, F., Ariel, F., Simpson, C. G., Romero-Barrios, N., Laporte, P., Balzergue, S., et al. (2014). Long noncoding RNA modulates alternative splicing regulators in *Arabidopsis*. *Dev. Cell* 30, 166–176. doi: 10.1016/j.devcel.2014.06.017
- Barry, G., Briggs, J. A., Vanichkina, D. P., Poth, E. M., Beveridge, N. J., Ratnu, V. S., et al. (2014). The long non-coding RNA Gomafu is acutely regulated in response to neuronal activation and involved in schizophrenia-associated alternative splicing. *Mol. Psychiatry* 19, 486–494. doi: 10.1038/mp.2013.45
- Bartel, D. P. (2009). MicroRNAs: target recognition and regulatory functions. *Cell* 136, 215–233. doi: 10.1016/j.cell.2009.01.002
- Batsché, E., Yaniv, M., and Muchardt, C. (2006). The human SWI/SNF subunit Brm is a regulator of alternative splicing. *Nat. Struct. Mol. Biol.* 13, 22–29. doi: 10.1038/nsmb1030
- Baylin, S. B., and Jones, P. A. (2011). A decade of exploring the cancer epigenome—biological and translational implications. *Nat. Rev. Cancer* 11, 726–734. doi: 10.1038/nrc3130
- Bazin, J., Romero, N., Rigo, R., Charon, C., Blein, T., Ariel, F., et al. (2018). Nuclear speckle rna binding proteins remodel alternative splicing and the non-coding arabidopsis transcriptome to regulate a cross-talk between auxin and immune responses. *Front. Plant Sci.* 9:1209. doi: 10.3389/fpls.2018.01209
- Blencowe, B. J. (2006). Alternative splicing: new insights from global analyses. *Cell* 126, 37–47. doi: 10.1016/j.cell.2006.06.023
- Boulay, G., Sandoval, G. J., Riggi, N., Iyer, S., Buisson, R., Naigles, B., et al. (2017). Cancer-Specific Retargeting of BAF complexes by a prion-like domain. *Cell* 171, 163–178.e19. doi: 10.1016/j.cell.2017.07.036
- Bu, Z., Yu, Y., Li, Z., Liu, Y., Jiang, W., Huang, Y., et al. (2014). Regulation of *Arabidopsis* flowering by the histone mark readers MRG1/2 via interaction with CONSTANS to modulate FT expression. *PLoS Genet.* 10:e1004617. doi: 10.1371/journal.pgen.1004617
- Cáceres, J. F., and Kornblihtt, A. R. (2002). Alternative splicing: multiple control mechanisms and involvement in human disease. *Trends Genet.* 18, 186–193. doi: 10.1016/S0168-9525(01)00262-9
- Calixto, C. P. G., Guo, W., James, A. B., Tzioutziou, N. A., Entizne, J. C., Panter, P. E., et al. (2018). Rapid and dynamic alternative splicing impacts the arabidopsis cold response transcriptome[CC-BY]. *Plant Cell* 30, 1424–1444. doi: 10.1105/tpc.18.00177
- Cech, T. R., and Steitz, J. A. (2014). Review the noncoding RNA revolution — trashing old rules to forge new ones. *Cell* 157, 77–94. doi: 10.1016/j.cell.2014.03.008
- Chaudhary, S., Khokhar, W., Jabre, I., Reddy, A. S. N., Byrne, L. J., Wilson, C. M., et al. (2019). Alternative splicing and protein diversity: plants versus animals. *Front. Plant Sci.* 10:708. doi: 10.3389/fpls.2019.00708
- Cheng, T. L., Chen, J., Wan, H., Tang, B., Tian, W., Liao, L., et al. (2017). Regulation of mRNA splicing by MeCP2 via epigenetic modifications in the brain. *Sci. Rep.* 7, 1–12. doi: 10.1038/srep42790
- Clapier, C. R., and Cairns, B. R. (2009). The biology of chromatin remodeling complexes. *Annu. Rev. Biochem.* 78, 273–304. doi: 10.1146/annurev.biochem.77.062706.153223
- Cooper, T. A., Wan, L., and Dreyfuss, G. (2009). RNA and disease. *Cell* 136, 777–793. doi: 10.1016/j.cell.2009.02.011
- Coustham, V., Vlad, D., Deremetz, A., Gy, I., Cubillos, F. A., Kerdaffrec, E., et al. (2014). SHOOT GROWTH1 maintains *Arabidopsis* epigenomes by regulating IBM1. *PLoS One* 9:e84687. doi: 10.1371/journal.pone.0084687
- Deremetz, A., Le Roux, C., Idir, Y., Brousse, C., Agorio, A., Gy, I., et al. (2019). Antagonistic actions of FPA and IBM2 regulate transcript processing from genes containing heterochromatin. *Plant Physiol.* 180, 392–403. doi: 10.1104/pp.18.01106
- Derti, A., Garrett-engele, P., Macisaac, K. D., Stevens, R. C., Sriram, S., Chen, R., et al. (2012). A quantitative atlas of polyadenylation in five mammals. *Genome Res.* 22, 1173–1183. doi: 10.1101/gr.132563.111
- Duan, C.-G., Wang, X., Zhang, L., Xiong, X., Zhang, Z., Tang, K., et al. (2017). A protein complex regulates RNA processing of intronic heterochromatin-containing genes in *Arabidopsis*. *Proc. Natl. Acad. Sci. U.S.A.* 114, E7377–E7384. doi: 10.1073/pnas.1710683114
- Duan, C. G., Zhu, J. K., and Cao, X. (2018). Retrospective and perspective of plant epigenetics in China. *J. Genet. Genomics* 45, 621–638. doi: 10.1016/j.jgg.2018.09.004
- Elkon, R., Ugalde, A. P., and Agami, R. (2013). Alternative cleavage and polyadenylation: extent, regulation and function. *Nat. Rev. Genet.* 14, 496–506. doi: 10.1038/nrg3482
- Fan, L., Zhang, F., Xu, S., Cui, X., Hussain, A., Fazli, L., et al. (2018). Histone demethylase JMJD1A promotes alternative splicing of AR variant 7 (AR-V7) in prostate cancer cells. *Proc. Natl. Acad. Sci. U.S.A.* 115, E4584–E4593. doi: 10.1073/pnas.1802415115
- Glaich, O., Leader, Y., Lev Maor, G., and Ast, G. (2019). Histone H1.5 binds over splice sites in chromatin and regulates alternative splicing. *Nucleic Acids Res.* 47, 6145–6159. doi: 10.1093/nar/gkz338
- Guo, Z., Li, Z., Liu, Y., An, Z., Peng, M., Shen, W. H., et al. (2020). MRG1/2 histone methylation readers and HD2C histone deacetylase associate in repression of the florigen gene FT to set a proper flowering time in response to day-length changes. *New Phytol.* 227, 1453–1466. doi: 10.1111/nph.16616
- Han, S. P., Tang, Y. H., and Smith, R. (2010). Functional diversity of the hnRNPs: past, present and perspectives. *Biochem. J.* 430, 379–392. doi: 10.1042/BJ20100396
- Happel, N., and Doenecke, D. (2009). Histone H1 and its isoforms: contribution to chromatin structure and function. *Gene* 431, 1–12. doi: 10.1016/j.gene.2008.11.003
- Harris, C. J., Scheibe, M., Wongpalee, S. P., Liu, W., Cornett, E. M., Vaughan, R. M., et al. (2018). A DNA methylation reader complex that enhances gene transcription. *Science* 362, 1182–1186. doi: 10.1126/science.aar7854
- Henikoff, S., and Shilatifard, A. (2011). Histone modification: cause or cog? *Trends Genet.* 27, 389–396. doi: 10.1016/j.tig.2011.06.006
- Hong, L., Ye, C., Lin, J., Fu, H., Wu, X., and Li, Q. Q. (2018). Alternative polyadenylation is involved in auxin-based plant growth and development. *Plant J.* 93, 246–258. doi: 10.1111/tjp.13771
- Hoque, M., Ji, Z., Zheng, D., Luo, W., Li, W., You, B., et al. (2013). Analysis of alternative cleavage and polyadenylation by 3' region extraction and deep sequencing. *Nat. Methods* 10, 133–139. doi: 10.1038/nmeth.2288
- Huang, C., Shi, J., Guo, Y., Huang, W., Huang, S., Ming, S., et al. (2017). A snoRNA modulates mRNA 3' end processing and regulates the expression of a subset of mRNAs. *Nucleic Acids Res.* 45, 8647–8660. doi: 10.1093/nar/gkx651
- Jabre, I., Reddy, A. S. N., Kalyna, M., Chaudhary, S., Khokhar, W., Byrne, L. J., et al. (2019). Does co-transcriptional regulation of alternative splicing mediate plant stress responses? *Nucleic Acids Res.* 47, 2716–2726. doi: 10.1093/nar/gkz121
- Jancewicz, I., Siedlecki, J. A., Sarnowski, T. J., and Sarnowska, E. (2019). BRM: the core ATPase subunit of SWI/SNF chromatin-remodelling complex – a tumour suppressor or tumour-promoting factor? *Epigenet. Chrom.* 12, 1–17. doi: 10.1186/s13072-019-0315-4
- Jelen, N., Ule, J., Živin, M., and Darnell, R. B. (2007). Evolution of Nova-dependent splicing regulation in the brain. *PLoS Genet.* 3:e173. doi: 10.1371/journal.pgen.0030173
- Ji, P., Diederichs, S., Wang, W., Böing, S., Metzger, R., Schneider, P. M., et al. (2003). MALAT-1, a novel noncoding RNA, and thymosin β 4 predict metastasis and survival in early-stage non-small cell lung cancer. *Oncogene* 22, 8031–8041. doi: 10.1038/sj.onc.1206928
- Kishore, S., and Stamm, S. (2006). The snoRNA HBII-52 regulates alternative splicing of the serotonin receptor 2C. *Science* 311, 230–232. doi: 10.1126/science.1118265

- Lai, Y., Cuzick, A., Lu, X. M., Wang, J., Katiyar, N., Tsuchiya, T., et al. (2019). The *Arabidopsis* RRM domain protein EDM3 mediates race-specific disease resistance by controlling H3K9me2-dependent alternative polyadenylation of RPP7 immune receptor transcripts. *Plant J.* 97, 646–660. doi: 10.1111/tpj.14148
- Law, J. A., and Jacobsen, S. E. (2010). Establishing, maintaining and modifying DNA methylation patterns in plants and animals. *Nat. Rev. Genet.* 11, 204–220. doi: 10.1038/nrg2719
- Lei, M., La, H., Lu, K., Wang, P., Miki, D., Ren, Z., et al. (2014). *Arabidopsis* EDM2 promotes IBM1 distal polyadenylation and regulates genome DNA methylation patterns. *Proc. Natl. Acad. Sci. U.S.A.* 111, 527–532. doi: 10.1073/pnas.1320106110
- Li, E., and Zhang, Y. (2014). DNA methylation in mammals. *Cold Spring Harb. Perspect. Biol.* 6:a019133. doi: 10.1101/cshperspect.a019133
- Li, T., Liu, Q., Garza, N., Kornblau, S., and Jin, V. X. (2018). Integrative analysis reveals functional and regulatory roles of H3K79me2 in mediating alternative splicing. *Genome Med.* 10, 1–11. doi: 10.1186/s13073-018-0538-1
- Liu, C., Lu, F., Cui, X., and Cao, X. (2010). Histone methylation in higher plants. *Annu. Rev. Plant Biol.* 61, 395–420. doi: 10.1146/annurev.arplant.043008.091939
- Luco, R. F., Pan, Q., Tominaga, K., Blencowe, B. J., Pereira-Smith, O. M., and Misteli, T. (2010). Regulation of alternative splicing by histone modifications. *Science* 327, 996–1000. doi: 10.1126/science.1184208
- Ma, W., Chen, C., Liu, Y., Zeng, M., Meyers, B. C., Li, J., et al. (2018). Coupling of microRNA-directed phased small interfering RNA generation from long noncoding genes with alternative splicing and alternative polyadenylation in small RNA-mediated gene silencing. *New Phytol.* 217, 1535–1550. doi: 10.1111/nph.14934
- Matzke, M. A., and Mosher, R. A. (2014). RNA-directed DNA methylation: an epigenetic pathway of increasing complexity. *Nat. Rev. Genet.* 15, 394–408. doi: 10.1038/nrg3683
- Maunakea, A. K., Chepelev, I., Cui, K., and Zhao, K. (2013). Intragenic DNA methylation modulates alternative splicing by recruiting MeCP2 to promote exon recognition. *Cell Res.* 23, 1256–1269. doi: 10.1038/cr.2013.110
- Memczak, S., Jens, M., Elefsinioti, A., Torti, F., Krueger, J., Rybak, A., et al. (2013). Circular RNAs are a large class of animal RNAs with regulatory potency. *Nature* 495, 333–338. doi: 10.1038/nature11928
- Movassat, M., Crabb, T. L., Busch, A., Yao, C., Derrick, J., Shi, Y., et al. (2016). Coupling between alternative polyadenylation and alternative splicing is limited to terminal introns. *RNA Biol.* 13, 646–655. doi: 10.1080/15476286.2016.1191727
- Naftelberg, S., Schor, I. E., Ast, G., and Kornblihtt, A. R. (2015). Regulation of alternative splicing through coupling with transcription and chromatin structure. *Annu. Rev. Biochem.* 84, 165–198. doi: 10.1146/annurev-biochem-060614-034242
- Nan, X., Campoy, F. J., and Bird, A. (1997). MeCP2 is a transcriptional repressor with abundant binding sites in genomic chromatin. *Cell* 88, 471–481. doi: 10.1016/S0092-8674(00)81887-5
- Nanavaty, V., Abrash, E. W., Hong, C., Park, S., Fink, E. E., Li, Z., et al. (2020). DNA methylation regulates alternative polyadenylation via CTCF and the cohesin complex. *Mol. Cell* 78, 752–764.e6. doi: 10.1016/j.molcel.2020.03.024
- Narayanan, R., Pirouz, M., Kerimoglu, C., Pham, L., Wagener, R. J., Kiszka, K. A., et al. (2015). Loss of BAF (mSWI/SNF) complexes causes global transcriptional and chromatin state changes in forebrain development. *Cell Rep.* 13, 1842–1854. doi: 10.1016/j.celrep.2015.10.046
- Neri, F., Rapelli, S., Krepelova, A., Incarnato, D., Parlato, C., Basile, G., et al. (2017). Intragenic DNA methylation prevents spurious transcription initiation. *Nature* 543, 72–77. doi: 10.1038/nature21373
- Ong, C. T., and Corces, V. G. (2014). CTCF: an architectural protein bridging genome topology and function. *Nat. Rev. Genet.* 15, 234–246. doi: 10.1038/nrg3663
- Ong-Abdullah, M., Ordway, J. M., Jiang, N., Ooi, S. E., Kok, S. Y., Sarpan, N., et al. (2015). Loss of Karma transposon methylation underlies the mantled somaclonal variant of oil palm. *Nature* 525, 533–537. doi: 10.1038/nature15365
- Pajoro, A., Severing, E., Angenent, G. C., and Immink, R. G. H. (2017). Histone H3 lysine 36 methylation affects temperature-induced alternative splicing and flowering in plants. *Genome Biol.* 18, 1–12. doi: 10.1186/s13059-017-1235-x
- Pan, Q., Shai, O., Lee, L. J., Frey, B. J., and Blencowe, B. J. (2008). Deep surveying of alternative splicing complexity in the human transcriptome by high-throughput sequencing. *Nat. Genet.* 40, 1413–1415. doi: 10.1038/ng.259
- Rataj, K., and Simpson, G. G. (2014). Message ends: RNA 3' processing and flowering time control. *J. Exp. Bot.* 65, 353–363. doi: 10.1093/jxb/ert439
- Regulski, M., Lu, Z., Kendall, J., Donoghue, M. T. A., Reinders, J., Llaca, V., et al. (2013). The maize methylome influences mRNA splice sites and reveals widespread paramutation-like switches guided by small RNA. *Genome Res.* 23, 1651–1662. doi: 10.1101/gr.153510.112
- Rigal, M., Kevei, Z., Pélessier, T., and Mathieu, O. (2012). DNA methylation in an intron of the IBM1 histone demethylase gene stabilizes chromatin modification patterns. *EMBO J.* 31, 2981–2993. doi: 10.1038/emboj.2012.141
- Rigo, R., Bazin, J., Romero-Barrios, N., Moison, M., Lucero, L., Christ, A., et al. (2020). The *Arabidopsis* Inc RNA ASCO modulates the transcriptome through interaction with splicing factors. *EMBO Rep.* 21, 1–19. doi: 10.15252/embr.201948977
- Rusconi, F., Grillo, B., Toffolo, E., Mattevi, A., and Battaglioli, E. (2017). NeuroLSD1: splicing-generated epigenetic enhancer of neuroplasticity. *Trends Neurosci.* 40, 28–38. doi: 10.1016/j.tins.2016.11.002
- Saint-André, V., Batsché, E., Rachez, C., and Muchardt, C. (2011). Histone H3 lysine 9 trimethylation and HP1 γ favor inclusion of alternative exons. *Nat. Struct. Mol. Biol.* 18, 337–344. doi: 10.1038/nsmb.1995
- Sanidas, I., Polyarchou, C., Hatzia Apostolou, M., Ezell, S. A., Kottakis, F., Hu, L., et al. (2014). Article phosphoproteomics screen reveals Akt isoform-specific signals linking RNA processing to lung cancer. *Mol. Cell* 53, 577–590. doi: 10.1016/j.molcel.2013.12.018
- Saze, H., Kitayama, J., Takashima, K., Miura, S., Harukawa, Y., Ito, T., et al. (2013). Mechanism for full-length RNA processing of *Arabidopsis* genes containing intragenic heterochromatin. *Nat. Commun.* 4:2301. doi: 10.1038/ncomms3301
- Saze, H., Shiraishi, A., Miura, A., and Kakutani, T. (2008). Control of genic DNA methylation by a jmjC domain-containing protein in *Arabidopsis thaliana*. *Science* 319, 462–465. doi: 10.1126/science.1150987
- Selvanathan, S. P., Graham, G. T., Erkizan, H. V., Dirksen, U., Natarajan, T. G., Dakic, A., et al. (2015). Oncogenic fusion protein EWS-FLI1 is a network hub that regulates alternative splicing. *Proc. Natl. Acad. Sci. U.S.A.* 112, E1307–E1316. doi: 10.1073/pnas.1500536112
- Selvanathan, S. P., Graham, G. T., Grego, A. R., Baker, T. M., Hogg, J. R., Simpson, M., et al. (2019). EWS-FLI1 modulated alternative splicing of ARID1A reveals novel oncogenic function through the BAF complex. *Nucleic Acids Res.* 47, 9619–9636. doi: 10.1093/nar/gkz699
- Shi, J., Huang, C., Huang, S., and Yao, C. (2017). snoRNAs associate with mRNA 3' processing complex: new wine in old bottles. *RNA Biol.* 6286, 1–4. doi: 10.1080/15476286.2017.1416278
- Shukla, S., Kavak, E., Gregory, M., Imashimizu, M., Shutinoski, B., and Kashlev, M. (2011). CTCF-promoted RNA polymerase II. *Nature* 479, 74–79. doi: 10.1038/nature10442
- Teixeira, F. K., Okuniewska, M., Malone, C. D., Coux, R. X., Rio, D. C., and Lehmann, R. (2017). PiRNA-mediated regulation of transposon alternative splicing in the soma and germ line. *Nature* 552, 268–272. doi: 10.1038/nature25018
- Terns, M. P., and Terns, R. M. (2002). Small nucleolar RNAs: versatile transacting molecules of ancient evolutionary origin. *Gene Expr.* 10, 17–39. doi: 10.0000/096020197390059
- Tian, B., and Manley, J. L. (2016). Alternative polyadenylation of mRNA precursors. *Nat. Rev. Mol. Cell Biol.* 18, 18–30. doi: 10.1038/nrm.2016.116
- Tsuchiya, T., and Eulgem, T. (2013). An alternative polyadenylation mechanism coopted to the *Arabidopsis* RPP7 gene through intronic retrotransposon domestication. *Proc. Natl. Acad. Sci. U.S.A.* 110, E3535–E3543. doi: 10.1073/pnas.1312545110
- Vyse, K., Faivre, L., Romich, M., Pagter, M., Schubert, D., Hinch, D. K., et al. (2020). Transcriptional and post-transcriptional regulation and transcriptional memory of chromatin regulators in response to low temperature. *Front. Plant Sci.* 11:39. doi: 10.3389/fpls.2020.00039
- Wang, H. L. V., and Chekanova, J. A. (2016). Small RNAs: essential regulators of gene expression and defenses against environmental stresses in plants. *Wiley Interdiscip. Rev. RNA* 7, 356–381. doi: 10.1002/wrna.1340
- Wang, T., Wang, H., Cai, D., Gao, Y., Zhang, H., Wang, Y., et al. (2017). Comprehensive profiling of rhizome-associated alternative splicing and

- alternative polyadenylation in moso bamboo (*Phyllostachys edulis*). *Plant J.* 91, 684–699. doi: 10.1111/tpj.13597
- Wang, X., Duan, C. G., Tang, K., Wang, B., Zhang, H., Lei, M., et al. (2013). RNA-binding protein regulates plant DNA methylation by controlling mRNA processing at the intronic heterochromatin-containing gene IBM1. *Proc. Natl. Acad. Sci. U.S.A.* 110, 15467–15472. doi: 10.1073/pnas.1315399110
- Wang, X., Hu, L., Wang, X., Li, N., Xu, C., Gong, L., et al. (2016). DNA methylation affects gene alternative splicing in plants: an example from rice. *Mol. Plant* 9, 305–307. doi: 10.1016/j.molp.2015.09.016
- Watkins, N. J., and Bohnsack, M. T. (2012). The box C/D and H/ACA snoRNPs: key players in the modification, processing and the dynamic folding of ribosomal RNA. *Wiley Interdiscip. Rev. RNA* 3, 397–414. doi: 10.1002/wrna.117
- Wong, J. J. L., Gao, D., Nguyen, T. V., Kwok, C. T., Van Geldermalsen, M., Middleton, R., et al. (2017). Intron retention is regulated by altered MeCP2-mediated splicing factor recruitment. *Nat. Commun.* 8, 1–13. doi: 10.1038/ncomms15134
- Xiao, X., Zhang, J., Li, T., Fu, X., Sathesh, V., Niu, Q., et al. (2019). A group of SUVH methyl-DNA binding proteins regulate expression of the DNA demethylase ROS1 in *Arabidopsis*. *J. Integr. Plant Biol.* 61, 110–119. doi: 10.1111/jipb.12768
- Xu, C., and Zhang, J. (2018). Alternative polyadenylation of mammalian transcripts is generally deleterious, not adaptive report alternative polyadenylation of mammalian transcripts is generally deleterious, not adaptive. *Cell Syst.* 6, 734–742.e4. doi: 10.1016/j.cels.2018.05.007
- Xu, Y., Gan, E. S., Zhou, J., Wee, W. Y., Zhang, X., and Ito, T. (2014). Arabidopsis MRG domain proteins bridge two histone modifications to elevate expression of flowering genes. *Nucleic Acids Res.* 42, 10960–10974. doi: 10.1093/nar/gku781
- Yang, X., Han, H., DeCarvalho, D. D., Lay, F. D., Jones, P. A., and Liang, G. (2014). Gene body methylation can alter gene expression and is a therapeutic target in cancer. *Cancer Cell* 26, 577–590. doi: 10.1016/j.ccr.2014.07.028
- Yearim, A., Gelfman, S., Shayevitch, R., Melcer, S., Glaich, O., Mallm, J. P., et al. (2015). HP1 is involved in regulating the global impact of DNA methylation on alternative splicing. *Cell Rep.* 10, 1122–1134. doi: 10.1016/j.celrep.2015.01.038
- Yin, Q. F., Yang, L., Zhang, Y., Xiang, J. F., Wu, Y. W., Carmichael, G. G., et al. (2012). Long noncoding RNAs with snoRNA ends. *Mol. Cell* 48, 219–230. doi: 10.1016/j.molcel.2012.07.033
- Yoshimi, A., Lin, K. T., Wiseman, D. H., Rahman, M. A., Pastore, A., Wang, B., et al. (2019). *Coordinated Alterations in RNA Splicing and Epigenetic Regulation Drive Leukaemogenesis*. New York, NY: Springer, doi: 10.1038/s41586-019-1618-0
- Yu, X., Meng, X., Liu, Y., Wang, X., Jing, T., Ai, W., et al. (2019). The chromatin remodeler ZmCHB101 impacts alternative splicing contexts in response to osmotic stress. *Plant Cell Rep.* 38, 131–145. doi: 10.1007/s00299-018-2354-x
- Yuan, H., Li, N., Fu, D., Ren, J., Hui, J., Peng, J., et al. (2017). Histone methyltransferase SETD2 modulates alternative splicing to inhibit intestinal tumorigenesis. *J. Clin. Invest.* 127, 3375–3391. doi: 10.1172/JCI94292
- Zhang, B., Arun, G., Mao, Y. S., Lazar, Z., Hung, G., Bhattacharjee, G., et al. (2012). The lncRNA malat1 is dispensable for mouse development but its transcription plays a cis-regulatory role in the adult. *Cell Rep.* 2, 111–123. doi: 10.1016/j.celrep.2012.06.003
- Zhao, Q. Q., Lin, R. N., Li, L., Chen, S., and He, X. J. (2019). A methylated-DNA-binding complex required for plant development mediates transcriptional activation of promoter methylated genes. *J. Integr. Plant Biol.* 61, 120–139. doi: 10.1111/jipb.12767

Conflict of Interest: The authors declare that the research was conducted in the absence of any commercial or financial relationships that could be construed as a potential conflict of interest.

Copyright © 2020 Zhang, Zhang, Jiang and Duan. This is an open-access article distributed under the terms of the Creative Commons Attribution License (CC BY). The use, distribution or reproduction in other forums is permitted, provided the original author(s) and the copyright owner(s) are credited and that the original publication in this journal is cited, in accordance with accepted academic practice. No use, distribution or reproduction is permitted which does not comply with these terms.



The Role of HDACs and HDACi in Cartilage and Osteoarthritis

He Zhang¹, Lu Ji², Yue Yang¹, Xiaoning Zhang³, Yi Gang⁴ and Lunhao Bai^{1*}

¹ Department of Orthopedic Surgery, Shengjing Hospital, China Medical University, Shenyang, China, ² Department of Gynecology and Obstetrics, Shengjing Hospital, China Medical University, Shenyang, China, ³ Department of Anesthesiology, Shengjing Hospital, China Medical University, Shenyang, China, ⁴ Department of Orthopedic Surgery, Panjin Central Hospital, Panjin, China

OPEN ACCESS

Edited by:

Kai Tang,
Purdue University, United States

Reviewed by:

Lei Zhao,
University of Wisconsin–Madison,
United States
Giuseppe Giannini,
Alfasigma SpA, Italy

*Correspondence:

Lunhao Bai
cmublh@163.com

Specialty section:

This article was submitted to
Epigenomics and Epigenetics,
a section of the journal
Frontiers in Cell and Developmental
Biology

Received: 08 May 2020

Accepted: 27 August 2020

Published: 30 September 2020

Citation:

Zhang H, Ji L, Yang Y, Zhang X,
Gang Y and Bai L (2020) The Role
of HDACs and HDACi in Cartilage
and Osteoarthritis.
Front. Cell Dev. Biol. 8:560117.
doi: 10.3389/fcell.2020.560117

Epigenetics plays an important role in the pathogenesis and treatment of osteoarthritis (OA). In recent decades, HDAC family members have been associated with OA. This paper aims to describe the different role of HDACs in the pathogenesis of OA through interaction with microRNAs and the regulation of relevant signaling pathways. We found that HDACs are involved in cartilage and chondrocyte development but also play a crucial role in OA. However, the distinct HDAC mechanism in the pathogenesis and treatment of OA require further investigation. Furthermore, HDAC inhibitors (HDACi) can protect cartilage from disease, which may represent a potential therapeutic approach against OA.

Keywords: osteoarthritis, HDAC, HDAC inhibitor, microRNA, cartilage

INTRODUCTION

Osteoarthritis (OA) is a common disease that not only causes physical disability but also imposes an economic burden on society (Litwic et al., 2013; Liu et al., 2018). The prevalence of OA is high and increases with age (Neogi, 2013). In Korea, 35% of people older than 65 years have been diagnosed radiographically with OA (Cho et al., 2015). The etiology of OA is multifactorial and complex. Mechanical stress, metabolic dysfunction and inflammation are all involved in OA progression (Sarzi-Puttini et al., 2005; Johnson and Hunter, 2014). Due to the aging population and the rising rate of obesity, the prevalence of OA is predicted to double by 2020 (Thomas et al., 2017).

OA is characterized by joint space narrowing, subchondral sclerosis, subchondral cysts, and osteophyte formation (Kuyinu et al., 2016). Its major clinical symptoms include joint pain and swelling and loss of movement (Shen and Chen, 2014; Moon et al., 2018). The pathological mechanism of OA includes increased dysfunction and death of chondrocytes and the disequilibrium of extracellular matrix synthesis and degradation (Zheng et al., 2018). There are many signaling pathways involved in OA pathogenesis that are activated by pro-inflammatory mediators and cytokines, such as interleukin-1 β (IL-1 β) (Jenei-Lanzl et al., 2019). Specifically, these cytokines promote OA through mitogen-activated protein kinase (MAPK) signaling (Malemud, 2017), NF- κ B, and other signaling pathways (Rigoglou and Papavassiliou, 2013; Jenei-Lanzl et al., 2019). The activation of catabolic signaling pathways and inhibition of anabolic signaling pathways lead to overexpression of matrix metalloproteinases (MMPs) and a disintegrin and metalloproteinase with thrombospondin motifs (ADAMTS).

Treatments for OA are developing rapidly. Platelet-rich plasma (PRP), mesenchymal stem cells (MSCs) and physical therapy are extensively applied to treatment of OA (Bennell et al., 2014; Bennell et al., 2017; Si et al., 2017; Toh et al., 2017). However, current medical management only focuses on the relief of symptoms, not the reversal of OA progression. It's unavoidable that OA patients suffer from the side effects of treatment. Therefore, it's essential to identify new therapeutic interventions for OA.

Recently, multiple studies have demonstrated that altered activity, expression, and distribution of histone deacetylases (HDACs) lead to the initiation and progression of OA. HDAC inhibitors (HDACi) can protect chondrocytes and prevent cartilage damage (Khan and Haqqi, 2018). This review focuses on the following insights: (1) the relationship between each HDAC and OA; (2) the relevant mechanisms governing HDACs involvement in OA; (3) the potential of HDACi in OA treatment.

HDAC STRUCTURE AND FUNCTION

HDACs, also called lysine deacetylases, are nuclear transcriptional regulatory proteins that regulate chromosome structure and the activity of transcription factors by removing acetyl groups from histones (Araki and Mimura, 2017). HDACs and histone acetyltransferases (HATs) are the two major components that maintain a balance in transcription activity, with HDACs inhibiting gene activation (Kroesen et al., 2014). The substrates of HDACs are abundant; HDACs can modify more than 3600 acetyl groups of over 1750 proteins. There are currently 18 HDACs, divided into four groups (**Figure 1**): Class I (HDAC1, HDAC2, HDAC3, and HDAC8), Class II (HDAC4, HDAC5, HDAC6, HDAC7, HDAC9, and HDAC10), Class III (sirtuins, sirt1–7), and Class IV (HDAC11). Class I and II HDACs require Zn^{2+} to maintain enzyme activity. The Class III HDACs are NAD^{+} -dependent (Hesham et al., 2018), and Class IV consists of a single HDAC11 (de Ruijter et al., 2003). Class I HDACs exist mostly in the nucleus, except for HDAC3 and HDAC8, which can shuttle between the nucleus and cytoplasm (Hull et al., 2016). The distribution of Class I HDACs is highly tissue-specific (Yoon and Eom, 2016). Most Class II HDACs are located in both the nucleus and cytoplasm and need to recruit Class I HDACs to obtain catalytic activity (Carpio and Westendorf, 2016).

In addition to transcriptional regulation, HDACs are involved in posttranslational modifications (PTMs). PTMs determine protein activity, stability, distribution and interaction (Yoon and Eom, 2016). Non-histone proteins such as NF- κ B, heat shock protein (HSP), P53, signal transducers and activators of transcription (STAT), forkhead transcription factor (FOXO) and mitogen-activated protein kinase (MAPK) are all modified by HDACs to regulate biological pathways (Gallinari et al., 2007; Spange et al., 2009; Jeong et al., 2014; Leus et al., 2016). Previous studies focused on the role of HDACs in cancer, pulmonary fibrosis, cardiovascular disease and rheumatoid

arthritis (Ooi et al., 2015; Angiolilli et al., 2017; Lyu et al., 2019). However, there are few articles indicating a role for HDACs in OA.

Class III HDACs (sirtuins) differ from the Class I and II HDACs structurally and mechanistically (NAD^{+} -dependent) (Dvir-Ginzberg et al., 2016). Meanwhile, there have been no reports indicating a role for the Class IV HDAC in OA. Therefore, we primarily discuss the role of the Class I and Class II HDACs in cartilage development and OA progression and the potential therapeutic effects of Class I and Class II HDAC inhibitors.

HDACs AND miRNA IN OA

MicroRNAs (miRNAs) are non-coding RNAs that regulate gene expression through post-transcriptional modifications. Altered miRNA expression is found in many diseases, including OA (Sondag and Haqqi, 2016). There have been many studies that identified a relationship between HDACs and miRNA in pathogenesis of OA (**Table 1**).

HDAC1

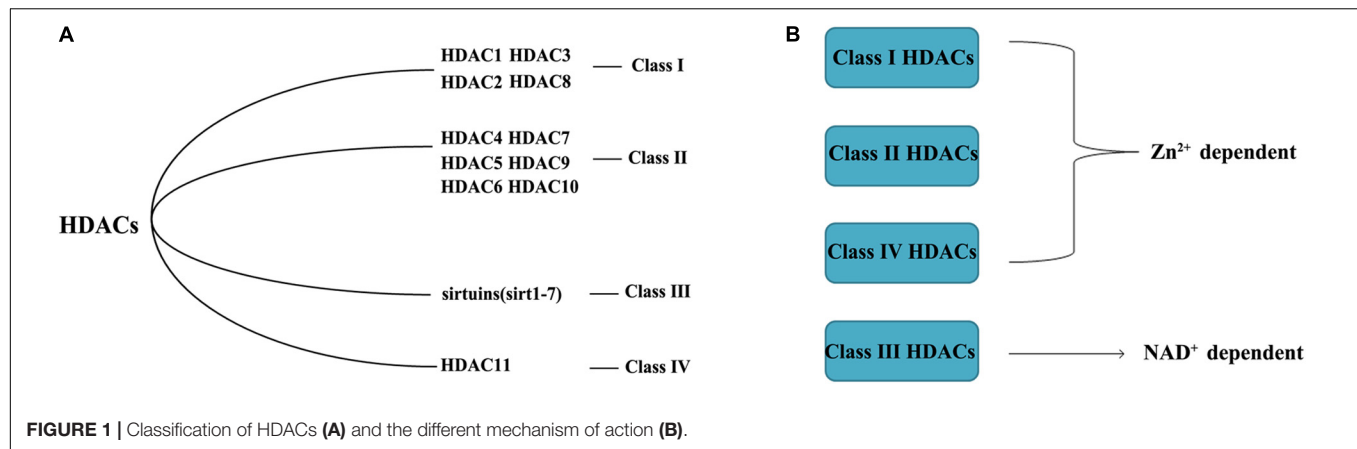
MiR-146a has a protective effect against OA by inhibiting inflammatory factors in cartilage and synovial tissues (Yang et al., 2014; Guan et al., 2018). In contrast, HDAC1 inhibits miR-146a expression in the synovium to aggravate cartilage damage (Wang et al., 2013). It's unclear whether HDAC1 regulates miR-146a expression in cartilage in OA.

HDAC2

HDAC2 has a similar structure to HDAC1 and also acts as a pro-inflammatory protein in OA pathogenesis (Brunmeir et al., 2009). Increased HDAC2 expression is observed in the cartilage and chondrocyte-secreted exosomes of OA patients and inhibits cartilage-specific gene expression in chondrocytes (Hong et al., 2009). Exosomal miR-95-5p delays OA progression and promotes cartilage matrix expression in chondrocytes by binding to the 3'-UTR of HDAC2 and inhibiting HDAC2 expression (Mao et al., 2018). Similarly, miR-92a-3p promotes cartilage matrix gene expression both in chondrogenic hMSCs and primary human chondrocytes (PHCs) by inhibiting HDAC2 expression through binding to the 3'-UTR of HDAC2 followed by increased H3 acetylation on the Aggrecan (ACAN), COMP and Col2a1 promoters and increased cartilage matrix expression (Mao et al., 2017). MiR-455-3p also has a protective effect on cartilage by inhibiting to the 3'-UTR of HDAC2, decreasing its expression, and promoting H3 acetylation on the Col2a1 promoter (Chen et al., 2016b).

HDAC3

HDAC3 is involved in the repression of cartilage matrix metabolism (Zhang et al., 2019b). MiR-193b-3p targets the 3'-UTR of HDAC3 and inhibits its expression. HDAC3 suppression

**TABLE 1 |** The relationship between HDACs and miRNAs in OA.

HDAC	miRNA	Differential expression in OA	Target gene(s)	miRNA Biological effects	References
HDAC2	miR-95-5p	Downregulated	HDAC2/8	Matrix synthesis	Mao et al. (2018)
	miR-92a-3p	Downregulated	HDAC2	Matrix synthesis	Mao et al. (2018)
	miR-455-3p	Downregulated	HDAC2/8	Matrix synthesis	Chen et al. (2016b)
HDAC3	miR-193b-3p	Downregulated	HDAC3	Matrix synthesis	Meng et al. (2018)
HDAC4	miR-381	Upregulated	HDAC4	Matrix degradation	Chen et al. (2016c)
	miR-438-5p	Upregulated	Matn3 and TIMP2	Chondrocyte hypertrophy and angiogenesis	Wang et al. (2018a)
	miR-365	Upregulated	HDAC4	Inhibition of MMP13 and Col X gene expression	Yang et al. (2016)
	miR-222	Downregulated	HDAC4	Inhibition of chondrocyte apoptosis and MMP13	Song et al. (2015)
HDAC7	miR-193b-5p	Downregulated	HDAC7	Matrix synthesis	Zhang et al. (2019a)
HDAC8	miR-95-5p	Downregulated	HDAC2/8	Matrix synthesis	Mao et al. (2018)
	miR-455-3p	Downregulated	HDAC2/8	Matrix synthesis	Chen et al. (2016b)

results in H3 acetylation and over-expression of Col2a1, ACAN, COMP, and SOX9 in hMSCs and PHC with or without IL-1 β stimulation (Meng et al., 2018).

HDAC4

The role of HDAC4 in OA has not been defined. Mammalian target of rapamycin complex 1 (mTORc1) activation induces extra cellular matrix (ECM) degradation through miR-483-5p-mediated downregulation of Matn3 and tissue inhibitor of metalloproteinase-2 (Timp2) in a Col2a1TSC1KO OA mouse model (Wang et al., 2018a). HDAC4 reverses OA symptoms by inhibiting miR-483-5p (Wang et al., 2018a). MiR-381 aggravates cartilage degradation and OA progression, whereas HDAC4 reverses this effect. The underlying mechanism involves the inhibition of HDAC4 expression by miR-381 binding to its 3'-UTR. Such inhibition decreases MMP13 and Runx-related transcription factor 2 (Runx2) expression in ATDC5 chondrocyte and SW1353 chondrosarcoma cell lines (Chen et al., 2016c). MiR-365 also promotes osteoarthritic cartilage destruction by targeting HDAC4 (Yang et al., 2016). Interestingly, HDAC4 also acting as a pro-inflammatory factor, can accelerate OA progression by inhibiting miR-146a in osteoarthritis synovial fibroblast-like cells (OA-FLS) (Wang et al., 2013). This contradictory phenomenon may be explained by the fact that this

latter study only focused on the effect of HDAC4 on miR-146a and the downstream proteins interleukin-1 receptor-associated kinase 1 (IRAK1) and tumor necrosis factor receptor-associated factor 6 (TRAF6), but HDAC4 can be a positive regulator in other processes. Thus, overall, HDAC4 has anti-inflammatory and anti-arthritis effect. The second reason might be that HDAC4 acts as a pro-inflammatory factor in FLS but not chondrocytes. However, Song et al. (2015) found that miR-222 over-expression suppressed chondrocyte apoptosis and MMP13 expression by inhibiting HDAC4. Thus, the distinct mechanism of HDAC4 in OA requires further investigation.

HDAC5 AND HDAC6

There are no article about relationship between HDAC9, HDAC10, and miRNAs in pathogenesis of OA.

HDAC7

HDAC7 evokes cartilage damage and ECM degradation through the over-expression of MMP3 and MMP13. In contrast, miR-193b-5p protects cartilage from injury by inhibiting HDAC7 through binding to its 3'-UTR (Zhang et al., 2019a). Interestingly, HDAC7 inhibition by siHDAC7 also promotes miR-193b-5p

expression, suggesting that HDAC7 regulates miR-193b-5p in OA via a positive-feedback loop.

HDAC8

Like HDAC2, HDAC8 exacerbates OA by inhibiting matrix metabolism, whereas miR-455-3p and miR-95-5p suppress HDAC8 expression to protect cartilage as mentioned above (Chen et al., 2016b; Mao et al., 2018).

HDAC9 AND HDAC10

There are no article about relationship between HDAC9, HDAC10, and miRNAs in pathogenesis of OA.

HDACs AND SIGNALING PATHWAYS IN CARTILAGE DEVELOPMENT AND OA

HDAC1

HDAC1 expression is elevated in OA cartilage (Hong et al., 2009). The carboxyl-terminal domain (CTD) of HDAC1 is the major regulatory unit in OA pathogenesis. While the CTD does not determine HDAC1 enzymatic activity, it does affect the target gene specificity. The HDAC1 CTD promotes Snail1 transcription factor activity, a known repressor of Collagen2 ($\alpha 1$) in chondrocytes (Hong et al., 2009). Leukemia/lymphoma-related factor (LRF) suppresses expression of the COMP gene. HDAC1 increases LRF activity and suppresses COMP transcription in chondrocytes (Liu et al., 2004). In addition, HDAC1 assists HDAC9 in weakening Nkx3.2 stability by regulating acetylation status, which is required for chondrocyte viability and chondrocyte hypertrophy (Choi et al., 2016). Interestingly, there have also been controversial observations. During chondrocyte proliferation and chondrogenesis, zinc finger nuclear regulator (Trps1) plays a critical role in mitosis. An interaction between Trps1 and HDAC1 increases the histone deacetylase activity of HDAC1, leading to normal chondrocyte mitosis (Wuelling et al., 2013). HDAC1 also promotes cartilage development through the canonical Wnt/ β -catenin pathway. HDAC1 suppresses β -catenin expression through its promoter and increases β -catenin degradation by regulating acetylation (Huang et al., 2014). Thus, HDAC1 plays a positive role in early cartilage formation and development but has a negative role in OA pathogenesis.

HDAC2

The HDAC2 CTD also interacts with the Snail transcription factor to promote its activity and inhibit COMP expression (Hong et al., 2009). Protein kinase epsilon (PKC ϵ) increases SOX9 expression, the deposition of glycosaminoglycans (GAGs) and inhibition of Runx2 expression in OA through HDAC2 down regulation (Queirolo et al., 2016).

HDAC3

HDAC3 plays an important role in the development of bone and cartilage but can also exacerbate OA progression. HDAC3 is required for chondrocyte maturation at the early stage of skeletal formation in mice (E10.5 and E16.5). Postnatal ablation of HDAC3 in chondrocytes delays chondrocyte endochondral maturation, ossification and induces inflammatory cytokines in normal chondrocytes (Carpio et al., 2016). HDAC3 also inhibits the Erk1/2 downstream proteins (Runx2 and MMP13) and promotes chondrocyte maturation in the growth plate, which inhibits temporal and spatial activation of Erk1/2 through the up-regulation of the dual-specific phosphatase Dusp6 (Carpio et al., 2017). HDAC3 also represses Phlpp1 transcription to promote Akt phosphorylation and activation of its downstream targets (mTOR and p70 SK6) in chondrocytes. These events are essential for regulating chondrocyte hypertrophy and the promotion of matrix gene expression (Bradley et al., 2013). In the pathogenesis of OA, HDAC3 promotes OA progression via the regulation of the nuclear transportation of NF- κ B in OA cartilage and chondrocytes with elevated MMP13 and ADAMTS5 expression (Zhang et al., 2019b). The contradictory phenomenon may be explained by the following: (1) HDAC3 is only essential for chondrocytes during the embryonic growth period; (2) HDAC3-deletion may slightly elevate inflammatory cytokines compared to normal chondrocytes, but significantly inhibit inflammation compared to chondrocytes treated with IL-1 β .

HDAC4

HDAC4 is the most thoroughly studied HDAC in OA pathogenesis. Decreased HDAC4 expression is observed in OA patients. HDAC4 not only inhibits the expression of Runx2, MMP1, MMP3, MMP13, ADAMTS4, and ADAMTS5 but also partially blocks the catabolic events in chondrocytes stimulated by IL-1 β (Cao et al., 2014). As mentioned earlier, PKC ϵ promotes SOX9 expression and the deposition of GAGs in chondrocytes via HDAC4 up-regulation (Queirolo et al., 2016). The PTHrp-Zfp521-HDAC4 pathway could negatively regulate chondrocyte hypertrophy. Zfp521 is a downstream target gene of PTHrp and forms a complex with HDAC4 and Runx2, leading to the repression of Runx2-mediated target gene activation (Correa et al., 2010).

Alterations in HDAC4 and cellular localization can regulate chondrocyte hypertrophy, OA progression and affect chondrocyte hemostasis. PTHrp promotes the nuclear translocation of HDAC4 and inhibition of MEF2 transcriptional activity to prevent chondrocyte hypertrophy (Kozhemyakina et al., 2009). In addition, HDAC4 is a mechanical-responsive protein; its expression can be regulated by mechanical compression in chondrocytes. Hydrostatic pressure (1–5 Hz) significantly decreases HDAC4 expression in OA chondrocytes to maintain the chondrocyte phenotype (Cheleschi et al., 2017). Furthermore, mechanical stimulation also alters the subcellular distribution of HDAC4 in these cells. Proper compression of chondrocytes promotes matrix-related gene expression through HDAC4 translocation to the nucleus (Chen et al., 2016a). This effect is dependent on PP2A-induced HDAC4

dephosphorylation. The relocation of HDAC4 associated with 14-3-3 to the cytoplasm also promotes CaMK IV-induced expression of Runx2 and related proteins in the chondrocytes (Guan et al., 2012). Interestingly, HDAC4 also has a destructive role in OA. HDAC4 is an upstream mediator of MAPK and promotes ADAMTS4, ADAMTS5, and cyclooxygenase 2 (Cox2) expression in rat articular chondrocytes stimulated with IL-1 β (Wang et al., 2018b). The reason for the inconsistent phenomenon is unclear and still need further explored.

HDAC5

Little is known on the role of HDAC5 in cartilage development and OA progression. HDAC5 acts as a co-activator of HDAC4 to inhibit chondrocyte hypertrophy through parathyroid hormone-related protein (PTHrP), which blocks the Mef2/Runx2 signaling pathway (Cheng et al., 2019).

HDAC6

Mechanical intervention and physical activity can modify the epigenetic state by regulating the HDACs. This process is called mechanico-epigenetics (Chen et al., 2013). HDAC6 is a mechanosensitive protein involved in OA. It promotes ADAMTS5 expression through cilia disassembly and hedgehog signaling at 0.33 Hz and 20% cyclic tensile strain (CTS). This effect is not observed at 10% CTS (Thompson et al., 2014). Mechanical loading also attenuates NF- κ B activity in chondrocytes stimulated with IL-1 β through the regulation of the intraflagellar transport (IFT)-dependent pathway. Under the conditions of 0.33 Hz and 10% CTS, HDAC6 activity increases followed by the recovery of cartilage (Fu et al., 2019).

HDAC7

HDAC7 plays a pivotal role in both cartilage development and OA. Increased HDAC7 expression is observed in the knee cartilage of OA patients, and HDAC7 induces MMP13 overexpression in OA (Higashiyama et al., 2010). Furthermore, insulin-like growth factor 1 (Igf1)/insulin-dependent signaling activates β -Catenin signaling, which promotes chondrocyte proliferation in immature chondrocytes. Igf1/insulin pathway also promotes HDAC7 translocation from the nucleus to the cytosol, where it is degraded by the proteasome (Bradley et al., 2015).

HDAC8

HDAC8 promotes JNK phosphorylation to increase the expression of ADAMTS4, ADAMTS5, ColX, and Cox-2 in chondrocytes (Wang et al., 2018b). This effect is inhibited by both HDAC8 siRNA and the HDAC8 inhibitor, PCI.

HDAC9

There are few reports on the role of HDAC9 in cartilage development, chondrocyte hypertrophy and OA. Nkx3.2/Bapx1 is a crucial protein for maintaining chondrocyte viability. The HDAC9-PIASy-RNF4 axis could promote chondrocyte hypertrophy by regulating the sumoylation and ubiquitination of Nkx3.2/Bapx1, leading to its degradation through the proteasome (Choi et al., 2016).

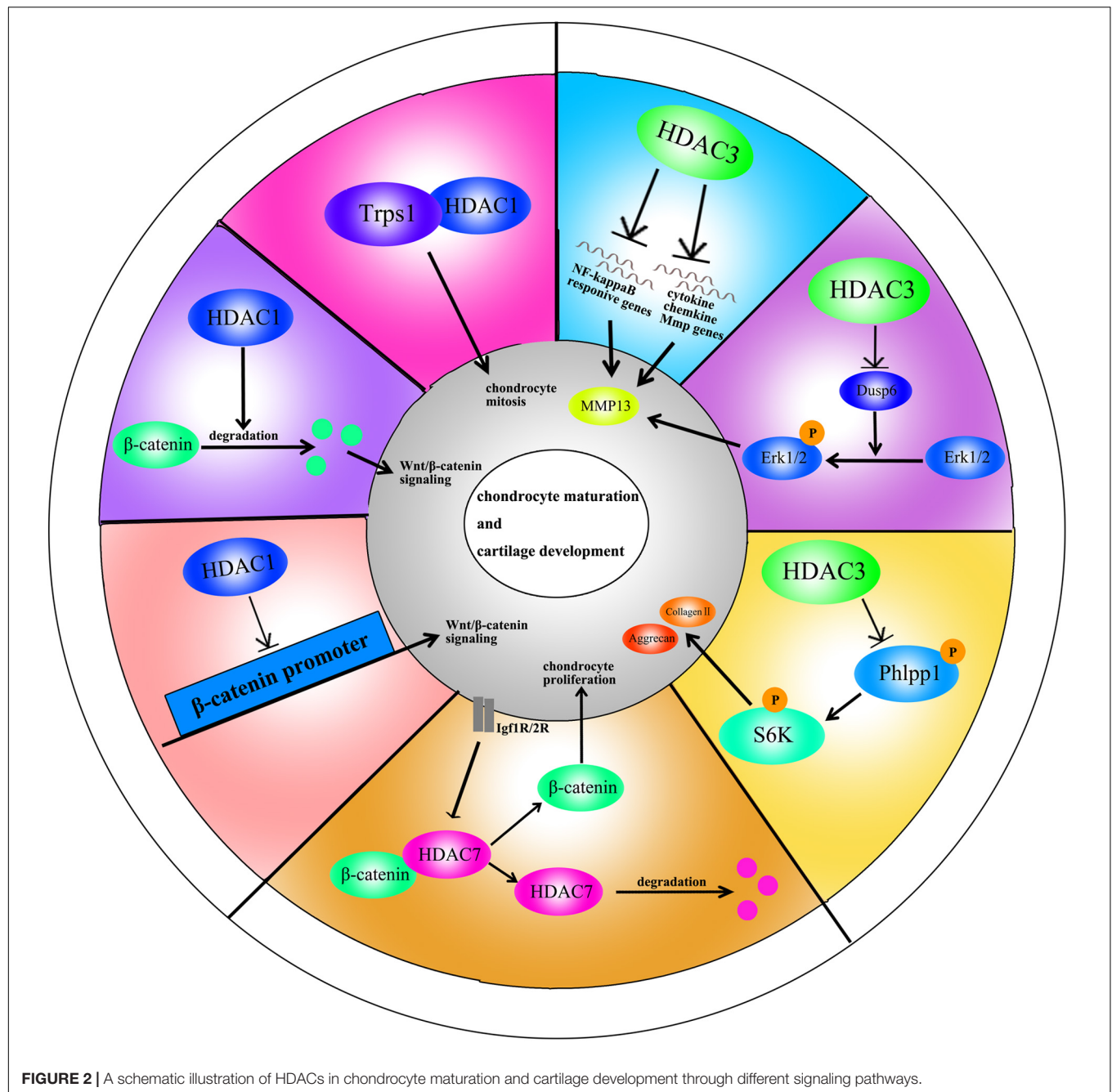
HDAC10

HDAC10 is involved in the regulation of collagen II expression through the epigenetic modification of enhancer elements in the collagen II gene. HDAC10 overexpression in Swarm rat chondrosarcoma (RCS) chondrocytes suppresses collagen II transcription through interaction with the E2 enhancer element in the collagen II gene, which locates 277 bp downstream of the transcription start site (Figures 2, 3; Nham et al., 2019).

HDAC INHIBITORS AND OA TREATMENT

HDACi inhibit the enzymatic activity of HDACs and promote acetylation of proteins. HDACi can be divided into four groups, according to their structures: short-chain fatty acids, hydroxamic acids, cyclic peptides, and benzamides (Carpio and Westendorf, 2016). Currently, there have been more than 609 completed/ongoing HDACi-related human clinical trials, including trials for kidney disease (Chun, 2018), cardiovascular disease (Yoon and Eom, 2016), neuronal memory and regeneration (Ganai et al., 2016), myeloma and solid tumors (Hull et al., 2016; Cengiz Seval and Beksac, 2019). Although, there have been many studies on the effects of HDACi on OA, none of the HDACi identified have been approved as an OA treatment by the United States Food and Drug Administration (FDA).

The hydroxamic acids consist of trichostatin (TSA), vorinostat (SAHA), ricolinostat (ACY-1215) and givinostat (ITF2357). TSA is the most common broad spectrum HDACi. *In vitro*, TSA inhibits MMP1, MMP3, MMP13, and IL-1 in OA chondrocytes (Chen et al., 2010). One of the mechanisms of TSA treatment is that TSA abolishes the pro-inflammatory effect of Kruppel-like factor 4 (KLF4) (Fujikawa et al., 2017). Although TSA inhibits the inflammatory response in OA, it decreases collagen II mRNA levels in primary human chondrocyte stimulated with IL-1 β or fibroblast growth factor-2 (FGF-2) (Wang et al., 2009). A Redox imbalance contributes to OA progression, TSA inhibits synthesis of NO and prostaglandin (PGE₂), and the expression of inducible nitric oxide synthase (iNOS) and Cox-2 in chondrocytes stimulated with IL-1 β (Chabane et al., 2008). Apoptosis is a crucial regulatory mechanism in OA. TSA suppresses apoptosis to protect chondrocytes (Song et al., 2015). In CTS-induced activation of the MAPK signaling pathway in chondrocytes, TSA downregulates MAPK and suppresses its downstream pro-inflammatory proteins (e.g., Runx2 and MMP13) at both the mRNA and protein levels (Saito et al., 2013). The protective effect of TSA is the same in leptin-stimulated human chondrocytes (Iliopoulos et al., 2007). *In vivo*, Cai et al. (2015) reported that TSA alleviates OA through the induction of Nrf2 and its downstream proteins. TSA also increases the Timp-1/MMP ratio in the OA model along with increased acetylation levels of H3 and H4. However, whether there is a relationship between histone acetylation and the Timp-1/MMP ratio needs additional study (Higashiyama et al., 2010). The protective effect of TSA was confirmed in an ACLT rabbit model through the inhibition of cathepsins (Chen et al., 2011). Furthermore, TSA also ameliorates OA by inhibiting synovial inflammation in an OA mouse model (Nasu et al., 2008).



Vorinostat (SAHA) is another HDACi composed of hydroxamic acids. It inhibits MMPs and iNOS by attenuating the NF- κ B and MAPK pathways in human chondrocytes stimulated with IL-1 β . However, vorinostat only inhibits p38 and Erk1/2 activation, not JNK activation (Zhong et al., 2013). Treatment with vorinostat also suppresses IL-6 expression in OA chondrocytes through the miR-9-MCPIP1 axis. Vorinostat promotes the recruitment of CEBP α to the promoter of MCPIP1 to inhibit IL-1 synthesis (Makki and Haqqi, 2017). Furthermore, IL-6-induced MMP13 expression in the chondrocytes can be

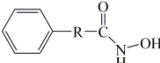
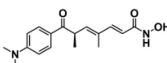
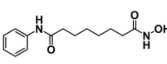
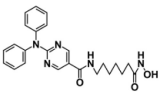
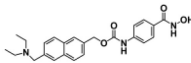
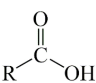
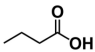
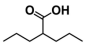
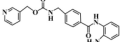
reversed by vorinostat, which promotes Col2a1 and ACAN expression in OA chondrocyte (Makki and Haqqi, 2016).

Ricolinostat (ACY-1215) is a selective HDAC6 inhibitor that has anti-inflammatory and chondroprotective properties. ACY-1215 inhibits MMP1 and MMP13 expression by down regulating NF- κ B and STAT3 activity in primary human chondrocyte stimulated with IL-1 β (Cheng et al., 2019).

Givinostat (ITF2357) is another anti-inflammatory compound that can inhibit MMPs expression in an experimental arthritis model (Joosten et al., 2011).



TABLE 2 | The classification of HDACi and effect of HDACi on OA.

Group and structure	HDAC inhibitor	HDAC selectivity	Effect of HDAC inhibitor	Mechanism	References
Hydroxamic acids 	TSA	Class I/II HDACs IC ₅₀ : 1.8 nM	Inhibition of MMPs and IL-1	ND and inhibition of KLF4	Chen et al. (2010); Fujikawa et al. (2017); Wang et al. (2009); Iliopoulos et al. (2007)
			Inhibition of NO and PGE ₂ synthesis; Inhibition of iNOS and Cox-2 expression	ND and not through NF-κB activity	Chabane et al. (2008)
			Inhibition of Runx2 and ADAMTS5	Inhibition of MAPK signaling	Saito et al. (2013)
			Inhibition of MMPs, TNF-α, IL-1, and IL-6	Promotion of Nrf2 signaling	Cai et al. (2015)
			Regulation of MMP/TIMP-1 ratio	ND	Higashiyama et al. (2010)
	Vorinostat (SAHA)	HDAC1 IC ₅₀ : 10 nM	Inhibition of cathepsins	ND	Chen et al. (2011)
			Inhibition of MMPs and iNOS	Attenuation of NF-κB and MAPK pathways	Zhong et al. (2013)
		HDAC3 IC ₅₀ : 20 nM	Inhibition of IL-1 synthesis	Recruitment of CEBPα to the promoter of MCP1	Makki and Haqqi (2017)
			Inhibition of MMP13 expression and promotion of Col2a1 and ACAN expression	ND	Makki and Haqqi (2016)
	Ricolinostat (ACY-1215)	HDAC6 IC ₅₀ : 5 nM	Inhibition of MMP1 and MMP13 expression	Down-regulation of NF-κB and STAT3 activity	Cheng et al. (2019)
					
	Givinostat (ITF-2357)	HDAC1 IC ₅₀ : 198 nM HDAC3 IC ₅₀ : 157 nM	Inhibition of MMPs	ND	Joosten et al. (2011)
					
Short-chain fatty acids 	Butyrate acid	Class I/II HDACs (except HDAC6 and HDAC10) IC ₅₀ : ND	Inhibition of pro-inflammatory cytokines and adipokines	Through G protein-coupled receptor (GPR)- 43	Pirozzi et al. (2018)
			Inhibition of MMPs	Through inactivation of NF-κB	Bo et al. (2018)
	Valproic acid	HDAC1 IC ₅₀ : 0.4mM HDAC2 IC ₅₀ : ND	Down-regulation of microsomal prostaglandin E2 (Mpges-1)	Promotion of NAB1 which suppressed promoter of Mpges-1	Zayed et al. (2011)
			Inhibition of MMP1, MMP3 and MMP13	ND	Culley et al. (2013)
	Entinostat (MS-275)	HDAC1 IC ₅₀ : 243 nM HDAC2 IC ₅₀ : 453 nM HDAC3 IC ₅₀ : 248 nM	Inhibition of MMP13 expression and prevention of cartilage absorption	ND	Queirolo et al. (2016); Culley et al. (2013)
			Suppression CTS- induced expression of Runx2, ADAMTS5 and MMP3	Through inhibition of MAPK signaling pathway	Saito et al. (2013)

ND: Not determined. IC₅₀ and chemical structure were cited by <https://www.medchemexpress.cn/>.

Furthermore, it suppresses CTS-induced expression of Runx2, ADAMTS5, and MMP3 at both the mRNA and protein levels in chondrocytes through inhibition of MAPK signaling pathway (Saito et al., 2013; **Table 2**).

There are also some major obstacles to using HDACi to treat OA. HDACi affect many systems and organs through blood flow after administration. Inevitably, unnecessary side effects and toxicity occur, including secondary malignancies (Bhaskara et al., 2010; Mendivil et al., 2013). Most HDACi are broad-spectrum inhibitors. Thus, some beneficial HDACs may also be inhibited, leading to side effects and a low efficiency of HDACi therapy. Furthermore, the HDACi dosage should be determined for individual patients (Khabele, 2014). Too much or too little dosage drug will fail to achieve the expected therapeutic effects against OA.

CONCLUSION

In recent years, HDACs have drawn more and more attention in the pathogenesis of OA. Previous studies demonstrated that HDACs not only regulate chondrocyte maturation and hypertrophy but also protect cartilage from damage. However, the mechanisms underlying the role of HDACs in OA are unclear and require additional investigation. Clarification of the roles of individual HDACs in cartilage will help define which HDAC(s) should be inhibited or activated for the treatment of OA. Moreover, a better understanding of the roles of individual HDACs in OA will reveal the major HDAC isoform(s) responsible for OA and allow the development of a selective HDACi to achieve a more precise and effective therapy for OA.

Based on this review, HDACi have protective roles in cartilage and enormous potential as new drugs to against OA. There are currently limitations to the use of HDACi as OA therapy. With non-selective HDACi, patients may suffer from severe side effect

and toxicity. The dosage is an important consideration for the clinical use of HDACi. An unoptimized dosage might not achieve the predicted effect and could even cause harm. Therefore it's essential to identify tissue-specific and HDAC-specific HDACi to avoid side effect and toxicity. In parallel, the development of specific HDACi will also help delineate the function of individual HDACs in OA. Finally, it's necessary to build a drug evaluation system to guide dosage selection for individual patients to achieve the best therapeutic effect.

In conclusion, although our knowledge of OA continues to grow, understanding the underlying mechanisms involved in OA pathogenesis and identifying effective treatments will require further investigation. Based on current data, HDACs and HDACi hold promise for the management of OA.

AUTHOR CONTRIBUTIONS

HZ contributed to conception and design for the manuscript. HZ and LJ drafted the article. HZ, YY, and XZ contributed to critical revision of the article. YG and JL provided the technical support. LB approved the final version of the article. All authors contributed to the article and approved the submitted version.

FUNDING

This research was funded by the National Natural Science Foundation of China, grant nos. 81772420 and 81272050.

ACKNOWLEDGMENTS

We appreciated the help from our fellows in the lab affiliated to China Medical University, Liaoning, China.

REFERENCES

- Angiolilli, C., Baeten, D. L., Radstake, T. R., and Reedquist, K. A. (2017). The acetyl code in rheumatoid arthritis and other rheumatic diseases. *Epigenomics* 9, 447–461. doi: 10.2217/epi-2016-0136
- Araki, Y., and Mimura, T. (2017). Matrix metalloproteinase gene activation resulting from disordered epigenetic mechanisms in rheumatoid arthritis. *Int. J. Mol. Sci.* 18:905. doi: 10.3390/ijms18050905
- Avery, L. B., and Bumpus, N. N. (2014). Valproic acid is a novel activator of AMP-activated protein kinase and decreases liver mass, hepatic fat accumulation, and serum glucose in obese mice. *Mol. Pharmacol.* 85, 1–10. doi: 10.1124/mol.113.089755
- Bennell, K. L., Egerton, T., Martin, J., Abbott, J. H., Metcalf, B., McManus, F., et al. (2014). Effect of physical therapy on pain and function in patients with hip osteoarthritis: a randomized clinical trial. *JAMA* 311, 1987–1997. doi: 10.1001/jama.2014.4591
- Bennell, K. L., Hunter, D. J., and Paterson, K. L. (2017). Platelet-rich plasma for the management of hip and knee osteoarthritis. *Curr. Rheumatol. Rep.* 19:24. doi: 10.1007/s11926-017-0652-x
- Bhaskara, S., Knutson, S. K., Jiang, G., Chandrasekharan, M. B., Wilson, A. J., Zheng, S., et al. (2010). Hdac3 is essential for the maintenance of chromatin structure and genome stability. *Cancer Cell* 18, 436–447. doi: 10.1016/j.ccr.2010.10.022
- Bo, W., Zhou, J., and Wang, K. (2018). Sodium butyrate abolishes the degradation of type II collagen in human chondrocytes. *Biomed. Pharmacother.* 102, 1099–1104. doi: 10.1016/j.biopha.2018.03.062
- Bradley, E. W., Carpio, L. R., Olson, E. N., and Westendorf, J. J. (2015). Histone deacetylase 7 (Hdac7) suppresses chondrocyte proliferation and beta-catenin activity during endochondral ossification. *J. Biol. Chem.* 290, 118–126. doi: 10.1074/jbc.M114.596247
- Bradley, E. W., Carpio, L. R., and Westendorf, J. J. (2013). Histone deacetylase 3 suppression increases PH domain and leucine-rich repeat phosphatase (Phlpp)1 expression in chondrocytes to suppress Akt signaling and matrix secretion. *J. Biol. Chem.* 288, 9572–9582. doi: 10.1074/jbc.M112.423723
- Brunmeir, R., Lagger, S., and Seiser, C. (2009). Histone deacetylase HDAC1/HDAC2-controlled embryonic development and cell differentiation. *Int. J. Dev. Biol.* 53, 275–289. doi: 10.1387/ijdb.082649rb
- Cai, D., Yin, S., Yang, J., Jiang, Q., and Cao, W. (2015). Histone deacetylase inhibition activates Nrf2 and protects against osteoarthritis. *Arthritis Res. Ther.* 17:269. doi: 10.1186/s13075-015-0774-3
- Cao, K., Wei, L., Zhang, Z., Guo, L., Zhang, C., Li, Y., et al. (2014). Decreased histone deacetylase 4 is associated with human osteoarthritis cartilage degeneration by releasing histone deacetylase 4 inhibition of runt-related transcription factor-2 and increasing osteoarthritis-related genes: a novel mechanism of human osteoarthritis cartilage degeneration. *Arthritis Res. Ther.* 16:491. doi: 10.1186/s13075-014-0491-3

- Carpio, L. R., Bradley, E. W., McGee-Lawrence, M. E., Weivoda, M. M., Poston, D. D., Dudakovic, A., et al. (2016). Histone deacetylase 3 supports endochondral bone formation by controlling cytokine signaling and matrix remodeling. *Sci. Signal.* 9:ra79. doi: 10.1126/scisignal.aaf3273
- Carpio, L. R., Bradley, E. W., and Westendorf, J. J. (2017). Histone deacetylase 3 suppresses Erk phosphorylation and matrix metalloproteinase (Mmp)-13 activity in chondrocytes. *Connect Tissue Res.* 58, 27–36. doi: 10.1080/03008207.2016.1236088
- Carpio, L. R., and Westendorf, J. J. (2016). Histone deacetylases in cartilage homeostasis and osteoarthritis. *Curr. Rheumatol. Rep.* 18:52. doi: 10.1007/s11926-016-0602-z
- Cengiz Seval, G., and Beksac, M. (2019). A comparative safety review of histone deacetylase inhibitors for the treatment of myeloma. *Expert Opin. Drug Saf.* 18, 563–571. doi: 10.1080/14740338.2019.1615051
- Chabane, N., Zayed, N., Afif, H., Mfuna-Endam, L., Benderdour, M., Boileau, C., et al. (2008). Histone deacetylase inhibitors suppress interleukin-1 β -induced nitric oxide and prostaglandin E2 production in human chondrocytes. *Osteoarthritis Cartilage* 16, 1267–1274. doi: 10.1016/j.joca.2008.03.009
- Cheleschi, S., De Palma, A., Pecorelli, A., Pascarelli, N. A., Valacchi, G., Belmonte, G., et al. (2017). Hydrostatic pressure regulates microRNA expression levels in osteoarthritic chondrocyte cultures via the Wnt/ β -catenin pathway. *Int. J. Mol. Sci.* 18:133. doi: 10.3390/ijms18010133
- Chen, C., Wei, X., Wang, S., Jiao, Q., Zhang, Y., Du, G., et al. (2016a). Compression regulates gene expression of chondrocytes through HDAC4 nuclear relocation via PP2A-dependent HDAC4 dephosphorylation. *Biochim. Biophys. Acta* 1863(7 Pt A), 1633–1642. doi: 10.1016/j.bbamcr.2016.04.018
- Chen, L. J., Wei, S. Y., and Chiu, J. J. (2013). Mechanical regulation of epigenetics in vascular biology and pathobiology. *J. Cell. Mol. Med.* 17, 437–448. doi: 10.1111/jcmm.12031
- Chen, W., Chen, L., Zhang, Z., Meng, F., Huang, G., Sheng, P., et al. (2016b). MicroRNA-455-3p modulates cartilage development and degeneration through modification of histone H3 acetylation. *Biochim. Biophys. Acta* 1863, 2881–2891. doi: 10.1016/j.bbamcr.2016.09.010
- Chen, W., Sheng, P., Huang, Z., Meng, F., Kang, Y., Huang, G., et al. (2016c). MicroRNA-381 regulates chondrocyte hypertrophy by inhibiting histone deacetylase 4 expression. *Int. J. Mol. Sci.* 17:1377. doi: 10.3390/ijms17091377
- Chen, W. P., Bao, J. P., Hu, P. F., Feng, J., and Wu, L. D. (2010). Alleviation of osteoarthritis by Trichostatin A, a histone deacetylase inhibitor, in experimental osteoarthritis. *Mol. Biol. Rep.* 37, 3967–3972. doi: 10.1007/s11033-010-0055-9
- Chen, W. P., Bao, J. P., Tang, J. L., Hu, P. F., and Wu, L. D. (2011). Trichostatin A inhibits expression of cathepsins in experimental osteoarthritis. *Rheumatol. Int.* 31, 1325–1331. doi: 10.1007/s00296-010-1481-7
- Cheng, C., Shan, W., Huang, W., Ding, Z., Cui, G., Liu, F., et al. (2019). ACY-1215 exhibits anti-inflammatory and chondroprotective effects in human osteoarthritic chondrocytes via inhibition of STAT3 and NF- κ B signaling pathways. *Biomed. Pharmacother.* 109, 2464–2471. doi: 10.1016/j.biopha.2018.11.017
- Cho, H. J., Morey, V., Kang, J. Y., Kim, K. W., and Kim, T. K. (2015). Prevalence and risk factors of spine, shoulder, hand, hip, and knee osteoarthritis in community-dwelling Koreans older than age 65 years. *Clin. Orthop. Relat. Res.* 473, 3307–3314. doi: 10.1007/s11999-015-4450-3
- Choi, H. J., Kwon, S., and Kim, D. W. (2016). A post-translational modification cascade employing HDAC9-PIASy-RNF4 axis regulates chondrocyte hypertrophy by modulating Nkx3.2 protein stability. *Cell. Signal.* 28, 1336–1348. doi: 10.1016/j.cellsig.2016.06.006
- Chun, P. (2018). Therapeutic effects of histone deacetylase inhibitors on kidney disease. *Arch. Pharm. Res.* 41, 162–183. doi: 10.1007/s12272-017-0998-7
- Correa, D., Hesse, E., Seriwatanachai, D., Kiviranta, R., Saito, H., Yamana, K., et al. (2010). Zfp521 is a target gene and key effector of parathyroid hormone-related peptide signaling in growth plate chondrocytes. *Dev. Cell* 19, 533–546. doi: 10.1016/j.devcel.2010.09.008
- Culley, K. L., Wang, H., Barter, M. J., Davidson, R. K., Swingle, T. E., Destrument, A. P. M., et al. (2013). Class I histone deacetylase inhibition modulates metalloproteinase expression and blocks cytokine-induced cartilage degradation. *Arthritis Rheum.* 65, 1822–1830. doi: 10.1002/art.37965
- de Ruijter, A. J., van Gennip, A. H., Caron, H. N., Kemp, S., and van Kuilenburg, A. B. (2003). Histone deacetylases (HDACs): characterization of the classical HDAC family. *Biochem. J.* 370(Pt 3), 737–749. doi: 10.1042/BJ20021321
- Dvir-Ginzberg, M., Mobasher, A., and Kumar, A. (2016). The role of sirtuins in cartilage homeostasis and osteoarthritis. *Curr. Rheumatol. Rep.* 18:43. doi: 10.1007/s11926-016-0591-y
- Fu, S., Thompson, Ph, D. C., Ali, A., Wang, Ph, D. W., et al. (2019). Mechanical loading inhibits cartilage inflammatory signalling via an HDAC6 and IFT-dependent mechanism regulating primary cilia elongation. *Osteoarthritis Cartilage* 27, 1064–1074. doi: 10.1016/j.joca.2019.03.003
- Fujikawa, J., Takeuchi, Y., Kanazawa, S., Nomi, A. G., Kito, A., Elkhassab, E., et al. (2017). Kruppel-like factor 4 regulates matrix metalloproteinase and aggrecanase gene expression in chondrocytes. *Cell Tissue Res.* 370, 441–449. doi: 10.1007/s00441-017-2674-0
- Gallinari, P., Di Marco, S., Jones, P., Pallaoro, M., and Steinkuhler, C. (2007). HDACs, histone deacetylation and gene transcription: from molecular biology to cancer therapeutics. *Cell Res.* 17, 195–211. doi: 10.1038/sj.cr.73.10149
- Ganai, S. A., Ramadoss, M., and Mahadevan, V. (2016). Histone Deacetylase (HDAC) Inhibitors - emerging roles in neuronal memory, learning, synaptic plasticity and neural regeneration. *Curr. Neuropharmacol.* 14, 55–71. doi: 10.2174/1570159x1366615102111609
- Guan, Y., Chen, Q., Yang, X., Haines, P., Pei, M., Terek, R., et al. (2012). Subcellular relocation of histone deacetylase 4 regulates growth plate chondrocyte differentiation through Ca²⁺/calmodulin-dependent kinase IV. *Am. J. Physiol. Cell Physiol.* 303, C33–C40. doi: 10.1152/ajpcell.00348.2011
- Guan, Y. J., Li, J., Yang, X., Du, S., Ding, J., Gao, Y., et al. (2018). Evidence that miR-146a attenuates aging- and trauma-induced osteoarthritis by inhibiting Notch1, IL-6, and IL-1 mediated catabolism. *Aging Cell* 17:e12752. doi: 10.1111/accel.12752
- Hesham, H. M., Lasheen, D. S., and Abouzid, K. A. M. (2018). Chimeric HDAC inhibitors: comprehensive review on the HDAC-based strategies developed to combat cancer. *Med. Res. Rev.* 38, 2058–2109. doi: 10.1002/med.21505
- Higashiyama, R., Miyaki, S., Yamashita, S., Yoshitaka, T., Lindman, G., Ito, Y., et al. (2010). Correlation between MMP-13 and HDAC7 expression in human knee osteoarthritis. *Mod. Rheumatol.* 20, 11–17. doi: 10.1007/s10165-009-0224-7
- Hong, S., Derfoul, A., Pereira-Mouries, L., and Hall, D. J. (2009). A novel domain in histone deacetylase 1 and 2 mediates repression of cartilage-specific genes in human chondrocytes. *FASEB J.* 23, 3539–3552. doi: 10.1096/fj.09-133215
- Huang, X., Xu, J., Huang, M., Li, J., Dai, L., Dai, K., et al. (2014). Histone deacetylase1 promotes TGF- β 1-mediated early chondrogenesis through down-regulating canonical Wnt signaling. *Biochem. Biophys. Res. Commun.* 453, 810–816. doi: 10.1016/j.bbrc.2014.10.021
- Hull, E. E., Montgomery, M. R., and Leyva, K. J. (2016). HDAC inhibitors as epigenetic regulators of the immune system: impacts on cancer therapy and inflammatory diseases. *Biomed. Res. Int.* 2016:8797206. doi: 10.1155/2016/8797206
- Iliopoulos, D., Malizos, K. N., and Tsezou, A. (2007). Epigenetic regulation of leptin affects MMP-13 expression in osteoarthritic chondrocytes: possible molecular target for osteoarthritis therapeutic intervention. *Ann. Rheum. Dis.* 66, 1616–1621. doi: 10.1136/ard.2007.069377
- Jenei-Lanzl, Z., Meurer, A., and Zaucke, F. (2019). Interleukin-1 β signaling in osteoarthritis - chondrocytes in focus. *Cell. Signal.* 53, 212–223. doi: 10.1016/j.cellsig.2018.10.005
- Jeong, Y., Du, R., Zhu, X., Yin, S., Wang, J., Cui, H., et al. (2014). Histone deacetylase isoforms regulate innate immune responses by deacetylating mitogen-activated protein kinase phosphatase-1. *J. Leukoc. Biol.* 95, 651–659. doi: 10.1189/jlb.1013565
- Johnson, V. L., and Hunter, D. J. (2014). The epidemiology of osteoarthritis. *Best Pract. Res. Clin. Rheumatol.* 28, 5–15. doi: 10.1016/j.berh.2014.01.004
- Joosten, L. A., Leoni, F., Meghji, S., and Mascagni, P. (2011). Inhibition of HDAC activity by ITF2357 ameliorates joint inflammation and prevents cartilage and bone destruction in experimental arthritis. *Mol. Med.* 17, 391–396. doi: 10.2119/molmed.2011.00058
- Khabele, D. (2014). The therapeutic potential of class I selective histone deacetylase inhibitors in ovarian cancer. *Front. Oncol.* 4:111. doi: 10.3389/fonc.2014.00111
- Khan, N. M., and Haqqi, T. M. (2018). Epigenetics in osteoarthritis: potential of HDAC inhibitors as therapeutics. *Pharmacol. Res.* 128, 73–79. doi: 10.1016/j.phrs.2017.08.007
- Kozhemyakina, E., Cohen, T., Yao, T. P., and Lassar, A. B. (2009). Parathyroid hormone-related peptide represses chondrocyte hypertrophy through a protein

- phosphatase 2A/histone deacetylase 4/MEF2 pathway. *Mol. Cell. Biol.* 29, 5751–5762. doi: 10.1128/MCB.00415-09
- Kroesen, M., Gielen, P., Brok, I. C., Armandari, I., Hoogerbrugge, P. M., and Adema, G. J. (2014). HDAC inhibitors and immunotherapy; a double edged sword? *Oncotarget* 5, 6558–6572. doi: 10.18632/oncotarget.2289
- Kuyinu, E. L., Narayanan, G., Nair, L. S., and Laurencin, C. T. (2016). Animal models of osteoarthritis: classification, update, and measurement of outcomes. *J. Orthop. Surg. Res.* 11:19. doi: 10.1186/s13018-016-0346-5
- Laufer, B. E., Mintzer, R., Fong, R., Mukund, S., Tam, C., Zilberleyb, I., et al. (2013). Histone deacetylase (HDAC) inhibitor kinetic rate constants correlate with cellular histone acetylation but not transcription and cell viability. *J. Biol. Chem.* 288, 26926–26943. doi: 10.1074/jbc.M113.490706
- Leus, N. G., Zwiderman, M. R., and Dekker, F. J. (2016). Histone deacetylase 3 (HDAC 3) as emerging drug target in NF-kappaB-mediated inflammation. *Curr. Opin. Chem. Biol.* 33, 160–168. doi: 10.1016/j.cbpa.2016.06.019
- Litwic, A., Edwards, M. H., Dennison, E. M., and Cooper, C. (2013). Epidemiology and burden of osteoarthritis. *Br. Med. Bull.* 105, 185–199. doi: 10.1093/bmb/ldo038
- Liu, C. J., Prazak, L., Fajardo, M., Yu, S., Tyagi, N., and Di Cesare, P. E. (2004). Leukemia/lymphoma-related factor, a POZ domain-containing transcriptional repressor, interacts with histone deacetylase-1 and inhibits cartilage oligomeric matrix protein gene expression and chondrogenesis. *J. Biol. Chem.* 279, 47081–47091. doi: 10.1074/jbc.M405288200
- Liu, Q., Wang, S., Lin, J., and Zhang, Y. (2018). The burden for knee osteoarthritis among Chinese elderly: estimates from a nationally representative study. *Osteoarthritis Cartilage* 26, 1636–1642. doi: 10.1016/j.joca.2018.07.019
- Lyu, X., Hu, M., Peng, J., Zhang, X., and Sanders, Y. Y. (2019). HDAC inhibitors as antifibrotic drugs in cardiac and pulmonary fibrosis. *Ther. Adv. Chronic Dis.* 10:2040622319862697. doi: 10.1177/2040622319862697
- Makki, M. S., and Haqqi, T. M. (2016). Histone deacetylase inhibitor vorinostat (SAHA) suppresses IL-1beta-induced matrix metalloproteinase-13 expression by inhibiting IL-6 in osteoarthritis chondrocyte. *Am. J. Pathol.* 186, 2701–2708. doi: 10.1016/j.ajpath.2016.06.010
- Makki, M. S., and Haqqi, T. M. (2017). Histone deacetylase inhibitor vorinostat (SAHA, MK0683) perturb miR-9-MCPIP1 axis to block IL-1beta-induced IL-6 expression in human OA chondrocytes. *Connect. Tissue Res.* 58, 64–75. doi: 10.1080/03008207.2016.1211113
- Malemud, C. J. (2017). Negative regulators of JAK/STAT signaling in rheumatoid arthritis and osteoarthritis. *Int. J. Mol. Sci.* 18:484. doi: 10.3390/ijms18030484
- Mao, G., Hu, S., Zhang, Z., Wu, P., Zhao, X., Lin, R., et al. (2018). Exosomal miR-95-5p regulates chondrogenesis and cartilage degradation via histone deacetylase 2/8. *J. Cell. Mol. Med.* 22, 5354–5366. doi: 10.1111/jcmm.13808
- Mao, G., Zhang, Z., Huang, Z., Chen, W., Huang, G., Meng, F., et al. (2017). MicroRNA-92a-3p regulates the expression of cartilage-specific genes by directly targeting histone deacetylase 2 in chondrogenesis and degradation. *Osteoarthritis Cartilage* 25, 521–532. doi: 10.1016/j.joca.2016.11.006
- Mendivil, A. A., Micha, J. P., Brown, J. V. III, Rettenmaier, M. A., Abaid, L. N., Lopez, K. L., et al. (2013). Increased incidence of severe gastrointestinal events with first-line paclitaxel, carboplatin, and vorinostat chemotherapy for advanced-stage epithelial ovarian, primary peritoneal, and fallopian tube cancer. *Int. J. Gynecol. Cancer* 23, 533–539. doi: 10.1097/IGC.0b013e31828566f1
- Meng, F., Li, Z., Zhang, Z., Yang, Z., Kang, Y., Zhao, X., et al. (2018). MicroRNA-193b-3p regulates chondrogenesis and chondrocyte metabolism by targeting HDAC3. *Theranostics* 8, 2862–2883. doi: 10.7150/thno.23547
- Moon, S. M., Lee, S. A., Han, S. H., Park, B. R., Choi, M. S., Kim, J. S., et al. (2018). Aqueous extract of *Codium fragile* alleviates osteoarthritis through the MAPK/NF-kappaB pathways in IL-1beta-induced rat primary chondrocytes and a rat osteoarthritis model. *Biomed. Pharmacother.* 97, 264–270. doi: 10.1016/j.biopha.2017.10.130
- Nasu, Y., Nishida, K., Miyazawa, S., Komiyama, T., Kadota, Y., Abe, N., et al. (2008). Trichostatin A, a histone deacetylase inhibitor, suppresses synovial inflammation and subsequent cartilage destruction in a collagen antibody-induced arthritis mouse model. *Osteoarthritis Cartilage* 16, 723–732. doi: 10.1016/j.joca.2007.10.014
- Neogi, T. (2013). The epidemiology and impact of pain in osteoarthritis. *Osteoarthritis Cartilage* 21, 1145–1153. doi: 10.1016/j.joca.2013.03.018
- Nham, G. T. H., Zhang, X., Asou, Y., and Shinomura, T. (2019). Expression of type II collagen and aggrecan genes is regulated through distinct epigenetic modifications of their multiple enhancer elements. *Gene* 704, 134–141. doi: 10.1016/j.gene.2019.04.034
- Ooi, J. Y., Tuano, N. K., Rafehi, H., Gao, X. M., Ziemann, M., Du, X. J., et al. (2015). HDAC inhibition attenuates cardiac hypertrophy by acetylation and deacetylation of target genes. *Epigenetics* 10, 418–430. doi: 10.1080/15592294.2015.1024406
- Pirozzi, C., Francisco, V., Guida, F. D., Gomez, R., Lago, F., Pino, J., et al. (2018). Butyrate modulates inflammation in chondrocytes via GPR43 receptor. *Cell. Physiol. Biochem.* 51, 228–243. doi: 10.1159/000495203
- Platta, C. S., Greenblatt, D. Y., Kunnimalaiyaan, M., and Chen, H. (2008). Valproic acid induces Notch1 signaling in small cell lung cancer cells. *J. Surg. Res.* 148, 31–37. doi: 10.1016/j.jss.2008.03.008
- Queirolo, V., Galli, D., Masselli, E., Borzi, R. M., Martini, S., Vitale, F., et al. (2016). PKCepsilon is a regulator of hypertrophic differentiation of chondrocytes in osteoarthritis. *Osteoarthritis Cartilage* 24, 1451–1460. doi: 10.1016/j.joca.2016.04.003
- Rigogliou, S., and Papavassiliou, A. G. (2013). The NF-kappaB signalling pathway in osteoarthritis. *Int. J. Biochem. Cell Biol.* 45, 2580–2584. doi: 10.1016/j.biocel.2013.08.018
- Saito, T., Nishida, K., Furumatsu, T., Yoshida, A., Ozawa, M., and Ozaki, T. (2013). Histone deacetylase inhibitors suppress mechanical stress-induced expression of RUNX-2 and ADAMTS-5 through the inhibition of the MAPK signaling pathway in cultured human chondrocytes. *Osteoarthritis Cartilage* 21, 165–174. doi: 10.1016/j.joca.2012.09.003
- Sarzi-Putini, P., Cimmino, M. A., Scarpa, R., Caporali, R., Parazzini, F., Zaninelli, A., et al. (2005). Osteoarthritis: an overview of the disease and its treatment strategies. *Semin. Arthritis Rheum.* 35(1 Suppl. 1), 1–10. doi: 10.1016/j.semarthrit.2005.01.013
- Shen, J., and Chen, D. (2014). Recent progress in osteoarthritis research. *J. Am. Acad. Orthop. Surg.* 22, 467–468. doi: 10.5435/JAAOS-22-07-467
- Si, H. B., Zeng, Y., Liu, S. Y., Zhou, Z. K., Chen, Y. N., Cheng, J. Q., et al. (2017). Intra-articular injection of microRNA-140 (miRNA-140) alleviates osteoarthritis (OA) progression by modulating extracellular matrix (ECM) homeostasis in rats. *Osteoarthritis Cartilage* 25, 1698–1707. doi: 10.1016/j.joca.2017.06.002
- Sondag, G. R., and Haqqi, T. M. (2016). The role of MicroRNAs and their targets in osteoarthritis. *Curr. Rheumatol. Rep.* 18:56. doi: 10.1007/s11926-016-0604-x
- Song, J., Jin, E. H., Kim, D., Kim, K. Y., Chun, C. H., and Jin, E. J. (2015). MicroRNA-222 regulates MMP-13 via targeting HDAC-4 during osteoarthritis pathogenesis. *BBA Clin.* 3, 79–89. doi: 10.1016/j.bbacli.2014.11.009
- Spange, S., Wagner, T., Heinzel, T., and Kramer, O. H. (2009). Acetylation of non-histone proteins modulates cellular signalling at multiple levels. *Int. J. Biochem. Cell Biol.* 41, 185–198. doi: 10.1016/j.biocel.2008.08.027
- Thomas, A. C., Hubbard-Turner, T., Wikstrom, E. A., and Palmieri-Smith, R. M. (2017). Epidemiology of posttraumatic osteoarthritis. *J. Athl. Train.* 52, 491–496. doi: 10.4085/1062-6050-51.5.08
- Thompson, C. L., Chapple, J. P., and Knight, M. M. (2014). Primary cilia disassembly down-regulates mechanosensitive hedgehog signalling: a feedback mechanism controlling ADAMTS-5 expression in chondrocytes. *Osteoarthritis Cartilage* 22, 490–498. doi: 10.1016/j.joca.2013.12.016
- Toh, W. S., Lai, R. C., Hui, J. H. P., and Lim, S. K. (2017). MSC exosome as a cell-free MSC therapy for cartilage regeneration: implications for osteoarthritis treatment. *Semin. Cell Dev. Biol.* 67, 56–64. doi: 10.1016/j.semcdb.2016.11.008
- Wang, H., Zhang, H., Sun, Q., Yang, J., Zeng, C., Ding, C., et al. (2018a). Chondrocyte mTORC1 activation stimulates miR-483-5p via HDAC4 in osteoarthritis progression. *J. Cell. Physiol.* 234, 2730–2740. doi: 10.1002/jcp.27088
- Wang, J. H., Shih, K. S., Wu, Y. W., Wang, A. W., and Yang, C. R. (2013). Histone deacetylase inhibitors increase microRNA-146a expression and enhance negative regulation of interleukin-1beta signaling in osteoarthritis fibroblast-like synoviocytes. *Osteoarthritis Cartilage* 21, 1987–1996. doi: 10.1016/j.joca.2013.09.008
- Wang, P., Mao, Z., Pan, Q., Lu, R., Huang, X., Shang, X., et al. (2018b). Histone deacetylase-4 and histone deacetylase-8 regulate interleukin-1beta-induced cartilage catabolic degradation through MAPK/JNK and ERK pathways. *Int. J. Mol. Med.* 41, 2117–2127. doi: 10.3892/ijmm.2018.3410

- Wang, X., Song, Y., Jacobi, J. L., and Tuan, R. S. (2009). Inhibition of histone deacetylases antagonized FGF2 and IL-1 β effects on MMP expression in human articular chondrocytes. *Growth Factors* 27, 40–49. doi: 10.1080/08977190802625179
- Wuelling, M., Pasdziernik, M., Moll, C. N., Thiesen, A. M., Schneider, S., Johannes, C., et al. (2013). The multi zinc-finger protein Trps1 acts as a regulator of histone deacetylation during mitosis. *Cell Cycle* 12, 2219–2232. doi: 10.4161/cc.25267
- Yang, C. R., Shih, K. S., Liou, J. P., Wu, Y. W., Hsieh, I. N., Lee, H. Y., et al. (2014). Denbinobin upregulates miR-146a expression and attenuates IL-1 β -induced upregulation of ICAM-1 and VCAM-1 expressions in osteoarthritis fibroblast-like synoviocytes. *J. Mol. Med.* 92, 1147–1158. doi: 10.1007/s00109-014-1192-8
- Yang, X., Guan, Y., Tian, S., Wang, Y., Sun, K., and Chen, Q. (2016). Mechanical and IL-1 β responsive miR-365 contributes to osteoarthritis development by targeting histone deacetylase 4. *Int. J. Mol. Sci.* 17:436. doi: 10.3390/ijms17040436
- Yoon, S., and Eom, G. H. (2016). HDAC and HDAC inhibitor: from cancer to cardiovascular diseases. *Chonnam Med. J.* 52, 1–11. doi: 10.4068/cmj.2016.52.1.1
- Zayed, N., El Mansouri, F. E., Chabane, N., Kapoor, M., Martel-Pelletier, J., Benderdour, M., et al. (2011). Valproic acid suppresses interleukin-1 α -induced microsomal prostaglandin E2 synthase-1 expression in chondrocytes through upregulation of NAB1. *J. Rheumatol.* 38, 492–502. doi: 10.3899/jrheum.100907
- Zhang, C., Zhang, Z., Chang, Z., Mao, G., Hu, S., Zeng, A., et al. (2019a). miR-193b-5p regulates chondrocytes metabolism by directly targeting histone deacetylase 7 in interleukin-1 β -induced osteoarthritis. *J. Cell. Biochem.* 120, 12775–12784. doi: 10.1002/jcb.28545
- Zhang, H., Ji, L., Yang, Y., Wei, Y., Zhang, X., Gang, Y., et al. (2019b). The therapeutic effects of treadmill exercise on osteoarthritis in rats by inhibiting the HDAC3/NF-KappaB pathway *in vivo* and *in vitro*. *Front. Physiol.* 10:1060. doi: 10.3389/fphys.2019.01060
- Zheng, G., Zhan, Y., Tang, Q., Chen, T., Zheng, F., Wang, H., et al. (2018). Monascin inhibits IL-1 β induced catabolism in mouse chondrocytes and ameliorates murine osteoarthritis. *Food Funct.* 9, 1454–1464. doi: 10.1039/c7fo01892d
- Zhong, H. M., Ding, Q. H., Chen, W. P., and Luo, R. B. (2013). Vorinostat, a HDAC inhibitor, showed anti-osteoarthritic activities through inhibition of iNOS and MMP expression, p38 and ERK phosphorylation and blocking NF-kappaB nuclear translocation. *Int. Immunopharmacol.* 17, 329–335. doi: 10.1016/j.intimp.2013.06.027

Conflict of Interest: The authors declare that the research was conducted in the absence of any commercial or financial relationships that could be construed as a potential conflict of interest.

Copyright © 2020 Zhang, Ji, Yang, Zhang, Gang and Bai. This is an open-access article distributed under the terms of the Creative Commons Attribution License (CC BY). The use, distribution or reproduction in other forums is permitted, provided the original author(s) and the copyright owner(s) are credited and that the original publication in this journal is cited, in accordance with accepted academic practice. No use, distribution or reproduction is permitted which does not comply with these terms.



The Histone Methyltransferase SETDB1 Modulates Survival of Spermatogonial Stem/Progenitor Cells Through NADPH Oxidase

Xueliang Li, Xiaoxu Chen, Yingdong Liu, Pengfei Zhang, Yi Zheng* and Wenxian Zeng*

Key Laboratory of Animal Genetics, Breeding and Reproduction of Shaanxi Province, College of Animal Science and Technology, Northwest A&F University, Yangling, China

OPEN ACCESS

Edited by:

Huiming Zhang,
Shanghai Institutes for Biological
Sciences (CAS), China

Reviewed by:

Danny Chi Yeu Leung,
Hong Kong University of Science
and Technology, Hong Kong
Matthew Wong,
Children's Cancer Institute Australia,
Australia

*Correspondence:

Yi Zheng
y.zheng@nwfau.edu.cn
Wenxian Zeng
zengwenxian2015@126.com

Specialty section:

This article was submitted to
Epigenomics and Epigenetics,
a section of the journal
Frontiers in Genetics

Received: 18 January 2020

Accepted: 05 August 2020

Published: 02 October 2020

Citation:

Li X, Chen X, Liu Y, Zhang P,
Zheng Y and Zeng W (2020) The
Histone Methyltransferase SETDB1
Modulates Survival of Spermatogonial
Stem/Progenitor Cells Through
NADPH Oxidase.
Front. Genet. 11:997.
doi: 10.3389/fgene.2020.00997

SETDB1, a histone H3 lysine 9 (H3K9) methyltransferase, is crucial in meiosis and embryo development. This study aimed to investigate whether SETDB1 was associated with spermatogonial stem cells (SSC) homeostasis. We found that knockdown of *Setdb1* impaired cell proliferation, led to an increase in reactive oxygen species (ROS) level through NADPH oxidase, and *Setdb1* deficiency activated ROS downstream signaling pathways, including JNK and p38 MAPK, which possibly contributed to SSC apoptosis. Melatonin scavenged ROS and rescued the phenotype of *Setdb1* KD. In addition, we demonstrated that SETDB1 regulated NADPH oxidase 4 (*Nox4*) and *E2F1*. Therefore, this study uncovers the new roles of SETDB1 in mediating intracellular ROS homeostasis for the survival of SSC.

Keywords: SETDB1, H3K9me3, NOX4, ROS, spermatogonial stem cell

INTRODUCTION

Male fertility depends on spermatogenesis, by which the haploid spermatozoa generate in the testes. This process starts with the mitosis of the spermatogonial stem cells (SSCs), followed by meiosis of spermatocytes. Finally, the haploid spermatids transform into spermatozoa (Kanatsu-Shinohara and Shinohara, 2013). This highly organized process of spermatogenesis requires timely coordinated gene expression that is regulated at the transcriptional and post-transcription levels (McSwiggin and O'Doherty, 2018). Histone modification has been implicated in the regulation of gene expression.

Histone H3 lysine 9 (H3K9) can be methylated by the methyltransferase SETDB1 (Mozzetta et al., 2015). Notably, the global level of H3K9me3 and SETDB1 gradually increases during development of the testes (An et al., 2014). Loss of *Setdb1* resulted in a reduced number of PGCs and postnatal hypogonadism (Liu et al., 2015). Moreover, depletion of *Setdb1* at postnatal day 7 caused germ cell apoptosis at the pachytene stage and defects in XY body formation (Hirota et al., 2018). *Setdb1* depletion induced SSC apoptosis through upregulating apoptotic inducers and downregulating apoptotic suppressors, and upregulating cytochrome *c* oxidase subunit IV isoform 2 (*Cox4i2*) through decreasing H3K9me3 (An et al., 2014). The up-regulation of COX4i2 is associated with elevated mitochondria-produced reactive oxygen species (ROS) (Singh et al., 2009).

The active NADPH oxidase (NOX) generates superoxide, which spontaneously recombines with other molecules to produce reactive free radicals (Katsuyama et al., 2012; Lambeth and Neish, 2014). Under physiological conditions, the intracellular ROS are thought to act as a second

messenger in cell signaling (Bigarella et al., 2014; Lambeth and Neish, 2014; Wang et al., 2018). Recent studies found that ROS generated by NOX1 and NOX3 was essential for SSC self-renewal (Morimoto et al., 2013, 2015). Ablation of *Nox1* severely compromises SSC self-renewal, and *Nox3*-depletion causes apoptosis and impairs SSC proliferation. However, the accumulated ROS is toxic to the cells. Enhancing the expression of NOX4 in cardiac myocytes induces apoptosis and mitochondrial dysfunction (Ago et al., 2010). Excessive ROS causes apoptosis through the p38 MAPK-p16 pathway in hematopoietic stem cells (Ito et al., 2006). High levels of ROS could also induce oxidative stress and activation of FOXO4 that is a regulator of cell cycle, cell death, and cell metabolism (Essers et al., 2004; Urbich et al., 2005; Eijkelenboom and Burgering, 2013). Importantly, oxidative stress is associated with male infertility (Bui et al., 2018). Thus, modest levels of ROS benefits cell proliferation, while accumulated ROS impairs cells. However, the function of SETDB1 in intracellular ROS homeostasis remains elusive. In this study, we revealed that *Setdb1* deficiency caused an increased ROS level via the NOX pathway and induced changes in the cell cycle through the JNK-FOXO4 pathway.

RESULTS

Knockdown of *Setdb1* Impairs Proliferation and Induces Apoptosis in Spermatogonial Stem Cells

Using the siRNA oligonucleotides of *Setdb1*, we efficiently downregulated *Setdb1* mRNA expression by approximately 70% (Supplementary Figure S1A). Western blotting analysis confirmed a significant decrease of SETDB1 at protein level after 48 h transfection (Supplementary Figures S1B,C). As shown in Figures 1A,B, the proliferation rate reduced in *Setdb1*-KD cells compared with the control group (Figures 1A,B). Flow cytometry analysis further confirmed that higher ratio of S phase cells in *Setdb1* KD than that of the control at 36 h post transfection (Figures 1C,D). Meanwhile, *Setdb1* depletion induced apoptosis at 48 h post transfection (Supplementary Figures S1D,E). Similar to the previous report, *Setdb1* KD caused an increase of double-strand DNA breaks (Figures 1E,F) (Supplementary Figures S1F,G) (Kim et al., 2016). Interestingly, overexpression of *Setdb1* had no effect on cell survival (Supplementary Figures S1H,J). These observations confirm that SETDB1 is required for the maintenance of SSCs.

Suppression of *Setdb1* Induces ROS Accumulation and NOX Expression

To clarify the expression of NOX4 in male germ cells, we carried out double-immunohistochemistry staining of testes tissue from 7-day-old and adult mice. NOX4 was co-localized with THY1 (SSC/undifferentiated spermatogonia marker) (Figure 2A). Intracellular ROS levels were detected by DCFH-DA and DHE staining. *Setdb1* KD increased the level of total intracellular ROS (Figures 2B,E; Supplementary

Figure S2). To test the potential roles of SETDB1 in mediating intracellular ROS homeostasis through NADPH oxidase, we detected NOX expression. *Setdb1* KD caused an increase of expression of *Nox3*, *Nox4*, and *p22phox* (NOX4 regulatory subunits) (Figure 2F). Western blot assay showed that the level of total NOX4 and p22phox were upregulated (Figure 2G,H). These data suggest that *Setdb1* KD resulted in ROS accumulation possibly by NOX expression in SSCs.

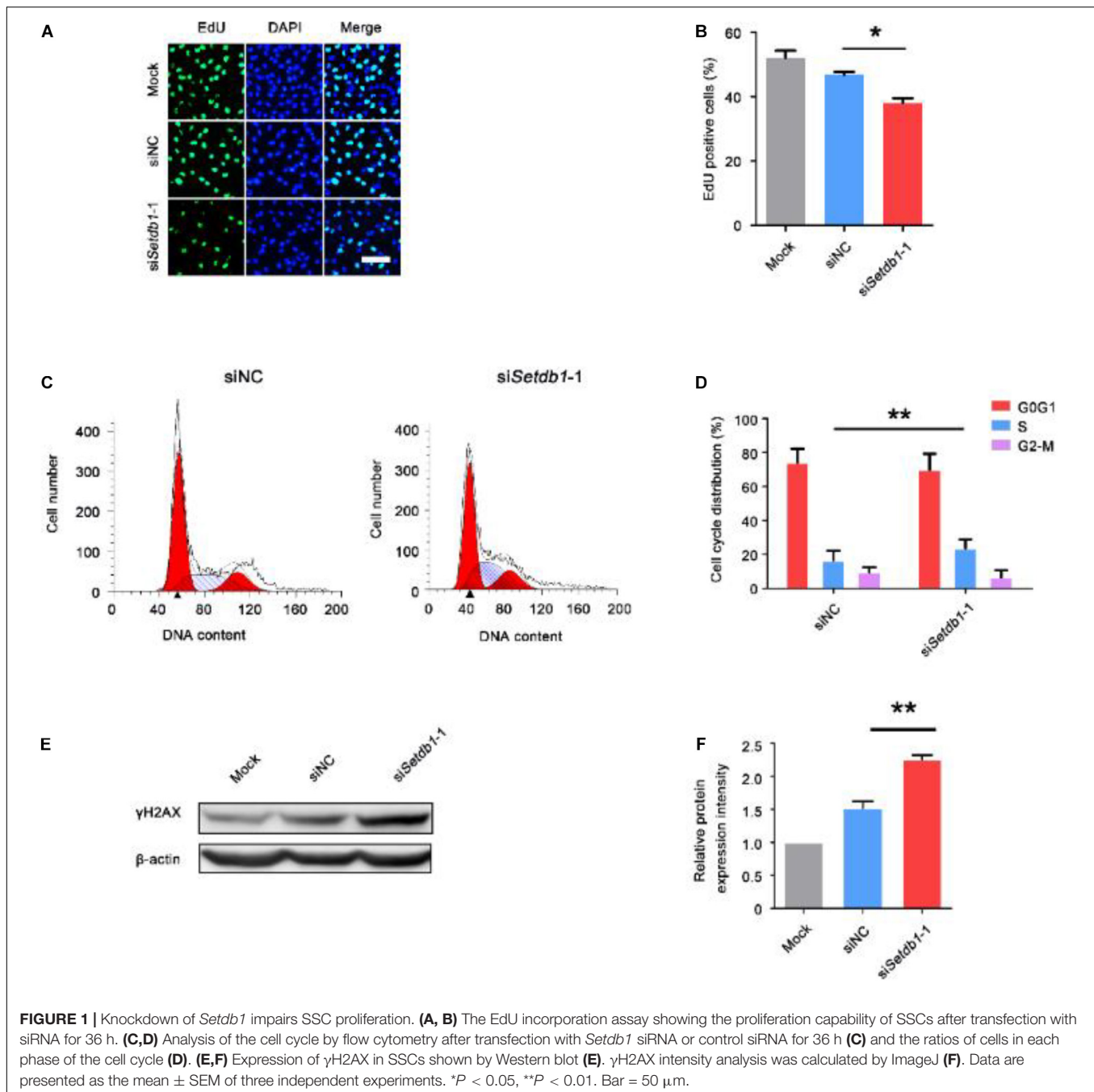
SETDB1 Activates *Nox4* Expression via Regulating E2F Transcription Factor 1 (E2F1)

Western blotting and RT-qPCR assay showed that knockdown of *Setdb1* led to an increase of *E2F1* expression at both mRNA and protein levels (Figures 3A,C). In order to determine whether E2F1 regulates the activity of *Nox4* promoter, the vector of luciferase containing *Nox4* promoter were co-transfected with *E2F1* overexpression vector or empty vector control. As shown in Figure 3D, luciferase reporter assay showed that *E2F1* overexpression significantly increased the luciferase activity compared with that in the empty control group. Hence, E2F1 modulated the activity of *Nox4* promoter (Figure 3D). Since *Setdb1* KD caused the upregulation of E2F1 and NOX4, we test whether *E2F1* and *Nox4* were repressed by SETDB1-mediated histone modification at their promoter region through H3K9me3 (Supplementary Figure S3). Chromatin immunoprecipitation (ChIP) followed by a quantitative real-time PCR (ChIP-qPCR) assay was performed to exam the tentative binding sites of SETDB1 in the promoters of *E2F1* and *Nox4* (Figures 3E,H). We found that the enrichment of SETDB1 and H3K9me3 in the *E2F1* promoter region were only 0.3–1.3% (Figures 3F,G) at these loci. ChIP-qPCR analysis confirmed that there is little enrichment of SETDB1 and H3K9me3 in the *Nox4* promoter region (Figure 3I,J), suggesting that the regulation of SETDB1 on *Nox4* expression is independent of H3K9me3.

SETDB1 Regulates Intracellular ROS Homeostasis Through NOX4

To clarify whether *Setdb1*-KD induces apoptosis via the ROS pathway, we pretreated the cells with melatonin, a ROS scavenger, before *Setdb1* knockdown (Tan et al., 2002; Schaefer et al., 2019). As shown in Figures 4A,B, addition of melatonin alleviated the apoptosis induced by *Setdb1* KD (Figures 4A,B), confirming that *Setdb1* KD induces apoptosis through the ROS pathway. We found that addition of melatonin reduced the expressions of *Nox2* and *Nox4* in SSCs, which are similar to previously published results (Supplementary Figure S4; Najafi et al., 2019). These results indicate that abolition of ROS partially rescued the death phenotype.

To test whether the ROS level is upregulated by NOX4, we co-transfected specific siRNA against *Setdb1* and *Nox4* and analyzed the knockdown efficiency (Supplementary Figure S5). As shown in Figures 4C,D, ROS were decreased in cells co-transfected with both siRNAs against *Setdb1* and *Nox4*

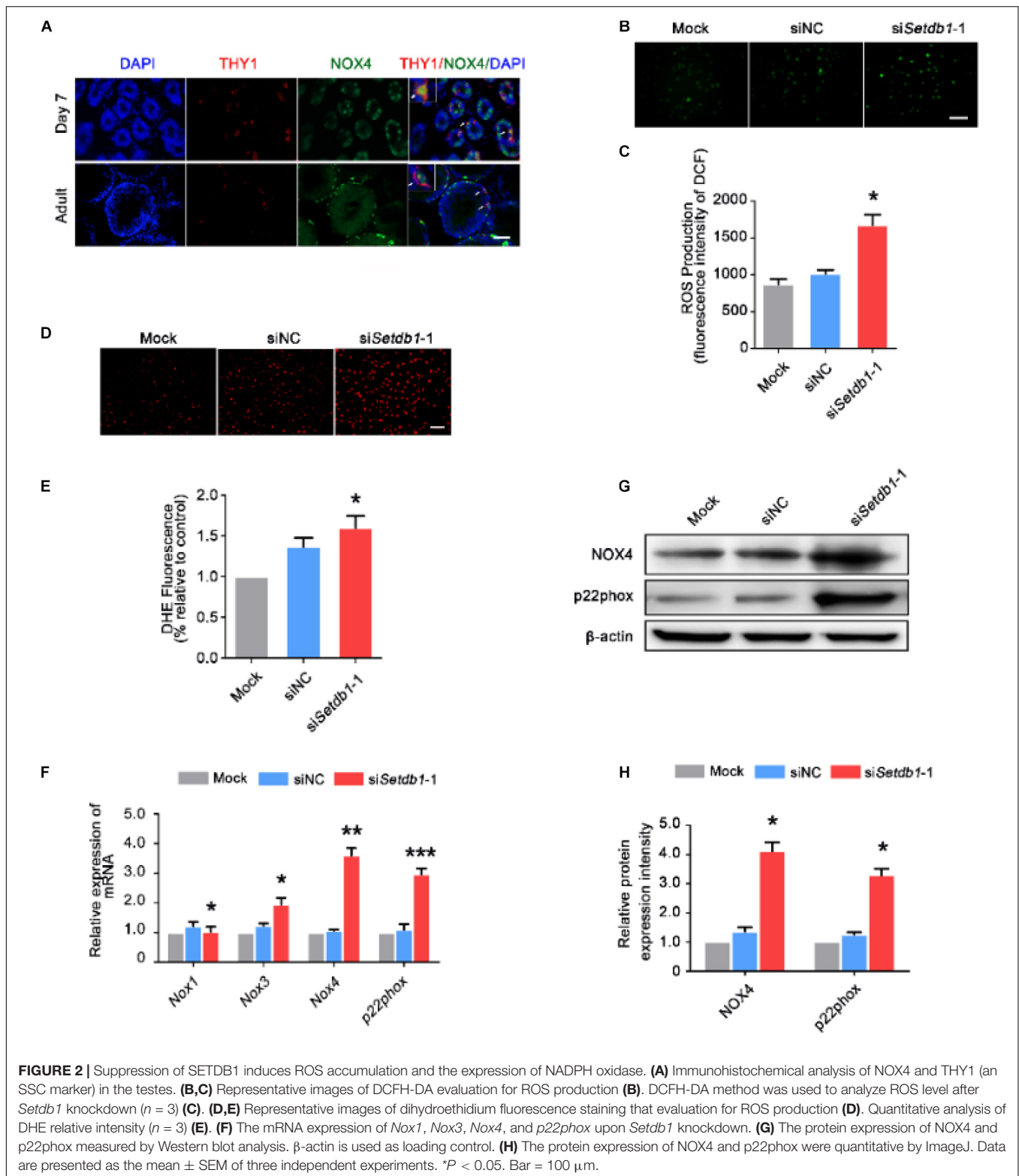


compared with the group that was solely transfected with the *Setdb1* siRNA (Figures 4C,D). To address whether *Setdb1* KD led to mitochondrial dysfunction by upregulating NOX4, both siRNAs of *Setdb1* and *Nox4* were introduced to the cells simultaneously. JC-1 assay showed that mitochondrial dysfunction was reduced in cells co-transfected with both siRNAs of *Setdb1* and *Nox4* compared with the group only transfected with the *Setdb1* siRNA (Figure 4E). Subsequently, we detected the role of NOX4 in apoptosis and cell proliferation. As shown in Figures 5A,B, *Nox4* KD could partly alleviate the phenotype induced by *Setdb1* KD (Figures 5A,B). In addition, TUNEL

positive cells were reduced in cells co-transfected with both *Setdb1* siRNA and *Nox4* siRNA compared with the group transfected with the *Setdb1* siRNA (Figures 5C,D). Based on these data, we conclude SETDB1 regulates intracellular ROS homeostasis through NOX4.

***Setdb1* Knockdown Activates p38/JNK-FOXO4 Pathway**

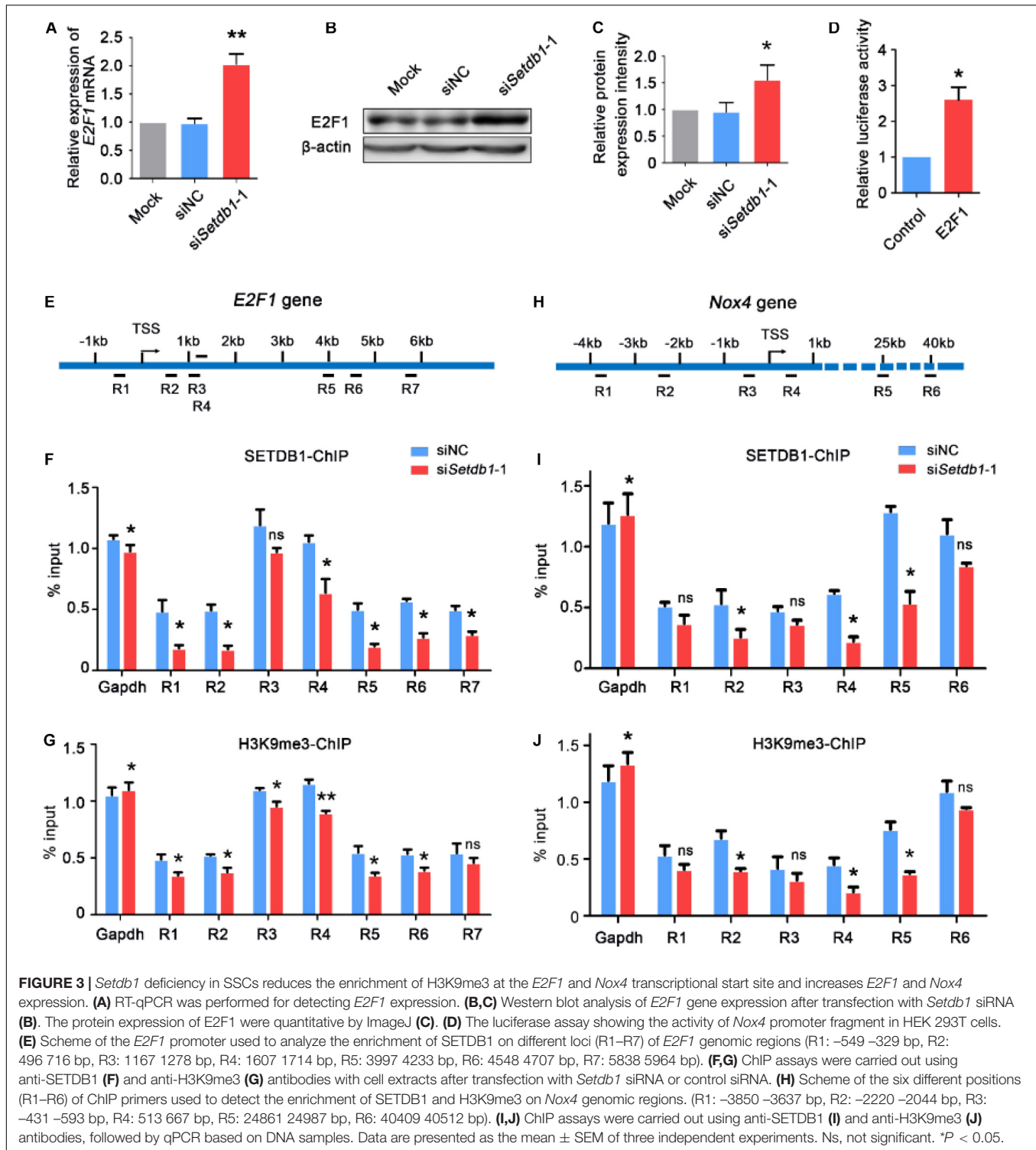
We examined whether SETDB1 mediated the phosphorylation of p38 MAPK and c-jun N-terminal kinase (JNK). We found that



Setdb1 KD led to the activation of p38 and JNK signaling in SSCs (Figures 6A,B).

We further investigated whether *Setdb1*-KD induced activation and translocation of FOXO4. The

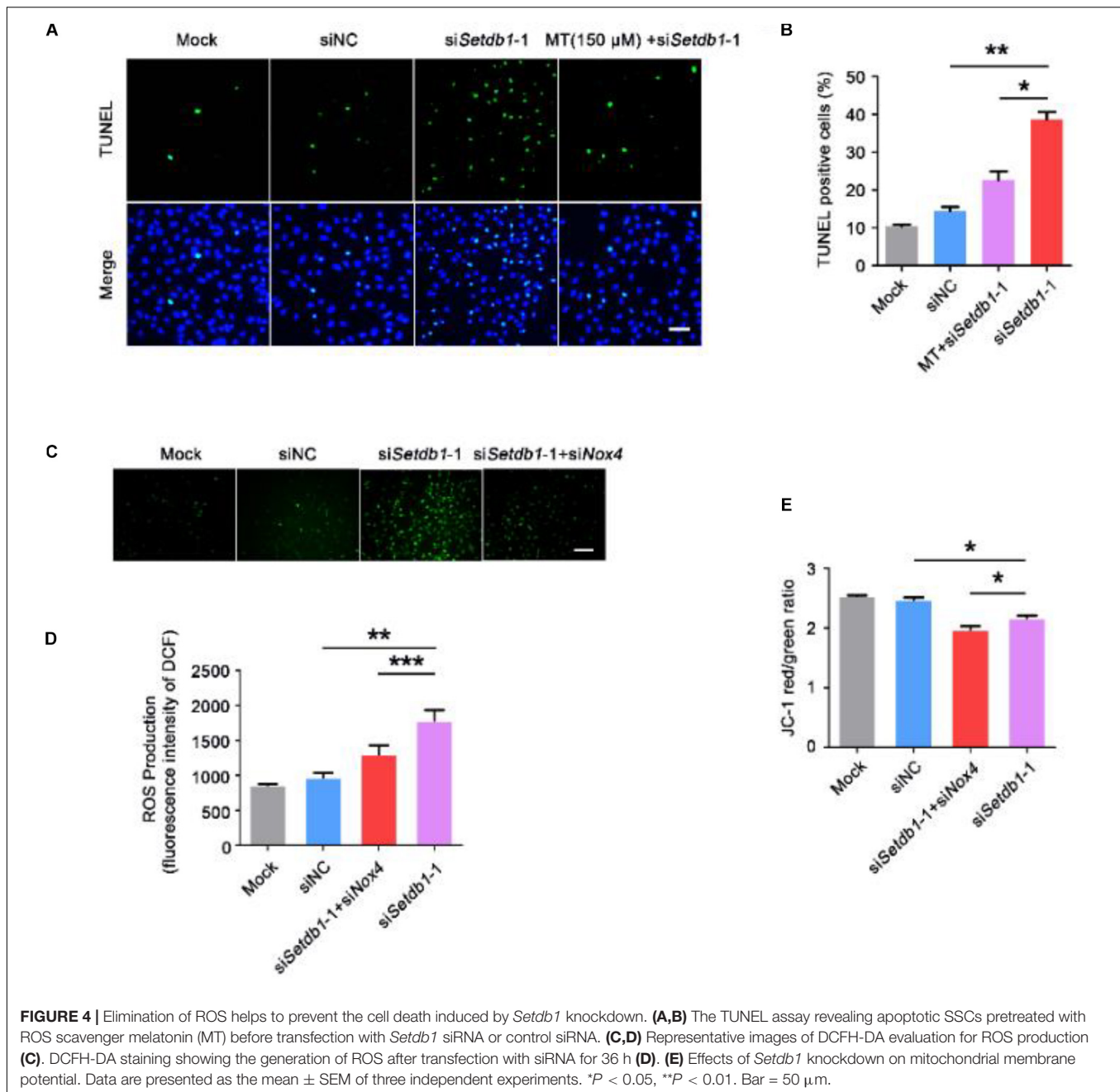
immunofluorescence assay showed *Setdb1* KD resulted in FOXO4 translocation (Figure 6C). To further confirm the nuclear translocation of FOXO4 after *Setdb1* KD, we extracted protein of the nucleus and cytoplasm. The western blot assay



confirmed that FOXO4 translocated from the cytoplasm to the nucleus (Figures 6D, E). However, the expression of FOXO4 almost did not change at 48 h after *Setdb1* KD (Figures 6F,G). *Setdb1* KD upregulated the expression of the target gene encoded Catalase (Figures 6H,I). These results suggest that *Setdb1* KD activates the p38/JNK-FOXO4 pathway.

DISCUSSION

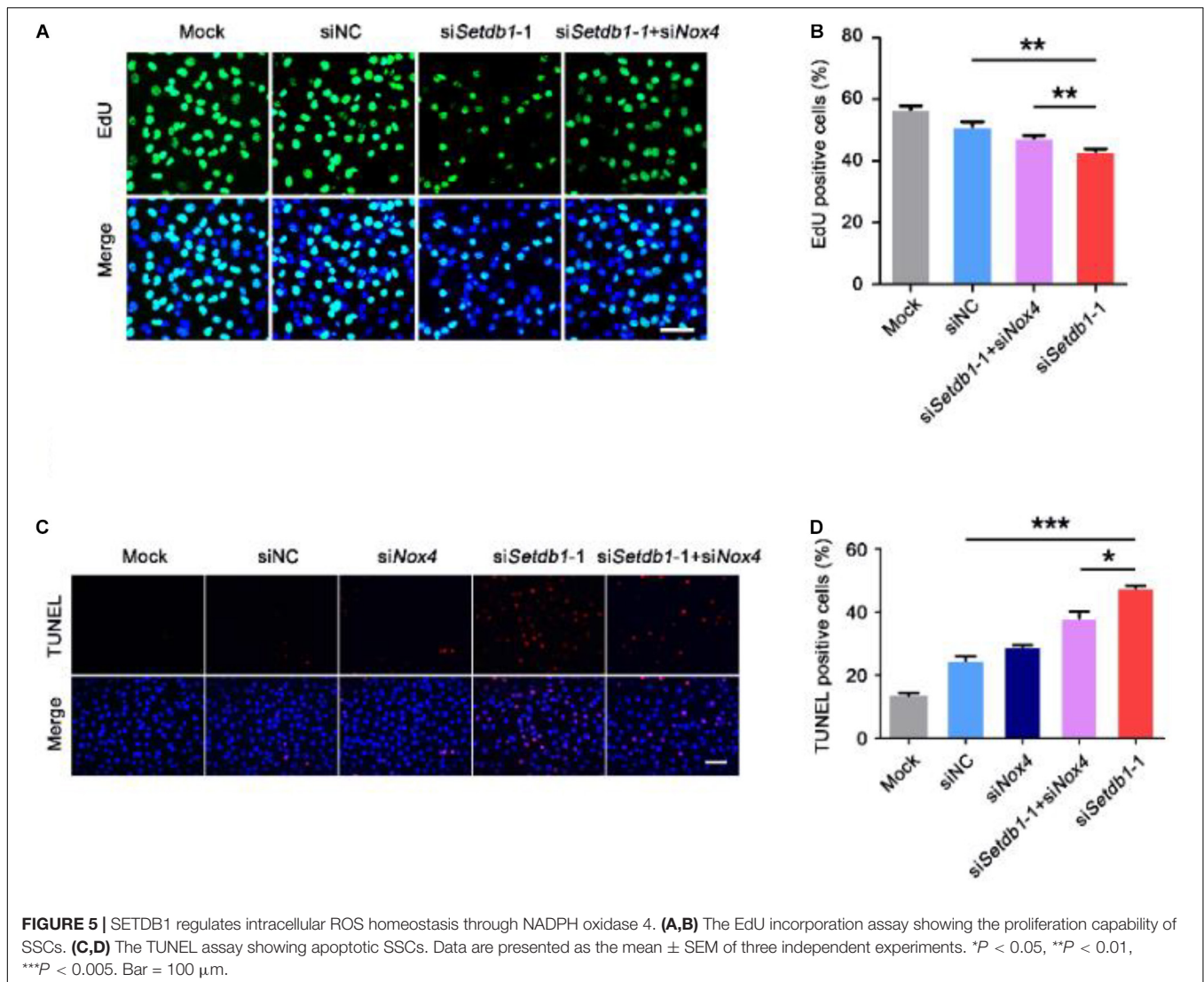
SETDB1 catalyzes H3K9me3, which is a repressive marker (Mozzetta et al., 2015). In the present study, we found that SETDB1 repressed expression of *Nox4* and *E2F1* and mediated ROS levels.



NOX consumes oxygen to generate O_2^- using NADPH as an electron donor, and the O_2^- subsequently forms H_2O_2 (Katsuyama et al., 2012; Bigarella et al., 2014). Previous studies have shown that ROS generated by NOX enhanced growth factor signaling and acts as anti-microbial molecules (Nathan and Cunningham-Bussell, 2013). Excessive ROS production induces cellular injury and lipid peroxidation (Su et al., 2019). In this study, we found that *Setdb1* KD induced accumulation of ROS and upregulation of *Nox3*, *Nox4*, *p22phox*, and *E2F1*. Importantly, melatonin alleviated the apoptosis in *Setdb1*-KD group. Co-transfecting with siRNAs of *Nox4* and *Setdb1* simultaneously resulted in the decrease of ROS and increase of

mitochondrial membrane potential compared with the *Setdb1* depleted cells. Furthermore, melatonin reduced the expression of *Nox2* and *Nox4*, which is consistent with the previous report (Najafi et al., 2019). Therefore, melatonin alleviated *Setdb1*-KD induced SSC apoptosis, probably by down-regulating *Nox2* and *Nox4*. The excess ROS was generated from NOX4 and was responsible for the apoptosis in *Setdb1*-KD cells. In this study, we also found that *Setdb1* KD led to increase of *Nox3*. Together, SETDB1 mediates ROS homeostasis and likely keeps ROS below a threshold level via NADPH oxidase.

It has been reported that ROS generated by NOX4 was associated with DNA damage (Weyemi et al., 2012), which

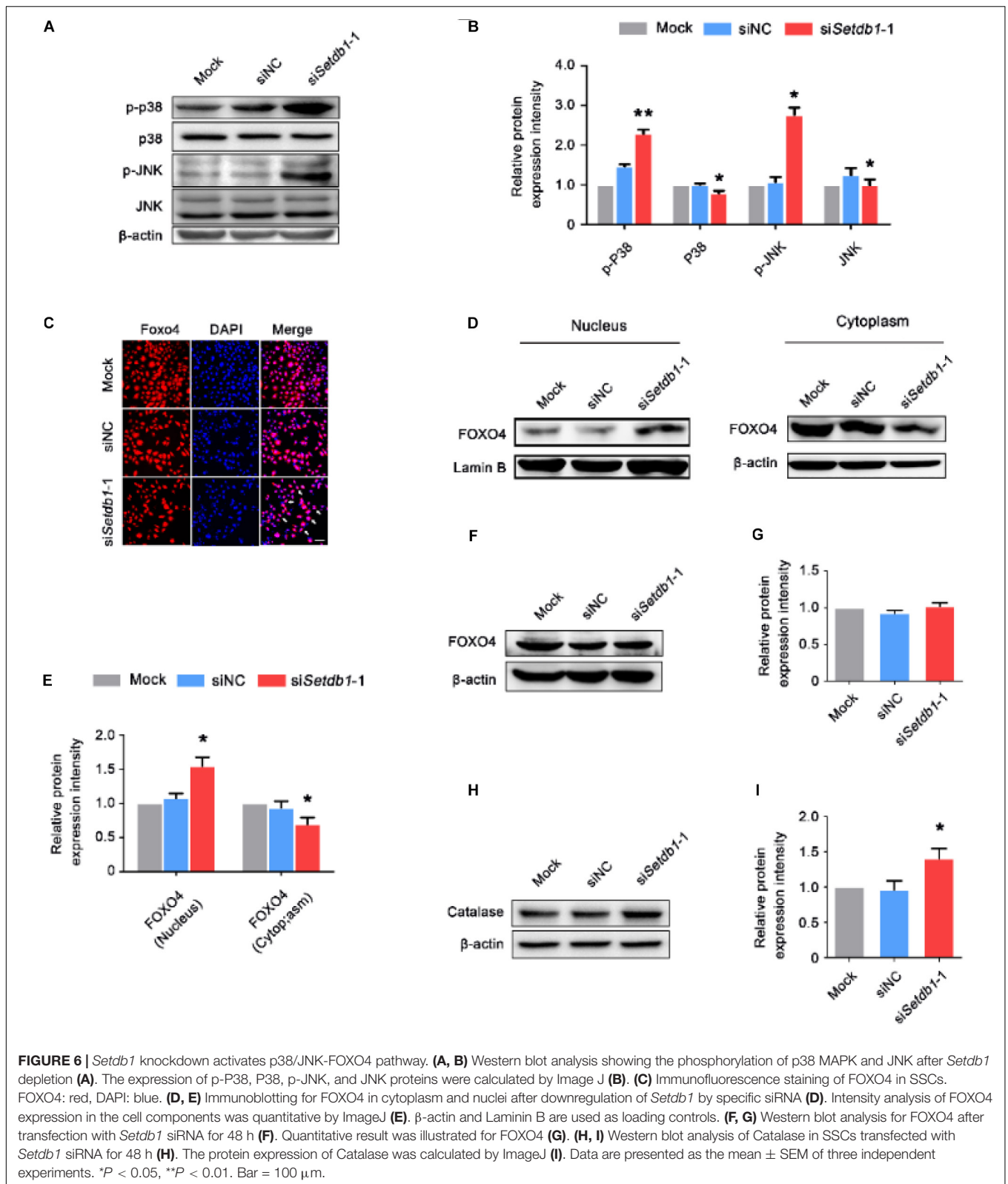


was consistent with the present findings on SSCs. Except for double-strand DNA breaks, ROS activates the signal-transducing molecules including JNK, p38, and FOXO4 (Ma et al., 2002; Essers et al., 2004; Hua et al., 2017; Zheng et al., 2017). In mammals, the FOXO family consists of four members (FOXO1, FOXO3, FOXO4, and FOXO6) (Eijkelenboom and Burgering, 2013). These FOXO transcription factors regulate multiple cellular pathways, including apoptosis, inflammation, proliferation, oxidative stress resistance, and aging (Henderson and Johnson, 2001; Lin et al., 2001; Tuteja and Kaestner, 2007a,b; Zanella et al., 2010; Genin et al., 2014; Webb and Brunet, 2014; Murtaza et al., 2017; Jiramongkol and Lam, 2020). Meanwhile, FOXO nuclear translocation triggers apoptosis by inducing the expression of death genes, such as the *FasL*, and thereby participates actively in the process of apoptosis (Brunet et al., 2004). In this study, knockdown of *Setdb1* activated the ROS-JNK signaling pathway and FOXO4 that was translocated into the nuclei, which led to an increase of expression of the *Catalase* gene (FOXO4 target gene) that

encodes an anti-oxidant enzyme (Nandi et al., 2019). Taken together, we propose that *Setdb1* KD activates ROS downstream signaling pathways, which partially contributes to the apoptotic phenotype in SSCs.

SETDB1 is involved in heterochromatin formation and transcription silencing via histone H3 methyltransferase activity (Zhu et al., 2020). In this study, we found that *Setdb1* KD led to the upregulation of *Nox4* and *E2F1*. ChIP-qPCR showed that 0.3–1.4% of input for SETDB1 and H3K9me3 at the loci of the *E2F1* and *Nox4* promoters, indicating that SETDB1 does not target *E2F1* and *Nox4* promoters. Recent studies revealed that *Setdb1* KD resulted in the activation of endogenous retroviruses (ERVs) and the long terminal repeat (LTR) and led to dysregulation expression of neighboring genes (Tan et al., 2012). Thus, SETDB1 may regulate the expression of *Nox4* and *E2F1* due to silencing of cis-regulatory elements or retrotransposons in SSCs.

NOX4 was involved in various physiological processes such as apoptosis and differentiation in various cell types (Pedrucci et al., 2004; McKallip et al., 2006; Carmona-Cuenca et al., 2008;



Caja et al., 2009). It was reported that SETDB1 was recruited to the *E2F1* promoter and co-operated with Alien complex to regulate the expression of *E2F1* (Hong et al., 2011). Meanwhile,

E2F1 positively regulates the transcription of *Nox4* in vascular smooth muscle cells (Zhang et al., 2008). In this study, the expression of E2F1 and NOX4 were elevated in *Setdb1*-KD group.

The expression of E2F1 was upregulated in *Setdb1*-KD cells, which in turn lead to upregulation of NOX4.

The role of SETDB1 has been explored extensively in the development of male germ lines (An et al., 2014; Liu et al., 2015, 2017; Hirota et al., 2018; Mochizuki et al., 2018). SETDB1 is recruited to repress ERVs transcription via H3K9me3 in primordial germ cells (Liu et al., 2015), and suppresses the expression of *Dppa2*, *Otx2*, and *Utf1* during PGC determination (Mochizuki et al., 2018). *Setdb1* knockout disrupts spermatogenesis and expression of meiosis-related genes (Hirota et al., 2018). Therefore, SETDB1 regulates different clusters of genes in the development of male germ cells. It would be interesting to further elucidate the mechanisms of recruitment in SETDB1 to different genes.

In conclusion, SETDB1 regulates the expression of *E2F1* and *Nox4*. *Setdb1* depletion causes the derepression of *E2F1* and upregulation of *Nox4*. On the other hand, NOX4 was upregulated by E2F1 dysregulation. Thus, NOX4 contributes to ROS generation and activates ROS downstream signaling pathways. Meanwhile, excessive amounts of ROS induces cell cycle arrest and apoptosis in SSCs. This study will provide a new perspective on SETDB1 function and understanding of male infertility.

MATERIALS AND METHODS

Cell Culture and Transfection

C18-4 cell line was obtained from Dr. Zuping He at Shanghai Jiao Tong University, China. The cell line was established from mouse type A spermatogonia from 6-day-old mice (Hofmann et al., 2005). C18-4 cells were maintained in Dulbecco modified Eagle medium (DMEM)/F12 (Hyclone, Logan, UT, United States) supplemented with 10% fetal bovine serum (BI, Israel), 100 U/ml penicillin and streptomycin (Gibco), 100 mM non-essential amino acids (Gibco), and 2 mM L-glutamine (Gibco) at 37°C and 5% CO₂. The 293T cell line was cultured in DMEM/Basic medium supplemented with 10% fetal bovine serum, 100 U/ml penicillin and streptomycin, 100 mM non-essential amino acids, and 2 mM L-glutamine at 37°C and 5% CO₂.

A pair of *Setdb1* small interfering RNAs (siRNAs), *Setdb1*-1 and *Setdb1*-2, were ordered from GenePharma (Shanghai, China). Sequences of mouse *Setdb1* siRNA were as follows: 5'-CCAACC UGUUUGUCCAGAAUGUGUU-3' (*Setdb1*-1), 5'-UCAAGUUUGGCAUCAUGAUGUAGC-3' (*Setdb1*-2), 5'-UU CUCCGAACGU GUCACGUTT-3' (Scramble). The sequence of mouse *Nox4* siRNA was as follows: 5'-GTAGGAGAC TGGACAGAAC-3'. The cells were transfected with siRNAs using Lipofectamine 2000 Transfection Reagent (Invitrogen) according to the manufacturer's instructions.

Reverse Transcription-Quantitative Polymerase Chain Reaction (RT-qPCR)

Total RNA was extracted using RNAiso Plus reagent (TaKaRa, Dalian, China). RT-qPCR was performed as described previously using the primers listed in **Supplementary Table S1** (Chen et al., 2017).

Western Blot

The cells were transfected with *Setdb1* siRNA for 48 h. Approximately 30 µg protein was separated by 8–12% SDS-PAGE and transferred to PVDF membranes (Millipore). The membranes were probed using the following primary antibodies: NOX4 (1:500; NB110-58849; Novus), beta-Actin (1:2000; CW0096; CWBIO), SETDB1 (1:1000; 11231-1-AP; Proteintech), E2F1 (1:500; sc-193; Santa Cruz Biotechnology), FOXO4 (1:500; sc-5221; Santa Cruz Biotechnology), Lamin B (1:500; sc-6217; Santa Cruz Biotechnology), JNK (1:500; sc-7345; Santa Cruz Biotechnology), p-JNK (1:400; WL01813; WanleiBio), γH2AX (1:1000; 2577; Cell signaling technology), p38 (1:500; sc-7972; Santa Cruz Biotechnology), and p-P38 (1:500; sc-17852-R; Santa Cruz Biotechnology). All were used as the manufacturer's recommendation. The secondary antibodies were horse radish peroxidase-linked anti-mouse, anti-rabbit, or anti-goat IgG for 2 h at room temperature. The membranes were visualized on a Bio-Rad Chemidoc XRS using a Western Bright ECL Kit (Bio-Rad, Berkeley, CA, United States).

ROS Measurement

Intracellular ROS was determined using the 2', 7'-dichlorofluorescein diacetate (DCFH-DA, Beyotime) and Dihydroethidium (DHE, Beyotime) according to the manufacturer's instructions. Cells were incubated with 10 µM 2', 7'-dichlorofluorescein diacetate or dihydroethidium at 37°C for 30 min. Subsequently, the fluorescence signals of the cells were observed using a multi-detection microplate reader. The excitation/emission of DCFH-DA is 488/525 nm, and the excitation/emission of DHE staining are 370/420 and 300/610 nm.

Cell Cycle Assay

The cell cycle analysis was performed with Flow cytometry. The cells were harvested at 36 h post transfection of *Setdb1* siRNA or control siRNA. After being fixed in 70% cold ethanol, the cells were incubated with RNase and finally stained with 4',6-diamidino-2-phenylindole (DAPI, Bioworld). DNA content was analyzed by Flow cytometry (BD FACSARIA™ III, United States). The data were analyzed with ModFit LT 5.0.

TUNEL Staining

Apoptotic cells were detected with TUNEL BrightGreen or BrightRed Apoptosis Detection Kit (Vazyme, Nanjing, China) according to the manufacturer's instructions. The cells were seeded on 96-well plates and transfected with siRNA. After washing with PBS, the cells were fixed in 4% paraformaldehyde (PFA) for 30 min. Then the cells were treated with proteinase K (20 mg/ml) for 5 min at room temperature and incubated in TUNEL reaction mixture at 37°C for 1 h in darkness. The nuclei were counterstained with DAPI (Bioworld). The cells were observed under a fluorescence microscope (Nikon, Tokyo, Japan).

Immunocytochemistry

The cells were seeded onto a 96-well plate and transfected with siRNA for 48 h. The cells were fixed with 4% PFA for 30 min, permeabilized in 0.5% TritonX-100 for 10 min, and blocked in 3% BSA for 2 h. The cells were incubated with primary antibody for FOXO4 (sc-5221; Santa Cruz Biotechnology) and γ H2AX (2577; Cell signaling technology) overnight at 4°C. After washing with PBS, the cells were incubated for 1 h with secondary antibody, followed by incubation with DAPI.

Immunohistochemistry

Testes from 6-d- and 3-m-old C57BL/6J mice were used for histologic analyses. In brief, the slides (5 μ m thick) were blocked with 10% donkey serum for 2 h to block non-specific reactions. The following primary antibodies were used: anti-NOX4 (NB110-58849; Novus) and anti-THY1 (sc-9163, Santa Cruz Biotechnology). The following secondary antibodies were used: Alexa 594-conjugated donkey anti-mouse IgG and Alexa 488-conjugated donkey anti-rabbit IgG (1: 400, Invitrogen). Photomicrographs were captured under a Nikon i90 microscope (Nikon, Tokyo, Japan).

Plasmid Construction

The 2 kb region of the *Nox4* gene promoter was amplified by polymerase chain reaction (PCR). Subsequently, PCR product was purified using AxyPrep™ PCR Clean-Up Kit (Axygen, CA, United States). The resulting fragments digested by *KpnI*/*Bgl* II were inserted into the *KpnI*/*Bgl* II restriction sites of digested pGL3-Basic vector. The ligated mixtures were transformed into competent cells of *Escherichia Coli* DH5 α using the heat shock method.

Transfections and Luciferase Assays

The 293T cells were transiently transfected using Turbofect™ (Thermo Fisher Scientific) reagent according to the manufacturer's protocol. The cells were seeded onto 24-well plates, and transfected with 1 μ g total plasmid containing 0.5 μ g pGL3-basic-*Nox4*, 0.5 μ g pCDNA3.1-*E2F1*, and 0.2 μ g pRL-CMV, which were transfected as reference plasmid. The transfected cells were cultured for 48 h and analyzed using a dual-luciferase reporter assay system kit (Promega, Madison, WI, United States) according to the manufacturer's protocol.

Chromatin Immunoprecipitation-qPCR

Chromatin Immunoprecipitation analysis was performed as previously described using EZ-Magna ChIP A/G (Millipore) (Liu et al., 2017). In brief, the cells were fixed with 1% formaldehyde and lysed in lysis buffer. After the sonication the cell lysates were immunoprecipitated with SETDB1 (11231-1-AP; Proteintech), H3K9me3 (07-442, millipore), or normal IgG (millipore) antibodies. IgG is as a background of the IP. The purified DNA was analyzed by RT-qPCR.

The primer was designed by published H3K9me3 ChIP-seq data in mouse undifferentiated spermatogonia cells (Liu et al., 2019). Then, ChIP-qPCR primers were designed around the transcription initiation site, and the size of the product was about 200 bp (Asp, 2018). Finally, the statistical calculation methodology was performed as described previously (Nelson et al., 2006). Briefly, the ChIP-qPCR data output from RT-qPCR software was in the form of Cycle threshold (Ct) values. The relative occupancy of the SETDB1 and H3K9me3 at a locus is measured by the equation $2^{-(Ct_{\text{mock}} - Ct_{\text{specific}})}$, where Ct_{mock} and Ct_{specific} are mean threshold cycles of RT-qPCR. Primers were listed in **supplementary Table S2**.

Statistics

The statistical analysis of the differences between two groups was performed by Student's *t*-test. $P < 0.05$ indicated statistical significance.

DATA AVAILABILITY STATEMENT

All data used to support the findings of this study are included in the article.

AUTHOR CONTRIBUTIONS

XL and XC: conceptualization and writing – original draft preparation. XL, YL, and PZ: methodology. XL: data curation. YZ and WZ: writing – review and editing and funding acquisition. All authors contributed to the article and approved the submitted version.

FUNDING

This study was supported by the National Natural Science Foundation of China (Grant No. 31772605) to WZ, the Natural Science Foundation of Shaanxi Province, China (Grant No. 2019JQ-430), Young Talent Fund of University Association for Science and Technology in Shaanxi, China (Grant No. 20180204), China Postdoctoral Science Foundation (Grant No. 2018M641032), and a startup fund from Northwest A&F University (Grant No. 2452018037) to YZ.

ACKNOWLEDGMENTS

We thank Dr. Zuping He for his generous gift of mouse progenitor spermatogonia cell line C18-4 cells and our laboratory members for technical support.

SUPPLEMENTARY MATERIAL

The Supplementary Material for this article can be found online at: <https://www.frontiersin.org/articles/10.3389/fgene.2020.00997/full#supplementary-material>

REFERENCES

- Ago, T., Kuroda, J., Pain, J., Fu, C., Li, H., and Sadoshima, J. (2010). Upregulation of Nox4 by hypertrophic stimuli promotes apoptosis and mitochondrial dysfunction in cardiac myocytes. *Circ. Res.* 106, 1253–1264. doi: 10.1161/circresaha.109.213116
- An, J., Zhang, X., Qin, J., Wan, Y., Hu, Y., Liu, T., et al. (2014). The histone methyltransferase ESET is required for the survival of spermatogonial stem/progenitor cells in mice. *Cell Death Dis.* 5:e1196. doi: 10.1038/cddis.2014.171
- Asp, P. (2018). How to combine ChIP with qPCR. *Methods Mol. Biol.* 1689, 29–42. doi: 10.1007/978-1-4939-7380-4_3
- Bigarella, C. L., Liang, R., and Ghaffari, S. (2014). Stem cells and the impact of ROS signaling. *Development* 141, 4206–4218. doi: 10.1242/dev.107086
- Brunet, A., Sweeney, L. B., Sturgill, J. F., Chua, K. F., Greer, P. L., Lin, Y., et al. (2004). Stress-dependent regulation of FOXO transcription factors by the SIRT1 deacetylase. *Science* 303, 2011–2015. doi: 10.1126/science.1094637
- Bui, A. D., Sharma, R., Henkel, R., and Agarwal, A. (2018). Reactive oxygen species impact on sperm DNA and its role in male infertility. *Andrologia* 50:e13012. doi: 10.1111/and.13012
- Caja, L., Sancho, P., Bertran, E., Iglesias-Serret, D., Gil, J., and Fabregat, I. (2009). Overactivation of the MEK/ERK pathway in liver tumor cells confers resistance to TGF- β -induced cell death through impairing up-regulation of the NADPH oxidase NOX4. *Cancer Res.* 69, 7595–7602. doi: 10.1158/0008-5472.can-09-1482
- Carmona-Cuenca, I., Roncero, C., Sancho, P., Caja, L., Fausto, N., Fernandez, M., et al. (2008). Upregulation of the NADPH oxidase NOX4 by TGF- β in hepatocytes is required for its pro-apoptotic activity. *J. Hepatol.* 49, 965–976. doi: 10.1016/j.jhep.2008.07.021
- Chen, X., Che, D., Zhang, P., Li, X., Yuan, Q., Liu, T., et al. (2017). Profiling of miRNAs in porcine germ cells during spermatogenesis. *Reproduction* 154, 789–798. doi: 10.1530/rep-17-0441
- Eijkelenboom, A., and Burgering, B. M. (2013). FOXOs: signalling integrators for homeostasis maintenance. *Nat. Rev. Mol. Cell Biol.* 14, 83–97. doi: 10.1038/nrm3507
- Essers, M. A., Weijzen, S., De Vries-Smits, A. M., Saarloos, I., De Ruiter, N. D., Bos, J. L., et al. (2004). FOXO transcription factor activation by oxidative stress mediated by the small GTPase Ral and JNK. *EMBO J.* 23, 4802–4812. doi: 10.1038/sj.emboj.7600476
- Genin, E. C., Caron, N., Vandenbosch, R., Nguyen, L., and Malgrange, B. (2014). Concise review: forkhead pathway in the control of adult neurogenesis. *Stem Cells* 32, 1398–1407. doi: 10.1002/stem.1673
- Henderson, S. T., and Johnson, T. E. (2001). daf-16 integrates developmental and environmental inputs to mediate aging in the nematode *Caenorhabditis elegans*. *Curr. Biol.* 11, 1975–1980. doi: 10.1016/s0960-9822(01)00594-2
- Hirota, T., Blakeley, P., Sangrithi, M. N., Mahadevaiah, S. K., Encheva, V., Snijders, A. P., et al. (2018). SETDB1 links the meiotic DNA damage response to sex chromosome silencing in mice. *Dev. Cell* 47:e646.
- Hofmann, M. C., Braydich-Stolle, L., Dettin, L., Johnson, E., and Dym, M. (2005). Immortalization of mouse germ line stem cells. *Stem Cells* 23, 200–210. doi: 10.1634/stemcells.2003-0036
- Hong, W., Li, J., Wang, B., Chen, L., Niu, W., Yao, Z., et al. (2011). Epigenetic involvement of Alien/ESET complex in thyroid hormone-mediated repression of E2F1 gene expression and cell proliferation. *Biochem. Biophys. Res. Commun.* 415, 650–655. doi: 10.1016/j.bbrc.2011.10.130
- Hua, X., Chi, W., Su, L., Li, J., Zhang, Z., and Yuan, X. (2017). ROS-induced oxidative injury involved in pathogenesis of fungal keratitis via p38 MAPK activation. *Sci. Rep.* 7:10421.
- Ito, K., Hirao, A., Arai, F., Takubo, K., Matsuo, S., Miyamoto, K., et al. (2006). Reactive oxygen species act through p38 MAPK to limit the lifespan of hematopoietic stem cells. *Nat. Med.* 12, 446–451. doi: 10.1038/nm1388
- Jiramongkol, Y., and Lam, E. W. (2020). FOXO transcription factor family in cancer and metastasis. *Cancer Metast. Rev.* 39, 681–709. doi: 10.1007/s10555-020-09883-w
- Kanatsu-Shinohara, M., and Shinohara, T. (2013). Spermatogonial stem cell self-renewal and development. *Annu. Rev. Cell Dev. Biol.* 29, 163–187. doi: 10.1146/annurev-cellbio-101512-122353
- Katsuyama, M., Matsuno, K., and Yabe-Nishimura, C. (2012). Physiological roles of NOX/NADPH oxidase, the superoxide-generating enzyme. *J. Clin. Biochem. Nutr.* 50, 9–22. doi: 10.3164/jcbs.11-06sr
- Kim, J., Zhao, H. B., Dan, J. M., Kim, S., Hardikar, S., Hollowell, D., et al. (2016). Maternal setdb1 is required for meiotic progression and preimplantation development in mouse. *PLoS Genet.* 12:e1005970. doi: 10.1371/journal.pgen.1005970
- Lambeth, J. D., and Neish, A. S. (2014). Nox enzymes and new thinking on reactive oxygen: a double-edged sword revisited. *Annu. Rev. Pathol.* 9, 119–145. doi: 10.1146/annurev-pathol-012513-104651
- Lin, K., Hsin, H., Libina, N., and Kenyon, C. (2001). Regulation of the *Caenorhabditis elegans* longevity protein DAF-16 by insulin/IGF-1 and germline signaling. *Nat. Genet.* 28, 139–145. doi: 10.1038/88850
- Liu, S., Brind'Amour, J., Karimi, M. M., Shirane, K., Bogutz, A., Lefebvre, L., et al. (2015). Setdb1 is required for germline development and silencing of H3K9me3-marked endogenous retroviruses in primordial germ cells (vol 28, pg 2041, 2014). *Genes Dev.* 29, 108–108.
- Liu, T. T., Chen, X. X., Li, T. J., Li, X. L., Lyu, Y. H., Fan, X. T., et al. (2017). Histone methyltransferase SETDB1 maintains survival of mouse spermatogonial stem/progenitor cells via PTEN/AKT/FOXO1 pathway. *Biochim. Biophys. Acta Gene Regul. Mech.* 1860, 1094–1102. doi: 10.1016/j.bbaggm.2017.08.009
- Liu, Y., Zhang, Y., Yin, J., Gao, Y., Li, Y., Bai, D., et al. (2019). Distinct H3K9me3 and DNA methylation modifications during mouse spermatogenesis. *J. Biol. Chem.* 294, 18714–18725. doi: 10.1074/jbc.ra119.010496
- Ma, X., Du, J., Nakashima, I., and Nagase, F. (2002). Menadione biphasically controls JNK-linked cell death in leukemia Jurkat T cells. *Antioxid. Redox. Signal.* 4, 371–378. doi: 10.1089/15230860260196173
- McKallip, R. J., Jia, W., Schlomer, J., Warren, J. W., Nagarkatti, P. S., and Nagarkatti, M. (2006). Cannabidiol-induced apoptosis in human leukemia cells: a novel role of cannabidiol in the regulation of p22phox and Nox4 expression. *Mol. Pharmacol.* 70, 897–908. doi: 10.1124/mol.106.023937
- McSwiggin, H. M., and O'Doherty, A. M. (2018). Epigenetic reprogramming during spermatogenesis and male factor infertility. *Reproduction* 156, R9–R21.
- Mochizuki, K., Tandot, Y., Sekinaka, T., Otsuka, K., Hayashi, Y., Kobayashi, H., et al. (2018). SETDB1 is essential for mouse primordial germ cell fate determination by ensuring BMP signaling. *Development* 145:dev164160. doi: 10.1242/dev.164160
- Morimoto, H., Iwata, K., Ogonuki, N., Inoue, K., Atsuo, O., Kanatsu-Shinohara, M., et al. (2013). ROS are required for mouse spermatogonial stem cell self-renewal. *Cell Stem Cell* 12, 774–786. doi: 10.1016/j.stem.2013.04.001
- Morimoto, H., Kanatsu-Shinohara, M., and Shinohara, T. (2015). ROS-generating oxidase Nox3 regulates the self-renewal of mouse spermatogonial stem cells. *Biol. Reprod.* 92:147.
- Mozzetta, C., Boyarchuk, E., Pontis, J., and Ait-Si-Ali, S. (2015). Sound of silence: the properties and functions of repressive Lys methyltransferases. *Nat. Rev. Mol. Cell Biol.* 16, 499–513. doi: 10.1038/nrm4029
- Murtaza, G., Khan, A. K., Rashid, R., Muneer, S., Hasan, S. M. F., and Chen, J. (2017). FOXO transcriptional factors and long-term living. *Oxid. Med. Cell Longev.* 2017:3494289.
- Najafi, M., Shirazi, A., Motevaseli, E., Geraily, G., Amini, P., Tooli, L. F., et al. (2019). Melatonin modulates regulation of NOX2 and NOX4 following irradiation in the lung. *Curr. Clin. Pharmacol.* 14, 224–231. doi: 10.2174/1574884714666190502151733
- Nandi, A., Yan, L. J., Jana, C. K., and Das, N. (2019). Role of catalase in oxidative stress- and age-associated degenerative diseases. *Oxid. Med. Cell Longev.* 2019:9613090.
- Nathan, C., and Cunningham-Bussell, A. (2013). Beyond oxidative stress: an immunologist's guide to reactive oxygen species. *Nat. Rev. Immunol.* 13, 349–361. doi: 10.1038/nri3423
- Nelson, J. D., Denisenko, O., and Bomsztyk, K. (2006). Protocol for the fast chromatin immunoprecipitation (ChIP) method. *Nat. Protoc.* 1, 179–185. doi: 10.1038/nprot.2006.27
- Pedruzzi, E., Guichard, C., Ollivier, V., Driss, F., Fay, M., Prunet, C., et al. (2004). NAD(P)H oxidase Nox-4 mediates 7-ketocholesterol-induced endoplasmic reticulum stress and apoptosis in human aortic smooth muscle cells. *Mol. Cell Biol.* 24, 10703–10717. doi: 10.1128/mcb.24.24.10703-10717.2004
- Schaefer, M., Gebhard, M. M., and Gross, W. (2019). The effect of melatonin on hearts in ischemia/reperfusion experiments without and with HTK

- cardioplegia. *Bioelectrochemistry* 129, 170–178. doi: 10.1016/j.bioelechem.2019.05.017
- Singh, S., Misiak, M., Beyer, C., and Arnold, S. (2009). Cytochrome c oxidase isoform IV-2 is involved in 3-nitropropionic acid-induced toxicity in *Striatal astrocytes*. *Glia* 57, 1480–1491. doi: 10.1002/glia.20864
- Su, L. J., Zhang, J. H., Gomez, H., Murugan, R., Hong, X., Xu, D., et al. (2019). Reactive oxygen species-induced lipid peroxidation in apoptosis, autophagy, and ferroptosis. *Oxid. Med. Cell Longev.* 2019:5080843.
- Tan, D. X., Reiter, R. J., Manchester, L. C., Yan, M. T., El-Sawi, M., Sainz, R. M., et al. (2002). Chemical and physical properties and potential mechanisms: melatonin as a broad spectrum antioxidant and free radical scavenger. *Curr. Top. Med. Chem.* 2, 181–197. doi: 10.2174/1568026023394443
- Tan, S. L., Nishi, M., Ohtsuka, T., Matsui, T., Takemoto, K., Kamio-Miura, A., et al. (2012). Essential roles of the histone methyltransferase ESET in the epigenetic control of neural progenitor cells during development. *Development* 139, 3806–3816. doi: 10.1242/dev.082198
- Tuteja, G., and Kaestner, K. H. (2007a). Forkhead transcription factors II. *Cell* 131:192. doi: 10.1016/j.cell.2007.09.016
- Tuteja, G., and Kaestner, K. H. (2007b). SnapShot: forkhead transcription factors I. *Cell* 130:1160.
- Urbich, C., Knau, A., Fichtlscherer, S., Walter, D. H., Bruhl, T., Potente, M., et al. (2005). FOXO-dependent expression of the proapoptotic protein Bim: pivotal role for apoptosis signaling in endothelial progenitor cells. *FASEB J.* 19, 974–976. doi: 10.1096/fj.04-2727fje
- Wang, Y., Branicky, R., Noe, A., and Hekimi, S. (2018). Superoxide dismutases: dual roles in controlling ROS damage and regulating ROS signaling. *J. Cell Biol.* 217, 1915–1928. doi: 10.1083/jcb.201708007
- Webb, A. E., and Brunet, A. (2014). FOXO transcription factors: key regulators of cellular quality control. *Trends Biochem. Sci.* 39, 159–169. doi: 10.1016/j.tibs.2014.02.003
- Weyemi, U., Lagente-Chevallier, O., Boufraqueh, M., Preno, F., Courtin, F., Caillou, B., et al. (2012). ROS-generating NADPH oxidase NOX4 is a critical mediator in oncogenic H-Ras-induced DNA damage and subsequent senescence. *Oncogene* 31, 1117–1129. doi: 10.1038/onc.2011.327
- Zanella, F., Link, W., and Carnero, A. (2010). Understanding FOXO, new views on old transcription factors. *Curr. Cancer Drug Targets* 10, 135–146. doi: 10.2174/156800910791054158
- Zhang, L., Sheppard, O. R., Shah, A. M., and Brewer, A. C. (2008). Positive regulation of the NADPH oxidase NOX4 promoter in vascular smooth muscle cells by E2F. *Free Radic. Biol. Med.* 45, 679–685. doi: 10.1016/j.freeradbiomed.2008.05.019
- Zheng, L., Wang, C., Luo, T., Lu, B., Ma, H., Zhou, Z., et al. (2017). JNK activation contributes to oxidative stress-induced parthanatos in glioma cells via increase of intracellular ROS production. *Mol. Neurobiol.* 54, 3492–3505. doi: 10.1007/s12035-016-9926-y
- Zhu, Y., Sun, D., Jakovcevski, M., and Jiang, Y. (2020). Epigenetic mechanism of SETDB1 in brain: implications for neuropsychiatric disorders. *Transl. Psychiatry* 10:115.

Conflict of Interest: The authors declare that the research was conducted in the absence of any commercial or financial relationships that could be construed as a potential conflict of interest.

Copyright © 2020 Li, Chen, Liu, Zhang, Zheng and Zeng. This is an open-access article distributed under the terms of the Creative Commons Attribution License (CC BY). The use, distribution or reproduction in other forums is permitted, provided the original author(s) and the copyright owner(s) are credited and that the original publication in this journal is cited, in accordance with accepted academic practice. No use, distribution or reproduction is permitted which does not comply with these terms.



Inhibition of DNA Methylation in *Picochlorum soloecismus* Alters Algae Productivity

Christina R. Steadman*, Shounak Banerjee, Yuliya A. Kunde, Claire K. Sanders, Babetta L. Marrone and Scott N. Twary

Los Alamos National Laboratory, Bioenergy and Biome Sciences, Los Alamos, NM, United States

OPEN ACCESS

Edited by:

Huiming Zhang,
Shanghai Institutes for Biological
Sciences (CAS), China

Reviewed by:

Honggui La,
Nanjing Agricultural University, China
Narendra Singh,
Stowers Institute for Medical
Research, United States

*Correspondence:

Christina R. Steadman
crt@lanl.gov

Specialty section:

This article was submitted to
Epigenomics and Epigenetics,
a section of the journal
Frontiers in Genetics

Received: 08 May 2020

Accepted: 03 September 2020

Published: 15 October 2020

Citation:

Steadman CR, Banerjee S,
Kunde YA, Sanders CK, Marrone BL
and Twary SN (2020) Inhibition
of DNA Methylation in *Picochlorum*
soloecismus Alters Algae Productivity.
Front. Genet. 11:560444.
doi: 10.3389/fgene.2020.560444

Eukaryotic organisms regulate the organization, structure, and accessibility of their genomes through chromatin remodeling that can be inherited as epigenetic modifications. These DNA and histone protein modifications are ultimately responsible for an organism's molecular adaptation to the environment, resulting in distinctive phenotypes. Epigenetic manipulation of algae holds yet untapped potential for the optimization of biofuel production and bioproduct formation; however, epigenetic machinery and modes-of-action have not been well characterized in algae. We sought to determine the extent to which the biofuel platform species *Picochlorum soloecismus* utilizes DNA methylation to regulate its genome. We found candidate genes with domains for DNA methylation in the *P. soloecismus* genome. Whole-genome bisulfite sequencing revealed DNA methylation in all three cytosine contexts (CpG, CHH, and CHG). While global DNA methylation is low overall (~1.15%), it occurs in appreciable quantities (12.1%) in CpG dinucleotides in a bimodal distribution in all genomic contexts, though terminators contain the greatest number of CpG sites per kilobase. The *P. soloecismus* genome becomes hypomethylated during the growth cycle in response to nitrogen starvation. Algae cultures were treated daily across the growth cycle with 20 μ M 5-aza-2'-deoxycytidine (5AZA) to inhibit propagation of DNA methylation in daughter cells. 5AZA treatment significantly increased optical density and forward and side scatter of cells across the growth cycle (16 days). This increase in cell size and complexity correlated with a significant increase (~66%) in lipid accumulation. Site specific CpG DNA methylation was significantly altered with 5AZA treatment over the time course, though nitrogen starvation itself induced significant hypomethylation in CpG contexts. Genes involved in several biological processes, including fatty acid synthesis, had altered methylation ratios in response to 5AZA; we hypothesize that these changes are potentially responsible for the phenotype of early induction of carbon storage as lipids. This is the first report to utilize epigenetic manipulation strategies to alter algal physiology and phenotype. Collectively, these data suggest these strategies can be utilized to fine-tune metabolic responses, alter growth, and enhance environmental adaption of microalgae for desired outcomes.

Keywords: algae, epigenetics, 5-aza-2'-deoxycytidine, DNA methylation, lipid accumulation, fatty acid synthesis, bisulfite sequencing

INTRODUCTION

Eukaryotic organisms control the organization and accessibility of their genomes via covalent modification of DNA and chromatin proteins. These modifications are collectively referred to as epigenetic modifications, which, under the purview of strict scrutiny, are reversible and yet heritable during mitotic activity (Feng et al., 2010b). Epigenetic mechanisms regulate a plethora of processes in mammalian and plant species, ranging from the fidelity of DNA replication, repair, and protection to DNA transcription and expression (Jaenisch and Bird, 2003). These processes are globally defined as either (1) covalent modification of basic amino acids located in the N-terminal domain of histone proteins that comprise nucleosome structures (i.e., histone modifications) or (2) covalent modification of the nucleic acids, adenosine or cytosine (i.e., DNA modifications). In plants, methylation of cytosines in DNA can occur in multiple genomic regions and dinucleotide contexts, including CpG, CHH, and CHG (where H corresponds to A, T or C). This DNA methylation is important for plant growth and dynamic responses to environmental perturbations and directly influences the plant's phenotype (Zhang et al., 2018).

Microalgae are photosynthetic, single-celled eukaryotes. Many microalgae species have relatively small genomes, particularly in comparison with humans and polyploid plant species. Of the thousands of algae species, very few have been sequenced, and even fewer have had their epigenomes measured (Blaby-Haas and Merchant, 2019). The model algae organism, *Chlamydomonas reinhardtii*, has been used extensively to study the mechanisms of epigenetic regulation, inheritance, and adaption (Cerutti, 1997; van Dijk et al., 2005; Shaver et al., 2010; Pandey et al., 2012; Fu et al., 2015; Kronholm et al., 2017). However, unlike mammalian species, in which the presence and functionality of epigenetic modifications is similar among several species, patterns of epigenetic modifications (and even function) have proven to be dissimilar (or not even present) in algae (Tirichine and Bowler, 2011; Veluchamy et al., 2014; Tirichine et al., 2017). This is likely attributed to either evolutionary divergence of algae and/or variable genome size. Organisms with smaller genomes use other mechanisms of genomic control, including operons and RNA interference (RNAi), both of which alter gene expression without the need for chromatin remodeling processes. Interestingly, despite the lack of differentiation and the relative compactness of their genomes, many microalgae tend to utilize some form of epigenetic modification, though relatively few have been tested (Müller et al., 1990; Umen and Goodenough, 2001; Babinger et al., 2007; Zemach et al., 2010; Lopez et al., 2015; Ngan et al., 2015). Thus, given the breadth of genetic diversity among microalgae, these organisms provide an opportunity to study the evolution of epigenetic mechanisms. However, this diversity requires that each modification must be assessed under environmental variability for each species of interest to determine the presence and function of epigenetic modifications in microalgae collectively.

We sought to determine the relative importance of DNA modifications, particularly 5-methylcytosine, for our microalgae species of interest, *Picochlorum soloecismus*, which has a small haploid genome (15.6 Mb) (Gonzalez-Esquer et al., 2018). We are interested in the phenotype of this species, particularly under nutrient-limited conditions that induce carbon sequestration into lipid and carbohydrate molecules. This “carbon accumulation” phenotype under duress has potential applications for the production of biofuels and other bioproducts (Alishah Aratboni et al., 2019). A recent algae biofuel consortium (the National Alliance for Advanced Biofuels and Bioproducts) denoted *P. soloecismus* as a promising feedstock for biofuel research (Unkefer et al., 2017). The *Picochlorum* genus is highly adaptive to environmental variation in salinity, temperature, pH, and nutrients; it readily alters its gene expression as such to induce particular phenotypes under these various conditions (Foflonker et al., 2015; Krasovec et al., 2018; Dahlin et al., 2019; Gonzalez-Esquer et al., 2019; Steadman Tyler et al., 2019). Bioengineering *P. soloecismus* includes the manipulation of gene expression to mimic environmental conditions that drive carbon sequestration, but efforts have been limited. Understanding the mechanisms by which this organism controls its genome is thus useful for maximizing its productivity. To aid in this challenge, we sought to quantify DNA methylation and determine its influence on the physiology and phenotype of *P. soloecismus*.

We used treatment with 5-aza-2'-deoxycytidine (5AZA) in cultivation of *P. soloecismus* to inhibit the formation of 5-methylcytosine (5mC) DNA methylation under baseline environmental conditions and during nitrogen starvation. This treatment inhibits binding of DNA methyltransferase enzymes to hemimethylated DNA during replication, thereby interfering with maintenance methylation on the lagging strand (Christman, 2002). After mitosis, daughter cells lack this epigenetic modification, and over the course of growth, each new cell has less 5mC DNA methylation (typically halved in each subsequent generation of cells). In mammalian cells, this treatment induces cell cycle arrest and apoptosis, thus demonstrating the importance of DNA methylation for maintaining cell function and physiology (Pall et al., 2008). Here, we report that 5mC DNA methylation occurs primarily in CpG contexts in *P. soloecismus*, though it was also found in CHG and CHH contexts. The relative abundance of DNA methylation is low but occurs in multiple genomic loci, including gene bodies, promoters, terminators, and intergenic regions. DNA methylation in *P. soloecismus* is dynamic and responsive over the algal growth cycle. Inhibition of 5mC propagation resulted in altered cell growth and increased lipid accumulation, suggesting this epigenetic modification has physiological relevance and control of the *P. soloecismus* stress phenotype. This study suggests that epigenetic manipulation of algal DNA methylomes may allow for fine-tuning metabolic responses, alteration of growth, and enhanced environmental adaption for biofuel and bioproduct outcomes.

MATERIALS AND METHODS

Data Mining for DNA Methyltransferase Genes in the *P. soloecismus* Genome

Using methods previously described, we interrogated the *P. soloecismus* genome for genes encoding epigenetic machinery with the capacity for DNA methylation (Hovde et al., 2018). Briefly, queries of known DNA methylation protein sequences were tested against the *P. soloecismus* protein sequence data. Sequences with similar homology were queried using BLASTP (Altschul et al., 1990) and for specific Pfam domains (El-Gebali et al., 2019). The presence of domains was confirmed in the annotated *P. soloecismus* genome using Pfam and InterPro domains considered essential for epigenetic function in each protein (Mitchell et al., 2019).

Microalgae Cultivation

For DNA methylation experiments, *P. soloecismus* was cultivated as previously described (Steadman Tyler et al., 2019). Briefly, cells were grown in 250 mL shaker flasks, maintained at ambient temperature, under $300 \mu\text{molm}^{-2}\text{s}^{-1}$ fluorescent light with a 16 h/8 h light:dark cycle in modified f/2 media with 8.8 mM sodium nitrate. Cultures were shaken and supplemented with 1% CO_2 . Cultures naturally depleted of nitrogen after 6 days of growth. Sterile sampling was used for obtaining aliquots on a daily basis. Optical density at 750 nm (OD_{750}) values were taken immediately after sampling. Samples for analysis were stored at 4°C until use. For cell cycle studies, triplicate *P. soloecismus* cultures were grown in 1 L volumes in 2.8 L spin flasks. Cultures were constantly bubbled with air and maintained at pH 8.25 by on-demand CO_2 injection. Cultures were mixed by magnetic stirring at 200 rpm and illuminated with $800 \mu\text{molm}^{-2}\text{s}^{-1}$ in a 16 h/8 h light:dark cycle. Cultures were sampled every 2 h for 48 h for cell cycle assessment.

Flow Cytometry Assessments (Cell Counts, FSC/SSC, DNA Ploidy, Lipid Accumulation)

Flow cytometry assessments were performed to determine cell concentration, relative cell size, DNA ploidy, and lipid accumulation in *P. soloecismus* as previously described (Unkefer et al., 2017; Steadman Tyler et al., 2019). Assessments were performed at the same time points and correlated to daily OD_{750} measurements 4 h into the light cycle. Unstained samples were used to determine cell concentration (cell/mL), relative size (FSC – forward scatter), and internal complexity (SSC – side scatter). Accumulation of neutral lipids was assessed using BODIPY 505/515 (D3921, Thermo Fisher Scientific, Waltham, MA, United States) staining and flow cytometry fluorescence assessment at selected time points during nitrogen replete, nitrogen starvation ($N = 0$), and nitrogen deplete culture conditions. For assessment of DNA content and replication, samples were taken every 2 h for 48 h, incubated with DyeCycle Orange (V35005, Thermo Fisher Scientific, Waltham, MA, United States), and assessed on the BD Accuri C6 Plus (BD Biosciences, San Jose, CA, United States) flow cytometer.

DNA Methylation Inhibition

5-aza-2'-deoxycytidine was purchased from Sigma (A3656). 5AZA is preferable to 5-azacytidine for its retention in the cell; both exert proapoptotic effects (Gnyszka et al., 2013). 5AZA was prepared in 50% DMSO and 50% ice cold MilliQ water in the least possible volume for all final concentrations (0–80 μM) in 250 mL shaker flasks. Stock solutions of 5AZA were stored at -20°C ; aliquots were thawed on ice prior to treatment to prevent drug instability and break down. Treatment occurred 4–5 h into the light cycle prior to DNA replication in *P. soloecismus* as determined by flow cytometry (see above) every day (days 1–16) of the growth cycle. The half-life of 5AZA in most mammalian cell cultures is between 8 and 10 h as determined in preclinical trials (Hollenbach et al., 2010).

DNA Extraction

A modified, combined protocol was generated from the manufacturer's instructions using E.Z.N.A. Plant DNA DS Mini Kit (D2411-01; Omega Bio-tek Inc., Norcross, GA, United States) and Quick-DNA Fungal/Bacterial Miniprep Kit (D6005; Zymo Research, Irvine, CA, United States) to isolate genomic DNA. Briefly, 400 μL of reconstituted cells were lysed using bead bashing lysis tubes and buffer at 4°C. Samples were treated with CSPL buffer and proteinase K solution and heated at 65°C for 30 min. Samples were centrifuged and cleared supernatant was passed through a mini column followed by RNase A treatment at RT. Cleared supernatant was treated with RBB Buffer and XP2 Buffer, vortexed, and transferred to a HiBind DNA Mini Column. HBC buffer and DNA wash buffers were added to the columns. Columns were allowed to air dry followed by 2 min incubation with elution buffer. DNA was purified using AMPure Purification Beads (100-265-900; PacBio, Menlo Park, CA, United States) in a 1:1 volumetric ratio per the manufacturer's instructions. After separation on a magnetic rack and washing with 70% ethanol, the beads were incubated with PacBio elution buffer (101-633-500; PacBio, Menlo Park, CA, United States) for 10 min at RT. Purified DNA was removed in the supernatant and quantified using a Qubit dsDNA HS Kit (32854; Thermo Fisher Scientific). Lambda HindIII DNA marker was used to determine the DNA size (SM0101; Thermo Fisher Scientific). DNA integrity and size were assessed on E-Gel EX 1% agarose gel (G402001; Thermo Fisher Scientific).

Global DNA Methylation Quantification

The presence of methylation on the 5' carbon of cytosine in DNA was determined using the 5mC DNA ELISA Kit (D5325; Zymo Research, Irvine, CA, United States) per manufacturer's instructions with minor changes. Modifications to the protocol included adding a 2.5% 5mC-DNA standard to the calibration curve, using 200 ng of input DNA, and quantification at 405 nm wavelength using a Tecan spectrophotometer (Tecan Life Sciences, Switzerland). For a positive control, *P. soloecismus* DNA was incubated with CpG Methylase (*M. SssI*) and 12 mM of s-adenosyl methionine substrate (E2010; Zymo Research, Irvine, CA, United States) for 12 h at 30°C. The %5mC in DNA was determined using a saturation binding curve (non-linear fit)

in GraphPad Prism 8 software (GraphPad, San Diego, CA, United States). Results are reported as %5mC.

Whole Genome Bisulfite Sequencing (WGBS)

Picochlorum soloecismus samples were processed and analyzed using the Methyl-MaxiSeq library preparation, sequencing, and bioinformatics pipeline from Zymo Research (Irvine, CA, United States). Triplicate biological replicates from 5AZA treated and untreated cells over 5 days of the growth cycle representing replete and deplete nitrogen conditions were used for analysis. Briefly, Methyl-MaxiSeq libraries were prepared from 1 µg gDNA digested with two units of dsDNA Shearase™ Plus (E2018-50; Zymo Research, Irvine, CA, United States). Fragments were end-blunted, the 3'-terminal-A extended, and purified using the DNA Clean & Concentrator Kit (D4003; Zymo Research, Irvine, CA, United States). A-tailed fragments were ligated to pre-annealed adapters containing 5mC instead of cytosine and adapter-ligated fragments were filled in. Fragments were treated with sodium bisulfite using the EZ DNA Methylation – Lightning Kit (D5030; Zymo Research, Irvine, CA, United States). Treated DNA was amplified with Illumina TruSeq indices; fragment DNA purity and size were confirmed on the Agilent 2200 TapeStation (Agilent Technologies, Santa Clara, CA, United States). DNA was sequenced using Illumina PE75 on the HiSeq (Illumina Inc., San Diego, CA, United States) instrument to 50X coverage.

Methylation Alignment and Calling

Three biological replicates over 5 days of the growth cycle were sequenced for the presence of methylated cytosines. Sequencing reads from bisulfite-treated EpiQuest libraries were identified using standard Illumina base-calling software and then analyzed using bismark bowtie2¹ for alignment. Methylation calling was performed using MethylDackel.² Index files were constructed by bismark_genome_preparation command using the entire reference genome of *P. soloecismus* (GenBank PJA000000000). The `-non-directional` parameter was applied while running bismark. All other parameters were set to default. For MethylDackel, parameters were also used to find sites in CHG and CHH contexts. All other parameters for MethylDackel were set to default. Methylation calls with greater than 20X coverage were validated against a list of all possible methylation sites in the genome. These validated sites were used to estimate global methylation profiles for each timepoint. All called sites are reported in **Supplementary Tables** (FigShare³). To obtain feature-length corrected methylation site frequencies in the genome, four features were used. These included “gene body,” “promoter,” “terminator,” and “intergenic regions.” Gene bodies denoted the protein coding regions and included introns and exons. Promoters and terminators were defined as the 500 bp 5' and 3' UTRs flanking gene bodies. Any sequence span not under these definitions of gene bodies, promoters, or terminators was marked as an intergenic region (IGR). These features are

available as extended versions of the genomic annotation file published for *P. soloecismus* in the **Supplementary Tables**. Methylation sites were mapped to genomic features using Pandas (McKinney, 2010). Briefly, counts of called sites were obtained for each feature and divided by the size (bp) of that feature. The resulting site density value (in counts/bp) was multiplied by 1000 to express density as counts per kb. Variables (averages and standard deviations) were calculated with or without filtering out zero-count entries; data is reported without zero-count entries. The script for this calculation is available in GitHub: https://github.com/lanl/DNA_methylation_analysis. All raw fastq files, processed methylation tracks, and methylation calls are provided on the Gene Expression Omnibus (GEO) website under the accession record GSE155500.

Differential Methylation Analysis

Data from Zymo Research included called sites, the number of total reads per site, and methylation ratio per site. The methylation ratio of each sampled cytosine is estimated as the number of reads reporting a cytosine divided by the total number of reads reporting a C or T [$C/(C + T)$]. Reads were culled according to NIH Roadmap Epigenomics Project (Bernstein et al., 2010). For the *P. soloecismus* genome (15.2 million base pairs, haploid), there was a median of 50X coverage for all sites. A Student's *t*-test was performed for each cytosine with a minimum coverage of 20X aligned sequence reads (for every day in culture) to identify statistically significant methylation differences in each comparison. The differences in methylation ratios between Day 4 and Day 10 in culture (the first and last day of sequencing) were used to determine overall changes in methylation across the time course. All significant methylation ratio changes less than 0.1 and greater than -0.1 were not considered in the analysis. The same parameters for calling were used for sequences from 5AZA treated samples. To determine the effect of 5AZA on methylation ratios per site, differences in methylation ratios were calculated for each day in culture between treated and untreated cultures. Data is plotted as methylation ratio per day in culture.

Methylation Visualization, Annotation, and Gene Cluster Analysis

To determine specific genes of interest that may contain sites of methylation, genomic annotations were added to sites with the most significant changes in methylation ratios (hyper or hypomethylation) from the LANL Greenhouse database.⁴ Open reading frames (ORF) extracted based on these annotations were assigned KEGG Orthologies (KOs) (Kanehisa et al., 2016a,b) using KofamKOALA (Aramaki et al., 2020), with an *E*-value cutoff of $1E-24$. For each predicted ORF encoded in the annotations, we retained the KO assignment with the lowest *E*-value. LANL in-house software was used to map KOs to KEGG pathways (Kanehisa et al., 2016a,b), to determine if genes with significantly different methylation ratios over the cultivation time course clustered into particular metabolic processes. To visualize sites in a gene (multiple sites per gene) under two

¹<http://www.bioinformatics.babraham.ac.uk/projects/bismark/>

²<https://github.com/dpryan79/MethylDackel/>

³https://figshare.com/authors/Christina_Steadman/8855753

⁴<https://greenhouse.lanl.gov>

different conditions (either day in culture or 5AZA treatment), the relevant methylation sites were added to the annotations extant in the greenhouse database and color coded in Microsoft Excel for Mac 2019. Separate, augmented annotation files were created for each timepoint and condition to enable simultaneous viewing in standard genome browsers capable of interpreting the GFF3 format. All scripts used for data analysis and methylation calling are provided in GitHub.⁵

Statistics

All statistical analyses were performed using GraphPad Prism8 software packages (version 8.4.1 (460), GraphPad Software, San Diego, CA, United States) with default parameters except when Bonferroni or Tukey's *post hoc* analyses were performed. One-way ANOVA repeated measures was performed to determine methylation ratio differences of *P. soloecismus* across the growth cycle. Two-way ANOVA repeated measures analysis was used to compare 5AZA treated and untreated *P. soloecismus* phenotypes over the time course for three biological replicate cultures. These phenotypes included optical density, cell counts, cell size (FSC), cell complexity (SSC), and lipid accumulation. A Student's *t*-test was used to evaluate %5mC and to evaluate the difference in methylation ratio between specific days in culture for treated or untreated cultures.

RESULTS

The Presence of Epigenetic Machinery for DNA Methylation in *P. soloecismus*

Prior to experimental determination of DNA methylation, we interrogated the *P. soloecismus* genome for signatures of epigenetic machinery. In plants, several enzymes are responsible for imparting DNA modifications. Each enzyme has a specific function for methylation in a particular cytosine context (CpG, CHG, or CHH). DNA methyltransferase enzymes contain specific DNA binding domains in addition to their methyltransferase enzymatic activity domains. We found homologs for a number of enzymes involved in DNA methylation in the *P. soloecismus* genome, suggesting the possibility of DNA methylation in multiple contexts (Table 1A). Some of these enzymes have domains for both DNA binding and 5mC methyltransferase activity. These domains can be found in several different databases. Pfam is a curated database of expertly built multiple sequence alignments representing clusters of proteins and/or protein domains (Finn et al., 2015). Clusters of sequences are organized into "families," and families are grouped at a higher level into "clans." InterPro is a similar but broader database that combines information from member databases like Pfam, including CATH-Gene3D, TIGRFAMs, and PROSITE among others (Haft et al., 2003; Sigrist et al., 2012; Lewis et al., 2017; Sillitoe et al., 2018; Mitchell et al., 2019). These databases are particularly useful in annotation of remote homologs of proteins that may be found in newly annotated genomes. Both are commonly used in unison by automated annotation pipelines

such as MAKER and AUGUSTUS (Stanke and Morgenstern, 2005; Cantarel et al., 2008). Interrogation of the *P. soloecismus* genome with InterPro and Pfam domains of interest (described in "Materials and Methods") produced 14 hits for possible methyltransferase enzymes (Table 1B). This information was cross referenced with the homologs from Table 1A. Two of these potential enzymes were aligned with DNA methyltransferase enzymes from other species, demonstrating sequence variation except in important catalytic domains required for DNA methylation activity (Figure 1). This *in situ* data suggested that *P. soloecismus* contains at least two enzymes capable of covalent modification of DNA on the 5' carbon of cytosine.

DNA Methylation Characteristics of *P. soloecismus*

DNA methylation was determined using two methods: 5mC ELISA and whole genome bisulfite sequencing (WGBS). Using the 5mC ELISA, 0.82% 5mC was detected in *P. soloecismus* gDNA. To generate a positive control, *P. soloecismus* gDNA was treated with CpG Methylase (*M. SssI*). This positive control had 1.3% 5mC methylation (Supplementary Figure 1, $p < 0.0001$). This initial assessment of global 5mC suggested that genomic DNA methylation of *P. soloecismus* was low but amenable to alteration (based on treatment with the *M. SssI* CpG methylase). Of note, the antibody-based ELISA from Zymo Research has a detection limit of $>0.5\%$ 5mC per 100 ng DNA.

Whole genome bisulfite sequencing provides metrics for global and site-specific DNA 5mC methylation, including sequencing metrics and calls for methylation (Table 2). For the 15.2 MB *P. soloecismus* genome, cytosine content should have been called for approximately 1,014,486 CpG sites, 1,316,811 CHG sites, and 4,430,371 CHH sites (or about 44% of the genome). Approximately 93% of CpG and CHG sites and 87% of CHH sites were called for WGBS (Table 2). The methylation fraction for each sample was determined for each context to provide a picture of global methylation. For example, for Day 4 Control 1, there were 944,940 called CpG sites with an approximate methylation ratio of 0.123. Thus, approximately 12.3% of these sites had methylation or, as noted later, most CpG sites from this day in culture had approximately 12.3% methylation based on read counts. Methylation ratios were calculated as the number of methylated reads from the bisulfite converted sequences divided by the total number of reads for that particular site (# methylated C reads/# total C + T reads). From this assessment, we determined that on average, methylation occurred in 12.1% of CpG contexts, 0.8% of CHG contexts, and 0.9% of CHH contexts (Figure 2A). From a genome-wide perspective, the *P. soloecismus* genome had approximately 1.15% cytosine methylation (Figure 2A). This was determined by calculating the number of sites with methylation divided by the total genome size and normalized based on the number of called sites for the sequencing run. This methylation was divided across all cytosine contexts, with the majority of methylation occurring at CpG sites.

For each cytosine context, we determined the relative abundance of DNA methylation in four genomic features: gene

⁵https://github.com/lanl/DNA_methylation_analysis

TABLE 1A | Top gene ID hits for homologs of DNA methyltransferases in *P. soloecismus*.

ID	Name	Domains
NSC_03941	s-adenosyl-methyltransferase	IPR002903, IPR023397
NSC_03950	Conserved hypothetical	PF13578
NSC_00652	Cytosine-5 DNA methyltransferase	IPR001525, IPR017198, IPR018117, IPR022702
NSC_01519	DNA-cytosine methyltransferase	IPR001525
NSC_00143	Hypothetical protein	IPR001025, IPR001357
NSC_06005	Meiosis expressed	IPR001025
NSC_00846	es43 protein	PR001025, IPR001965, IPR011011, IPR013083, IPR019786, IPR019787
NSC_03065	Chromodomain-helicase-DNA-binding protein	IPR000330, IPR000953, IPR001650, IPR014001, IPR016197, IPR023780
NSC_05938	Ankyrin repeat domain	IPR000953, IPR002110, IPR016197, IPR020683, IPR023780
NSC_03492	Elongation factor ef-3	IPR003439, IPR003593, IPR011989, IPR015688, IPR016024, IPR017871, IPR021133, IPR023780
NSC_00815	Arid bright DNA binding domain protein	IPR001487, IPR001606, IPR022702

The IPR domains associated with genes of interest (Name and ID) in the *P. soloecismus* genome are provided.

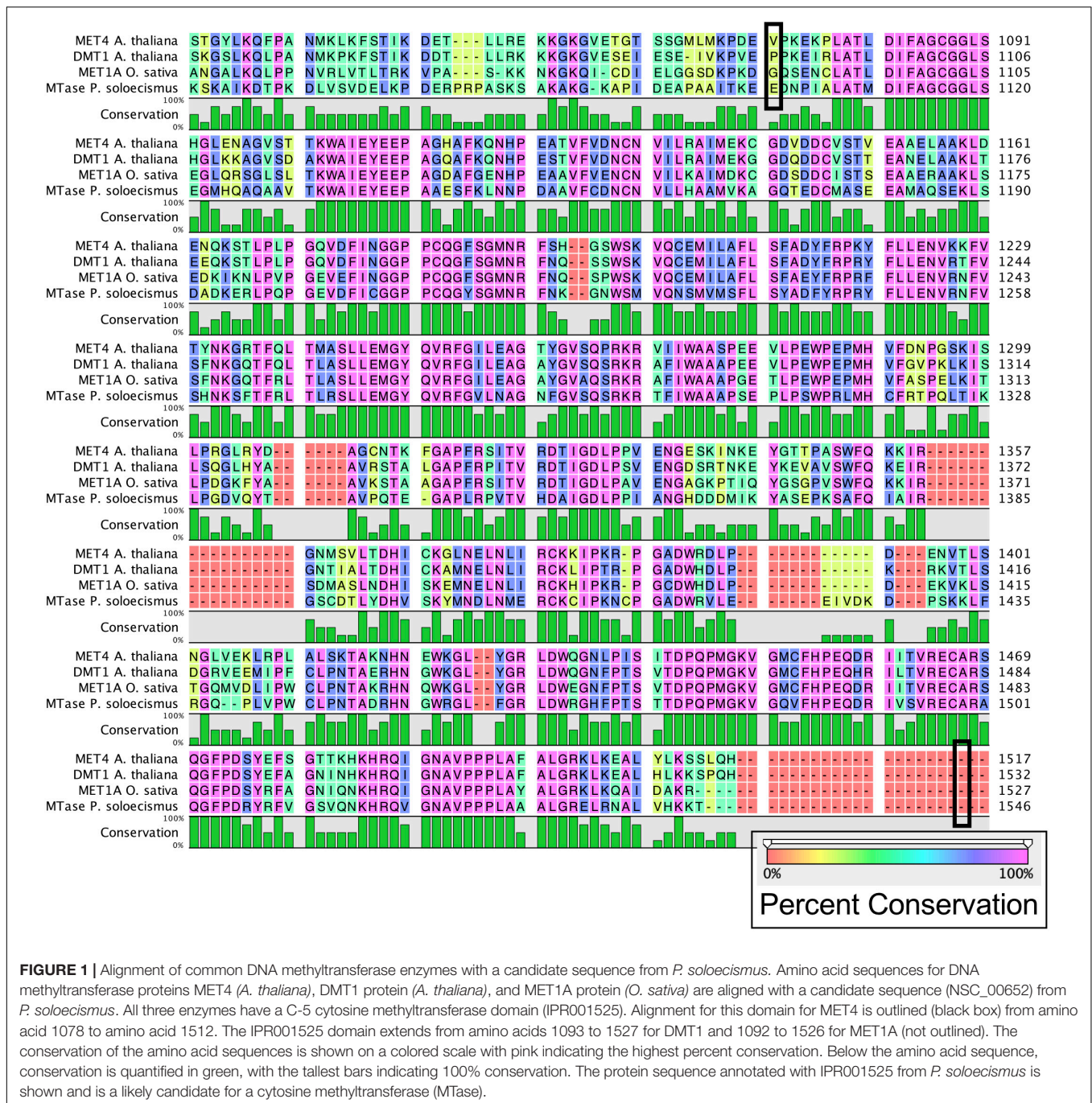
TABLE 1B | Epigenetic machinery domains of interest for 5mC DNA methylation and hits within the *P. soloecismus* genome.

Domain	Name	Hits	Function
IPR001025	BAH_dom	3	Protein-protein interaction module specialized in gene silencing
IPR001091	RM_Methylase	0	Site-specific DNA-methyltransferase, N-6 adenine-specific DNA methylase and cytosine-N4-specific
IPR001525	C5_MeTfrase	2	Methylates the C-5 carbon of cytosines in DNA
IPR002941	DNA_methylase_N4/N6	2	Family contains both N-4 cytosine-specific DNA methylases and N-6 Adenine-specific DNA methylases
IPR015270	RDM1_plant	0	Small protein that binds single-stranded methylated DNA; co-localizes with RNA polymerase II, AGO4 and DRM2 in the nucleus
IPR017198	DNMT1-like	1	Methylates CpG residues with a preference for hemimethylated DNA
IPR017985	MeTfrase_CN4_CS	0	Methylates the amino group at the C-4 position of cytosines in DNA
IPR018117	C5_DNA_meth_AS	1	Methylates the C-5 carbon of cytosines in DNA
IPR022702	Cytosine_MeTfrase1_RFD	2	Part of DNA (cytosine-5)-methyltransferase 1 that targets the protein towards replication foci
IPR023780	Chromo_domain	3	Conserved region of around 60 amino acids; condenses morphology of heterochromatin
IPR025794	Hist-Lys_N-MeTfrase_plant	0	Silencing mechanism; interacts with DNA CpNpG methylation requires the targeting of chromomethylase CMT3 to methylated histone
IPR029063	SAM-dependent_MTases	0	Transfer a methyl group from a donor (S-adenosyl methionine) to an acceptor
IPR030380	SAM_MeTfrase_DRM	0	Domains Rearranged Methylases (DRM1 and DRM2) are <i>de novo</i> cytosine methyltransferases from plants involved in the initial methylation of unmethylated DNA sequences
IPR030486	DNMT3L	0	Inactive regulatory factor of <i>de novo</i> DNA methyltransferases DNMT3A and DNMT3AB
IPR030487	C5_MeTfrase	0	Propagates methylation patterns with DNMT3B stimulating DNMT3A activity by promoting its association with nucleosomes
IPR030488	DNMT3B_ADD	0	ADD domain of DNMT3B
IPR033375	Cggbp1	0	A repetitive DNA-binding transcription regulator with target sites at CpG-rich sequences such as CGG repeats and Alu-SINEs and L1-LINES
IPR036319	RDM1_sf	0	Superfamily includes protein RDM1 from <i>Arabidopsis thaliana</i>
IPR040175	TET1/2/3	0	Converts 5-methylcytosine to 5-hydroxymethylcytosine
PF00145	DNA methylase	0	Methylates the C-5 carbon of cytosines in DNA
PF00385	Chromo	0	Conserved region of 60 amino acids; condenses morphology of heterochromatin
PF01426	BAH	0	Protein-protein interaction module specialized in gene silencing; commonly found in chromatin-associated proteins including eukaryotic DNA (cytosine-5) methyltransferases and recognition complex 1 (Orc1) proteins
PF02182	SAD_SRA	0	Binds hemi-methylated CpG dinucleotides and other 5mC containing dinucleotides
PF09187	RDM1_plant	0	Family of plant proteins includes RDM1 from <i>Arabidopsis thaliana</i> ; a component of the RNA-directed DNA methylation (RdDM) effector complex
PS51058	ZF_CXXC	0	Binds specifically to non-methylated CpG DNA; sequence found in mammalian DNMT1, MBD1, and MLL1

IPR domain names and numbers involved in DNA methylation are listed; the number of hits per IPR domain found in the *P. soloecismus* genome is provided along with the function of the domain.

bodies, promoters, terminators, and intergenic regions. For CpG sites, there were, on average, 4.95 sites per kb for gene bodies, 5.83 sites per kb for promoters, 6.39 sites per kb for terminators,

and 5.86 sites per kb for intergenic regions. Given that gene bodies are larger than most other features, there were more CpG sites of methylation found in genes; however, per kb,



terminators had the most CpG sites (Figure 2B). The distribution of methylation in all contexts is bimodal (Figures 2C–E). Of the 699,653 called CpG sites on Day 4 in the first control sample (Supplementary Table 1), approximately 7% (48667) sites were largely methylated (>0.8 methylation ratio), and approximately 83% of sites were largely unmethylated (<0.2 methylation ratio). Approximately 2% of sites had moderate methylation (0.4–0.6). This finding correlated with the global methylation analysis indicating that 12.3% of CpG called sites for Day 4 had some methylation. Of that 12.3%, most sites were

largely methylated (Figure 2C). Validation of called CpG sites resulted in other called CHG and CHH sites, which showed a bimodal distribution of methylation as well. Thus, while there were very few methylated CHG and CHH sites, the degree of methylation at those sites was large.

Changes in global and site-specific DNA methylation of *P. soleocismus* across its growth cycle were determined from the WGBS data. Global CpG DNA methylation decreased (hypomethylation) across the growth cycle (Figure 2F), with significant differences between early days (nitrogen replete) in the

TABLE 2 | Metrics for global and site-specific DNA 5mC methylation from whole genome bisulfite sequencing.

	Sequencing metrics				Median coverage of all sites			Called sites			Methylation fraction		
	Read pairs	Mapping efficiency	Unique CpGs	Coverage	CpG	CHG	CHH	CpG	CHG	CHH	CpG	CHG	CHH
Day 4 Control 1	41,023,876	75%	972,932	73	62	57	40	944940	1228396	3846923	0.123	0.008	0.009
Day 4 Control 2	33,648,831	77%	973,618	63	81	78	59	942047	1223285	3817927	0.122	0.006	0.007
Day 4 Control 3	29,579,086	76%	973,104	53	44	41	28	928325	1202508	3674044	0.121	0.005	0.007
Day 5 Control 1	25,654,725	77%	973,344	54	47	45	33	937428	1219080	3780033	0.123	0.008	0.010
Day 5 Control 2	29,937,985	79%	971,660	54	44	40	26	910613	1176724	3483664	0.126	0.005	0.007
Day 5 Control 3	45,111,988	77%	975,224	92	52	48	33	964233	1257465	4098185	0.123	0.010	0.013
Day 6 Control 1	36,639,600	80%	973,029	69	58	54	37	938805	1219379	3782740	0.123	0.005	0.007
Day 6 Control 2	40,794,105	74%	972,768	74	63	59	41	943226	1226052	3830516	0.122	0.007	0.009
Day 6 Control 3	29,191,188	74%	972,574	52	43	40	26	916792	1186033	3549572	0.123	0.006	0.007
Day 7 Control 1	33,885,815	77%	972,102	61	52	47	33	934725	1212452	3731159	0.123	0.007	0.009
Day 7 Control 2	40,610,069	72%	972,679	66	54	49	35	941356	1221066	3827818	0.120	0.007	0.008
Day 7 Control 3	26,226,738	77%	972,111	50	44	41	30	931596	1209022	3711732	0.119	0.007	0.008
Day 10 Control 1	44,523,335	72%	972,336	77	65	60	41	942568	1224561	3816369	0.119	0.008	0.009
Day 10 Control 2	31,106,461	73%	972,473	55	48	44	32	937025	1216470	3783515	0.115	0.008	0.009
Day 10 Control 3	31,278,928	71%	976,178	63	57	56	45	965823	1260295	4140910	0.117	0.011	0.013
Day 4 AZA 1	35,175,861	78%	974,284	68	58	54	39	953024	1240912	3971269	0.121	0.005	0.007
Day 4 AZA 2	25,810,214	80%	979,296	72	68	67	62	972892	1269534	4252504	0.119	0.017	0.018
Day 4 AZA 3	51,025,989	81%	973,858	103	53	49	34	956954	1247256	3995715	0.124	0.009	0.011
Day 5 AZA 1	23,711,109	77%	974,016	50	44	42	31	934472	1215456	3753189	0.122	0.009	0.011
Day 5 AZA 2	38,010,117	80%	976,674	88	81	79	65	970660	1266406	4206109	0.119	0.010	0.012
Day 5 AZA 3	24,571,651	78%	972,998	59	49	46	33	927143	1204554	3706979	0.129	0.009	0.010
Day 6 AZA 1	32,609,015	78%	973,530	62	46	43	29	935134	1213880	3753222	0.121	0.005	0.007
Day 6 AZA 2	36,869,188	78%	974,719	75	69	66	51	963066	1255704	4086914	0.119	0.009	0.010
Day 6 AZA 3	26,727,193	80%	974,765	59	53	51	40	955764	1245567	3991086	0.122	0.011	0.014
Day 7 AZA 1	37,076,497	78%	972,230	68	48	44	30	939065	1218808	3778410	0.120	0.007	0.008
Day 7 AZA 2	27,862,914	81%	973,613	54	46	43	29	934476	1212377	3747479	0.118	0.005	0.006
Day 7 AZA 3	32,739,443	80%	973,978	64	54	50	35	945266	1229569	3875733	0.120	0.005	0.007
Day 10 AZA 1	32,085,678	77%	974,843	77	66	63	46	950340	1237985	3940037	0.124	0.009	0.011
Day 10 AZA 2	31,462,613	79%	973,459	58	88	84	58	931975	1208968	3716882	0.121	0.006	0.007
Day 10 AZA 3	25,019,781	80%	972,153	47	39	36	24	908946	1173978	3481932	0.119	0.005	0.006

WGBS was performed for *P. soloecismus* untreated (control) and treated (5-aza-2'-deoxycytidine, 5AZA) cultures over five days in triplicate. The read pairs, mapping efficiency, unique CpGs identified, and sequencing coverage per sample are provided. The median coverage per cytosine context is provided, along with the number of called sites and the average methylation fraction per context, per sample, per day in culture.

time course (Days 4, 5, 6) and late (nitrogen deplete) in the time course (Day 10) ($p < 0.05$). No significant changes in global DNA methylation in the CHG and CHH contexts across the growth cycle were observed (Figures 2G,H). All Supplementary Tables can be found on FigShare (see text footnote 3).

Site Specific DNA Methylation Characteristics of *P. soloecismus*

To determine site specific hyper or hypomethylation across the time course, WGBS data was trimmed according to significant differences ($p < 0.01$) between Day 4 and Day 10 in culture for control cultures. Methylation differences between -0.1 and 0.1 were not considered in this analysis. Called sites were validated for cytosine context, some of which were CHH and CHG sites and removed from the analysis. There were 1102 significantly hypomethylated sites from Day 4 to

Day 10 in culture with methylation differences ranging from $-0.36 > x > -0.1$ (Supplementary Table 2). There were 41 significantly hypermethylated sites from Day 4 to Day 10 in culture with methylation differences ranging from $0.19 > x > 0.1$ (Supplementary Table 3). These sites were annotated and assigned KEGG orthologies, which were in turn, mapped to KEGG Pathways to determine the most impacted metabolic processes (also shown in the tables) using LANL in house software (Kanehisa et al., 2016a).

There were two main features of the sites that became hypomethylated across the *P. soloecismus* growth cycle. First, most sites were largely methylated (average methylation ratio was 0.72) and became hypomethylated but not completely demethylated (average methylation ratio was 0.58 by Day 10 in culture). Very few sites started with low methylation and became even less methylated, though there were some sites

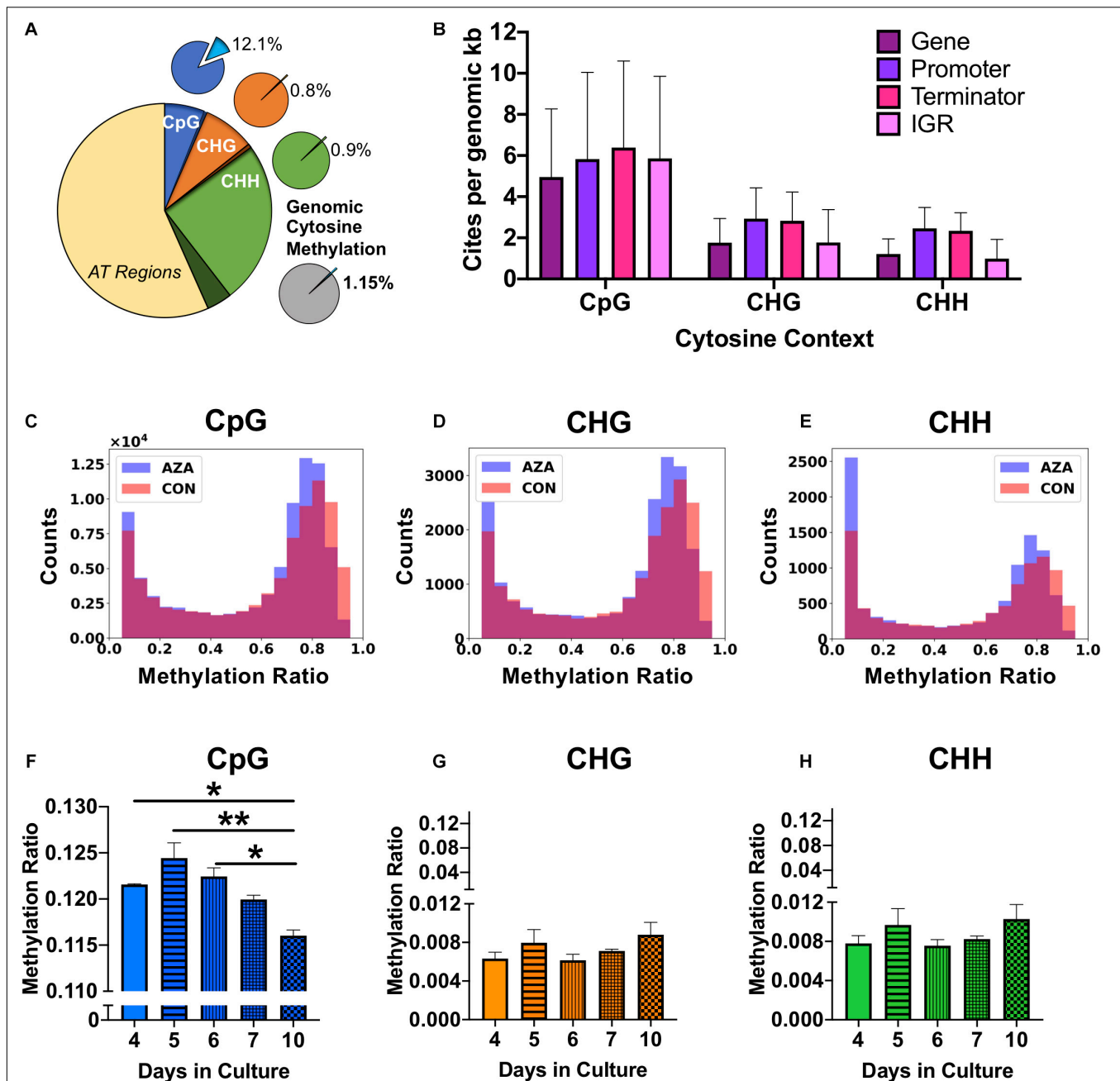


FIGURE 2 | Genomic DNA methylation characteristics of *P. soloecismus*. **(A)** Graphical representation of genomic cytosine methylation in *P. soloecismus*. The larger circle depicts the *P. soloecismus* genome of 15.6 MB nucleic acids with AT content of 66% and GC content of 44%. The total number of CpG sites is shown in dark blue (1,014,486 sites) with called sites shown in lighter blue and labeled as CpG (94,195,597 sites). This constitutes approximately 93% of total CpG sites in the genome. The same quantification is presented for CHG (in orange) and CHH (in green), where 93% and 87% of sites were called, respectively. Of those called sites for CpG, the average methylation ratio is 0.121 or 12.1% (light blue slice of smaller pie). The average methylation ratio for CHG is 0.08% (orange) and for CHH is 0.09% (green). The gray circle depicts the sum total of 1.15% cytosine methylation with the majority derived from the CpG context (blue). **(B)** 5mC DNA methylation can be found in four features of the *P. soloecismus* genome: gene bodies, promoters, terminators, or intergenic regions (IGR). The number of sites per genomic kb for each of these four features in all three cytosine contexts is shown. Data is presented as mean \pm SD (standard deviation). Representative histograms showing the distribution of 5mC DNA methylation in *P. soloecismus* for **(C)** CpG, **(D)** CHG, and **(E)** CHH cytosine contexts. Control samples are shown in orange, 5AZA samples are shown in purple, and the overlap is shown in magenta. The number of sites for each methylation ratio is shown in 0.1 bins. Given the low percentage of genomic methylation for *P. soloecismus*, sites from bin 0 to 0.05 were removed as most cytosines are unmethylated. **(F)** Global methylation ratios for CpG sites across the growth cycle of *P. soloecismus* as determined by WGBS. Tukey *post hoc* correction was performed for Student's *t*-tests; the significance of those *post hoc* assessments is shown between days 4, 5, and 6 compared with day 10 in culture. **(G)** Global methylation ratios for CHG sites and **(H)** CHH sites across the growth cycle of *P. soloecismus* as determined by WGBS. No significant differences in global methylation across the growth cycle for CHG and CHH sites were found. Data are presented as mean \pm SEM (standard error of the mean). * $p < 0.05$ and ** $p < 0.01$.

with moderate methylation that became hypomethylated. This pattern can be seen in the top 100 sites with the greatest change in methylation ratio (Figure 3, $p < 0.01$). The third most significantly hypomethylated site was annotated as acetyl CoA synthetase, an important protein involved in lipid synthesis (Figure 3). The 1102 significantly hypomethylated sites were mapped to specific metabolic pathways deemed important for algal biofuel species (Figure 4). Of note, several sites aligned with genes involved in the cell cycle, fatty acid synthesis, amino acid metabolism, glycolysis, gluconeogenesis, MAPK signaling,

and photosynthesis. Other significantly hypomethylated sites were annotated to genes involved in ribosome formation, RNA synthesis, splicing, transport, and degradation (Supplementary Table 4). All Supplementary Tables can be found on FigShare (see text footnote 3).

DNA Replication in *P. soloecismus*

Modifications to the epigenome of an organism can be induced by altering the expression and function of epigenetic machinery within the cell using drugs such as 5AZA. To determine the

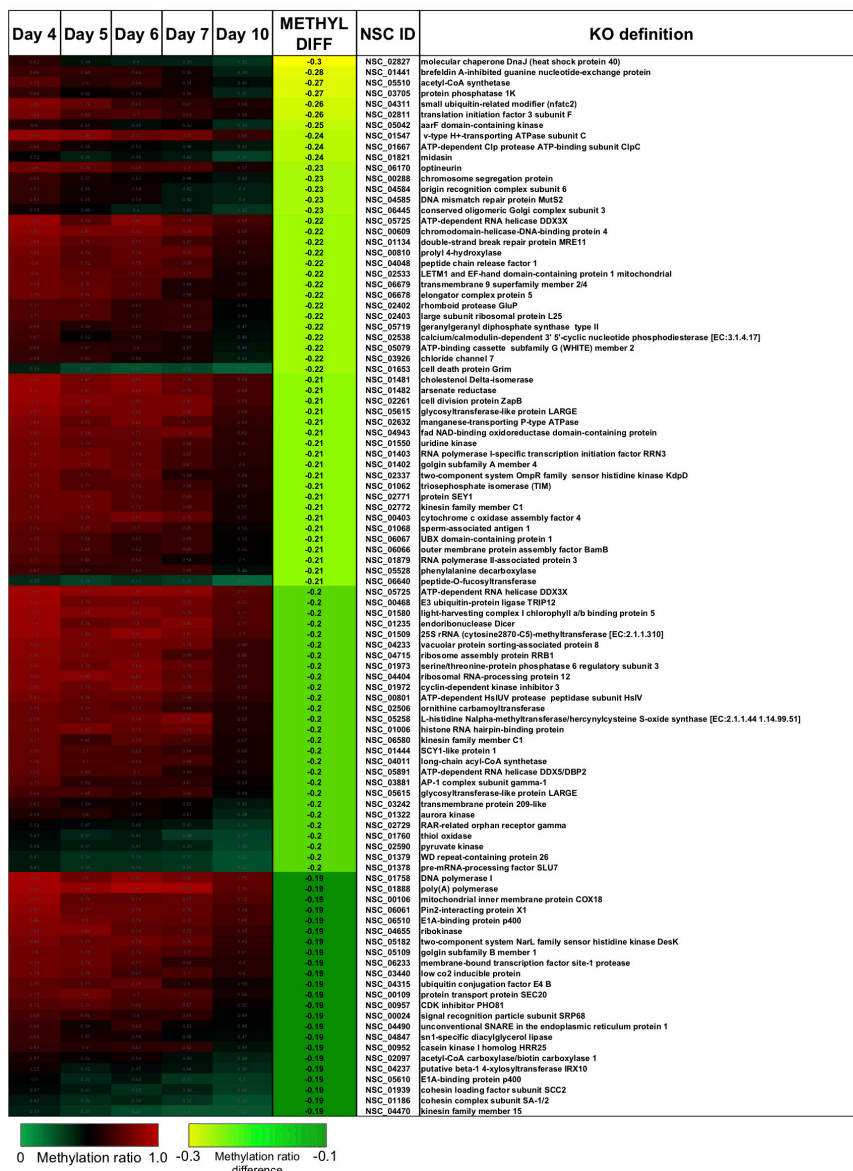


FIGURE 3 | The top 100 CpG sites that became significantly hypomethylated across the growth cycle of *P. soloecismus*. The top 100 annotated sites with the greatest change in methylation ratio across the growth cycle from Day 4 to Day 10 are listed ($p < 0.01$ for all sites). The greatest change in methylation ratio (-0.3) is shown under the column METHYL DIFF in yellow; change in methylation ratio decreases in absolute value down the column (dark green). Sites are largely methylated (red) and become less methylated (darker, black). Few sites have lower methylation (lighter green) and become less methylated over time (darker green). Some sites start with moderate methylation (black) and become hypomethylated (green). Annotations (NSC_ID corresponding to the *P. soloecismus* genomic ID) and the KO (KEGG Orthologies, within E-24) definitions are provided.

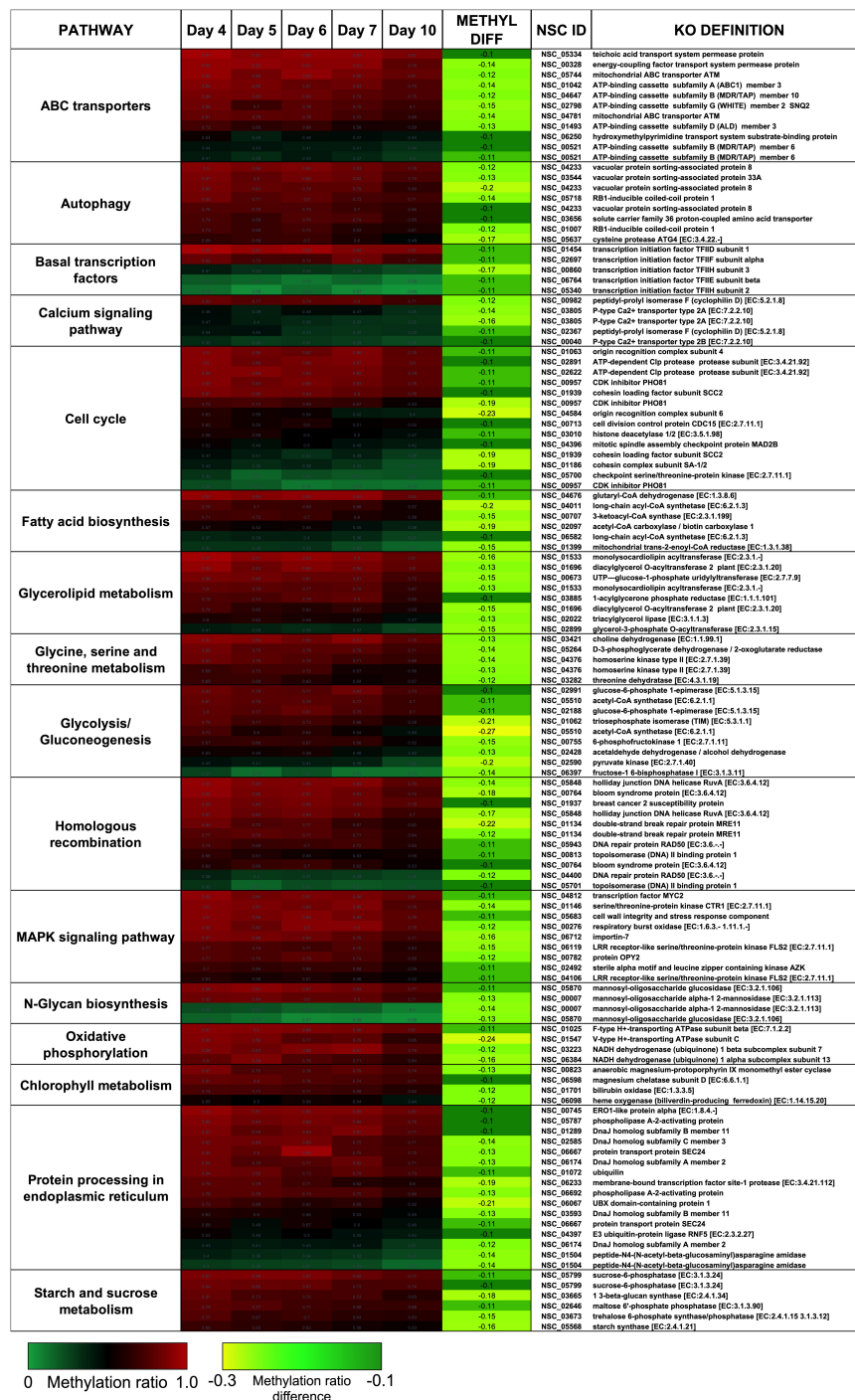


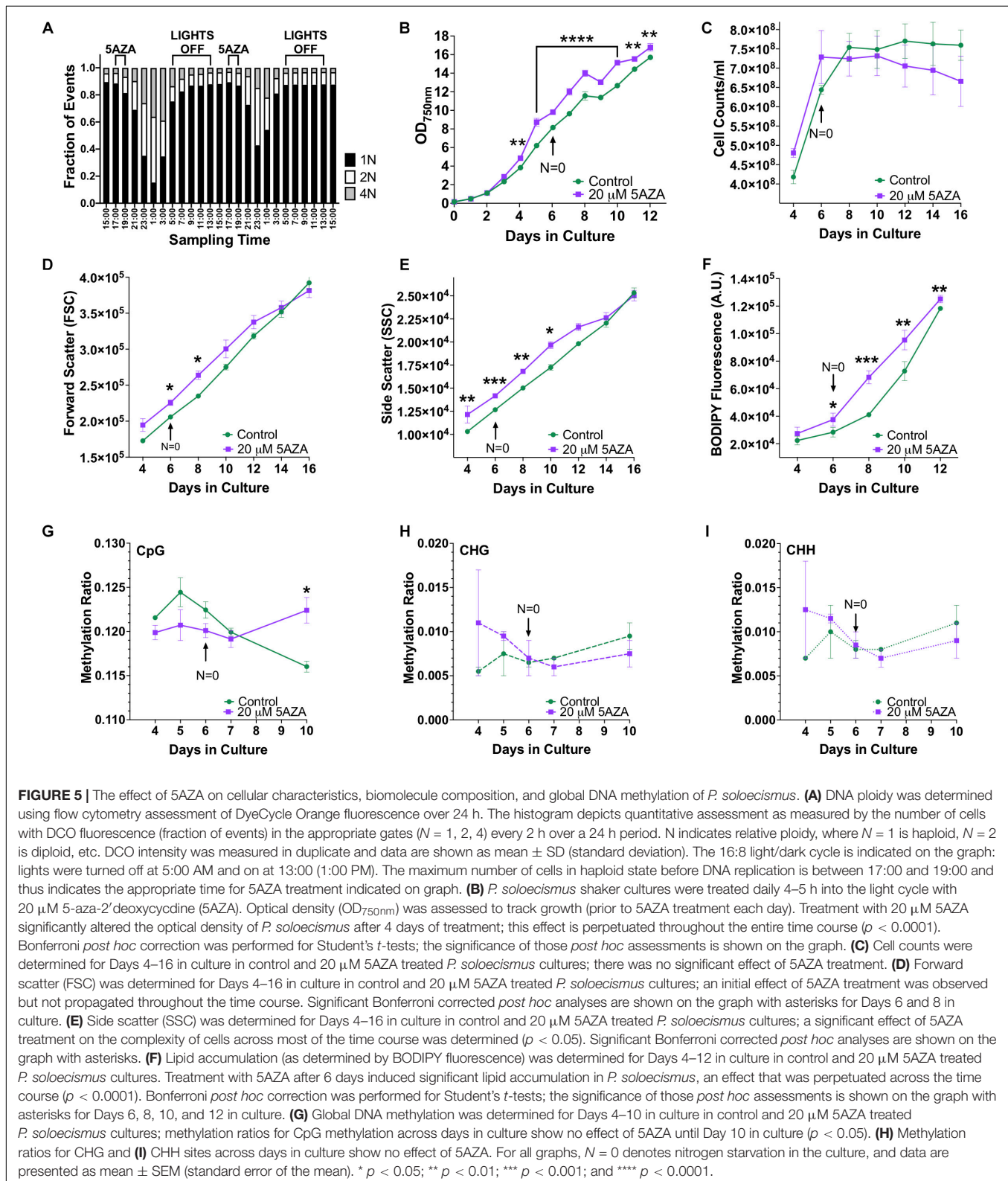
FIGURE 4 | CpG sites that became hypomethylated across the growth cycle of *P. soleocismus* belong to metabolic pathways important for algal biofuel characteristics. CpG sites from the 1102 most significantly hypomethylated sites are shown; these were chosen based on their annotations to specific metabolic pathways, and their role in lipid accumulation and the cell cycle. All pathways have sites with decreased methylation ratios across the time course (labeled as METHYL DIFF, derived from subtracting Day 4 methylation ratio from Day 10, shown as negative values). All methylation differences are significant ($p < 0.009$). Annotations (NSC_ID corresponding to the *P. soleocismus* genomic ID) and the KO (KEGG Orthologies, within E-24) definitions are provided.

optimal time of drug delivery, DNA ploidy of *P. soleocismus* was assessed every 2 h over a 48 h period. As previously described, *P. soleocismus* has a haploid genome; DNA populations are

denoted as $N = 1$, $N = 2$, and $N = 4$ in flow cytometry data (Gonzalez-Esquer et al., 2018; Steadman Tyler et al., 2019). The stable haploid population ($N = 1$) was present 3–5 h into the

light cycle (Figure 5A). The $N = 1$ population increased during the “dark” part of the diurnal cycle and had the greatest number of cells from 17:00–19:00 h, or 4–6 h into the light cycle. As

$N = 1$ population diminished, the $N = 2$ and $N = 4$ populations increased due to DNA replication. A large $N = 4$ population emerged 10 h into the light cycle (23:00). At 14 h into the



light cycle (3:00) the cells started to divide. Cell counts and forward scatter (FSC, indicative of cell size) were also determined for these time points. From these experiments, we determined introduction of 5AZA prior to DNA replication would induce the most efficacious phenotype. Thus, drug treatment occurred 4–5 h into the light cycle (between 17:00 and 18:00).

5AZA Treatment Altered Growth of *P. soloecismus*

Picochlorum soloecismus was cultivated in shaker flasks and optical density measurements were taken approximately 4–5 h into the light phase of growth every 24 h for 16 days. Algae were treated with 0–20 μ M 5AZA and the dose response was determined (Supplementary Figure 2). Drug treatment pharmacodynamics follow an inverted-U dose response with low and high concentrations of the same drug not eliciting a significant response (Tyler et al., 2018). We assessed 0–80 μ M of 5AZA treatment and found this inverted -U dose response (data not shown); 20 μ M 5AZA induced the most distinct growth response. The treatment effect of 20 μ M 5AZA was repeated with biological triplicates and appropriate controls. Optical density at 750 nm (OD₇₅₀) is an appropriate initial measurement of growth phenotype for *P. soloecismus*. We did not observe a decrease in OD₇₅₀ in response to drug treatment as expected; in fact, treatment with 20 μ M 5AZA increased the OD₇₅₀ (Figure 5B, $p < 0.0001$). The effect of 5AZA treatment became apparent (and significant) after 4 days of treatment in culture. Statistical analysis suggested a significant main effect of time in culture and treatment with 5AZA with a significant interaction between the factors ($p < 0.0001$) (All ANOVA statistical analyses, including F and p values are provide in Table 3). Nitrogen starvation occurred on Day 6 of culture (data not shown) and may have had a combined effect with 5AZA treatment. It is typical of all algae cultures to utilize available nitrogen for rapid growth, and thus, “nitrogen starvation” occurs later in cultivation (Sharma et al., 2012; Banerjee et al., 2017). Overall, treatment with 20 μ M 5AZA significantly altered the optical density of *P. soloecismus* after 4 days of treatment; this effect was perpetuated throughout the growth cycle (Figure 5B, $p < 0.0001$).

5AZA Treatment Altered Cellular Characteristics and Biomolecule Composition of *P. soloecismus*

Increased optical density of algae cells can result from a number of cellular and physiological changes. Cell counts, forward scatter (FSC, indicative of cell size), and side scatter (SSC, indicative of cell complexity) were assessed via flow cytometry (Figures 5C–E). Cell counts were not significantly impacted by 5ZA treatment (Figure 5C), though this lack of significance is likely due to the large variance in measurement. Both FSC and SSC were impacted by 5AZA treatment in similar ways: initially 5AZA significantly increased both FSC (Figure 5D, $p < 0.01$) and SSC (Figure 5E, $p < 0.001$) until Days 8 and 10, respectively, but this effect was abrogated as the days in culture increase. In other studies of microalgae cultivation, lack of change in cell counts accompanied by an increase optical density, FSC,

and SSC suggests altered cellular composition particularly of biomolecules like neutral lipids (Bono et al., 2015; Gonzalez-Esquer et al., 2019; Steadman Tyler et al., 2019). Using a BODIPY fluorescent probe (Steadman Tyler et al., 2019), we found that lipid accumulation was significantly increased after 4 days of 5AZA treatment (Figure 5F). This increase remained apparent across the growth cycle of *P. soloecismus* ($p < 0.0001$). Every day in culture had significantly increased lipid accumulation in response to 5AZA (Figure 5F). While Day 4 showed a 22% increase in lipid accumulation, this was not significant as the coefficient of variance was 12.92 and 15.27 for the control and 5AZA treated cultures, respectively. This increased variance in measurement likely contributed to the lack of significance. Similarly, Day 12 showed a 5% increase in lipid accumulation, but the coefficient of variance was low for both control (0.72) and 5AZA treated cultures (1.98), providing statistical significance. 5AZA significantly increased lipid accumulation on Day 6 (32%), Day 8 (66%), and Day 10 (31%) all of which had nominal coefficients of variance (CoV < 1%) (All ANOVA statistical analyses, including F and p values are provide in Table 3).

The Effect of 5AZA Treatment on DNA Methylation in *P. soloecismus*

Whole genome bisulfite sequencing was performed on samples treated with 5AZA across the time course (Days 4, 5, 6, 7, and 10 in culture). There was no change in total global methylation for any cytosine context (CpG, CHH, and CHG) in response to 5AZA treatment except on CpG sites on the last day assessed (Day 10, $p < 0.05$ for CpG) (Figures 5G–I). The methylation ratios across all called sites for each day in culture for all three replicates were averaged for these calculations.

Treatment with 5AZA did not impact the percent of global DNA methylation for the entire *P. soloecismus* genome. Yet, for specific sites, 5AZA treatment induced hypomethylation and hypermethylation (Figures 6A,B). Differences in methylation ratios were determined for each day comparing control versus 5AZA treated cultures. The most significant differences ($p < 0.05$) were kept, and sites with methylation ratio differences in the $-0.1 < x < 0.1$ range were trimmed from the analysis (as performed in all analyses). Called sites were validated for context and annotated (see methods). By Day 4 in culture, 855 sites were hypomethylated and 407 sites were hypermethylated in response to 5AZA treatment (Figure 6A). The most significant impact of 5AZA treatment occurred on Day 10 in culture: 2255 sites were hypermethylated and 161 sites were hypomethylated (Figure 6A). Given that mitosis does not occur after Day 6 in culture, this effect is likely due to the lack of efficacy of the 5AZA drug, which begins on Day 7 with 607 sites of hypermethylation. Days 4, 6, and 10 had the most significant effect of 5AZA coinciding with the most physiologically relevant days in culture (Figures 5F, 6A). All sites with significant methylation ratio differences (hyper and hypomethylation) are provided in Supplementary Tables 5–9 for all days in culture; these sites are also annotated. A subset of hypomethylated CpG sites (~190) in response to nitrogen starvation had significantly differential methylation in response to 5AZA treatment on Day 4

TABLE 3 | F and *p*-values for ANOVA statistical analyses.

Assessment	Main effect of time in culture (Factor 1)	Main effect of 5AZA treatment (Factor 2)	Interaction between factors	Post-hoc Analyses
Effect of time on CpG methylation ratios (Figure 2F) 1-way ANOVA repeated measures	$F(4,5) = 11.98$ $p = 0.0089$	No AZA treatment	N/A	Tukey corrected <i>post hoc</i> : Day 4 to Day 10: $p < 0.05$ Day 5 to Day 10: $p < 0.01$ Day 6 to Day 10: $p < 0.05$
Effect of 5AZA on optical density (Figure 5B) 2-way ANOVA repeated measures	$F(12,120) = 2868$ $p < 0.0001$	$F(1,10) = 34.88$ $p < 0.0001$	$F(12,120) = 19.88$ $p < 0.0001$	Bonferroni corrected <i>post-hoc</i> : Days 4, 10, 11: $p < 0.01$ Days 5-10: $p < 0.0001$
Effect of 5AZA on cell counts (Figure 5C) 2-way ANOVA repeated measures	$F(6,48) = 45.25$ $p < 0.0001$	$F(1,9) = 0.02904$ ns	$F(6,48) = 2.778$ $p < 0.05$	Bonferroni corrected <i>post-hoc</i> : ns
Effect of 5AZA on forward scatter (FSC) (Figure 5D) 2-way ANOVA repeated measures mixed effects	$F(2.482,24.21) = 431.1$ $p < 0.0001$ Geisser-Greenhouse's epsilon 0.4137	$F(1,10) = 4.083$ ns	$F(6,59) = 3.721$ $p < 0.01$	Bonferroni corrected <i>post-hoc</i> : Day 6, 8: $p < 0.05$
Effect of 5AZA on side scatter (SSC) (Figure 5E) 2-way ANOVA repeated measures mixed effects	$F(2.205,21.31) = 521.0$ $p < 0.0001$ Geisser-Greenhouse's epsilon 0.3675	$F(1,10) = 9.694$ $p < 0.05$	$F(6,58) = 4.458$ $p < 0.001$	Bonferroni corrected <i>post-hoc</i> : Days 4 and 8: $p < 0.01$ Day 5: $p < 0.001$ Day 10: $p < 0.05$
Effect of 5AZA on lipid accumulation (Figure 5F) 2-way ANOVA repeated measures	$F(1.138,11.38) = 784.5$, $p < 0.0001$	$F(1,10) = 3677$ $p < 0.0001$	$F(4, 40) = 12.49$ $p < 0.0001$	Bonferroni corrected <i>post-hoc</i> : Day 6: $p < 0.05$ Day 8: $p < 0.001$ Days 10 and 12: $p < 0.01$

All ANOVA statistical analyses for each type of assessment is provided. The *F* and *p*-values for the main effect of time in culture, the main effect of treatment in culture, the factors' interaction, and any post-hoc analyses are listed.

of the time course (Figure 6C, $p < 0.05$). The methylation ratios for the following days in culture, starting on Day 5 for control cultures, were more similar (closer in color) to the 5AZA-treated culture on Day 4. Thus, 5AZA-induced hypomethylation early in treatment was similar to the hypomethylation that occurred across the growth cycle in response to nitrogen starvation (Figure 6C). This trend suggests that the 5AZA simply shifted the hypomethylation status of specific sites sooner than would normally occur during nitrogen starvation. For sites that were significantly hypomethylated during the growth cycle that were mapped to metabolic pathways deemed important for algal biofuel species (Figure 4), the pattern was not as clear. These sites were either not impacted by 5AZA or were hypomethylated early after 5AZA treatment (Day 4); many of these sites became hypermethylated after several days of 5AZA treatment (Day 10) (Figure 7).

Interestingly, there was a subset of sites where 5AZA induced significant hypomethylation on Day 4 and significant changes in methylation ratio on Day 10 (Figure 8, $p < 0.05$). For this analysis, sites with significant methylation differences between $-0.1 < x < 0.1$ were not considered unless either Day 4 or Day 10 fulfilled the criteria for selection. All of these sites became significantly hypomethylated across the time course without 5AZA treatment due to nitrogen starvation. Of note, a pattern emerged of significant hypomethylation on Day 4 followed by hypermethylation of the same site by Day 10 (Figure 8). The genes associated with these sites did not fall into a particular category. Of the 855 CpG sites that became hypomethylated on Day 4 by 5AZA, 283 of these sites remained hypomethylated with no significant change by Day 10 (Supplementary Figure 3).

There were several sites of cytosine methylation found within or near genes involved in epigenetic regulation. Some of these sites (CpG and CHG) became hypomethylated across the time course (Figure 9) and were impacted by 5AZA treatment; many of them became significantly hypermethylated in response to 5AZA treatment by Day 10 in culture. These sites included histone methyltransferases (MLL and SET proteins), histone acetyltransferases (MYST1), histone deacetylases (HDAC1/2), and chromatin remodeling proteins (SWI/SNF). To date, histone modifications have not been measured in *P. soloecismus*. However, this data suggests that this microalgae may use histone modifications for regulation and that these sites are themselves regulated by DNA methylation. All Supplementary Tables can be found on FigShare (see text footnote 3).

DISCUSSION

Approximately 40,000 species of microalgae have been reported, though some estimates are double (Khan et al., 2018). Many of these species have not been sequenced and even fewer have epigenome characterization. The handful of algal methylomes available do not show a distinctive pattern of DNA methylation; further, there is some disagreement on the amount and distribution of methylation within the same species (Hattman et al., 1978; Feng and Chiang, 1984; Cerutti, 1997; Wu-Scharf et al., 2000; Babinger et al., 2001, 2007; Jeong et al., 2002; Feng et al., 2010a; Zemach et al., 2010; Maumus et al., 2011; Veluchamy et al., 2014; Lopez et al., 2015). Collectively, the methylation

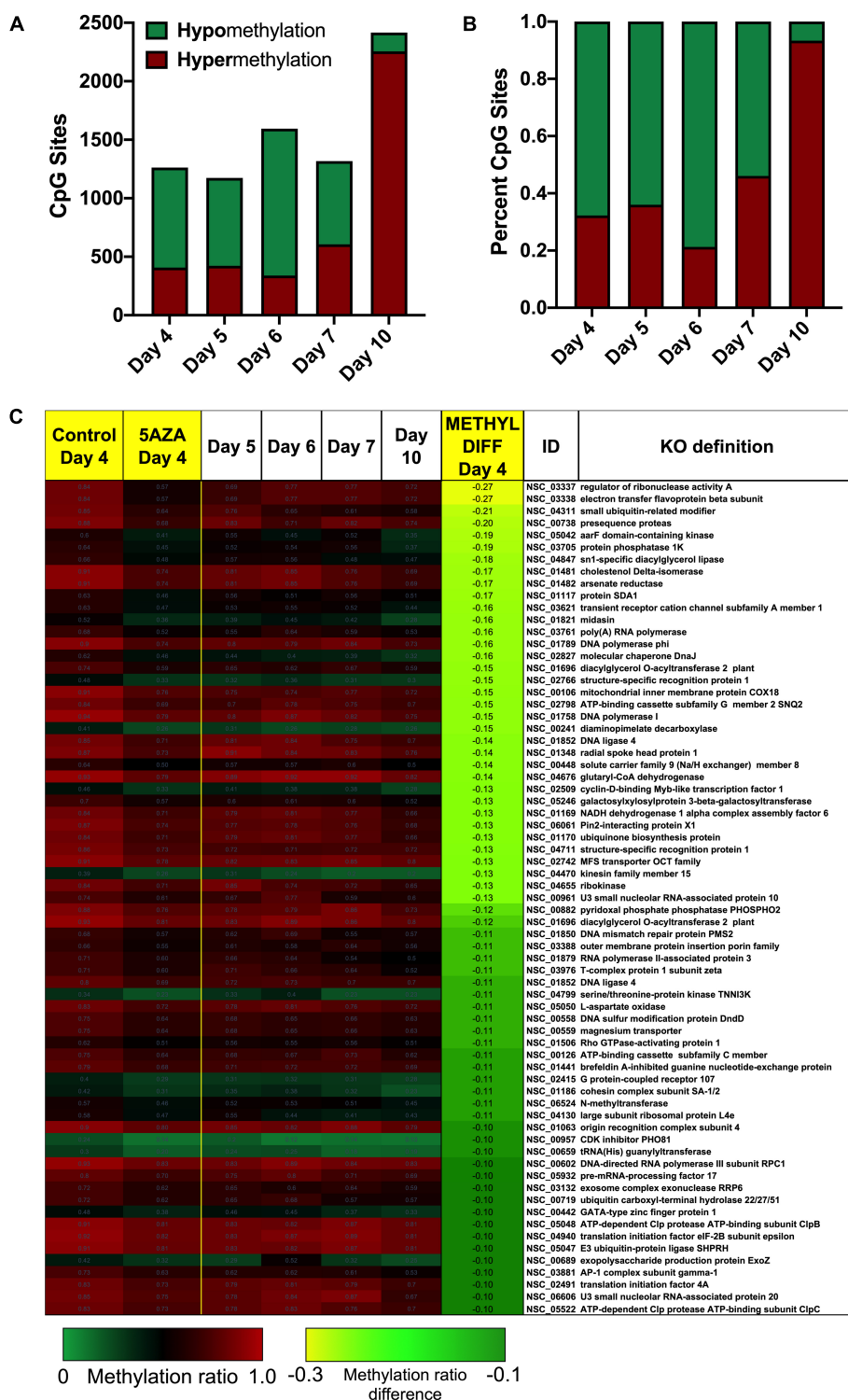
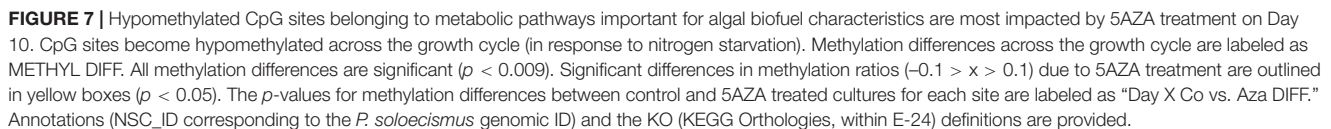


FIGURE 6 | Sites-specific changes in CpG methylation ratios due to 5AZA treatment. **(A)** The number of CpG sites with significantly altered methylation ratios after 5AZA treatment ($p < 0.05$) per day in culture are shown. **(B)** The percent of hypomethylated or hypermethylated sites normalized to total sites affected by 5AZA per day are shown. Green, hypomethylation; Red, hypermethylation **(C)** CpG sites in *P. soleocismus* that are significantly hypomethylated on Day 4 of 5AZA treatment are shown. Methylation ratios from control and 5AZA treated cultures on Day 4 are side by side, followed by methylation ratios for control cultures for Days 5–10, all of which are significantly hypomethylated. Methylation differences between control and 5AZA treated cultures on Day 4 are labeled as METHYL DIFF Day 4; all methylation differences are significant ($p < 0.05$). Annotations (NSC_ID corresponding to the *P. soleocismus* genomic ID) and the KO (KEGG Orthologies, within E-24) definitions are provided.



but quantifiable amount of global DNA methylation; (2) this methylation changes during the growth cycle of *P. soloecismus* in response to nitrogen starvation and 5AZA treatment, leading to the induction of lipids; and (3) CpG sites exhibit dynamic methylation in genes involved in fatty acid biosynthesis and the cell cycle. All three findings suggest that epigenetic regulation plays a key role in the growth and productivity of *P. soloecismus*.

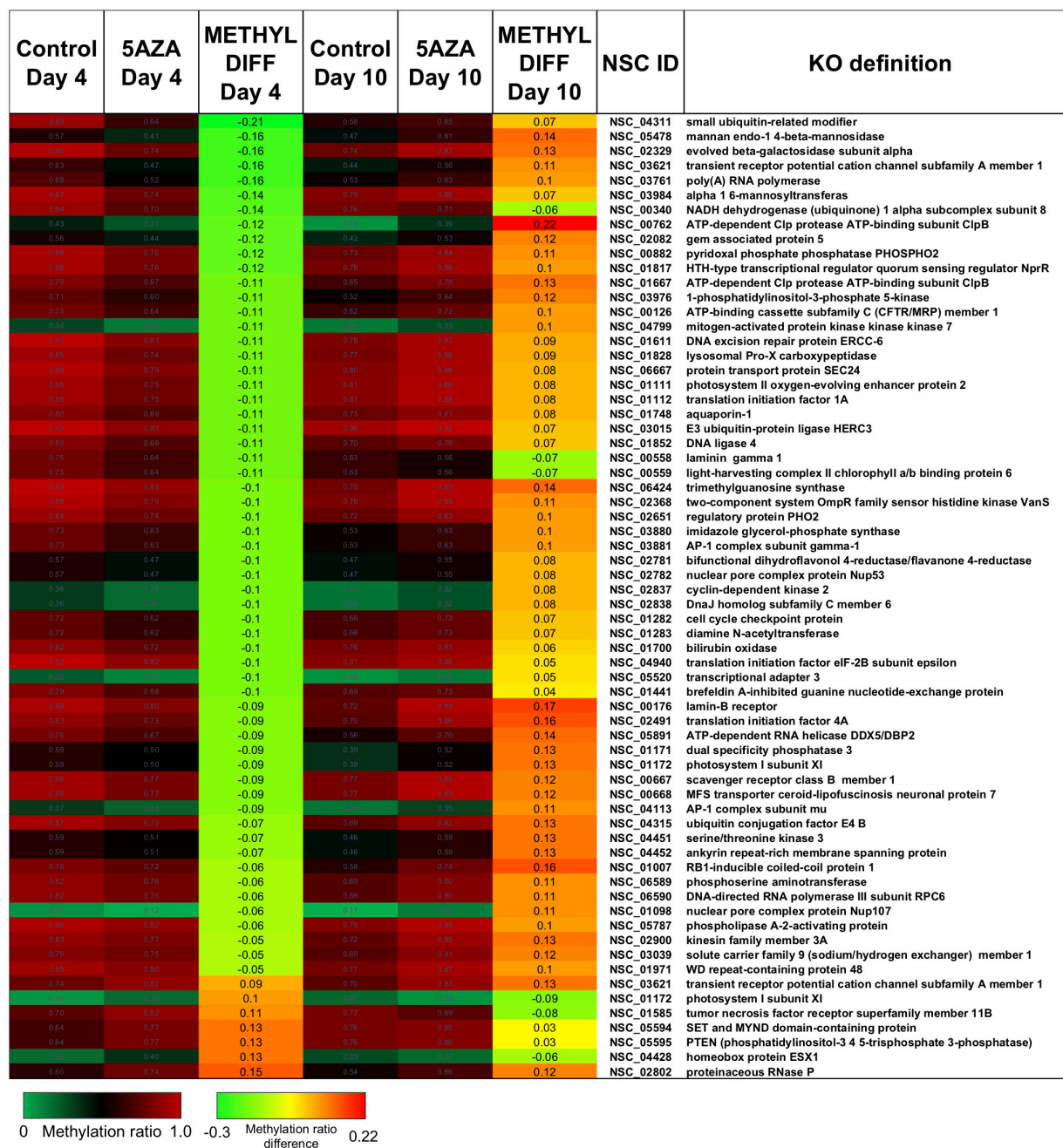


FIGURE 8 | The top CpG sites with significantly altered methylation ratios due to 5AZA treatment on Day 4 and Day 10. Average methylation ratios are shown for control and 5AZA treated cultures on Day 4 and Day 10. All methylation ratio differences between control and 5AZA treated cultures, labeled as METHYL DIFF Day 4 or Day 10, are significant ($p < 0.05$). Annotations (NSC_ID corresponding to the *P. solocismus* genomic ID) and the KO (KEGG Orthologies, within E-24) definitions are provided.

We determined the following features of DNA methylation in *P. solocismus*. First, the *P. solocismus* genome encodes for at least two putative DNA methyltransferases. Approximately 1.15% of the *P. solocismus* 15.2 MB genome contains some form of cytosine methylation. Contextually, this methylation occurs in a bimodal distribution predominately in (~12.1%) CpG sites, though there are some (<1%) CHH and CHG

sites of methylation. Methylated sites are found in all genomic features, though terminators have the most abundant CpG sites per kilobase of the genome. For context, DNA methylation in microalgae varies from less than 1% CpG methylation in *C. reinhardtii* (Lopez et al., 2015) and *Volvox carteri* (Babinger et al., 2007) to almost 80% CpG methylation in *Chlorella variabilis* NC64A (Zemach et al., 2010).

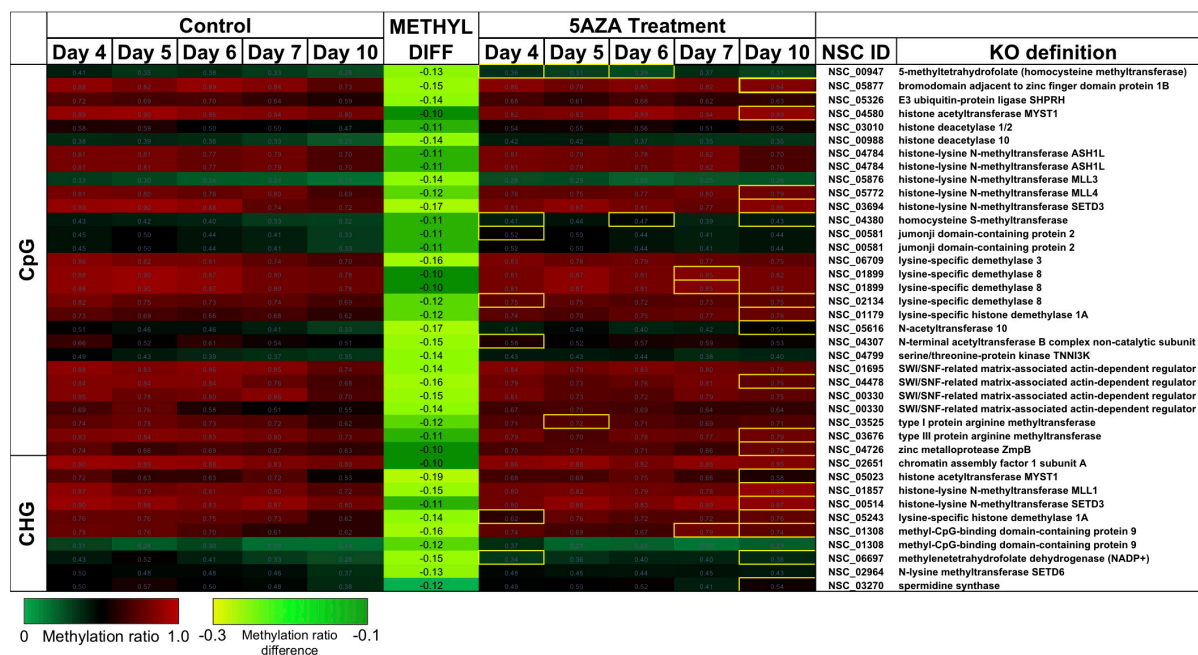


FIGURE 9 | CpG and CHG sites in *P. soloecismus* belonging to genes for chromatin modifying proteins with differential methylation ratios. Methylation ratios across the growth cycle (control) and in response to 5AZA treatment are shown for sites annotated to epigenetic machinery. Significant hypomethylation across the growth cycle (for controls) occurs for all sites shown (labeled as METHYL DIFF) ($p < 0.009$). Methylation ratios significantly altered by 5AZA are outlined in yellow with the majority of differences (hypermethylation) occurring on Day 10 of 5AZA treatment. These are calculated by subtracting the methylation ratios for a specific day in the controls from the 5AZA treated methylation ratios (i.e., methyl ratio Day 4 5AZA – methyl ratio Day 4 control). Annotations (NSC_ID corresponding to the *P. soloecismus* genomic ID) and the KO (KEGG Orthologies, within E-24) definitions are provided.

We found that DNA methylation in *P. soloecismus* is dynamic and responsive to the environment. Treatment of *P. soloecismus* gDNA with a methylase derived from *Escherichia coli* increased global DNA methylation, suggesting sites of methylation are responsive to perturbation. Global hypomethylation on CpG sites occurred across the growth cycle of *P. soloecismus*, potentially in response to nitrogen starvation, with the greatest impact occurring by Day 10 in culture under severe nitrogen depletion conditions. We have previously observed that during nitrogen starvation, *P. soloecismus* ceases dividing and accumulates lipids in response to this stress. Several of the hypomethylated CpG sites are annotated as genes in pathways involved in lipid biosynthesis, including acetyl-CoA synthetase, long-chain acyl-CoA synthetase, 3-ketoacyl-CoA synthetase, acetyl-CoA carboxylase, and glutaryl-CoA dehydrogenase. Acyl-CoA synthetases have been shown to stimulate the release of lipids in *C. reinhardtii* (Jia et al., 2016), while acetyl-CoA production is associated with increased lipid accumulation in green algae (Avidan et al., 2015). The last step of lipid biosynthesis dependent on acyl-CoA is catalyzed by diacylglycerol acyltransferase (DGAT) (Wei et al., 2017); a CpG site within this gene (annotated as diacylglycerol O-acyltransferase 2) became hypomethylated across the growth cycle of *P. soloecismus* as well. Further, several CpG sites within genes involved in glycolysis and gluconeogenesis also became hypomethylated; the formation of glucose 6-phosphate eventually leads to the synthesis of pyruvate for fatty acid biosynthesis (Xue et al., 2017). This suggests

that DNA methylation plays a role in nitrogen responses in *P. soloecismus* and potentially regulates genes that are involved in stress responses and lipid accumulation.

To determine how important DNA methylation is for the survival of *P. soloecismus*, we employed the use of 5AZA in culture. Once inside a cell, 5AZA forms a covalent bond with the DNA methyltransferase (DNMT) enzyme during DNA replication and inhibits the DNMT from binding to the newly synthesized DNA. Maintenance DNA methylation from hemimethylated DNA on the lagging strand is impeded by the presence of 5AZA. Over the growth cycle, daughter cells generated during mitosis lose DNA methylation (Stresemann and Lyko, 2008). Previous studies have demonstrated significant DNA demethylation and cellular responses (including apoptosis and DNA damage) after 5AZA treatment in several cell types (Christman, 2002; Madlung et al., 2002; Chang and Pikaard, 2005; Akimoto et al., 2007; Karahoca and Momparler, 2013). We anticipated that 5AZA would exert similar effects on *P. soloecismus*.

We did not observe global changes in DNA methylation in response to daily 20 μ M 5AZA treatment: markedly, despite obvious differences in phenotype, it seemed that cytosine methylation was unaffected by the drug, except on Day 10 in culture when there was a striking increase in global methylation with drug treatment. Deeper analysis into site-specific changes in methylation ratios in response to 5AZA provided a clearer picture. 5AZA induced site-specific changes in DNA methylation

for each day in culture: most sites became hypomethylated early in treatment and then became hypermethylated after several days of treatment. Given that *P. soloecismus* eventually undergoes hypomethylation during its growth cycle (and lipid accumulation), it is possible that 5AZA simply induced hypomethylation early on these particular sites to drive the same phenotype. This early hypomethylation pattern due to 5AZA treatment occurred on several genes involved in lipid synthesis and the cell cycle, including on the CpG site within diacylglycerol O-acyltransferase 2. As many as 40% of sites became hypermethylated in response to 5AZA after several days of 5AZA treatment; however, this hypermethylation coincided with lack of cell division in *P. soloecismus* cultures. It is unlikely that 5AZA interfered with *de novo* methylation; thus, the reversal in the methylation pattern was likely due to lack of efficacy of 5AZA given that mitosis had ceased. A subset of genes involved in fatty acid synthesis and elongation have CpG sites and were hypomethylated by 5AZA treatment on Day 6. These included the very-long-chain enoyl-CoA reductase (TER), which catalyzes the last of the four reactions of the long-chain fatty acids elongation cycle; DGAT1, an enzyme that catalyzes the terminal and only committed step in triacylglycerol synthesis by using diacylglycerol and fatty acyl CoA as substrates; and phosphoglycolate phosphatase, which regulates the cellular levels of glycerol-3-phosphate (a metabolic intermediate of glucose) and thus lipid and energy metabolism (Mueller et al., 2017). Thus, while we did not observe global hypomethylation in response to 5AZA treatment, these site specific changes may have been sufficient to alter phenotype.

One of the more interesting findings in this study was the significant hypomethylation of CpG and CHG sites located within genes encoding for chromatin modifying enzymes. These included histone methyltransferase and demethylases, histone acetyltransferases and deacetylases, and the SWI/SNF chromatin remodeling complex. Histone modifications have yet to be measured in *P. soloecismus*; however, the data suggests that in addition to DNA methylation, *P. soloecismus* may use histone modifications. The enzymes responsible for histone modifications are themselves regulated by DNA methylation and responsive to environmental conditions during growth of this species. Indeed, 5AZA treatment altered the methylation ratios of many of these sites within chromatin modifying genes. Several studies demonstrate the importance of histone modifications in regulation of the life cycle and even lipid metabolism in *C. reinhardtii* (Waterborg et al., 1995; van Dijk et al., 2005; Casas-Mollano et al., 2007; Ngan et al., 2015). Our ongoing efforts in analyzing genomic regulation of *P. soloecismus* will explore these mechanisms as well.

In addition to altering methylation ratios on specific CpG sites, 5AZA treatment, remarkably, impacted the phenotype of *P. soloecismus* during the growth cycle. Significant increases in optical density, cell size, cell complexity, and accumulation of lipid biomolecules resulted from 5AZA treatment. 5AZA did not statistically impact cell proliferation, though the variance in this measurement was large. Given the limited number of studies on the effects of 5AZA in microalgae cultures (Xue et al., 2019), it is difficult to put these findings into context. To our knowledge this

is the first report of repeated treatments with 5AZA for any algae species. In microalgae cultivation, an increase in optical density, cell size, and cell complexity accompanied by a lack of cellular proliferation, suggests that cellular composition has changed. Using an established flow cytometry assay for assessing lipid content (Steadman Tyler et al., 2019), we measured a significant increase in lipids in the 5AZA treated cultures, beginning on Day 6 in culture. This increase was as much as 66% by Day 8 in culture. Lipid accumulation is a hallmark phenotype that algal researchers seek in selecting a biofuel platform species. Potentially, this finding has far reaching implications, suggesting that manipulation of DNA methylomes (and perhaps other epigenetic modifications) could drive microalgae phenotypes toward any desired feature, including lipid accumulation.

CONCLUSION

We sought to determine the role DNA methylation plays in regulating growth and lipid accumulation of *P. soloecismus*, a promising algal biofuel production species. We found genomic sequences for putative DNA methyltransferase enzymes, and initially measured low, but adaptable, 5mC levels. WGBS revealed that approximately 1.15% of the *P. soloecismus* genome contains cytosine methylation in all three contexts, localized to several genomic regions, with approximately 12.1% CpG methylation. The genome becomes hypomethylated across the algal growth cycle, suggesting that nutrient deprivation has an impact on epigenetic regulation of the *P. soloecismus* genome. DNA methylation was further altered by treatment with a DNA methyltransferase inhibitor, 5AZA, across the growth cycle. Hypomethylation of site-specific CpGs in genes involved in fatty acid synthesis and the cell cycle correlated with changes in phenotype, including larger cell size and complexity and accumulation of lipids. Potentially, DNA methylation regulates the cellular response to environmental stressors, such as nitrogen limitation, resulting in carbon sequestration into lipid biomolecules; deeper molecular investigation is needed to assess the validity of this assertion. This is the first report on manipulation of epigenetic mechanisms in algae for the purposes of enhanced biofuel production.

DATA AVAILABILITY STATEMENT

All datasets presented in this study are included in the article/Supplementary Material can be found on FigShare (see text footnote 3).

AUTHOR CONTRIBUTIONS

CSt, SB, CSa, BM, and ST conceived the research and designed the experiments. CSt, YK, and CSa performed the experiments. CSt and SB analyzed the data. CSt performed the statistical analysis and wrote the manuscript. SB, YK, CSa, BM, and ST critically revised and edited the manuscript. CSt, BM, and ST obtained the funding. All authors read and approved the final manuscript.

FUNDING

This work was supported by the Office of Energy Efficiency and Renewable Energy under contract from the Bioenergy Technologies Office (agreement number NL0026328).

SUPPLEMENTARY MATERIAL

The Supplementary Material for this article can be found at: <https://www.frontiersin.org/articles/10.3389/fgene.2020.560444/full#supplementary-material> and on FigShare at: https://figshare.com/authors/Christina_Steadman/8855753

SUPPLEMENTARY FIGURE 1 | Global DNA methylation of *P. soleocismus* determined by ELISA. *P. soleocismus* gDNA percent 5mC was determined using an antibody-based ELISA. *P. soleocismus* gDNA contains 0.82% 5mC content, while *P. soleocismus* gDNA treated for 12 h with CpG methylase has 1.3% 5mC content ($p < 0.0001$); comparison done using Student's *t*-test. Data are presented as mean \pm SEM (standard error of the mean).

SUPPLEMENTARY FIGURE 2 | Dose response of *P. soleocismus* after treatment with 5AZA. *P. soleocismus* shaker cultures were treated daily 4–5 h into the light cycle with 0, 5, 10, and 20 μ M 5-aza-2'-deoxycytidine (5AZA). Prior to treatment each day, optical density (OD_{750nm}) was assessed to track growth. 20 μ M 5AZA induced the greatest change in optical density of the cultures after 4 days of treatment.

SUPPLEMENTARY FIGURE 3 | Top CpG sites with the largest methylation ratio differences between control and 5AZA treated cultures on Day 4. These sites

remain hypomethylated through the time course. Average methylation ratios are shown for control and 5AZA treated cultures on Day 4. Methylation ratio differences between control and 5AZA treated cultures on Day 4 are labeled as METHYL DIFF and are significant ($p < 0.05$). Annotations (NSC_ID corresponding to the *P. soleocismus* genomic ID) and the KO (KEGG Orthologies, within E-24) definitions are provided.

SUPPLEMENTARY TABLE 1 | All cytosine sites called from whole genome bisulfite sequencing analysis (WGBS).

SUPPLEMENTARY TABLE 2 | All significantly hypomethylated CpG sites for all days in culture.

SUPPLEMENTARY TABLE 3 | All significantly hypermethylated CpG sites across all days in culture with KO annotations.

SUPPLEMENTARY TABLE 4 | Hypomethylated CpG sites belonging to specific KO pathways.

SUPPLEMENTARY TABLE 5 | Day 4 in culture with 5AZA treatment; all significantly hypomethylated and hypermethylated CpG sites.

SUPPLEMENTARY TABLE 6 | Day 5 in culture with 5AZA treatment; all significantly hypomethylated and hypermethylated CpG sites.

SUPPLEMENTARY TABLE 7 | Day 6 in culture with 5AZA treatment; all significantly hypomethylated and hypermethylated CpG sites.

SUPPLEMENTARY TABLE 8 | Day 7 in culture with 5AZA treatment; all significantly hypomethylated and hypermethylated CpG sites.

SUPPLEMENTARY TABLE 9 | Day 10 in culture with 5AZA treatment; all significantly hypomethylated and hypermethylated CpG sites.

REFERENCES

- Akimoto, K., Katakami, H., Kim, H.-J., Ogawa, E., Sano, C. M., Wada, Y., et al. (2007). Epigenetic inheritance in rice plants. *Ann. Bot.* 100, 205–217. doi: 10.1093/aob/mcm110
- Alishah Aratboni, H., Rafiei, N., Garcia-Granados, R., Alemzadeh, A., and Morones-Ramirez, J. R. (2019). Biomass and lipid induction strategies in microalgae for biofuel production and other applications. *Microb. Cell Fact* 18:178. doi: 10.1186/s12934-019-1228-4
- Altschul, S. F., Gish, W., Miller, W., Myers, E. W., and Lipman, D. J. (1990). Basic local alignment search tool. *J. Mol. Biol.* 215, 403–410. doi: 10.1016/S0022-2836(05)80360-2
- Aramaki, T., Blanc-Mathieu, R., Endo, H., Ohkubo, K., Kanehisa, M., Goto, S., et al. (2020). KofamKOALA: KEGG Ortholog assignment based on profile HMM and adaptive score threshold. *Bioinformatics* 36, 2251–2252. doi: 10.1093/bioinformatics/btz859
- Avidan, O., Brandis, A., Rogachev, I., and Pick, U. (2015). Enhanced acetyl-CoA production is associated with increased triglyceride accumulation in the green alga *Chlorella desiccata*. *J. Exp. Bot.* 66, 3725–3735. doi: 10.1093/jxb/erv166
- Babinger, P., Kobl, I., Mages, W., Schmitt, R., Genetik, L., Regensburg, U., et al. (2001). A link between DNA methylation and epigenetic silencing in transgenic *Volvox carteri*. *Science* 29, 1261–1271. doi: 10.1093/nar/29.6.1261
- Babinger, P., Völkl, R., Cakstina, I., Maftai, A., and Schmitt, R. (2007). Maintenance DNA methyltransferase (Met1) and silencing of CpG-methylated foreign DNA in *Volvox carteri*. *Plant Mol. Biol.* 63, 325–336. doi: 10.1007/s11103-006-9091-1
- Banerjee, A., Maiti, S. K., Guria, C., and Banerjee, C. (2017). Metabolic pathways for lipid synthesis under nitrogen stress in *Chlamydomonas* and *Nannochloropsis*. *Biotechnol. Lett.* 39, 1–11. doi: 10.1007/s10529-016-2216-y
- Barry, A., Wolfe, A., English, C., Ruddick, C., and Lambert, D. (2016). *National Algal Biofuels Technology Review*. Washington, DC: United States Department of Energy. doi: 10.2172/1259407
- Bernstein, B. E., Stamatoyannopoulos, J. A., Costello, J. F., Ren, B., Milosavljevic, A., Meissner, A., et al. (2010). The NIH roadmap epigenomics mapping consortium. *Nat. Biotechnol.* 28, 1045–1048. doi: 10.1038/nbt1010-1045
- Blaby-Haas, C. E., and Merchant, S. S. (2019). Comparative and functional algal genomics. *Annu. Rev. Plant Biol.* 70, 605–638. doi: 10.1146/annurev-arplant-050718-095841
- Bono, M. S. Jr., Garcia, R. D., Sri-Jayanthi, D. V., Ahner, B. A., and Kirby, B. J. (2015). Measurement of lipid accumulation in *Chlorella vulgaris* via flow cytometry and liquid-state ¹H NMR Spectroscopy for development of an NMR-traceable flow cytometry protocol. *PLoS One* 10:e0134846. doi: 10.1371/journal.pone.0134846
- Cantarel, B. L., Korf, I., Robb, S. M. C., Parra, G., Ross, E., Moore, B., et al. (2008). MAKER: an easy-to-use annotation pipeline designed for emerging model organism genomes. *Genome Res.* 18, 188–196. doi: 10.1101/gr.6743907
- Casas-Mollano, J. A., van Dijk, K., Eisenhart, J., and Cerutti, H. (2007). SET3p monomethylates histone H3 on lysine 9 and is required for the silencing of tandemly repeated transgenes in *Chlamydomonas*. *Nucleic Acids Res.* 35, 939–950. doi: 10.1093/nar/gkl1149
- Cerutti, H. (1997). Epigenetic silencing of a foreign gene in nuclear transformants of *Chlamydomonas*. *Plant Cell Online* 9, 925–945. doi: 10.1105/tpc.9.6.925
- Chang, S., and Pikaard, C. S. (2005). Transcript profiling in arabidopsis reveals complex responses to global inhibition of DNA methylation and histone deacetylation. *J. Biol. Chem.* 280, 796–804. doi: 10.1074/jbc.M409053200
- Christman, J. K. (2002). 5-Azacytidine and 5-aza-2'-deoxycytidine as inhibitors of DNA methylation: mechanistic studies and their implications for cancer therapy. *Oncogene* 21, 5483–5495. doi: 10.1038/sj.onc.1205699
- Dahlin, L. R., Gerritsen, A. T., Henard, C. A., Van Wychen, S., Linger, J. G., Kunde, Y., et al. (2019). Development of a high-productivity, halophilic, thermotolerant microalga *Picochlorum renovo*. *Commun. Biol.* 2:388. doi: 10.1038/s42003-019-0620-2
- El-Gebali, S., Mistry, J., Bateman, A., Eddy, S. R., Luciani, A., Potter, S. C., et al. (2019). The Pfam protein families database in 2019. *Nucleic Acids Res.* 47, D427–D432. doi: 10.1093/nar/gky995

- Feng, S., Cokus, S. J., Zhang, X., Chen, P. Y., Bostick, M., Goll, M. G., et al. (2010a). Conservation and divergence of methylation patterning in plants and animals. *Proc. Natl. Acad. Sci. U.S.A.* 107, 8689–8694. doi: 10.1073/pnas.1002720107
- Feng, S., Jacobsen, S. E., and Reik, W. (2010b). Epigenetic reprogramming in plant and animal development. *Science* 330, 622–627. doi: 10.1126/science.1190614
- Feng, T. Y., and Chiang, K. S. (1984). The persistence of maternal inheritance in *Chlamydomonas* despite hypomethylation of chloroplast DNA induced by inhibitors. *Proc. Natl. Acad. Sci. U.S.A.* 81, 3438–3442. doi: 10.1073/pnas.81.11.3438
- Finn, R. D., Coghill, P., Eberhardt, R. Y., Eddy, S. R., Mistry, J., Mitchell, A. L., et al. (2015). The Pfam protein families database: towards a more sustainable future. *Nucleic Acids Res.* 44, D279–D285. doi: 10.1093/nar/gkv1344
- Foflonker, F., Price, D. C., Qiu, H., Palenik, B., Wang, S., and Bhattacharya, D. (2015). Genome of the halotolerant green alga *Picochlorum* sp. Reveals strategies for thriving under fluctuating environmental conditions. *Environ. Microbiol.* 17, 412–426. doi: 10.1111/1462-2920.12541
- Fu, Y., Luo, G., Chen, K., Deng, X., Yu, M., Han, D., et al. (2015). N6-methyldeoxyadenosine marks active transcription start sites in *Chlamydomonas*. *Cell* 161, 879–892. doi: 10.1016/j.cell.2015.04.010.N
- Gnyska, A., Jastrzębski, Z., and Flis, S. (2013). DNA methyltransferase inhibitors and their emerging role in epigenetic therapy of cancer. *Anticancer Res.* 33, 2989–2996.
- Gonzalez-Esquer, C. R., Twary, S. N., Hovde, B. T., and Starkenburg, S. R. (2018). Nuclear, chloroplast, and mitochondrial genome sequences of the prospective microalgal biofuel strain *Picochlorum soloecismus*. *Genome Announc.* 6, 1–2. doi: 10.1128/genomeA.01498-17
- Gonzalez-Esquer, C. R., Wright, K. T., Sudasinghe, N., Carr, C. K., Sanders, C. K., Turmo, A., et al. (2019). Demonstration of the potential of *Picochlorum soloecismus* as a microalgal platform for the production of renewable fuels. *Algal Res.* 43:658. doi: 10.1016/j.algal.2019.101658
- Haft, D. H., Selengut, J. D., and White, O. (2003). The TIGRFAMs database of protein families. *Nucleic Acids Res.* 31, 371–373. doi: 10.1093/nar/gkg128
- Hattman, S., Kenny, C., Berger, L., and Pratt, K. (1978). Comparative study of DNA methylation in three unicellular eucaryotes. *J. Bacteriol.* 135, 1156–1157. doi: 10.1128/JB.135.3.1156-1157.1978
- Hollenbach, P. W., Nguyen, A. N., Brady, H., Williams, M., Ning, Y., Richard, N., et al. (2010). A comparison of azacitidine and decitabine activities in acute myeloid leukemia cell lines. *PLoS One* 5:e9001. doi: 10.1371/journal.pone.0009001
- Hovde, B. T., Hanschen, E. R., Steadman Tyler, C. R., Lo, C.-C., Kunde, Y., Davenport, K., et al. (2018). Genomic characterization reveals significant divergence within *Chlorella sorokiniana* (Chlorellales, Trebouxiophyceae). *Algal Res.* 35:12. doi: 10.1016/j.algal.2018.09.012
- Jaenisch, R., and Bird, A. (2003). Epigenetic regulation of gene expression: how the genome integrates intrinsic and environmental signals. *Nat. Genet.* 33(Suppl.), 245–254. doi: 10.1038/ng1089
- Jeong, B. B., Wu-Scharf, D., Zhang, C., and Cerutti, H. (2002). Suppressors of transcriptional transgenic silencing in *Chlamydomonas* are sensitive to DNA-damaging agents and reactivate transposable elements. *Proc. Natl. Acad. Sci. U.S.A.* 99, 1076–1081. doi: 10.1073/pnas.022392999
- Jia, B., Song, Y., Wu, M., Lin, B., Xiao, K., Hu, Z., et al. (2016). Characterization of long-chain acyl-CoA synthetases which stimulate secretion of fatty acids in green algae *Chlamydomonas reinhardtii*. *Biotechnol. Biofuels* 9:184. doi: 10.1186/s13068-016-0598-7
- Kanehisa, M., Sato, Y., Kawashima, M., Furumichi, M., and Tanabe, M. (2016a). KEGG as a reference resource for gene and protein annotation. *Nucleic Acids Res.* 44, D457–D462. doi: 10.1093/nar/gkv1070
- Kanehisa, M., Sato, Y., and Morishima, K. (2016b). BlastKOALA and GhostKOALA: KEGG tools for functional characterization of genome and metagenome sequences. *J. Mol. Biol.* 428, 726–731. doi: 10.1016/j.jmb.2015.11.006
- Karahoca, M., and Momparker, R. L. (2013). Pharmacokinetic and pharmacodynamic analysis of 5-aza-2'-deoxycytidine (decitabine) in the design of its dose-schedule for cancer therapy. *Nucleic Acids Res.* 2013, 1–16. doi: 10.1186/1868-7083-5-3
- Khan, M. I., Shin, J. H., and Kim, J. D. (2018). The promising future of microalgae: current status, challenges, and optimization of a sustainable and renewable industry for biofuels, feed, and other products. *Microb. Cell Fact* 17:36. doi: 10.1186/s12934-018-0879-x
- Krasovec, M., Vancaester, E., Rombauts, S., Buccini, F., Yau, S., Hemon, C., et al. (2018). Genome analyses of the *Microalga picochlorum* provide insights into the evolution of thermotolerance in the green lineage. *Genome Biol. Evol.* 10, 2347–2365. doi: 10.1093/gbe/evy167
- Kronholm, I., Bassett, A., and Baulcombe, D. (2017). Epigenetic and genetic contributions to adaptation in *Chlamydomonas*. *Mol. Biol. Evol.* 34, 2285–2306. doi: 10.1093/molbev/msx166
- Lewis, T. E., Sillitoe, I., Dawson, N., Lam, S. D., Clarke, T., Lee, D., et al. (2017). Gene3D: extensive prediction of globular domains in proteins. *Nucleic Acids Res.* 46, D435–D439. doi: 10.1093/nar/gkx1069
- Lopez, D. A., Hamaji, T., Kropat, J., De Hoff, P., Morselli, M., Rubbi, L., et al. (2015). Dynamic changes in the transcriptome and methylome of *Chlamydomonas reinhardtii* throughout its life cycle. *Plant Physiol.* 2015:00861. doi: 10.1104/pp.15.00861
- Madlung, A., Masuelli, R. W., Watson, B., Reynolds, S. H., Davison, J., and Comai, L. (2002). Remodeling of DNA methylation and phenotypic and transcriptional changes in synthetic *Arabidopsis allotetraploids*. *Plant Physiol.* 129, 733–746. doi: 10.1104/pp.003095
- Maumus, F., Rabinowicz, P., Bowler, C., and Rivarola, M. (2011). Stemming epigenetics in marine stramenopiles. *Curr. Genomics* 12, 357–370. doi: 10.2174/138920211796429727
- McKinney, W. (2010). "Data structures for statistical computing in python," in *Proceedings of the 9th Python Science Conference*, New York, NY. doi: 10.25080/Majors-92bf1922-00a
- Mitchell, A. L., Attwood, T. K., Babbitt, P. C., Blum, M., Bork, P., Bridge, A., et al. (2019). InterPro in 2019: improving coverage, classification and access to protein sequence annotations. *Nucleic Acids Res.* 47, D351–D360. doi: 10.1093/nar/gky1100
- Mueller, S. P., Unger, M., Guender, L., Fekete, A., and Mueller, M. J. (2017). Phospholipid:diacylglycerol acyltransferase-mediated triacylglycerol synthesis augments basal thermotolerance. *Plant Physiol.* 175, 486–497. doi: 10.1104/pp.17.00861
- Müller, K., Lindauer, A., Brüderlein, M., and Schmitt, R. (1990). Organization and transcription of *Volvox* histone-encoding genes: similarities between algal and animal genes. *Gene* 93, 167–168. doi: 10.1016/0378-1119(90)90221-C
- Ngan, C. Y., Wong, C.-H., Choi, C., Yoshinaga, Y., Louie, K., Jia, J., et al. (2015). Lineage-specific chromatin signatures reveal a regulator of lipid metabolism in microalgae. *Nat. Plants* 1, 1–11. doi: 10.1038/NPLANTS.2015.107
- Palii, S. S., Emburgh, B. O., Van Sankpal, U. T., Brown, K. D., and Robertson, K. D. (2008). DNA Methylation inhibitor 5-Aza-2'-deoxycytidine induces reversible genome-Wide DNA damage that is distinctly influenced by DNA methyltransferases 1 and 3B. *Mol Cell Biol.* 28, 752–771. doi: 10.1128/MCB.01799-07
- Pandey, M., Kaur, P., Shukla, S., Abbas, A., Fu, P., and Gupta, S. (2012). Plant flavone apigenin inhibits HDAC and remodels chromatin to induce growth arrest and apoptosis in human prostate cancer cells: in vitro and in vivo study. *Mol. Carcinog* 51, 952–962. doi: 10.1002/mc.20866
- Sharma, K. K., Schuhmann, H., and Schenk, P. M. (2012). High lipid induction in microalgae for biodiesel production. *Energies* 5, 1532–1553. doi: 10.3390/en5051532
- Shaver, S., Casas-Mollano, J. A., Cerny, R. L., and Cerutti, H. (2010). Origin of the polycomb repressive complex 2 and gene silencing by an E(z) homolog in the unicellular alga *Chlamydomonas*. *Epigenetics* 5, 301–312. doi: 10.4161/epi.5.4.11608
- Sigrist, C. J. A., de Castro, E., Cerutti, L., Cuche, B. A., Hulo, N., Bridge, A., et al. (2012). New and continuing developments at PROSITE. *Nucleic Acids Res.* 41, D344–D347. doi: 10.1093/nar/gks1067
- Sillitoe, I., Dawson, N., Lewis, T. E., Das, S., Lees, J. G., Ashford, P., et al. (2018). CATH: expanding the horizons of structure-based functional annotations for genome sequences. *Nucleic Acids Res.* 47, D280–D284. doi: 10.1093/nar/gky1097
- Stanke, M., and Morgenstern, B. (2005). AUGUSTUS: a web server for gene prediction in eukaryotes that allows user-defined constraints. *Nucleic Acids Res.* 33, W465–W467. doi: 10.1093/nar/gki458

- Steadman Tyler, C. R., Sanders, C. K., Erickson, R. S., Dale, T., Twary, S. N., and Marrone, B. L. (2019). Functional and phenotypic flow cytometry characterization of *Picochlorum soloecismus*. *Algal Res.* 43:101614. doi: 10.1016/j.algal.2019.101614
- Stresemann, C., and Lyko, F. (2008). Modes of action of the DNA methyltransferase inhibitors azacytidine and decitabine. *Int. J. Cancer* 13, 8–13. doi: 10.1002/ijc.23607
- Tirichine, L., and Bowler, C. (2011). Decoding algal genomes: tracing back the history of photosynthetic life on Earth. *Plant J.* 66, 45–57. doi: 10.1111/j.1365-3113X.2011.04540.x
- Tirichine, L., Rastogi, A., and Bowler, C. (2017). Recent progress in diatom genomics and epigenomics. *Curr. Opin. Plant Biol.* 36, 46–55. doi: 10.1016/j.pbi.2017.02.001
- Tyler, C. R. S., Smoake, J. J. W., Solomon, E. R., Villicana, E., Caldwell, K. K., and Allan, A. M. (2018). Sex-dependent effects of the histone deacetylase inhibitor, sodium valproate, on reversal learning after developmental arsenic exposure. *Front. Genet.* 9:200. doi: 10.3389/fgene.2018.00200
- Umen, J. G., and Goodenough, U. W. (2001). Chloroplast DNA methylation and inheritance in *Chlamydomonas*. *Genes Dev.* 15, 2585–2597. doi: 10.1101/gad.906701
- Unkefer, C. J., Sayre, R. T., Magnuson, J. K., Anderson, D. B., Baxter, I., Blaby, I. K., et al. (2017). Review of the algal biology program within the national alliance for advanced biofuels and bioproducts. *Algal Res.* 22, 187–215. doi: 10.1016/j.algal.2016.06.002
- van Dijk, K., Marley, K. E., Jeong, B., Xu, J., Hesson, J., Cerny, R. L., et al. (2005). Monomethyl Histone H3 Lysine 4 as an epigenetic mark for silenced euchromatin in *Chlamydomonas*. *Plant Cell* 17, 2439–2453. doi: 10.1105/tpc.105.034165
- Veluchamy, A., Lin, X., Maumus, F., Rivarola, M., Bhavsar, J., Creasy, T., et al. (2014). Insights into the role of DNA methylation in diatoms by genome-wide profiling in *Phaeodactylum tricornutum*. *Nat. Commun.* 4:2091. doi: 10.1038/ncomms3091
- Waterborg, J. H., Robertson, A. J., Tatar, D. L., Borza, C. M., and Davie, J. R. (1995). Histones of *Chlamydomonas reinhardtii*. synthesis, acetylation, and methylation. *Plant Physiol.* 109, 393–407. doi: 10.1104/pp.109.2.393
- Wei, H., Shi, Y., Ma, X., Pan, Y., Hu, H., Li, Y., et al. (2017). A type-I diacylglycerol acyltransferase modulates triacylglycerol biosynthesis and fatty acid composition in the oleaginous microalga, *Nannochloropsis oceanica*. *Biotechnol. Biofuels* 10:174. doi: 10.1186/s13068-017-0858-851
- Wu-Scharf, D., Jeong, B., Zhang, C., and Cerutti, H. (2000). Transgene and transposon silencing in *Chlamydomonas reinhardtii* by a DEAH-box RNA helicase. *Science* 290, 1159–1162. doi: 10.1126/science.290.5494.1159
- Xue, J., Balamurugan, S., Li, D. W., Liu, Y. H., Zeng, H., Wang, L., et al. (2017). Glucose-6-phosphate dehydrogenase as a target for highly efficient fatty acid biosynthesis in microalgae by enhancing NADPH supply. *Metab. Eng.* 41, 212–221. doi: 10.1016/j.ymben.2017.04.008
- Xue, J.-H., Chen, G.-D., Hao, F., Chen, H., Fang, Z., Chen, F.-F., et al. (2019). A vitamin-C-derived DNA modification catalysed by an algal TET homologue. *Nature* 569, 581–585. doi: 10.1038/s41586-019-1160-0
- Zemach, A., McDaniel, I. E., Silva, P., and Zilberman, D. (2010). Genome-wide evolutionary analysis of eukaryotic DNA methylation. *Science* 328, 916–919. doi: 10.1126/science.1186366
- Zhang, H., Lang, Z., and Zhu, J.-K. (2018). Dynamics and function of DNA methylation in plants. *Nat. Rev. Mol. Cell Biol.* 19, 489–506. doi: 10.1038/s41580-018-0016-z

Conflict of Interest: The authors declare that the research was conducted in the absence of any commercial or financial relationships that could be construed as a potential conflict of interest.

Copyright © 2020 Steadman, Banerjee, Kunde, Sanders, Marrone and Twary. This is an open-access article distributed under the terms of the Creative Commons Attribution License (CC BY). The use, distribution or reproduction in other forums is permitted, provided the original author(s) and the copyright owner(s) are credited and that the original publication in this journal is cited, in accordance with accepted academic practice. No use, distribution or reproduction is permitted which does not comply with these terms.



FAIM Is Regulated by MiR-206, MiR-1-3p and MiR-133b

Elena Coccia^{1,2,3}, Marc Masanas⁴, Joaquín López-Soriano^{1,2,3}, Miguel F. Segura⁴, Joan X. Comella^{1,2,3*} and M. José Pérez-García^{1,2,3*}

¹ Cell Signaling and Apoptosis Group, Vall d'Hebron Research Institute, Barcelona, Spain, ² Centro de Investigación Biomédica en Red sobre Enfermedades Neurodegenerativas (CIBERNED), Madrid, Spain, ³ Institut de Neurociències, Departament de Bioquímica i Biologia Molecular, Facultat de Medicina, Universitat Autònoma de Barcelona, Bellaterra, Spain, ⁴ Group of Translational Research in Child and Adolescent Cancer, Vall d'Hebron Research Institute (VHIR)-UAB, Barcelona, Spain

OPEN ACCESS

Edited by:

Kai Tang,

Purdue University, United States

Reviewed by:

Abhijit Shukla,

Cornell University, United States

Arun Upadhyay,

Northwestern University,

United States

Hiroaki Kaku,

Western Michigan University,

United States

*Correspondence:

M. José Pérez-García

maria.perez@vhir.org

Joan X. Comella

joan.comella@vhir.org

Specialty section:

This article was submitted to

Epigenomics and Epigenetics,

a section of the journal

Frontiers in Cell and Developmental

Biology

Received: 17 July 2020

Accepted: 27 November 2020

Published: 23 December 2020

Citation:

Coccia E, Masanas M,

López-Soriano J, Segura MF,

Comella JX and Pérez-García MJ

(2020) FAIM Is Regulated by MiR-206,

MiR-1-3p and MiR-133b.

Front. Cell Dev. Biol. 8:584606.

doi: 10.3389/fcell.2020.584606

Apoptosis plays an important role during development, control of tissue homeostasis and in pathological contexts. Apoptosis is executed mainly through the intrinsic pathway or the death receptor pathway, i.e., extrinsic pathway. These processes are tightly controlled by positive and negative regulators that dictate pro- or anti-apoptotic death receptor signaling. One of these regulators is the Fas Apoptotic Inhibitory Molecule (FAIM). This death receptor antagonist has two main isoforms, FAIM-S (short) which is the ubiquitously expressed, and a longer isoform, FAIM-L (long), which is mainly expressed in the nervous system. Despite its role as a death receptor antagonist, FAIM also participates in cell death-independent processes such as nerve growth factor-induced neuritogenesis or synaptic transmission. Moreover, FAIM isoforms have been implicated in blocking the formation of protein aggregates under stress conditions or de-regulated in certain pathologies such as Alzheimer's and Parkinson's diseases. Despite the role of FAIM in physiological and pathological processes, little is known about the molecular mechanisms involved in the regulation of its expression. Here, we seek to investigate the post-transcriptional regulation of FAIM isoforms by microRNAs (miRNAs). We found that miR-206, miR-1-3p, and miR-133b are direct regulators of FAIM expression. These findings provide new insights into the regulation of FAIM and may provide new opportunities for therapeutic intervention in diseases in which the expression of FAIM is altered.

Keywords: microRNA, neurodegenerative diseases, nervous system, death receptor, FAIM, Fas apoptotic inhibitory molecule

INTRODUCTION

Several types of molecules are able to block apoptotic pathways, conferring cells with protection against threatening stimuli. The extrinsic apoptotic pathway is mediated by death receptors that integrate and transmit the extracellular apoptotic stimuli. In the last 20 years, mounting evidence has shed light on the physiological and pathological functions of these molecules and has widened the array of identified responses elicited by these receptors beyond cell death. Indeed, Fas receptor and TNF receptors (TNFRs) are paradigmatic cases of receptors that can

trigger apoptotic and non-apoptotic responses depending on the cellular and molecular context (Marques-Fernandez et al., 2013).

The molecular response upon death receptor activation, depends on the activity of proteins called death receptor antagonists. Among these, FAIM (Fas apoptosis inhibitory molecule) was first identified as a negative regulator of Fas signaling (Schneider et al., 1999). It was later found to play multifaceted roles in other physiological processes such as the protective or deleterious effects of TNF α in neurodegenerative disorders (Carriba et al., 2015), regulating axon-selective pruning, hippocampal long-term depression (LTD) (Martinez-Marmol et al., 2016) and opposition to stress-induced accumulation of protein aggregates (Kaku and Rothstein, 2020).

Two main FAIM isoforms generated by alternative splicing have been found at the protein level. While the shorter isoform, named FAIM-S, is ubiquitously expressed, FAIM-L is expressed exclusively in neurons and testes (Zhong et al., 2001; Segura et al., 2007). In the nervous system, FAIM-S participates in neurite outgrowth by activating Ras-ERK and NF- κ B pathways. On the other hand, FAIM-L has been shown to modulate death receptor-induced apoptosis and caspase activation by binding to the receptor (Segura et al., 2007), as well as through interaction with X-linked inhibitor of apoptosis (XIAP) (Moubarak et al., 2013).

Alterations in the expression of FAIM may be relevant in several types of human diseases. For example, in multiple myeloma (MM) patients, FAIM expression is increased in B lymphocyte cells compared with normal individuals and its expression is higher in symptomatic MM patients compared with asymptomatic and premalignant individuals (Huo et al., 2013). FAIM expression is also elevated in CD34 hematopoietic stem cells and leukocytes. This deregulation is associated with chronic myeloproliferative pathogenesis (Tognon et al., 2011).

Other results show FAIM as an important molecule in metabolic processes. When both isoforms of FAIM are knocked out, mice spontaneously develop non-hyperphagic obesity, as well as also manifest hepatosteatosis, adipocyte hypertrophy, dyslipidemia, hyperglycemia, and hyperinsulinemia. In obese patients, FAIM expression is lower in blood cells and is inversely correlated with insulin resistance biomarkers (Huo et al., 2016).

Moreover, FAIM-L levels have been found to be relevant in neurodegenerative diseases. FAIM-L was found to be reduced in the hippocampus of Alzheimer's disease patients (Carriba et al., 2015) and in the entorhinal and hippocampal cortex of Alzheimer's disease mouse models (APP-PS1) (Carriba et al., 2015). In Parkinson's disease, the expression of FAIM-L was found to be reduced in midbrain dopaminergic neurons after trophic factor deprivation, as well as to sensitize them to Fas-induced cell death (Yu et al., 2008). Recent findings also show that FAIM could play a role in Amyotrophic Lateral Sclerosis inhibiting the aggregation of mutant SOD1, suggesting that FAIM participates in maintaining cell homeostasis (Kaku and Rothstein, 2020). Kaku et al. (2020) also described that FAIM is recruited to cellular stress-induced ubiquitinated proteins, and the levels of stress-induced protein aggregates are much greater in FAIM-deficient cell lines.

Despite the pathological consequences of FAIM de-regulation, little is known about how its expression is modulated. Kaku et al.

reported that murine Faim promoter contains three interferon regulatory factor (IRF) binding sites, and Faim expression is positively regulated through IRF4 in primary B cells (Kaku and Rothstein, 2009). At post-transcriptional level, FAIM can also be regulated by MicroRNAs (miRNAs) (Patron et al., 2012; Santosa et al., 2015). MiRNAs are short non-coding RNA of 18–25 base pairs in length that are involved in the regulation of gene expression at the post-transcriptional level. Mature miRNAs repress gene expression through binding to the 3'UTR of the mRNA with the miRNA seed region, a 6–8 bases located at the 5' end of the mature miRNA and perfectly complementary to the target mRNA sequence (Mullany et al., 2016), thereby inhibiting mRNA translation or inducing mRNA degradation (Alvarez-Garcia and Miska, 2005; Shingara et al., 2005). Thus far, the evidence of FAIM being regulated by miRNA was reported by Patron and colleagues who showed that miR-133b directly impairs the expression of FAIM, thereby enhancing Fas-induced cell death in HeLa and PC3 cells (Patron et al., 2012).

Owing to the pathological consequences that FAIM de-regulation may have for certain human diseases like are those involved in neurodegeneration, we sought to screen for other miRNA that could bind to the FAIM 3'UTR and modulate its expression. Our study identified miR-206, miR-1-3p and miR-133b as direct regulators of FAIM, thereby providing a deeper knowledge on the FAIM regulation mechanisms and opening up new opportunities for therapeutic intervention.

MATERIALS AND METHODS

FAIM 3'UTR Analysis

The miRWalk 2.0 database using five miRNA-target prediction algorithms (miRDB (RRID:SCR_010848), miRWalk (Vlachos et al., 2015), miRanda (Betel et al., 2010), miRMap (RRID:SCR_016508) and TargetScan; version 6.2 (Agarwal et al., 2015) were used for the computational miRNA target prediction analysis. The miRNA target search was restricted to the 3'UTR of FAIM and with a minimum complementarity of 7 nucleotides in the seeding region. Probability distribution of random matches was set at 0.05 (Poisson *p*-value). MiRNAs with *p* \leq 0.05 predicted by all five algorithms were selected for further analysis.

Cell Culture and Transfection

SH-SY5Y (Cat# CRL-2266, RRID:CVCL_0019), SK-N-AS (Cat# CRL-2137, RRID:CVCL_1700), HEK293T (Cat# CRL-3216, RRID:CVCL_0063) and HeLa (CLS Cat# 300194/p772_HeLa, RRID:CVCL_0030) cell lines were purchased from American Type Culture Collection (ATCC, Rockville, MD, United States). SH-SY5Y, SK-N-AS and HEK293T were grown in Dulbecco's modified Eagle's medium (DMEM, Thermo Fisher Scientific, Waltham, MA, United States) containing 10% fetal bovine serum (HEK293T, SK-N-AS) or 15% fetal bovine serum (SH-SY5Y) (Thermo Fisher Scientific, Waltham, MA, United States). HeLa cells were cultured in Roswell Park Memorial Institute (RPMI) 1640 (Thermo Fisher Scientific) supplemented with 10% fetal bovine serum, sodium pyruvate 1 mM (Thermo

Fisher Scientific) and 1% of non-essential amino acids (Thermo Fisher Scientific). All media were supplemented with 100 U/mL penicillin, 100 µg/mL streptomycin (Thermo Fisher Scientific) and 5 µg/mL PlasmocinTM (InvivoGen). Culture conditions were maintained at 37°C in a humidified atmosphere containing 5% CO₂. For miRNA transfection, SH-SY5Y, SK-N-AS and HeLa were seeded at 6×10^5 , 4.5×10^5 , and 4×10^5 cells in 60 mm dishes, respectively, and transfected 24 h later with the indicated miRIDIAN microRNA mimic oligonucleotides (25 nM, Dharmacon), GE Healthcare using Lipofectamine 2000 transfection reagent (Thermo Fisher Scientific, Waltham, MA, United States), following the manufacturer's instructions. Mimic Transfection Control with Dy547 was used as a negative control.

Luciferase Reporter Assay

Wild type and mutated 3'UTR sequences of *FAIM* were synthesized using the GeneArt Gene synthesis platform (Thermo Fisher Scientific, Waltham, MA, United States) and cloned into the psiCheckTM-2 dual luciferase reporter vector (Promega, C8021). For luciferase assays, HEK293T (Cat# CRL-3216, RRID:CVCL_0063) cells were co-transfected with 50 ng of psiCheckTM-2 vectors containing wild type or mutated *FAIM* 3'UTR and 25 nM of the indicated miRNAs, using Lipofectamine 2000 (Invitrogen, Carlsberg, CA, United States), following the manufacturer's protocol. Luciferase activity was measured 24 h post-transfection using the Dual Luciferase Reporter Assay System (Promega Corporation, Madison, WI, United States). Luminescence was measured in an Appliskan (Thermo Fisher Scientific) microplate reader. Renilla luciferase activity was normalized to corresponding firefly luciferase activity and plotted as a percentage of the control.

Quantitative Real-Time PCR

Total RNA, including small RNA, was isolated from human cell lines using the miRNeasy Mini Kit (Qiagen) following the manufacturer's instructions. Equal amounts of RNA (1 µg) were converted to cDNA using the High Capacity RNA-to-cDNA Kit (Applied Biosystems), following the manufacturer's instructions. The quantitative real-time PCR (RT-qPCR) was performed using TaqMan Universal PCR Master Mix Kit (Thermo Fisher Scientific). Samples were subjected to a PCR amplification protocol using an AB7900HT Real Time PCR System (Thermo Fisher Scientific, Waltham, MA, United States) using the following primers for *FAIM-L* (Hs00992098_m1; Thermo Fisher Scientific, Waltham, MA, United States) and for *FAIM* (Hs00216756_m1; Thermo Fisher Scientific, Waltham, MA, United States). The PCR conditions were: 94°C for 3 min, 40 cycles of 45 s at 94°C, followed by 30 s at 55°C, 72°C for 1 min and 72°C for 10 min. The data were analyzed using the SDS 2.3 software (Thermo Fisher Scientific, Waltham, MA, United States) and normalized using GAPDH as a housekeeping gene. TaqMan MicroRNA Assay (Applied Biosystems) was used to convert miRNA to cDNA for the analysis of mature miRNAs. cDNA was quantified by Taqman Universal Master Mix (Applied Biosystems). MiRNA expression was normalized against RNU-44 small RNA. The reactions were performed in triplicate for each

sample and incubated in optical 384-well reaction plates. *FAIM* mRNA expression level was calculated as (Rao et al., 2013).

Western Blot

Proteins were extracted using SET lysis buffer [10 mM Tris-HCl pH7.4, 150 mM NaCl, 1 mM EDTA and 1% sodium dodecyl sulfate (SDS)] and then quantified using a modified Lowry assay (DC protein assay, Bio-Rad). Equal amounts of protein (30 µg per lane) were separated by 10% sodium dodecyl sulfate polyacrylamide gel (SDS-PAGE) electrophoresis, and then transferred onto a polyvinylidene fluoride membrane (PVDF, Merck Millipore, MA, United States). Membranes were blocked with 5% non-fat milk at room temperature for 1 h and then incubated with the primary antibodies against *FAIM* (1:1000) (Segura et al., 2007) and α -tubulin (1:10000, Cat# T9026, RRID:AB_477593; Sigma-Aldrich) overnight at 4°C. The membranes were then incubated with horseradish peroxidase-conjugated goat anti-rabbit IgG secondary antibody (1:10000, Cat# AP132, RRID:AB_11214051; Sigma-Aldrich) and anti-mouse (1:20000, Cat# AP124, RRID:AB_92455; Sigma-Aldrich) for 1 h at room temperature. An enhanced chemiluminescence detection System, EZ-ECL detection kit (Biological Industries) was used to develop signals, using α -tubulin as a loading control.

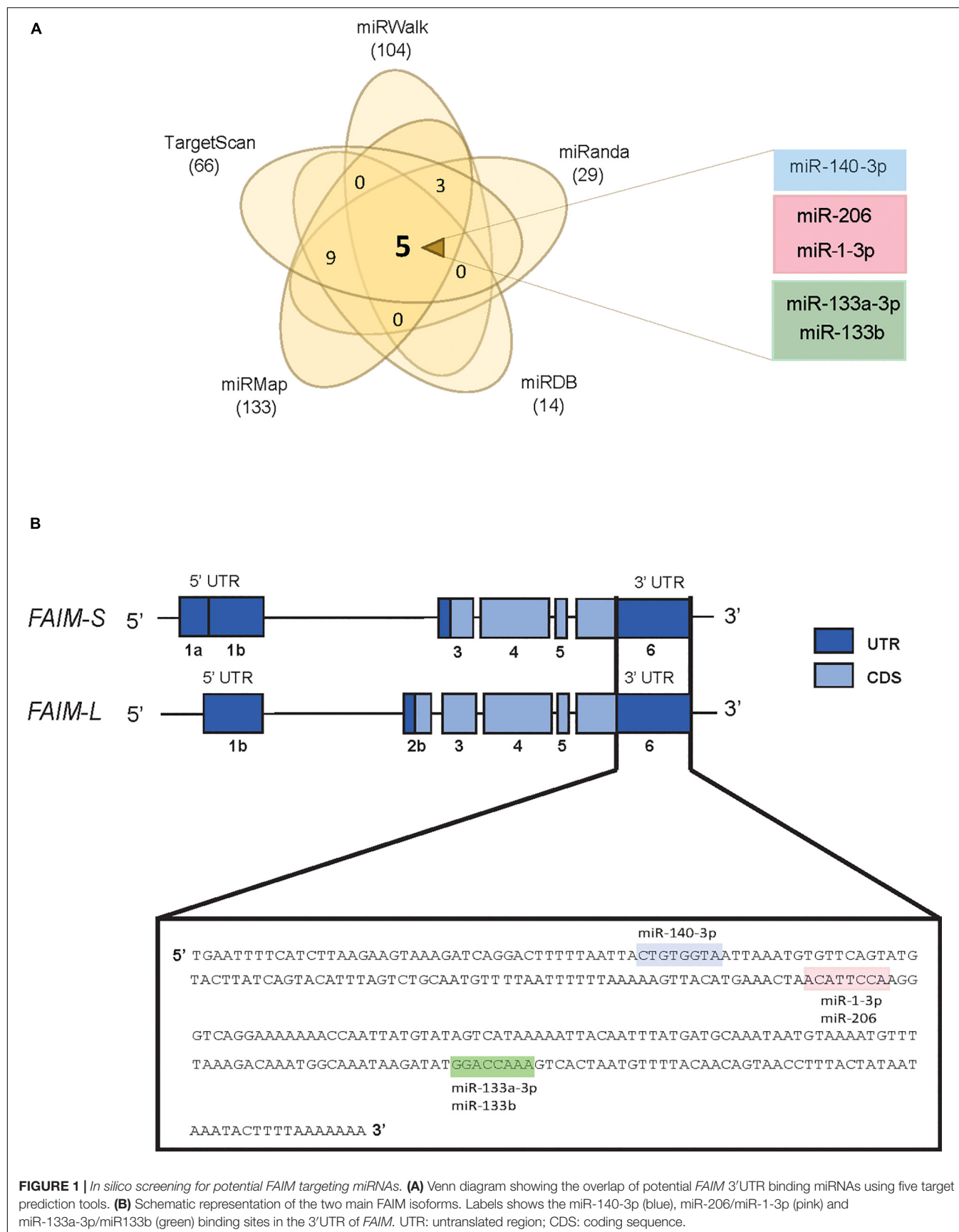
Statistical Analysis

Statistical analysis was performed using GraphPad Prism 7.0. All data in this study were shown as the mean of three independent experiments \pm SEM. Statistical differences in multiple groups were examined by one-way ANOVA followed by Dunnett's multiple range test. *P* value < 0.05 was considered as statistically significant.

RESULTS

Five MiRNAs Are Predicted to Target *FAIM* by Five Different MiRNA-Binding Algorithms

In order to screen for potential miRNAs able to modulate the expression of *FAIM*, we compared the prediction of putative miRNA-binding sites in the 3'UTR of *FAIM* from five different prediction algorithms, i.e., TargetScan, miRanda, miRWalk, miRMap, and miRDB (see **Supplementary Table 1**). When predictions from the different algorithms were overlapped, five miRNAs were commonly found, namely miR-140-3p, miR-206, miR-1-3p, miR-133a-3p, and miR-133b (**Figure 1A**). The two main isoforms codified by *FAIM* gene, *FAIM-S* and *FAIM-L*, differ in their 5'UTR composition, and in the inclusion of the exon 2b in the neuronal isoform *FAIM-L*. On the other hand, the 3' UTR which includes the predicted target sites of these 5 miRNAs, is common to both isoforms (**Figure 1B**). Of note, while the protein sequence is highly conserved during the evolution, the 3'UTR, and more precisely, the identified miRNA-binding sites are conserved only among vertebrates, thereby suggesting that this mechanism of regulation was incorporated lately in the evolution (**Supplementary Figure 1**).



MiR-206, MiR-1-3p and MiR-133b Can Bind Directly to the 3'UTR of *FAIM*

To confirm whether the identified miRNAs are truly direct regulators of *FAIM* expression, a luciferase-reporter vector containing the wild type 3'UTR was cloned and co-transfected with control mimic oligonucleotides or the indicated miRNA mimics. Since miR-133a-3p and miR-133b are almost identical (20/21 nucleotides) and share the exact same seed region, we proceeded with our analyses only with miR-133b. A remarkable reduction in luciferase activity was observed upon transfection of miR-206, miR-1-3p, and miR-133b but not with the transfection of miR-140-3p (**Figure 2A**). The 3'UTR region of *FAIM* contains one binding site common to miR-206 and miR-1-3p, and one binding site for miR-133b. In order to confirm the interactions were sequence specific we engineered specific mutations in the 3'UTR, giving rise to correspondingly 3'UTR mut206/1-3p and 3'UTR mut 133b, respectively (**Figure 2B**). Luciferase activity reduction found in the wild type- 3'UTR was almost completely restored to control levels when miRNAs were co-transfected with the respective 3'UTR mutated forms (**Figure 2C**). Of note, Clip-seq data mining also showed binding of Ago2 in the 3'UTR of *FAIM* for miR-133a-3p, miR-133b, miR-206, and miR-1-3p but not for miR-140-3p (**Supplementary Table 2**). Overall, we were able to show that miR-206, miR-1-3p, and miR-133 have the capacity to directly bind *FAIM* 3'UTR.

MiR-206, MiR-1-3p, and MiR-133b Modulate *FAIM* Expression

To elucidate whether the direct binding of miRNAs to the 3'UTR causes a downregulation of *FAIM* expression, we decided to transfect miRNA mimics oligonucleotides into human cells lines that could represent different tissues where one or both *FAIM* isoforms are expressed (**Figure 3A**). On the one hand, we selected the neuroblastoma cell line SH-SY5Y that express both *FAIM-L* and *FAIM-S*, and SK-N-AS that only express *FAIM-S*. Furthermore, we added HeLa cells, since is one of the few models where the functionality of *FAIM* in human models has been tested (Patron et al., 2012). The expression at mRNA and protein levels was measured in the indicated cell lines after transfection of miR-140-3p, miR-206, miR-1-3p, and miR-133b (**Figures 3B,C**). While miR-140-3p did not modulate the levels of *FAIM* in any of the cell lines tested, transfection of miR-206, miR-1-3p, and miR-133b caused a ~2-fold reduction in *FAIM* mRNA levels (**Figure 3B**). Similarly, *FAIM* protein levels decreased in presence of miR-206, miR-1-3p, and miR-133b overexpression in the three cell lines tested (**Figure 3C**). Overall, we were able to confirm that among the predicted miRNAs targeting *FAIM* 3'UTR, miR-206, miR-1-3p, and miR-133b regulate *FAIM* isoforms levels, while miR-140 does not.

DISCUSSION

Death receptor-induced cell death is essential during development due to its role regulating tissue homeostasis and differentiation. In the adult, death receptor signaling can be important under physiological or pathological circumstances.

FAIM acts as a death receptor antagonist by binding directly to the death receptor (Segura et al., 2007) or by interacting with downstream effectors such as X-linked inhibitor of apoptosis protein (XIAP) (Moubarak et al., 2013). De-regulation of *FAIM* is associated with the pathophysiology of cancer and neurodegenerative diseases among others. In Alzheimer's disease (AD), the levels of *FAIM-L* were shown to be decreased according to Braak stages in AD patients (Braakman et al., 1991; Carriba et al., 2015). At molecular level, *FAIM-L* levels reduction abolished TNF α protection against amyloid- β neurotoxicity (Carriba et al., 2015). Thus, a better understanding on how *FAIM* levels are modulated can be paramount for better characterization of human disease and for the design of new therapeutic approaches.

MiRNAs have important roles in regulating diverse biological processes, such as cell proliferation, immunity, development, differentiation, metabolism and cell death, and generally they act as a negative feedback factor in cell signaling (Ha, 2011). Furthermore, miRNA deregulation is a frequent event in human disease, and they can be used as therapeutic tools to treat pathologies with unbalanced cell death and survival pathways (Paul et al., 2018).

We found that miR-206, miR-1-3p, and miR-133b directly regulate *FAIM* by binding to 3'UTR, decreasing the mRNA and protein levels. MiR-133b has already been described to target *FAIM* in PC3 and HeLa cells (Patron et al., 2012). The authors showed that *FAIM* silencing or miR-133b overexpression exacerbated death receptor-induced cell death. Our results confirmed that miR-133b is a direct regulator of *FAIM* in a broader spectrum of cell types including the neuronal lineage. As regards the potential connection of miR-133b-*FAIM* in neurodegenerative diseases, Jimenez-Jimenez et al. (2014) reported that variations in miR-133b could contribute to the risk of developing Parkinson's disease. In this regard, the expression of *FAIM-L* was also described to be reduced in dopaminergic neurons in Parkinson's disease (Yu et al., 2008), thus making this type of neurons more vulnerable to Fas-induced death. Thus, high levels of miR-133b could contribute to lowering the expression of *FAIM* in these neurons. However, in Alzheimer's disease, miR-133b was found to be significantly downregulated after A β 25-35 treatment (Yang et al., 2019). In a different study, *FAIM* levels also appear to be reduced in hippocampal samples from AD patients (Carriba et al., 2015), thus suggesting that the miR-133b-*FAIM* axis would not be relevant in this disease and opens up the question of whether other miRNAs could be responsible for *FAIM* downregulation.

Here, we report, for the first time, that miR-206 and miR-1-3p can also be direct modulators of *FAIM*. Interestingly, miR-206 and miR-1-3p belong to the same miRNA family, which means that, they share the same seed region, thereby suggesting a major overlap in their targets. Furthermore, miR-206, is clustered with miR-133b in the short arm of chromosome 6, indicating that these miRNAs can be co-regulated and provide a strong mechanism in the regulation of *FAIM*. MiR-206 was found to be significantly upregulated in blood samples from Alzheimer's disease patients compared with age-matched normal controls. Furthermore, upregulation of miR-206 has been detected in serum from patients with mild cognitive

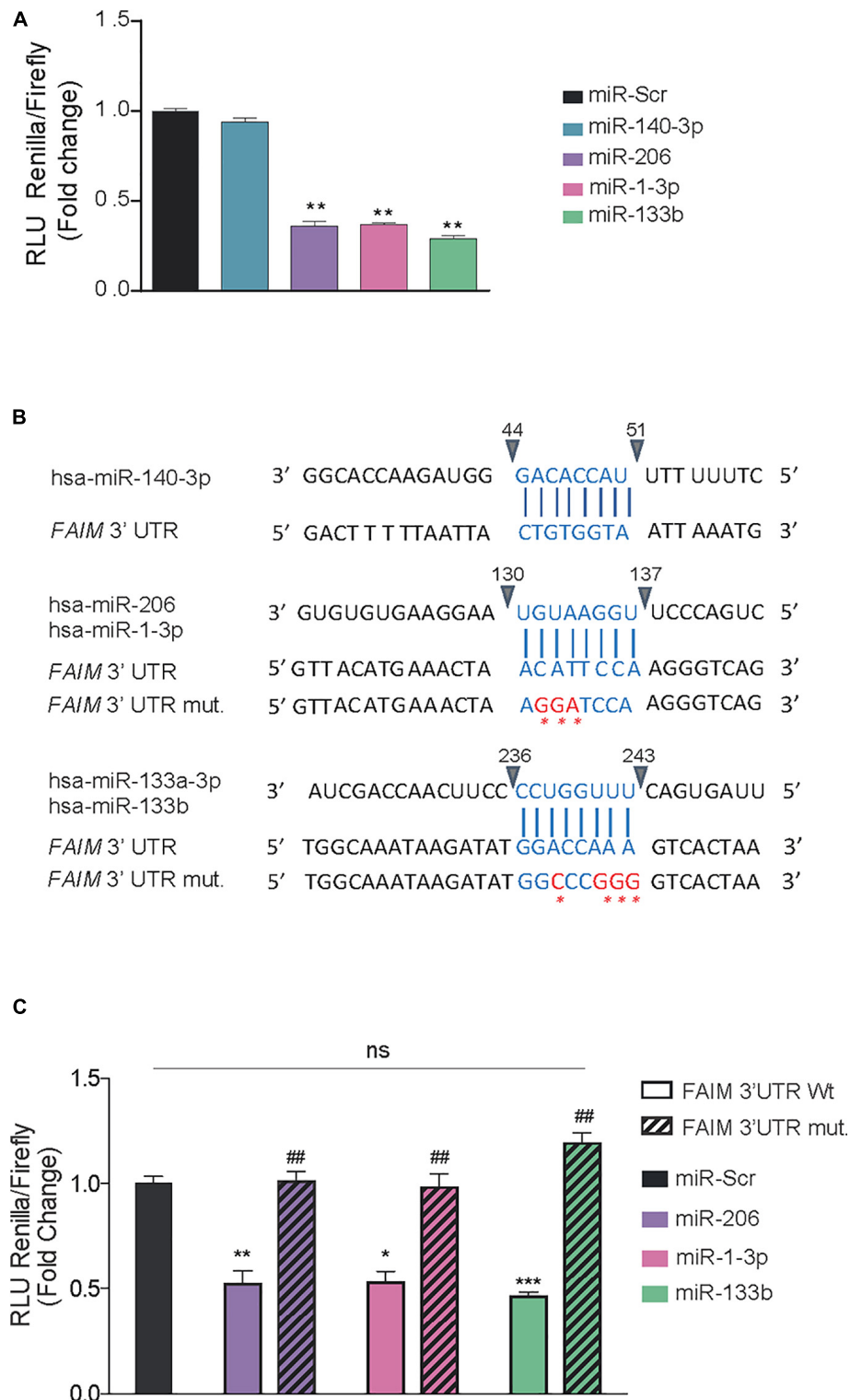


FIGURE 2 | *miR-206*, *miR-1-3p*, and *miR-133b* bind directly to *FAIM* 3'UTR. **(A)** Dual luciferase activity assay in HEK293T cells after the transfection of 25 nM of the indicated miRNAs using psiCheckTM-2 vectors encoding the wild type 3'UTR of *FAIM*. **(B)** Schematic representation of the indicated miRNA binding sites in the wild type (wt) and mutated (mut) 3'UTR of *FAIM*. The mutated nucleotides are indicated in red. **(C)** Dual luciferase activity assay in HEK293T cells after the transfection of 25 nM of the indicated miRNAs using psiCheckTM-2 vectors encoding the wild type and mutated forms of *FAIM* 3'UTR. Graph represents the values of luciferase activity and are the mean of three independent experiments \pm SEM. * $P < 0.05$, ** $P < 0.01$, and *** $P < 0.001$, compared with control vector. ## $P < 0.05$ compared with the wild type 3'UTR of *FAIM*.

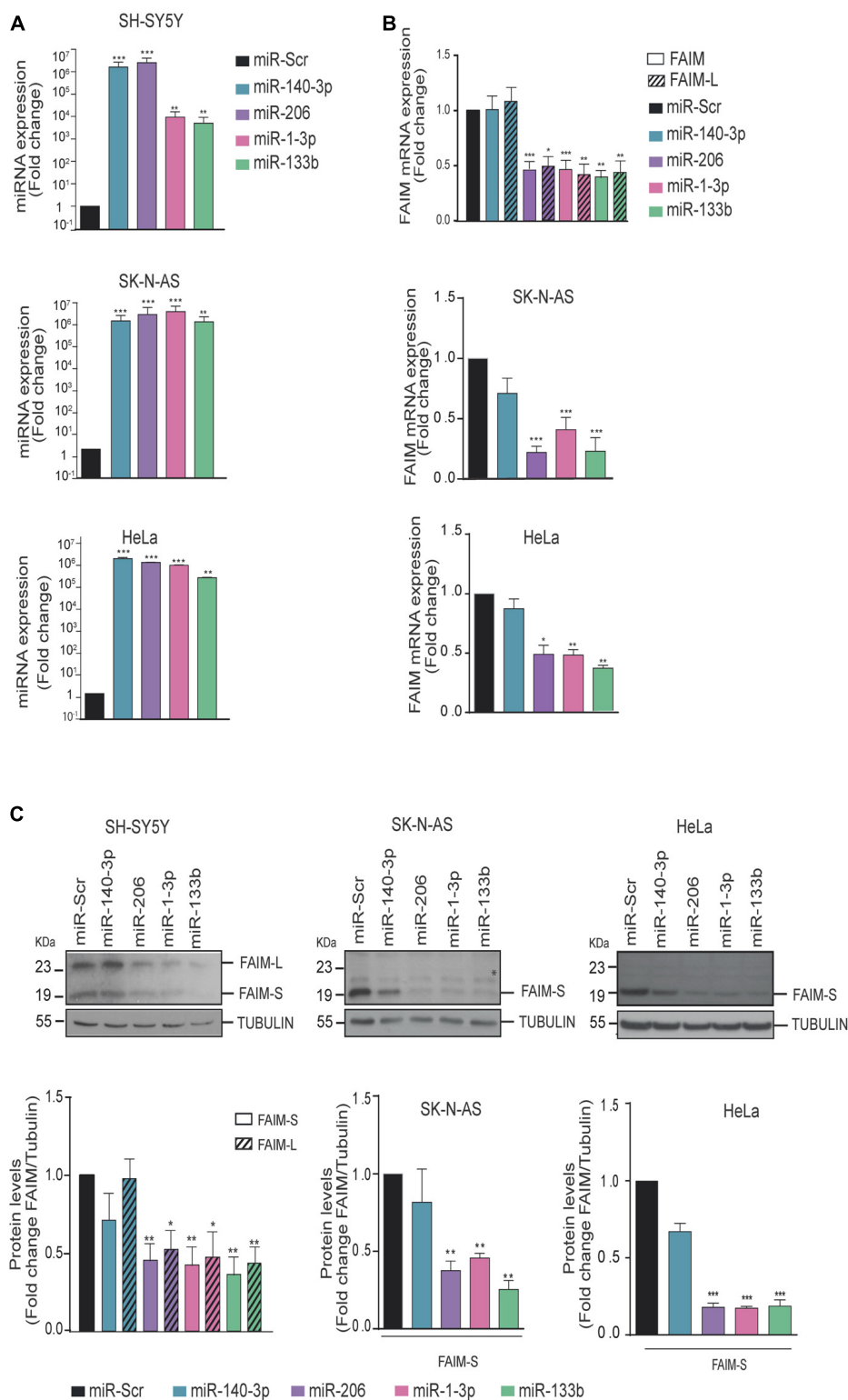


FIGURE 3 | *FAIM* expression is modulated by *miR-206*, *miR-1-3p*, and *miR-133b*. **(A)** MiRNAs expression levels were assessed by RT-qPCR. **(B)** SK-N-AS, SH-SY5Y and HeLa cells were transfected with 25 nM of *miR-140-3p*, *miR-206*, *miR-1-3p*, *miR-133b* or a control miRNA (*miR-Scr*) and *FAIM* mRNA expression levels were assessed by RT-PCR. **(C)** Representative western blots of *FAIM* in neuroblastoma and HeLa cells transfected with the indicated miRNAs. Lower panels show the quantification of the band intensity of the western blots normalized to the control miRNA (*miR-Scr*) condition. *Unspecific band. Graphs represent the mean of four independent experiments \pm SEM. Tubulin was used as a loading control. * $P < 0.05$, ** $P < 0.01$, *** $P < 0.005$.

impairment (Xie et al., 2015), and in the temporal cortex of human AD brains (Lee et al., 2012). Previous studies using microglial BV-2 cells and miR-206 mimics demonstrated that a pro-inflammatory stimulus (LPS treatment), increased miR-206 expression and enhanced the release of pro-inflammatory cytokines, including IL-1 β and TNF α . Thus, in a scenario with high levels of TNF α and low levels of FAIM as reported in some neurodegenerative diseases, TNF α signaling can be switched from a pro-survival to a pro-apoptotic response. Previous results from our lab showing that A β treatment decreased the levels of FAIM-L and blocked TNF α protection against A β toxicity (Carriba et al., 2015) would support this hypothesis.

To date, there are no effective therapies for these diseases and new strategies are needed. Given the encouraging results of profiling studies and preclinical testing, miRNAs are now being integrated into human clinical trials. For example, miR-122 has successfully reached clinical trials as a targeted therapy for hepatitis C (Lanford et al., 2010). Disrupting the miRNA-mediated reduction of anti-apoptotic proteins such as FAIM, could represent a new neuroprotective strategy against neurodegenerative diseases such as Alzheimer's or Parkinson's.

DATA AVAILABILITY STATEMENT

The raw data supporting the conclusions of this article will be made available by the authors, without undue reservation.

AUTHOR CONTRIBUTIONS

EC and MM performed the experiments. MS, JC, and MP-G designed the experiments and wrote the

manuscript. EC, MM, MS, and JL-S analyzed data. All authors contributed to the article and approved the submitted version.

FUNDING

This work was funded by grants awarded by the Spanish "Ministerio de Economía y Competitividad" (SAF2016-80236-R and PID2019-107286RB-I00), CIBERNED (CB06/05/1104) and Generalitat de Catalunya (2017SGR996) to JC. EC was supported by a pre-doctoral fellowship from the Vall d'Hebron Research Institute (VHIR) and MM was awarded by the FPU-Ph.D. fellowship (Grant No. FPU16/01099) from the Spanish Ministry of Education.

SUPPLEMENTARY MATERIAL

The Supplementary Material for this article can be found online at: <https://www.frontiersin.org/articles/10.3389/fcell.2020.584606/full#supplementary-material>

Supplementary Figure 1 | Multiple sequence alignment of 3'UTR FAIM from different species. Sequences included in the alignment are those of *Homo sapiens*, *Mus musculus*, *Rattus norvegicus*, and *Sus scrofa*. The sequences of miRNA are boxed in blue (miR-140-3p), pink (miR-206;miR-1-3p), and green (miR-133b;miR-133a-3p).

Supplementary Table 1 | MiRNA-binding sites in the 3'UTR of FAIM.

Supplementary Table 2 | AGO2-ClipSeq studies (Li et al., 2014 and Zhou, ENCORI: the encyclopedia of RNA interactomes).

REFERENCES

- Agarwal, V., Bell, G. W., Nam, J. W., and Bartel, D. P. (2015). Predicting effective microRNA target sites in mammalian mRNAs. *eLife* 4:e05005.
- Alvarez-Garcia, I., and Miska, E. A. (2005). MicroRNA functions in animal development and human disease. *Development* 132, 4653–4662. doi: 10.1242/dev.02073
- Betel, D., Koppal, A., Agius, P., Sander, C., and Leslie, C. (2010). Comprehensive modeling of microRNA targets predicts functional non-conserved and non-canonical sites. *Genome Biol.* 11:R90.
- Braakman, R., Fontijne, W. P., Zeegers, R., Steenbeek, J. R., and Tanghe, H. L. (1991). Neurological deficit in injuries of the thoracic and lumbar spine. A consecutive series of 70 patients. *Acta Neurochir.* 111, 11–17. doi: 10.1007/bf01402507
- Carriba, P., Jimenez, S., Navarro, V., Moreno-Gonzalez, I., Barneda-Zahonero, B., Moubarak, R. S., et al. (2015). Amyloid-beta reduces the expression of neuronal FAIM-L, thereby shifting the inflammatory response mediated by TNF α from neuronal protection to death. *Cell Death Dis.* 6:e1639. doi: 10.1038/cddis.2015.6
- Ha, T. Y. (2011). The role of MicroRNAs in regulatory T cells and in the immune response. *Immune Netw.* 11, 11–41. doi: 10.4110/in.2011.11.1.11
- Huo, J., Ma, Y., Liu, J. J., Ho, Y. S., Liu, S., Soh, L. Y., et al. (2016). Loss of Fas apoptosis inhibitory molecule leads to spontaneous obesity and hepatosteatosis. *Cell Death Dis.* 7:e2091. doi: 10.1038/cddis.2016.12
- Huo, J., Xu, S., Lin, B., Chng, W. J., and Lam, K. P. (2013). Fas apoptosis inhibitory molecule is upregulated by IGF-1 signaling and modulates Akt activation and IRF4 expression in multiple myeloma. *Leukemia* 27, 1165–1171. doi: 10.1038/leu.2012.326
- Jimenez-Jimenez, F. J., Alonso-Navarro, H., Garcia-Martin, E., and Agundez, J. A. (2014). Cerebrospinal fluid biochemical studies in patients with Parkinson's disease: toward a potential search for biomarkers for this disease. *Front. Cell. Neurosci.* 8:369. doi: 10.3389/fncel.2014.00369
- Kaku, H., Ludlow, A. V., Gutknecht, M. F., and Rothstein, T. L. (2020). FAIM opposes aggregation of mutant SOD1 that typifies some forms of familial amyotrophic lateral sclerosis. *Front. Neurosci.* 14:110. doi: 10.3389/fnins.2020.00110
- Kaku, H., and Rothstein, T. L. (2009). Fas apoptosis inhibitory molecule expression in B cells is regulated through IRF4 in a feed-forward mechanism. *J. Immunol.* 183, 5575–5581. doi: 10.4049/jimmunol.0901988
- Kaku, H., and Rothstein, T. L. (2020). FAIM Is a non-redundant defender of cellular viability in the face of heat and oxidative stress and interferes with accumulation of stress-induced protein aggregates. *Front. Mol. Biosci.* 7:32. doi: 10.3389/fmolb.2020.00032
- Lanford, R. E., Hildebrandt-Eriksen, E. S., Petri, A., Persson, R., Lindow, M., Munk, M. E., et al. (2010). Therapeutic silencing of microRNA-122 in primates with chronic hepatitis C virus infection. *Science* 327, 198–201. doi: 10.1126/science.1178178
- Lee, S. T., Chu, K., Jung, K. H., Kim, J. H., Huh, J. Y., Yoon, H., et al. (2012). miR-206 regulates brain-derived neurotrophic factor in Alzheimer disease model. *Ann. Neurol.* 72, 269–277. doi: 10.1002/ana.23588
- Li, J. H., Liu, S., Zhou, H., Qu, L. H., and Yang, J. H. (2014). starBase v2.0: decoding miRNA-ceRNA, miRNA-ncRNA and protein-RNA interaction networks from large-scale CLIP-Seq data. *Nucleic Acids Res.* 42, D92–D97.

- Marques-Fernandez, F., Planells-Ferrer, L., Gozzelino, R., Galenkamp, K. M., Reix, S., Llecha-Cano, N., et al. (2013). TNF α induces survival through the FLIP-L-dependent activation of the MAPK/ERK pathway. *Cell Death Dis.* 4:e493. doi: 10.1038/cddis.2013.25
- Martinez-Marmol, R., Barneda-Zahonero, B., Soto, D., Andres, R. M., Coccia, E., Gasull, X., et al. (2016). FAIM-L regulation of XIAP degradation modulates synaptic long-term depression and axon degeneration. *Sci. Rep.* 6:35775.
- Moubarak, R. S., Planells-Ferrer, L., Urresti, J., Reix, S., Segura, M. F., Carriba, P., et al. (2013). FAIM-L is an IAP-binding protein that inhibits XIAP ubiquitinylation and protects from Fas-induced apoptosis. *J. Neurosci.* 33, 19262–19275. doi: 10.1523/jneurosci.2479-13.2013
- Mullany, L. E., Herrick, J. S., Wolff, R. K., and Slattery, M. L. (2016). MicroRNA seed region length impact on target messenger RNA expression and survival in colorectal cancer. *PLoS One* 11:e0154177. doi: 10.1371/journal.pone.0154177
- Patron, J. P., Fendler, A., Bild, M., Jung, U., Muller, H., Arntzen, M. O., et al. (2012). MiR-133b targets antiapoptotic genes and enhances death receptor-induced apoptosis. *PLoS One* 7:e35345. doi: 10.1371/journal.pone.0035345
- Paul, P., Chakraborty, A., Sarkar, D., Langthasa, M., Rahman, M., Bari, M., et al. (2018). Interplay between miRNAs and human diseases. *J. Cell. Physiol.* 233, 2007–2018. doi: 10.1002/jcp.25854
- Rao, X., Huang, X., Zhou, Z., and Lin, X. (2013). An improvement of the 2⁻($\Delta\Delta$ CT) method for quantitative real-time polymerase chain reaction data analysis. *Biostat. Bioinforma. Biomath.* 3, 71–85.
- Santosa, D., Castoldi, M., Paluschinski, M., Sommerfeld, A., and Haussinger, D. (2015). Hyperosmotic stress activates the expression of members of the miR-15/107 family and induces downregulation of anti-apoptotic genes in rat liver. *Sci. Rep.* 5:12292.
- Schneider, T. J., Fischer, G. M., Donohoe, T. J., Colarusso, T. P., and Rothstein, T. L. (1999). A novel gene coding for a Fas apoptosis inhibitory molecule (FAIM) isolated from inducibly Fas-resistant B lymphocytes. *J. Exp. Med.* 189, 949–956. doi: 10.1084/jem.189.6.949
- Segura, M. F., Sole, C., Pascual, M., Moubarak, R. S., Perez-Garcia, M. J., Gozzelino, R., et al. (2007). The long form of Fas apoptotic inhibitory molecule is expressed specifically in neurons and protects them against death receptor-triggered apoptosis. *J. Neurosci.* 27, 11228–11241. doi: 10.1523/jneurosci.3462-07.2007
- Shingara, J., Keiger, K., Shelton, J., Laosinchai-Wolf, W., Powers, P., Conrad, R., et al. (2005). An optimized isolation and labeling platform for accurate microRNA expression profiling. *RNA* 11, 1461–1470. doi: 10.1261/rna.2610405
- Tognon, R., Gasparotto, E. P., Leroy, J. M., Oliveira, G. L., Neves, R. P., Carrara Rde, C., et al. (2011). Differential expression of apoptosis-related genes from death receptor pathway in chronic myeloproliferative diseases. *J. Clin. Pathol.* 64, 75–82. doi: 10.1136/jcp.2010.080895
- Vlachos, I. S., Zagganas, K., Paraskevopoulou, M. D., Georgakilas, G., Karagkouni, D., Vergoulis, T., et al. (2015). DIANA-miRPath v3.0: deciphering microRNA function with experimental support. *Nucleic Acids Res.* 43, W460–W466.
- Xie, B., Zhou, H., Zhang, R., Song, M., Yu, L., Wang, L., et al. (2015). Serum miR-206 and miR-132 as potential circulating biomarkers for mild cognitive impairment. *J. Alzheimers. Dis.* 45, 721–731. doi: 10.3233/jad-14-2847
- Yang, Q., Zhao, Q., and Yin, Y. (2019). miR-133b is a potential diagnostic biomarker for Alzheimer's disease and has a neuroprotective role. *Exp. Ther. Med.* 18, 2711–2718.
- Yu, L. Y., Saarma, M., and Arumae, U. (2008). Death receptors and caspases but not mitochondria are activated in the GDNF- or BDNF-deprived dopaminergic neurons. *J. Neurosci.* 28, 7467–7475. doi: 10.1523/jneurosci.1877-08.2008
- Zhong, X., Schneider, T. J., Cabral, D. S., Donohoe, T. J., and Rothstein, T. L. (2001). An alternatively spliced long form of Fas apoptosis inhibitory molecule (FAIM) with tissue-specific expression in the brain. *Mol. Immunol.* 38, 65–72. doi: 10.1016/s0161-5890(01)00035-9

Conflict of Interest: The authors declare that the research was conducted in the absence of any commercial or financial relationships that could be construed as a potential conflict of interest.

Copyright © 2020 Coccia, Masanas, López-Soriano, Segura, Comella and Pérez-García. This is an open-access article distributed under the terms of the Creative Commons Attribution License (CC BY). The use, distribution or reproduction in other forums is permitted, provided the original author(s) and the copyright owner(s) are credited and that the original publication in this journal is cited, in accordance with accepted academic practice. No use, distribution or reproduction is permitted which does not comply with these terms.

Advantages of publishing in Frontiers



OPEN ACCESS

Articles are free to read
for greatest visibility
and readership



FAST PUBLICATION

Around 90 days
from submission
to decision



HIGH QUALITY PEER-REVIEW

Rigorous, collaborative,
and constructive
peer-review



TRANSPARENT PEER-REVIEW

Editors and reviewers
acknowledged by name
on published articles

Frontiers

Avenue du Tribunal-Fédéral 34
1005 Lausanne | Switzerland

Visit us: www.frontiersin.org

Contact us: frontiersin.org/about/contact



REPRODUCIBILITY OF RESEARCH

Support open data
and methods to enhance
research reproducibility



DIGITAL PUBLISHING

Articles designed
for optimal readership
across devices



FOLLOW US

@frontiersin



IMPACT METRICS

Advanced article metrics
track visibility across
digital media



EXTENSIVE PROMOTION

Marketing
and promotion
of impactful research



LOOP RESEARCH NETWORK

Our network
increases your
article's readership